ELECTRON MICROSCOPE OBSERVATIONS OF EMBRYOS FROM MATERNAL RATS TREATED WITH TRYPAN BLUE

by

Karmen LaVer Bingham Schmidt

A THESIS
Presented to the Department of Anatomy
and the Graduate Division of the University of Oregon Medical School
in partial fulfillment of
the requirements for the degree of
Doctor of Philosophy

June 1971

For my Mother and Father

APPROVED:

[redacted]

.....

(Professor in Charge of Thesis)

[redacted]

.....

(Chairman, Graduate Council)

ACKNOWLEDGEMENT

This investigation was supported by United States Public Health Service training grant number 4 F01 GM30813 from the National Institutes of Health.

TABLE OF CONTENTS

TABLE OF FIGURES

EXPERIMENTAL

	9-day	10-day	11-day	12-day
Embryo:	1	2		
Neurectoderm:		3, 4, 5, 6, 7, 8, 9, 10*, 12	13, 14	15
Myocardium:				20, 21, 22, 23, 24*
Gut:		28, 29, 30, 31*	33, 34, 35, 36	37, 38, 39, 40, 41*, 43, 44, 45, 46, 47, 48
Mesenchyme:			53, 54, 55, 57, 58, 59	56, 60
Extra-embryonic membranes:				
Visceral yolk sac:	63, 64, 65*, 66*	67, 70	68, 71	69, 72
Trophoblast:		78, 79*, 81, 82, 83*		
Amnion:		87, 88, 89, 90*, 92, 93		
Maternal:				
Proximal convoluted tubules of kidney:				95, 96*

*Denotes 1 μ thick sections. All other figures are electron micrographs.

TABLE OF FIGURES

CONTROL

	9-day	10-day	11-day	12-day
Embryo:				
Neurectoderm:		11*, 16, 17	18	19
Myocardium:				25*, 26, 27
Gut:		32*, 49	50	42*, 51, 52
Mesenchyme:				61, 62
Extra-embryonic membranes:				
Visceral yolk sac:	73	74	75, 76	77
Trophoblast:		80*, 84*, 85, 86		
Amnion:		91*, 94		
Maternal:				
Proximal convoluted tubules of kidney				97*, 98

*Denotes 1 μ thick sections. All other figures are electron micrographs.

INTRODUCTION

Congenital malformations have often been described in animal offspring. It is estimated that 1 of every 65 live human births displays one or more anomalies (Murphy 1956). Abnormalities are produced in laboratory animals by dietary alterations and by exogenous agents. The colloidal disazo dye, Trypan blue, is an exogenous agent widely employed in the production of a variety of embryonic and fetal anomalies in laboratory animals. The teratogenic effects of this dye were first reported by Gillman, Gilbert, Gillman, and Spence (1948) in their experiments with rats. Subsequent studies reported Trypan blue-produced anomalies in other animal species: the mouse (Hamburgh 1952, Hamburgh et al. 1967), the rabbit (Harm 1954, Ferm 1956), the guinea pig (Hoar et al. 1961), the hamster (Geber 1969, Ferm 1958), the avian (Critchfield et al. 1965, Stéphan et al. 1961), the frog (Greenhouse et al. 1968), and the fish (Battle et al. 1960).

Trypan Blue Effects:

Three embryonic organ systems serve as major targets for the disruptive effects of the dye: the central nervous system, the cardiovascular system, and the vertebral axis. Neural tissues are those most frequently compromised, yielding such anomalies as hydrocephalus, exencephaly, anencephaly, and the Arnold-Chiari deformity (Hamburgh 1954, Waddington et al. 1953, Warkany et al. 1958, Gilbert et al. 1954). Fox and Goss (1955, 1956, 1957, 1958), Monie, Takacs and Warkany (1966), and Smith (1963) have described the following cardiovascular malformations: transposition of arterial trunks, pulmonary stenosis, auricular displacement, septal defects, and vena caval deformities. Abnormalities of the vertebral axis, such as torsion defects, taillessness and spina

bifida, have been characterized by Stéphan and Sutter (1960), Hamburgh (1952, 1954), Gunberg (1954, 1956), and Murakami (1952).

Other embryonic tissues not belonging to these three major organ systems can also be affected by Trypan blue, although the frequency of such malformations is low. These systems include the eye (Gillman et al. 1948, Gilbert et al. 1954), the ear (Gillman et al. 1948, Myers 1955), and the genito-urinary tracts (Goldstein 1957, Gillman et al. 1948).

The malforming effects of the dye vary widely among experiments, mainly due to differences in time of injection, route of injection (subcutaneous, intraperitoneal, or intravenous), and species of animal. For example, Gillman et al. (1948) found that the highest level of malformation resulted from injection of the maternal animal on the 6th day of gestation, whereas Wilson, Beaudoin and Free (1959) showed the greatest incidence to occur if injected subcutaneously on day 7-8, if intravenously on day 8-9. Wilson et al. (1959) also demonstrated the decrease in frequency of anomalies produced by injection in later stages of gestation; if injection was delayed until day 11 or longer, no teratogenic effects were observed. Gunberg (1958) demonstrated the differences in incidences and types of malformations which resulted among three strains of rats; Hamburgh and Callahan (1967) found similar differences among strains of mice.

Malformation parameters may also be markedly affected by the dye sample lot employed, as studied by Beck, Spencer and Baxter (1960), Beck (1961), Tuchmann-Duplessis and Mercier-Parot (1959), and Carpent (1962). Depending upon the manufacturer, the titratable azo-linkages varied from 20 to 86%. Kelly and co-workers (1964) noted that com-

mercial samples of Trypan blue ranged from 50 to 80% in dye content, and 4 to 15% in red impurities.

Other studies demonstrated that malformation parameters may also be affected by the variations in concentrations of the various colored components of a dye sample. Dijkstra and Gillman (1961) fractionated Trypan blue into three colored components, red, purple, and blue. The purple fraction was held to be responsible for the reticuloendothelial proliferation noted in the maternal liver. Barber and Geer (1964) found the blue fraction to be responsible for teratogenicity in the mouse; such a finding was later confirmed in the rat by Beck and Lloyd (1963b) and by Kelly et al. (1964). Although a recent study by Bertini and Sacerdote (1970) attributes some teratogenic capacity to the red impurity, the great bulk of information indicates that this capability is confined to the blue fraction (Barber et al. 1964, Beck et al. 1963b, and Kelly et al. 1964).

Site of Dye Action:

A. Maternal animal:

Despite its wide usage, the site of action of the dye remains unknown. Three possibilities have been suggested, that of the maternal animal, the visceral yolk sac placenta, or the embryo. Teratogenic action via the maternal animal is a concept which had received wide support in early experimentation due to the numerous alterations in maternal metabolism noted after dye usage. For example, Beaudoin and Ferm (1961) demonstrated an elevation of the alpha- and beta-globulin fractions of treated maternal rabbit sera, and reasoned that such alteration might be causative of embryonic malformation. However, Wilson (1955) reported that an azo dye of relatively low teratogenicity, Evans

blue, produced almost identical serum protein alterations. Beaudoin and Roberts (1965) found that serum globulins obtained from dye-treated maternal rats did not produce malformations when administered to other pregnant rats. Further contraindication of the importance of serum protein alteration in the production of malformation is the report that the teratogenic azo dye Congo red does not affect the respective proportions of serum protein fractions (Beaudoin, 1964).

A theory of thyroid-mediated teratogenicity resulted from observations of gland suppression after dye injection (Christie 1964). Yamada et al. (1965) and Beaudoin et al. (1966) found that Trypan blue competes with thyroxine for the same serum binding sites, resulting in increased amounts of free thyroxine, inhibition of TSH secretion, and thyroid gland suppression, yet Beck and Lloyd (1966) determined that administration of free thyroxine to the maternal rat had no effect upon the incidence of malformations.

That malformations result from maternal liver damage was a concept proposed by the discoverers of the teratogenic properties of the dye (Gillman et al. 1948). However, Wilson (1954) produced almost total liver failure in rats by using carbon tetrachloride without producing malformations. Dye-induced maternal anemia was proposed as another possible scheme of teratogenicity by the original workers (Gillman et al. 1948) yet no malformations were produced by major depletion of maternal blood stores (Wilson 1953).

Hommes (1958) suggested that adrenal hyperactivity might be responsible for malformation for three reasons: first, both Trypan blue and ACTH produce similar alterations in concentrations of individual serum protein components. Second, the dye produces a hypertrophy of the

maternal adrenal gland. Third, cortisone usage has produced anomalies in mice (Fraser et al. 1951). However, Ferm (1959) reported that maternal adrenal hypertrophy followed the administration of non-teratogenic dyes, while Schnurer (1963) produced similar maternal adrenal effects with formalin injection without producing abnormalities. In addition, Gunberg (1957) found that hydrocortisone did not produce malformations in rats.

Blockage of the maternal reticuloendothelial system as a possible cause of malformation was one concept suggested by Gillman and co-workers (1948), but a later report by this group (Gillman et al. 1951) demonstrated that non-teratogenic disazo dyes also yield such a response. In addition, India ink and Niagara blue 2B, both of which possess colloidal properties similar to those of Trypan blue, did not produce malformations (Wilson et al. 1959). As a further contradiction to such a concept of malformation, Dijkstra et al. (1961) reported that the non-teratogenic purple component was that fraction responsible for production of maternal reticulosis.

The case for a maternal site of dye action is further weakened by the observations that quite similar malformations have been produced in species lacking the maternal factor, as in the avian, frog, and fish (Stéphan et al. 1960, Greenhouse et al. 1968, Battle et al. 1960), and in mammalian animals cultured in vitro (Mulherkar 1960, Turbow 1966, Gunberg 1969).

B. Yolk sac placenta:

The yolk sac placenta has received the bulk of support as the site of Trypan blue teratogenicity, for two reasons: first, its inner or visceral layer phagocytizes large quantities of dye. Second, the cessa-

tion of the teratogenic period roughly coincides with the time of completion of enclosure of the embryo by the yolk sac. Unlike the embryos of most mammalian species, the rodent embryo grows into and thus becomes enclosed by its own bilaminar yolk sac, an organ which provides nourishment until such a role can begin to be assumed by the chorio-allantoic placenta on day 11. Waddington et al. (1953) first offered the hypothesis that the heavy accumulations of dye in the visceral yolk sac could "clog" this tissue and thus prevent the transmission of essential nutrients to the embryo. Hamburgh's (1952) experimentation with mice provided additional support for such a rationale. Subsequently, Beck and co-workers (1967) and Lloyd and Beck (1969) have suggested that the dye phagocytized in this visceral yolk sac layer compromises the lysosomal apparatus and thus prevents transfer of nutrients, for they demonstrated in rat visceral yolk sacs an in vitro inhibition of five lysosomal enzymes. Some in vivo studies of dye-laden mouse visceral yolk sacs revealed a reduction in activity of acid phosphatase and of monoamine oxidase, but no reduction in activity of alkaline phosphatase (Nebel et al. 1966, Hamburgh et al. 1966). Greenhouse (1969) found diminution in the activity levels of acid phosphatase, but not of thiamine pyrophosphatase, succinic dehydrogenase, or glucose-6-dehydrogenase. Padykula and Richardson (1963) found no differences in the glycogen content of dye-laden and control yolk sacs. Furthermore, in an attempt to correlate dye concentration in the yolk sac with degree of malformation, Davis (1968) showed that those yolk sacs containing the heaviest concentrations of dye were more likely to surround normal rather than abnormal embryos. Tuchmann-Duplessis and Mercier-Parot (1955) found that the non-teratogenic dye Azo blue is also intensively collected

by the visceral yolk sac. Thus, while Trypan blue does affect yolk sac functions, the evidence to support the concept that the visceral yolk sac is the site of malformation is equivocal.

C. Embryo:

The third suggested site of malformation, that of the embryo, has received very little support because of the failure to demonstrate Trypan blue within embryonic tissues (Waddington et al. 1953, Hamburgh 1954, Wilson et al. 1959), and especially because Wilson et al. (1963) demonstrated no significant radioactivity in embryonic tissues after C^{14}-labelled Trypan blue was injected into maternal rats. A few indications exist, however, that the dye crosses the maternal-embryonic barriers. Blue coloration of the rabbit blastocyst fluid was reported by Ferm (1956). Barber and Geer (1964) observed a diffuse blue staining of the mouse embryonic mass, prior to the time of yolk sac closure. Kaplan and Johnson (1970) produced malformations in chick embryos after direct injections of Trypan blue into the vitelline circulation. Finally, Davis and Gunberg (1968) reported conclusively the presence of the dye within the embryonic hindgut of 11 to 13 day embryos. Because the latter study unequivocally demonstrated the presence of small quantities of dye in embryonic tissues, an electron microscope investigation of selected embryonic tissues was deemed necessary.

Statement of Objectives:

The objective of this dissertation is to utilize the resolving powers of the electron microscope for the following purposes:

1. to describe the ultrastructural morphology of certain normal embryonic tissues of the rat. Mandatory prerequisites include the development (Appendix, Tables 1, 2, 3, 4) of a fixative

adequate for the preservation of such delicate tissues.

2. to characterize any intra- or extra-cellular abberations of embryonic tissues from dye-treated maternal animals which might signal a forthcoming malformation. This necessitates intensive examinations of those tissues most commonly compromised by the dye, namely, the central nervous system and the heart.
3. to search for evidence of the dye within embryonic tissues, particularly in the region of the hindgut where small amounts can be seen in whole mounts. Because numerous reports have failed to describe the dye with light microscopy (Waddington et al. 1953, Hamburgh 1954, Wilson et al. 1959, Greenhouse et al. 1968), any possible aggregations of dye must necessarily be minute.
4. to relate any ultrastructural dye-produced alterations to the mode and/or the site of action of the dye. For example, do those sites of ultrastructural alteration relate to those organ systems most affected by the dye, namely, the central nervous system, heart and great vessels, and vertebral axis? In addition, how might the nature of such cellular changes relate to any concept of site and/or mode of action of this teratogen?

MATERIALS AND METHODS

Animal care and breeding:

Simonsen Laboratories of Gilroy, California, provided Sprague-Dawley rats of breeding age. The animals were housed in metal cages in a windowless room in which the period of artificial light lasted from 10:00 P.M. to 10:00 A.M. This arrangement served as a convenience in the procurement of accurately timed rat gestational ages. An ad libitum diet of Purina rat chow was supplemented with green vegetables twice each week. Only healthy, female animals between 80 and 100 days of age were utilized. Each female was checked daily for stage of estrus by vaginal swabbing. A rat in late pro-estrus or early estrus was housed with a male rat for the first two-hour period of darkness (10:00-12:00 A.M.), then checked for the presence of sperm by vaginal swabbing. The beginning of gestation was estimated as occurring at the midpoint of the two-hour breeding period.

Teratogenic agent:

Each experimental female was anesthetized with ether and injected intraperitoneally with a 2% aqueous solution of Trypan blue (Color Index #23850, National Aniline Division, Allied Chemical Corporation, Lot #2062P) at a dosage level of 100 mg./kg. body weight. Trypan blue, the sodium salt of the disazo dye formed by coupling tetrazotized o-tolidine with two molecular portions of 8-amino-1-napthol-3,6-di-sulphonic acid (Hartwell et al. 1936), has a molecular weight of 960.83. Its structural and chemical formulae are displayed below:

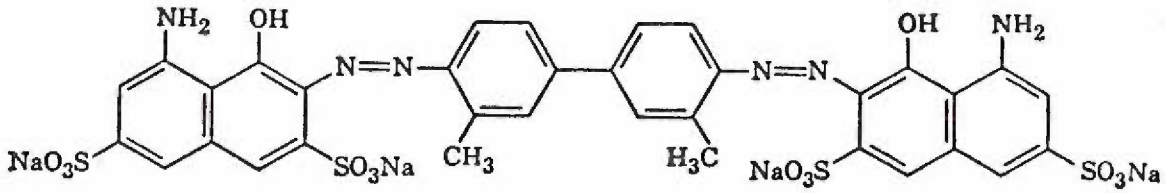

3,3'- [(3,3'-dimethyl-4,4'biphenylene)bis(azo)] bis [5-amino-4-hydroxy-2,7-naphthalenedisulfonic acid]

The pregnant females received the teratogen 8.5 days after the estimated initiation of gestation. Control animals were neither anesthetized nor injected with Trypan blue.

Collection of embryos and fetuses:

On gestation day 9, 10, 11, 12, 16, or 20, each maternal animal in the control and experimental groups received a subcutaneous injection of aqueous sodium pentobarbital at a dosage level of 60 mg./kg. body weight. Each embryo or fetus was dissected in freshly prepared solutions of either fixative or physiological saline, respectively. During such dissection, the uterine horns were kept moist with saline-soaked gauze.

Nine- and 10-day embryos were freed of any maternal tissue remnants during immersion in cold (4° C.) fixative. The embryo, encased in its yolk sac, was then transferred by glass pipette to a vial containing fresh fixative. Eleven- and 12-day embryos were likewise freed of any maternal tissue remnants during immersion in cold fixative. Each yolk sac was gently removed with micro-dissecting forceps and transferred to a vial of cold fixative. Head, heart, and tail areas were removed with a razor blade in fixative-containing dishes.

While immersed in physiological saline, 16- and 20-day fetuses were freed of all extra-embryonic membranes and examined for the

presence of external malformations. Records were kept on each fetus with respect to uterine position, wet weight, and type of external malformation (Appendix, Tables 5, 6).

A variant of Pease's formaldehyde mixture (1964) proved to be the most satisfactory fixative. It was constituted as follows:

Stock solution A:	8.5 ml. of 2.25 gm.% NaOH 41.5 ml. of 2.26 gm.% $NaH_2PO_4 \cdot H_2O$
Stock solution B:	30.0 gm. of paraformaldehyde 5.0 gm. of glucose Distilled water to 100 ml.
Fixative (pH 7.4):	45.0 ml. Stock solution A 5.0 ml. Stock solution B 0.5 ml. of 50% glutaraldehyde

The fixative utilized paraformaldehyde in order to avoid the methanol contaminant present in commercial formaldehyde solutions. The fixative was maintained at room temperature to prevent the formation of trioxymethylene (Stecher 1960), a contaminant which forms at cooler temperatures. Each tissue segment was immersed for 10 minutes in fixative, rinsed in three changes of phosphate buffer (Stock solution A), and post-fixed for 30 minutes. The post-fixative solution was prepared as follows:

Post-fixative:	45.0 ml. of Stock solution A 5.0 ml. of 5.0 gm.% aqueous glucose 0.5 gm. of osmium tetroxide

The tissue was dehydrated in a graded series of aqueous solutions of ethyl alcohol (50, 70, 95, 100%), further dehydrated in propylene oxide, and infiltrated with a 1:1 mixture of propylene oxide and epoxy resin. After 4 to 6 hours of infiltration, the tissue blocks were embedded in the following resin mixture:

11.0	cc.	Epon 812 (Ladd Research Industries; Burlington, Vermont)
7.0	cc.	dodecenyl succinic anhydride
5.0	cc.	nadic methyl anhydride
0.345	cc.	tri (dimethyl amino methyl) phenol

To polymerize the resin mixture, the blocks were first exposed to room temperature for 24 hours, then to 60° C. temperature for an equal period of time.

Maternal kidney:

Because Trypan blue is avidly phagocytized by cells of the proximal convoluted tubules, samples of kidney were obtained from control and dye-treated maternal rats to assist in the ultrastructural identification of Trypan blue. Tissue blocks of maternal kidney were prepared for electron microscopy as described above.

Dye reduction:

The reducing agent, sodium hydrosulfite, has been employed by Lloyd and Beck (1964) to render Trypan blue colorless by reductive cleavage of the disazo bond. Since either embryonic or adult tissues could conceivably harbor enzyme systems capable of cleaving the dye molecule, it became of interest to investigate the ultrastructural characteristics of tissues housing deposits of dye exposed to such a reducing agent.

Tissue samples of maternal kidney and of embryonic gut were treated with a 10% aqueous solution of sodium hydrosulfite until the blue color of the dye either disappeared or was visibly diminished.

Glycogen determination:

Bacterial alpha-amylase (4 X crystallized) and bovine pancreatic ribonuclease (Sigma Chemical Company; St. Louis, Missouri) were employed as aids in the identification of glycogen in 12-day embryonic gut tis-

sue. Alpha-amylase was utilized to cleave any 1,4 linkages uniting the glucose sub-units of glycogen. The ribonuclease was used to discriminate between cytoplasmic ribonucleoproteins, such as free and bound ribosomes, and somewhat larger granules suspected of being glycogen. Tissue blocks were fixed for 10 minutes in the chosen fixative and incubated in the enzyme solutions (Biava 1963) described below.

The tissues were immersed in either an alpha-amylase or an RNA-ase solution (1:100,000 in 0.1 M $NaH_2PO_4 \cdot H_2O$, pH 7.2) for 24 hours at 40° C. These concentrations were similar to those utilized by Lillie (1965). Control blocks were prepared by immersion of experimental gut tissue for 24 hours in the phosphate buffer solution minus the enzyme. The tissues were subsequently post-fixed and embedded in the manner previously described.

Sectioning and staining:

An LKB Ultratome was utilized for sectioning the embedded tissue blocks. One-micron sections cut with glass knives were transferred to glass slides and affixed with heat. These sections were either unstained, stained with Richardson's stain (1960), or treated with a periodic acid-Schiff solution sequence (Lane et al. 1965).

Thin sections, 500 to 800 Å in thickness, were cut with a diamond knife and transferred to 200- or 300-mesh copper grids. To enhance tissue contrast, sections were stained in a saturated aqueous solution of uranyl acetate (Watson 1958) for 15 minutes, and then in Reynolds' basic lead citrate solution (Reynolds 1963) for 1.5 minutes. Sections were viewed with an RCA EMU 3f electron microscope.

RESULTS

All of the light and electron microscope observations of embryonic tissues obtained from maternal rats injected with Trypan blue were performed on tissue samplings from those 9- through 12-day embryos which appeared to be normal. No embryos were utilized which exhibited tissues identified as containing either well-defined or probable areas of malformation. The reader is directed to Figures 1 and 2 for the purpose of relating descriptions of tissue sample areas to the spatial relationships of the cells, tissues, and organs involved as component parts of rodent embryogenesis.

A. Embryonic tissues:

1. Neurectoderm:

a. Experimental:

The amniotic cavity directly overlying the flattened 10-day neural plate frequently contained aggregations of fibrillar material (Figure 3) which usually were detected in the mid-sagittal plane. These aggregations were composed of randomly distributed fibrin polymers, identified as such because the polymers displayed an axial periodicity of 225-235 Å in longitudinal section (Figure 4). In cross-section, these polymers exhibited the following morphology: an outer, electron-dense sheath of 300-400 mμ diameter surrounded a circular, clear area of 100-150 mμ diameter. Some of the tangential sections of the neural plate (Figure 5) revealed portions of the amniotic cavity among neurectoderm cells. These portions of the amniotic cavity sometimes contained a fibrous material which displayed no clear indications of axial periodicity.

The neurectoderm cells of the 10-day experimental embryos con-

tained numerous accumulations of electron-dense glycogen particles (Figure 5). These accumulations of glycogen were composed of individual particles which measured 20-40 mμ in diameter and larger rosettes which measured 60-80 mμ in diameter. The individual glycogen particles were larger than adjacent free and bound ribosomes, which measured 15-20 mμ in diameter (Figure 6). These accumulations of glycogen particles were observed either free within the cytoplasm, adjacent to residual bodies, or within residual bodies (Figure 7).

Another prominent component of 10-day experimental neurectoderm cells was a vacuole which in this study was termed the "dye-like" vacuole. This "dye-like" vacuole exhibited a homogeneous, electron-dense center surrounded by a clear peripheral area. These "dye-like" vacuoles usually formed small clusters, although occasionally they appeared individually (Figure 8). The "dye-like" vacuoles were often situated adjacent to deposits of glycogen (Figures 3, 4, 6, 7), or to large residual bodies (Figures 5, 9). In 1 μ thick sections of 10-day experimental neurectoderm stained with Richardson's stain, the "dye-like" vacuoles displayed dark blue centers with clear peripheral areas (Figure 10). One μ thick sections of control 10-day neural plate stained with Richardson's stain, failed to demonstrate the presence of the "dye-like" vacuoles (Figure 11).

Residual bodies were prevalent within neurectoderm cells of 10-day experimental embryos. These large vacuoles displayed heterogeneous arrays of materials of different electron densities; usually the contents were composed of a floccular material of high electron-density (Figure 12). These residual bodies often contained, or were adjacent to, glycogen deposits and "dye-like" vacuoles (Figures 5, 7, 9).

Cells which exhibited the morphology and function of phagocytes were not identified in the neurectoderm from 10-day experimental embryos.

Eleven-day neural tissue was formed as a neural tube composed of a layer of pseudostratified columnar epithelium. In the midbrain, the only neural area sampled in 11-day embryos, fibrin was not detected in the neural tube lumen. The neurectoderm cells did not exhibit glycogen. The frequency of "dye-like" vacuoles was less than that observed in neurectoderm cells of the 10-day experimental embryos. The "dye-like" vacuoles (Figure 13) exhibited a morphology and distribution identical to those observed in the 10-day experimental tissue. The 11-day neurectoderm exhibited numerous residual bodies which were morphologically similar to those within 10-day experimental neurectoderm. These residual bodies were encountered more frequently in the 11-day than in the 10-day experimental neurectoderm cells and were often either adjacent to or contained "dye-like" vacuoles. The 11-day neurectoderm, in contrast to the 10-day neurectoderm, contained numerous phagocytic cells (Figure 14).

Fibrin, a common feature of the 10-day experimental amniotic cavity, was not evident in the 12-day experimental midbrain lumen. The 12-day midbrain cells contained no glycogen. The frequency of "dye-like" vacuoles was less than that of the 11-day midbrain. Residual bodies (Figure 15), morphologically identical to those of the 11-day experimental neurectoderm, were encountered more frequently than in the 11-day experimental neurectoderm. Phagocytic cells, first observed in the 11-day experimental neurectoderm, were observed in greater numbers in the 12-day experimental neurectoderm.

b. Control:

In 10- through 12-day control embryos, samples of neurectoderm comparable in location to those of 10- through 12-day experimental embryos did not contain fibrin, glycogen, or "dye-like" vacuoles. Residual bodies appeared infrequently in control embryos. These organelles usually contained a heterogeneous material, some of which was identified as remnants of other organelles (Figure 16).

The cells comprising the neural plate of 10-day control embryos were joined together by terminal bars at their luminal ends. Contiguous cells displayed large intercellular spaces; desmosomal junctions appeared infrequently (Figure 17).

Cells of the 11-day control neural tube resembled those of the 10-day control neural plate except for the development in the former of cytoplasmic processes which extended toward the neural tube lumina (Figure 18).

Cells of the 12-day control neural tube exhibited a morphology identical to that of the 11-day control neurectoderm. Those cells in some phase of mitosis demonstrated organelles composed of paired tubules which were similar to profiles of the endoplasmic reticulum (Figure 19). This organelle appeared to be a normal component of the mitotic process.

2. Myocardium:

a. Experimental:

The most apparent characteristic of 12-day experimental myocardial cells was glycogen, which appeared as large numbers of very electron-dense particles measuring approximately 30 mμ in diameter (Figure 20). These accumulations of glycogen were often sufficiently concentrated to either obscure the cytoplasmic organelles or to crowd them into a

peripheral intra-cellular position (Figure 21). Some of the glycogen appeared in an extra-cellular position (Figures 22, 23); a particulate mass often extended over the outer surfaces of several contiguous cells. Cell and organelle membranes were poorly defined (Figure 21). In addition, the myofibrils appeared to lack the organization observed in comparable control tissues. The application of the periodic acid-Schiff reagent to 1 μ sections (Figure 24) resulted in the appearance of highly PAS-positive areas which coincided with those areas identified ultrastructurally as containing glycogen. These PAS-positive areas were larger and more intensely colored than those in comparable sections of control tissues (Figure 25).

b. Control:

The most prominent feature of 12-day control myocardial cells was the diminution in numbers of glycogen particles, in comparison with 12-day experimental myocardial cells (Figure 26). The myofibrillae, which displayed clear evidence of axial banding, appeared to be integral parts of the intercalated discs. Numerous polyribosomes either were scattered among the myofilaments or were gathered into small clusters elsewhere in the cytoplasm. The sarcoplasm also contained particles which appeared to be glycogen (Figure 27).

3. Visceral endoderm and primitive gut:

a. Experimental:

The ventral surface of the 10-day embryo (Figure 2) displayed a simple epithelium which was continuous laterally with the visceral yolk sac. This cell layer, the visceral endoderm, possessed a luminal border of irregular micro-villi. Dense concentrations of "dye-like" vacuoles were observed in the cytoplasm of these visceral endoderm cells. Each

vacuole exhibited a compact, homogeneous material in the center of an otherwise clear vacuole (Figures 28, 29). Underlying the visceral endoderm was the splanchnic mesoderm, which separated the visceral endoderm from the intra-embryonic coelom. This splanchnic mesoderm also contained "dye-like" vacuoles (Figure 30). One μ thick sections of visceral endoderm exhibited small vacuoles with dark blue centers and clear peripheries (Figure 31). These small vacuoles were identical to the "dye-like" vacuoles seen ultrastructurally. Comparable 1 μ sections of control tissues did not demonstrate the presence of such vacuoles (Figure 32).

The 11-day embryo possessed a primitive gut tube which developed by invagination of the visceral endoderm. Randomly distributed fibrin polymers, displaying a 225-235 Å axial periodicity, filled the gut lumen (Figure 33). The cross-sectional diameter of these fibrin polymers usually measured between 300-700 mμ, although in some instances diameters as large as 1.5 μ were observed. The cross-sectional morphology of the fibrin polymer (Figure 34) was essentially identical to that of the fibrin observed in the amniotic cavities of the 10-day experimental embryos (Figure 34).

Electron-dense glycogen particles measuring 35-55 mμ in diameter were conspicuous in the 11-day hindgut epithelium (Figure 35), both in an inter-cellular and an extra-cellular position, as noted in 12-day myocardium. Large rosettes of glycogen, measuring 100 mμ in diameter, were more electron-dense than the individual particles of which they were composed.

"Dye-like" vacuoles were frequently observed in the 11-day hindgut endoderm (Figure 36).

The 12-day hindgut lumina contained fibrin polymers similar in quantity and morphology (Figure 37) to those noted in the 11-day hindgut lumina. However, the glycogen content of the 12-day hindgut cells was markedly increased over that of 11-day hindgut cells. Glycogen particles were often observed to fill the epithelial cells (Figure 38). Glycogen rosettes, measuring 40-200 mμ in diameter, were more electron-dense than their component 20-40 mμ particles (Figure 39). Cell organelles often possessed poorly defined membranes. Figure 40 suggests the possibility that accumulations of glycogen passed from an intra-cellular to an extra-cellular position.

To assist in the identification of glycogen in the 12-day hindgut, 1 μ thick sections of these tissues were reacted with the periodic acid-Schiff reagent (PAS). Numerous PAS-positive areas were apparent (Figure 41) which coincided in position with ultrastructural deposits of glycogen. Comparable sections of control 12-day hindgut did not exhibit these large PAS-positive areas (Figure 42), although some PAS-positive staining was exhibited.

Alpha-amylase digestion of 12-day hindgut tissues removed particles resembling those identified as glycogen. Nearly all of the membrane-bound and free ribosomes were retained after this treatment (Figures 43, 44).

Incubation of the 12-day hindgut tissues in a solution of ribonuclease resulted in loss of nearly all of the bound ribosomes, and in loss of all of the free ribosomes. All of the particles similar to those identified as glycogen remained apparent (Figures 45, 46).

The 12-day hindgut cells displayed "dye-like" vacuoles, sometimes situated in close proximity to aggregations of glycogen (Figure 47).

To strengthen the identification of the contents of "dye-like" vacuoles as being dye, 12-day hindguts were immersed in a solution of sodium hydrosulfite. This compound cleaves the disazo bond of Trypan blue, rendering it colorless. As seen in Figure 48, a definite alteration in the appearance of the contents of the "dye-like" vacuoles was observed, for the formerly compact, electron-dense vacuole center appeared now to be filamentous. This sodium hydrosulfite treatment also altered the appearance of the nuclear chromatin and enhanced the definition of the cellular membranes.

b. Control:

The "dye-like" vacuoles which were prominent in the visceral endoderm cells of the 10-day experimental embryos were never observed in comparable tissue from the 10-day control embryos (Figure 49). All other morphological aspects of the experimental endoderm cells were similar to those of the experimental tissue cells.

The lumen of the 11-day control hindgut did not exhibit any fibrin polymers (Figure 50). These control endoderm cells demonstrated neither "dye-like" vacuoles nor accumulations of glycogen.

The hindgut lumen of one 12-day control embryo exhibited cross-sections of two structures (Figure 51) bearing a morphology similar to that of the fibrin cross-sections described in embryos of the experimental group. No longitudinal sections demonstrating axial periodicity were observed in these structures to positively identify them as fibrin. This was the only control embryo in this study which contained any evidence of fibrin formation. Neither glycogen nor "dye-like" vacuoles were evident in the endoderm cells from control 12-day hindgut areas.

The cell-to-cell membrane associations were simple in 11-day hindgut

tissues, more complex in 12-day hindgut endoderm. Numerous free ribosomes filled the cell cytoplasm of the 12-day control endoderm, and rough endoplasmic reticulum surrounded oval-shaped mitochondria (Figure 52). The dense coagula filling the gut lumina often contained debris, some of which was cellular debris; Figure 51 demonstrates an example of sloughing of dead cells.

4. Mesenchyme:

a. Experimental:

The mesenchyme of 10-day experimental embryos exhibited intracellular clusters of "dye-like" vacuoles and of residual bodies. Ten-day mesenchyme also displayed cells of phagocytic capabilities.

The mesenchyme of 11-day experimental embryos contained large accumulations of glycogen. When these tissues were treated with aqueous uranyl acetate, the glycogen appeared as clumps of white fibrous material, among which smaller, electron-dense ribosomes were seen (Figure 53). Residual bodies were prevalent; sometimes they were situated adjacent either to glycogen fields (Figure 54) or to clusters of "dye-like" vacuoles (Figure 55).

Deposits of glycogen were frequently observed in the mesenchyme of 12-day experimental embryos. In comparison with experimental group mesenchyme of the previous day, "dye-like" vacuoles remained in evidence, and the number of residual bodies increased significantly (Figure 56).

Stellate or rounded cells of phagocytic capabilities were seen in 11- and 12-day mesenchyme tissues, as well as in the 10-, 11-, and 12-day neural tube. The numerous free ribosomes caused these cells to appear very electron-dense (Figures 57, 58). Although areas of chromatin material were observed in most tissue sections, it could not be deter-

mined whether the cells were multinucleated or multilobated. Occasionally, these cells displayed glycogen, perhaps derived by phagocytosis (Figures 57, 58). Figure 59 pictures such a cell in the act of phagocytising two residual bodies. Figure 60 demonstrates a portion of a phagocytic cell which contained a residual body and several "dye-like" vacuoles.

b. Control:

The mesenchyme of 10-, 11-, and 12-day control embryos exhibited neither glycogen deposits, "dye-like" vacuoles, nor residual bodies. Phagocytic cells were observed only in 12-day control embryos, in the regions of the developing palatal shelves and mesonephros. In fact, phagocytic cells were never observed in the present study in any of the tissues from 10-, 11-, and 12-day control embryos, except for the two aforementioned areas of 12-day embryos.

Figure 61 depicts a mesenchymal cell which exhibited a morphology typical of mesenchyme of 11- and 12-day embryos. Occasionally, such cells which were in some phase of mitosis exhibited an organelle similar to sub-components of the rough endoplasmic reticulum. This organelle, called "paired cisternae", appeared to be formed of components of rough endoplasmic reticulum (Figure 62).

B. Extra-embryonic membranes:

1. Visceral yolk sac:

a. Experimental:

Because of its ability to phagocytize large quantities of Trypan blue, the visceral yolk sac was studied for additional information on dye ultrastructure. Twelve hours after maternal injection of Trypan blue, the 9-day visceral yolk sac was heavily laden with dye (Figure 63).

Very electron-dense vacuoles were seen to contain a dense, homogeneous material similar to that comprising the contents of the "dye-like" vacuoles previously described in embryonic tissues. Small, fuzzy vesicles or caveolae were detected among the bases of contiguous microvilli; these vesicles appeared to coalesce into larger supra-nuclear vacuoles. These supra-nuclear vacuoles displayed contents which varied in electron density (Figure 64). Such a phenomenon probably represented the variation among vacuoles in concentration of Trypan blue, for stained and unstained 1 μ thick sections displayed the same variation among vacuoles in the intensity of the blue-colored contents (Figures 65, 66). These 1 μ thick sections showed no correlation between size of vacuole and intensity of blue coloration.

The 10-day experimental visceral yolk sacs displayed numerous, electron-dense, supra-nuclear vacuoles (Figure 67) which were larger in diameter than those noted in comparable 9-day tissues.

The vacuolar population of 11-day visceral yolk sacs (Figure 68) was more heterogeneous than that of 10-day visceral yolk sacs. Only an occasional vacuole of high electron-density and homogeneous content was observed. Most vacuoles contained either a floccular or granular material of moderate electron density. A new kind of vacuole was apparent, one which contained clumps of spicular material. Still other vacuoles exhibited tiny globules of electron-dense material, a material which has formerly been described as the only evidence of dye in this kind of tissue (St. Krzyzowska-Gruca et al. 1967, Beck et al. 1967).

The 12-day visceral yolk sacs displayed even more heterogeneous populations of vacuoles. Few of the electron-dense, homogeneous vacuoles were seen. The vacuole containing a spicular substance was

observed more frequently (Figure 69) than in cells of 11-day experimental yolk sacs.

Figure 70 demonstrates a collection of dead cells in the 10-day yolk sac cavity. These cells contained large vacuoles filled with a material of high electron-density similar to that of the dye vacuoles in the 9- or 10-day visceral yolk sacs. These degenerating cells may have been derived from the yolk sac endoderm.

A layer of mesothelial cells in 11- and 12-day experimental embryos separated the visceral yolk sac from the extra-embryonic coelom. These mesothelial cells exhibited clusters of "dye-like" vacuoles (Figures 71, 72).

b. Control:

The very electron-dense, homogeneous vacuoles exhibited in 9-day experimental yolk sacs were not observed in 9-day control yolk sacs. However, the normal phagocytic activities of the control tissue was demonstrated by the presence of numerous caveolae (Figure 73). These coalesced to form apical vesicles or larger supra-nuclear vacuoles. The supra-nuclear vacuoles contained a fine granular or floccular material of moderate electron density.

The 10-day control yolk sacs did not demonstrate the large, electron-dense, homogeneous vacuoles which characterized the 10-day experimental yolk sacs. The control yolk sacs did exhibit fuzzy caveolae and large supra-nuclear vacuoles filled with a granular material of moderate electron density (Figure 74).

The spicular vacuoles and the few electron-dense, homogeneous vacuoles which characterized the 11-day experimental yolk sacs were not evident in the 11-day control yolk sacs. However, the control tissue

did exhibit a vacuolar population more heterogeneous than that of 10-day control yolk sacs. The supra-nuclear vacuoles displayed moderately electron-dense contents both granular and floccular (Figure 75).

The 12-day control yolk sacs did not demonstrate either the electron-dense, homogeneous vacuoles or the spicular vacuoles which were observed in 12-day experimental yolk sacs. The control tissues did exhibit supra-nuclear vacuoles composed of minute membranous components (Figure 76).

Tortuous, foot-like processes characterized the basal ends of the visceral yolk sac cells of 10- through 12-day embryos (Figure 77). A serosal basement membrane supported the simple layer of visceral yolk sac cells. This serosal basement membrane, composed of vascular endothelium and loose mesenchyme, was seen to separate the visceral yolk sac epithelium from the mesothelium lining the extra-embryonic coelom. No "dye-like" vacuoles were observed in these 10- through 12-day mesothelial layers of control embryos.

2. Trophoblast:

a. Experimental:

The junctional zone trophoblast of 10-day experimental embryos exhibited numerous vacuoles, some of which resembled "dye-like" vacuoles (Figure 78). These "dye-like" vacuoles coincided in morphology and location to vacuoles with dark blue centers which were observed in 1 μ thick sections stained with Richardson's stain (Figure 79). Comparable sections of control trophoblast did not demonstrate any "dye-like" vacuoles (Figure 80).

The 10-day chorionic trophoblast cells exist between the extra-embryonic coelom and the ectoplacental cavity (Figure 2). This chorionic

trophoblast joins with the allantois and the ectoplacental cone to form the chorio-allantoic placenta. The 10-day experimental chorionic trophoblast cells contained clusters of "dye-like" vacuoles (Figure 81). The visceral yolk sac adjacent to the chorionic trophoblast also contained "dye-like" vacuoles (Figure 82). One μ thick sections of 10-day experimental chorionic trophoblast stained with Richardson's stain showed numerous vacuoles with dark blue centers and clear peripheral areas (Figure 83) which corresponded in morphology and intra-cellular position to the "dye-like" vacuoles seen ultrastructurally. "Dye-like" vacuoles can also be seen in Figure 83 in the distal yolk sac. One μ thick sections of 10-day control chorionic trophoblast stained with Richardson's stain showed clear vacuoles (Figure 84).

b. Control:

The "dye-like" vacuoles observed in the junctional zone trophoblast of 10-day experimental embryos were not apparent in comparable control tissues. The control trophoblast did contain numerous, very large vacuoles containing membranous profiles and smaller vacuoles (Figure 85).

The 10-day control chorionic trophoblast cells did not demonstrate any "dye-like" vacuoles (Figure 86). Other ultrastructural characteristics of these cells were identical to those of the comparable experimental tissues. The visceral yolk sac adjacent to the chorionic trophoblast did not contain "dye-like" vacuoles.

3. Amnion:

a. Experimental:

The 10-day amnion from experimental embryos was an attenuated membrane composed both of a layer of mesoderm lining the extra-embryonic coelom and of a layer of ectoderm lining the amniotic cavity

(Figure 87). The experimental amnions contained clusters of "dye-like" vacuoles (Figures 88, 89). One μ thick sections of light microscope sections, 10-day experimental amnions stained with Richardson's stain, demonstrated numerous "dye-like" vacuoles (Figure 90); such vacuoles were not evident in comparable control sections (Figure 91).

Phagocytic cells were detected in 10-day experimental amnions (Figures 92, 93). These phagocytic cells contained glycogen, "dye-like" vacuoles, and residual bodies.

b. Control:

The 10-day control amnions demonstrated neither "dye-like" vacuoles nor phagocytic cells, both of which characterized comparable experimental amnions (Figure 94). All other ultrastructural features were identical to those of the 10-day experimental amnions.

C. Maternal proximal convoluted tubules:

a. Experimental:

Because Trypan blue was seen to accumulate within the proximal convoluted tubules of the adult rat kidney, this tissue was examined in order to add to the ultrastructural characterization of the dye. Electron micrographs of these tubules demonstrated the presence of very large, electron-dense, homogeneous vacuoles (Figure 95). The contents of these vacuoles appeared similar to the contents both of dye-containing vacuoles of 9- and 10-day experimental yolk sacs and of "dye-like" vacuoles of 10-, 11-, and 12-day experimental embryos and extra-embryonic membranes. These vacuoles, located in the basilar portions of the tubule cells, displayed sizes comparable to those of cell nuclei. Unstained 1 μ thick sections of the tubules showed large, blue structures in the basilar portions of the tubule cells (Figure 96) which coincided in size and

intra-cellular position to vacuoles seen ultrastructurally. Unstained 1 μ thick sections of control tubules demonstrated refractile bodies within their basilar cytoplasm (Figure 97). These uncolored refractile bodies were neither as large nor as prevalent as the large, blue structures noted in experimental tubule cells.

b. Control:

Proximal convoluted tubule cells from control maternal rats did not exhibit the large, electron-dense, homogeneous vacuoles observed in comparable experimental tissues. The control cells contained vacuoles of the cytosome type (Figure 98). These cytosome-like vacuoles, located in the basilar portions of the tubule cells, displayed heterogeneous contents.

DISCUSSION

Two considerations must preface discussion of the results of the present study. (1) All light and electron microscope observations of embryonic tissues taken from maternal rats injected with Trypan blue were performed on tissues obtained from embryos which appeared normal to the naked eye. (2) Embryos of control and experimental litters aged 16- and 20-days of gestation were grossly examined in order to establish those rates and types of malformations which would be expected to develop if gestation in the embryos studied with microscopy had been allowed to proceed to such fetal stages. The results of these gross examinations appear in Tables 6 and 7 of the Appendix.

Fixation:

The electron microscope has been employed in the examination of tissues obtained from a large number of animal species, but only a small minority of such studies have utilized mammalian species, and only a small fraction of the latter studies have investigated embryonic stages of gestation. The most prevalent reason for this paucity of reports on the ultrastructure of mammalian embryos seems to be that of inadequate fixation. The mouse, rat, and rabbit blastocysts have been described by Izquierdo et al. (1962), Reinius (1967), Schlafke et al. (1963, 1967), and Anderson et al. (1970). The mouse neural tube, palate and pancreas has been studied by Herman et al. (1966), Smiley et al. (1966), Farbman (1968), Wessels et al. (1968), and Sweney et al. (1970). Rabbit neural tube has been described by Tennyson (1970). The rat gut and heart have been characterized by Hayward et al. (1964), Hayward (1967), Dunn (1967), Cornell et al. (1969), and Henningsen et al. (1970).

The reports of Dossel (1966) and Tennyson (1970) have included

extensive investigations of the effects produced by alteration of fixative components. Because the fixatives ordinarily employed for electron microscopy failed to provide adequate fixation for the tissues studied in the current investigation, an extensive series of experiments were performed in the search for an acceptable fixative; these experiments were patterned after the methodology of Maunsbach (1966b). Tables 1, 2, 3, and 4 of the Appendix summarize the compositions of these fixatives.

The fixative finally chosen proved to be superior to those which have been utilized in other studies of embryonic ultrastructure, but some undesirable effects were noted. Membranes of cells within tissues of the experimental group were often absent or difficult to identify, implying some membrane alterations by Trypan blue. These membranes displayed an improved preservation subsequent to exposure to sodium hydrosulfite, a compound utilized to cleave the Trypan blue molecule. The gut and neural tube tissues frequently demonstrated wide spacing among cells of their epithelial component. Although other ultrastructural studies have indicated that such spacing was characteristic of early rat embryo neural tissue (del Cerro et al. 1968, Sumi 1969), much of the spacing was interpreted as artifact.

The fixative employed in the present study did prevent the appearance of myelin figures within embryonic neurons. In chick embryos, such figures have been interpreted by Candiollo and Filogamo (1966) as "the morphological expression of a resettlement process of lipo-protein materials" which would be extruded from the cell during states of high metabolic activity. However, because these myelin figures were apparent within neurons in the present study only after utilization of the trial fixatives composed entirely of glutaraldehyde, these figures were inter-

preted as artifact.

Fibrin deposits:

An axial periodicity of 230 Å, which has been postulated by Hall (1949) to be characteristic of the fibrin polymer, has been confirmed by other investigations (Still et al. 1957, Majno et al. 1961, White 1964, 1965, Kay et al. 1967, Cuddigan et al. 1968, Karges et al. 1970). Because such a periodicity was consistent with that described in the polymer of the present study, this material can be identified as fibrin.

Although this periodicity was that of fibrin of adult rats (Majno et al. 1961) and of other species (Still et al. 1957, Kay et al. 1967), the cross-sectional morphology of this embryonic fibrin (Figures 3, 4) was unique. The adult fibrin polymer is a solid fiber in transverse section; the embryonic fibrin displayed an outer, fibrous sheath surrounding a central area composed of fine granules. Such an embryonic fibrin morphology may represent either a configuration characteristic of the prenatal rat or an arrangement in which some unknown substance served as a nucleus around which fibrin formed. In future studies, it would be important to search for the presence of fibrin in rat embryos older than those examined in the present study.

At least two possibilities exist which could explain the presence of fibrin in each of the 10-day, and older, embryos of the experimental group. (1) Trypan blue could have produced an increase in the amount of fibrinogen precursors, from whatever source. Dye treatment does increase the beta-globulin levels of both maternal and fetal sera (Beaudoin 1963), and fibrinogen does possess the solubility characteristics of a globulin (West et al. 1966). Although dye-bound serum proteins are not teratogenic (Beaudoin et al. 1965), those azo dyes most

potent as teratogens cause the greatest alterations in the individual components of serum proteins (Beaudoin 1969). Furthermore, the protein contents of the blastocyst cavity, the extra-embryonic coelom, the amniotic cavity, and the gut lumen of fetal rabbits, plus those of the sera of fetal rats mimic the maternal sera protein fraction changes resulting from dye treatment (Brambell et al. 1953, Hommes 1958, Beaudoin et al. 1961, Beaudoin et al. 1963). Finally, that dye treatment can produce a shift in metabolism to a more adult state is one of the effects on cardiac tissue suggested by Smith (1963). (2) Trypan blue could have caused the polymerization of fibrinogen precursors, for the polymerization of fibrin has been produced by substances other than thrombin. Stewart et al. (1969) and Horn et al. (1969) have produced the formation of fibers exhibiting the same axial periodicity as that of fibrin by the utilization of a non-enzymatic substance, protamine sulfate. Protamine sulfate is a basic protein component of nucleoproteins, and, like Trypan blue, is a colloidal material of low molecular weight (West et al. 1966).

The presence of fibrin aggregations in every experimental embryo, but in only one control embryo, coincides with other reports of fibrin formation produced by the dye. Scott (1963) has found that an injection of Trypan blue prior to that of a bacterial endotoxin greatly increased the number of thrombi found in the lung, kidney, and visceral organs of the non-pregnant rabbit. Even more relevant to the present study, he has detected some thrombi after dye treatment alone. These thrombi contained material displaying the histochemical properties of fibrin; vascular intimae contained a "fibrinoid" material. In a later ultrastructural study (Scott 1964), the fibrin of thrombi displayed the

characteristic 230 Å axial periodicity, but the intimal "fibrinoid" did not.

Fibrin has been implicated in rabbit embryo pathology by Brambell et al. (1947). A high embryonic mortality among several populations of wild rabbits was correlated with dense accumulations of fibrin in the yolk sac cavity. Their study of domesticated rabbits indicated that fibrinogen was a normal protein component of the yolk sac fluid. When the yolk sac contents from embryos of the domesticated rabbits were artificially polymerized by additions of thrombin, no histochemical differences were found between the resultant fibrin and that in the yolk sac contents from embryos of wild rabbits. It was suggested that possibly a dietary influence had caused fibrin formation.

The present results added to the concept outlined above (Brambell et al. 1947) of the correlation between fibrin deposition and embryonic mortality, by suggesting that fibrin deposition can lead to malformation. The two areas of heaviest fibrin deposition, those of the neural plate and hindgut, were those tissue sites displaying the highest incidences of malformations in older embryos (Appendix, Table 6). For example, defects of the neural tube, such as exencephaly, hydrocephalus, and meningocoele, accounted for 28% of the malformations observed in the 16-day fetuses, and 34% of the malformations in the 20-day fetuses. The vertebral axis, which bears a close spatial relationship to the neural plate, showed anomalies comprising 19% of the malformations noted in the 16-day fetuses, and 24% of the malformations in the 20-day fetuses. Abnormalities of the hindgut area, such as taillessness, tail atrophy, and imperforate anus, accounted for 14% of the anomalies observed in the 16-day fetuses, and 18% of the anomalies in the 20-day

fetuses. As to the mechanism by which fibrin deposition could have effected malformations, other studies have noted that Trypan blue treatment reduced rates of cell proliferation (Hamburgh 1954, Fox et al. 1957, Turbow 1966), and such diminutions in growth rate, whether or not caused by the presence of fibrin, could conceivably have produced such anomalies as torsion of the body axis, spina bifida, and taillessness. To extend the rationale even further, the present evidence suggested that the in situ presence of Trypan blue caused deposition of fibrin, for the area of most concentrated fibrin deposition, that of the hindgut, was the area displaying the most intense blue coloration in embryonic whole mounts.

Although concentrated deposits of fibrin were observed in the neural plates of 10-day embryos, no fibrin was detected in the neural tubes of 11- or 12-day embryos. It is possible that fibrin was present in the neural tubes of the latter stages, but was not detected because only midbrain tissues were sampled.

Glycogen:

Four methods for the identification and characterization of glycogen were employed in the experimental basis for this dissertation: 1) the ultrastructural morphology and staining characteristics of glycogen particles were described and compared with the results of other studies. 2) The ultrastructural localizations of glycogen were compared with those of 1 μ thick epoxy resin sections which had been treated with the periodic acid-Schiff reagent (Lane et al. 1965). The PAS reaction is designed to identify tissue sites where 1,2-glycol endings are localized, such as those located on the sugars comprising the glycogen molecule (Lillie 1965). 3) The enzyme alpha-amylase was employed

for the *in situ* digestion of glycogen; this enzyme cleaves any 1,4 linkages existing among the glucose subunits of glycogen (Lillie 1965). 4) The incubation of tissues in a solution of bovine pancreatic ribonuclease was utilized to digest cytoplasmic riboproteins (Lillie 1965), which were numerous in these embryonic tissues. This process does not digest glycogen, and hence aids in the differentiation between riboproteins and glycogen. In a comprehensive review of methods for glycogen identification, Revel (1964) has endorsed the following scheme for the accurate identification of glycogen deposits seen with the electron microscope: glycogen extraction and its qualitative analysis, then ultrastructural examination of the pelleted extract. In the present study, however, such a sequence of procedures was not performed because of the small size of the embryos utilized.

Luft (1956) has attempted to develop a potassium permanganate fixative which would specifically identify ultrastructural deposits of glycogen. The application of potassium permanganate fixative to the rat embryo tissues utilized in the present study resulted in complete tissue destruction. Although Watson (1958b) has demonstrated that lead stains enhance glycogen contrast, Revel (1964) has emphasized their non-specificity by showing that ribosomes stained with equal intensity. Biava (1963) has found than an aqueous solution of uranyl acetate failed to stain glycogen. Similar results have been produced by Vye *et al.* (1970); they have reported that an *en bloc* treatment with aqueous uranyl acetate did not stain clumps of white fibrous material suspected of being glycogen. The latter description coincides with that of the present study, in which certain tissues of dye-treated embryos were stained only with uranyl acetate (Figures 53, 54, 57, 58).

At the ultrastructural level of magnification, the tissues of experimental embryos contained pools of intra- and extracellular glycogen composed of particles measuring 20 to 30 mμ in diameter. In the specific instance of 11- and 12-day hindgut, larger "rosettes" of glycogen measuring 40 to 200 mμ in diameter were prevalent. Both dimensions coincide with those of glycogen within adult rat liver (Drochmans 1960, 1962).

As expected, all control and experimental embryonic tissues demonstrated some degree of positive periodic acid-Schiff (PAS) response. However, the tissues obtained from the experimental group showed extensive areas of highly positive reaction, especially those tissues from the 11- and 12-day hindgut and the 12-day heart. The localizations of these PAS-positive areas coincided with ultrastructural sites of glycogen. Although alpha-amylase digestion of these 1 μ thick epoxy resin sections is a desirable control procedure, it was not feasible in the present study; after the epoxy resin was removed, the unsupported tissues disintegrated in the enzyme solution.

Attempts to employ alpha-amylase for the digestion of glycogen in tissue sections fixed with osmium tetroxide have yielded equivocal results: Steiner et al. (1961) reported success, Karrer (1960) reported failure. Watson (1958a) has demonstrated that although alpha-amylase abolished the staining of liver glycogen by phosphomolybdic acid, the heat-inactivated enzyme produced the same effect. These discrepancies emphasize that fixation in osmium tetroxide prior to alpha-amylase digestion is a technique which sometimes produces unreliable results. Biava (1963) has overcome this problem by using an en bloc alpha-amylase digestion subsequent to fixation in formalin. An adap-

tation of this procedure was employed in the present study, with good results: few 20 to 30 mμ particles or 40 to 200 mμ particles remained after such treatment. Although minor protease activity has been reported to exist in repeatedly crystallized bacterial alpha-amylase (Fisher et al. 1960), such activity was observed only up to dilutions of 1:3000 (Lillie 1965), and was therefore probably abolished at the 1:100,000 dilution employed in the present study.

Although ribonuclease (RNA-ase) has been commonly used in light microscopy studies to discriminate between cytoplasmic riboproteins and glycogen, the results of its application in the present study must be interpreted with caution, for two reasons. First, ribonuclease has not often been employed in ultrastructural studies for such a purpose. Second, a slight glycogenolytic activity has been reported in solutions of RNA-ase at dilutions of 1:5000 (Lillie 1965). Such an activity was probably abolished in the 1:100,000 dilution utilized in the present study. The RNA-ase digestion of the hindgut tissue blocks from the experimental group resulted in the loss of all 10-17 mμ ribosomal elements, and in the retention of the beta and alpha glycogen particles.

The dense accumulations of glycogen in 11- and 12-day hindgut and 12-day myocardium of experimental embryos is significant in the light of other studies of embryonic glycogen. The "glycogen body" of the embryonic chick is a structure which has displayed a heavy concentration of glycogen (Revel et al. 1960). Although glycogen has been detected in human embryonic myocardium and chick embryonic liver (Leak et al. 1964, Karrer 1960), it did not appear as precociously, or in such high concentrations, as it did in the present study. Ultrastructural studies of intestinal epithelium from fetal rats ranging in

age from 13 days to term have not identified glycogen (Hayward et al. 1964, Hayward 1967, Dunn 1967). In addition the alpha or rosette form of glycogen, noted in the hindgut tissues of the experimental embryos of the present study, was quite unique, because only the smaller, beta glycogen particle has been detected in mammalian, avian, and amphibian embryos (Karrer 1960, Leak et al. 1964, Perry 1967, Ruggeri 1969). Furthermore, the alpha form of glycogen has been described only in the liver parenchyma of the adult rat and adult mouse (Luft 1956, Drochmans 1960, Revel 1964). The present results also indicated a close proximity between "dye-like" vacuoles and glycogen in the early neural plate, in mesenchyme, and in hindgut, but no such proximity in myocardial cells. This is of interest in light of Ruggeri's (1969) observation that a close proximity existed between glycogen and yolk inclusions of the chick blastoderm cell; he has inferred that yolk stimulates the formation of glycogen. Ruggeri's observations are made even more pertinent in noting that Trypan blue often has been treated by embryonic cells in a fashion similar to their treatment of yolk (Sander et al. 1967, Ramamurty 1968, Telfer et al. 1968, Anderson et al. 1970). Although the significance of the alpha and beta forms of glycogen in 11- and 12-day hindgut is not known, one can speculate that the presence of glycogen may signal the presence of Trypan blue in embryonic cells.

The accumulations of the beta form of glycogen in myocardial tissues of the experimental embryos were seen in quantities sufficient to suggest significant metabolic alterations. The light microscope study of Smith (1963) has noted the increased PAS-positive response of cardiac tissues from similarly treated embryos, as well as noting a diminution in the cardiac jelly and a thinning of the myocardium. He has suggested that

Trypan blue produced a "precocious transition to the biochemical characteristics of adult tissue with a consequent decrease in the amount of cardiac jelly formed." In light of the fact that the atrio-ventricular cushions may depend upon the presence of cardiac jelly for proper development (Smith 1963), and because normal formation of the septum primum, membranous interventricular septum, and conus do depend upon normal growth of these cushions (Fox et al. 1958, Smith 1963), an inadequacy of cardiac jelly could conceivably have resulted in the cardiac abnormalities observed in embryos from Trypan blue-treated rats (Fox et al. 1956, 1957, 1958). Other evidence of disturbances of carbohydrate metabolism in cardiac tissue following dye treatment has been offered by Cox (1970), who has reported a reduced glucose utilization in rat embryo hearts cultured in a Trypan blue-containing medium.

Disturbances in glycogen metabolism have frequently been noted in tumor cells, which often have displayed glycogen in the alpha form (Karasaki et al. 1969, Rudolph et al. 1969). Furthermore, at least eight, and possibly ten, glycogen storage diseases have been described in man, each disease displaying a separate, inborn error in the enzymes necessary for normal carbohydrate metabolism (Baudhuin et al. 1964, Hug et al. 1966, Cardiff 1966, Hug et al. 1967, Bruni et al. 1970, Garancis et al. 1970). These diseases were partially characterized by massive accumulations of glycogen in striated muscle, and often further characterized by a decreased myofibrillar development; phenomena also noted in the 12-day myocardium of the experimental embryos of the present study (Figures 21, 22).

The significance of glycogen accumulations in extra-cellular loci is unknown, although such loci also have been identified in the glycogen

storage diseases of man (Garancis et al. 1970). The extra-cellular disposition could have resulted from a seepage of glycogen from disrupted cells, a suggestion supported by the fragile appearance of the membranes surrounding the cells of these experimental myocardial and hindgut tissues.

Trypan blue:

Light microscopy and whole mounts:

Numerous studies have demonstrated the lack of blue coloration in embryos from Trypan blue-treated maternal rats (Goldmann 1909, Gillman et al. 1948, Waddington et al. 1953, Hamburgh 1954, Wilson 1955). However, light microscope examinations have provided some evidence of intra-embryonic dye. A diffuse, blue staining of the mouse embryonic mass has been reported by Barber et al. (1964). Davis (1968) and Davis and Gunberg (1968) have described a blue staining of the definitive embryo, in rat embryos from 11 to 13 days of gestation; a blue "allantoic patch" was detected in the hindgut, and blue coloration was detected in the pericardium and branchial pouches. The present study confirmed Davis' observations, for blue coloration was detected at low magnifications (x20) in every experimental embryo hindgut. Because both the study of Davis et al. (1968) and the present study indicated coloration to exist in loci detectable only upon careful light microscope examination, the electron microscope was utilized in the search for further evidence of dye within the embryo.

Electron microscopy:

The few ultrastructural studies utilizing Trypan blue have described the difficulty in detection of this substance because of its non-specific morphology. Trump (1960, 1961), in studying some effects of the

dye on renal tissues of adult rats, has mentioned such a difficulty. An attempt (Takada 1963) to use Trypan blue as a marker for electrolyte passage through venous capillary walls has had little success because the dye could not be positively identified. St. Krzyzowska-Gruca et al. (1967), in examining dye-laden fetal rodent visceral yolk sacs, has described the dye as small globules of electron-dense material within larger vacuoles. Other studies of this organ have confirmed this description (Beck et al. 1967, Lloyd et al. 1968). Lastly, a study of the cat blood-brain barrier has reported the presence of sequestered dye in neural tissues, but it contained no micrographs (Koenig et al. 1969).

Maternal animal:

Because cells of proximal convoluted tubules have been shown to actively phagocytize Trypan blue (Trump 1960, 1961), maternal kidney tissue was sampled in order to study the dye's morphology. In epoxy resin sections 1 μ in thickness (Figure 96), large, blue bodies occupied the basilar regions of the tubule cells; these bodies corresponded in size and intra-cellular position to the large vacuoles, composed of an electron-dense, homogeneous material, seen in thin sections (Figure 95). These large vacuoles, being absent from control tissues (Figures 97, 98), probably were composed largely of Trypan blue. Kidney studies by Trump (1960, 1961) have noted that, with increasing time, apically situated vacuoles move into a basilar position, and concomitantly, that the characterization of their contents changed from dense to sparse aggregations of granular particles. In the present study, the fact that the Trypan blue injection dosages used were 2 to 20 times those of Trump's probably accounts for the heavier concentrations of dye in all vacuoles.

Thus, with the exception of vacuolar dye concentration, the present findings coincide with those of Trump.

Yolk sac placenta:

The large quantities of dye phagocytized by the visceral yolk sac rendered this tissue suitable for the ultrastructural study of Trypan blue morphology. Unstained, 1 μ thick sections of 9-day experimental yolk sacs revealed the presence of blue vacuoles (Figure 66) which coincided in intra-cellular position to dark blue vacuoles in 1 μ sections stained with Richardson's stain (Figure 65). In both kinds of preparations, color intensity varied among vacuoles (Figures 65, 66), probably indicating that Trypan blue was being selectively concentrated. Electron micrographs of 9-day yolk sacs also indicated a variability of electron density among vacuoles (Figure 64). Many of the 9- and 10-day yolk sac cells contained electron-dense apical vacuoles, which may contain Trypan blue (Figures 63, 67); control tissues possessed vacuoles displaying contents of a floccular nature (Figures 73, 74). By the 11- to 12-day period, the contents of vacuoles in cells from experimental yolk sacs now assumed either a granular, floccular, or spicular appearance; few vacuoles of high electron density remained (Figures 68, 69). This change in vacuolar contents with increasing age has been noted in kidney tubule cells after Trypan blue treatment (Trump 1961).

Studies of experimental fetal rodent yolk sacs (Beck et al. 1967, St. Krzyzowska-Gruca et al. 1967, Lloyd et al. 1968) have not depicted any large, electron-dense vacuoles similar to those seen in the 9- and 10-day experimental tissues of the present study. The former group of reports have identified the dye solely as tiny electron-dense globules within larger vacuoles. Similar globules were also observed within

vacuoles in the yolk sacs of the present study (Figures 68, 69, 82) these could represent Trypan blue. However, other large vacuoles (Figures 63, 67) probably also contained the dye because they exhibited homogeneous, electron-dense contents similar to those within the "tiny globules."

Extra-embryonic membranes:

An unusual vacuole was first noticed during examinations of the ultrastructural morphology of extra-embryonic membranes from experimental embryos. Each of these "dye-like", membrane-bound vacuoles possessed an electron-dense homogeneous center and a clear periphery (Figures 71,72). These vacuoles were observed in cells of every extra-embryonic membrane from experimental embryos older than 9 days, with the exception of the definitive visceral yolk sac. Cells of the junctional zone trophoblast and the chorionic trophoblast, each destined to contribute to the definitive chorio-allantoic placenta, contained numerous vacuoles of this nature (Figures 78, 81, 82). Further distribution of this vacuole was observed in cells of the 10-day distal yolk sac, the amnion, and the yolk sac mesothelium (Figures 71, 72, 83, 87, 88, 89). Although its size approached the limit of resolution, the vacuole was observed in the light microscope in 1 μ thick sections of the extra-embryonic membranes (Figures 79, 83, 90). The possibility that the vacuoles contained Trypan blue is supported both by light microscope evidence (Goldmann 1909, Wislocki 1920, Latta et al. 1922) and by a study which utilized dye labelled with C^{14} (Wilson et al. 1963). These four studies have demonstrated that small amounts of dye enter extra-embryonic tissues. This conclusion is further strengthened by the absence of similar vacuoles in micrographs both of the present control tissues and

of other studies of normal rodent extra-embryonic membranes (Wislocki et al. 1961, Jollie 1964, Enders 1965, Connell 1967, Carlson et al. 1969).

Embryo:

The "dye-like" vacuole first noted in studying extra-embryonic membranes was observed in cells of every 10-, 11-, and 12-day embryo, but rarely in those of 9-day experimental embryos. This period of latency subsequent to experimental injection may have been necessary for penetration and sequestration of the dye. Dense accumulations of these vacuoles occurred, at light and electron microscope levels of magnification, in 10-day visceral endoderm (Figures 28, 29, 30, 31). By the 11- to 12-day period, visceral endoderm has developed into the primitive gut tube. Because "dye-like" vacuoles were detected in the visceral endoderm and hindgut (Figures 28, 36, 47), and because another study has shown that the hindgut contained blue coloration in the "allantoic patch" region (Davis et al. 1968), dye access to the embryo may have occurred by this route. Such "dye-like" vacuoles coincided with blue deposits which have been described by other workers in the light microscopy of cells from similarly treated embryos (Wislocki 1921, Barber et al. 1964, Davis 1968, Davis et al. 1968). One must not, however, exclude the possibilities of additional pathways of entry for dye into extra-embryonic membranes. One such route may start with the desquamation of dead, dye-laden cells from the yolk sac (Figure 70) or chorion, as has been suggested by Davis et al. (1968). Such cell masses could slough into the extra-embryonic coelom and release the dye which could then be taken up by the embryo and its membranes.

Although numerous "dye-like" vacuoles were observed by light and

electron microscopy in 10-day neural plate cells (Figures 8, 9, 10) they were observed with decreasing frequency in 11- and 12-day neurectoderm (Figures 13, 15). Twelve-day myocardial cells never displayed these inclusions (Figures 21, 22, 23). Because both neural tissue and myocardium were incipient sites of malformation (Appendix, Table 6, Fox et al. 1955, 1956, 1957, 1958), yet the "dye-like" vacuoles were absent from myocardium and were diminished in number in neurectoderm as age increased, some incongruity exists. Two possible explanations serve to reconcile these conflictions. First, those cells which can sequester the dye may have been protected from its effects, or, stated conversely, the unsequestered form of Trypan blue may have been the only form capable of compromising normal cell functions. Thus, the inability to "wall off" the dye may have been related to the advanced degree of tissue maturity. Such an argument is reinforced by noting the numerous "dye-like" vacuoles in mesenchyme (Figures 54, 55, 60), an undifferentiated tissue which compromises a large portion of the cells of 10-, 11-, and 12-day embryos. Second, some tissues or tissue stages may have possessed a system, similar to the azo reductase system (Fouts et al. 1957), capable of cleaving the disazo bond and thus rendering the dye colorless. Although this could account for the equivocal evidence of blue coloration at malformation sites in a light microscope study of similarly treated embryonic tissues (Davis et al. 1968), teratogenic action must have occurred prior to dye cleavage, because the components of the cleaved dye molecule have been shown to be non-teratogenic (Beaudoin et al. 1960).

Dye identification:

The above considerations are based upon the probability that the

"dye-like" vacuolar contents were, indeed, Trypan blue. The following circumstantial evidence supports such a contention. 1) "Dye-like" vacuoles were never present in control tissues, yet were observed in the tissues of every experimental embryo older than 9 days. 2) The vacuolar contents resembled lipid, yet no evidence exists that Trypan blue disturbs embryonic or fetal lipid metabolism. 3) The vacuolar contents were similar in appearance to dye deposits in the maternal kidney (Figure 95) and in the yolk sac placenta (Figures 63, 67). 4) The high incidence of "dye-like" vacuoles in visceral endoderm coincided in location with the "allantoic patch" of blue coloration noted in 11- and 12-day hindgut. 5) "Dye-like" vacuoles were identified in every tissue containing blue granules revealed by light microscopy, and were absent from myocardium, which contained no such granules. 6) Following sodium hydrosulfite treatment, the vacuolar contents were altered in appearance (Figure 48). However, chromatin material was also modified by this procedure, so this piece of evidence was equivocal.

Further ultrastructural studies of embryonic tissues from dye-treated rats are indicated, if only to search for "dye-like" vacuoles in other tissues which have shown high rates of malformation, such as the eye and the 10- and 11-day myocardium. In these studies, it is suggested that attempts be made to label the dye molecule to facilitate ultrastructural identification. A heavy metal linkage to a halogen addition to the dye molecule might provide such an electron-dense marker for both free and sequestered dye. It is imperative, however, to establish the teratogenic properties of this altered form of Trypan blue, because isomers of this teratogen nearly always have been shown to lack teratogenic capabilities (Beaudoin et al. 1960).

Residual body formation:

Cell death in embryogenesis is a well-known phenomenon which has been studied both with the light microscope and with the electron microscope (Glücksmann 1951, Bellairs 1961, Saunders 1966, Angelici et al. 1968, DeAngelis et al. 1968, Sweney et al. 1970). Cell death as a necessary element in normal differentiation is exemplified in such processes as bone growth, limb bud formation, and regression of the mesonephros (Levi-Montalcini 1964, Saunders 1966). The intra-cellular presence of residual bodies sometimes indicates that a cell is approaching death (Ericsson et al. 1965, 1969a, 1969b, de Duve et al. 1966), although residual bodies may be a manifestation, rather than a cause, of cell death (de Duve et al. 1966, Saunders 1966). Residual bodies were detected in the present study in greater abundance within cells obtained from tissues of the experimental group than within cells of the control group. This relationship has been confirmed in a light microscope study of similarly treated tissues (Davis et al. 1968).

Trypan blue elicited a multiplicity of effects in the rat embryo, one of which was death and resorption (Appendix, Table 5, Ferm 1958, Beck et al. 1960, 1963a, 1964). Because embryonic death was presumably preceded by extensive cell death, the noted abundance of residual bodies within cells obtained from tissues of the experimental group may in some instances have been indicative of approaching embryo death. However, death could have been averted by reparative processes in at least some of those embryonic cells and tissue areas which displayed residual bodies, because such processes have been demonstrated to exist in mouse embryos by Hamburgh et al. 1967.

A reduction in embryo wet weight was an additional effect of dye

administration to the maternal animal (Appendix, Table 5), and it is reasonable to suggest that extensive embryo cell death could have contributed to this phenomenon. Other studies have also noted that both malformed and grossly normal embryos from dye-treated rats displayed a reduction in body weight and total protein content (Jensh et al. 1967, Berry 1970).

Could cell death have participated in the etiology of malformations? Such a proposal is not unreasonable, for the normal development of epithelial systems has been shown to rely on unknown influences of the underlying mesenchyme (McLoughlin 1961a, 1961b, Grobstein 1963), and the present results indicated that mesenchyme was markedly altered by Trypan blue, as shown by the cellular presence of residual bodies and "dye-like" vacuoles.

The role of the tissue macrophage is to attend sites of tissue death or of foreign-body invasion (Clark et al. 1928, 1930, Levi-Montalcini 1964, Saunders 1966), and Trypan blue was identified by cells as a foreign body, for phagocytic cells in the embryo and adult have been seen to engulf dye particles (Clark et al. 1918, Evans et al. 1920, Latta et al. 1929, Gillman et al. 1949, Barber et al. 1964, Davis et al. 1968). In the present study a phagocytic cell was described which bore similarities to the "dark cell" which has been seen in necrotic zones of amphibian larvae (Weber 1964, Fox 1970). Other ultrastructural studies of mouse and chick embryos have labelled such a cell as a "degenerative body" (Bellairs 1961, Smiley et al. 1966, Farbman 1968). However, the present observations indicated that the cell's function and distribution were consistent with those characteristics of a phagocyte. Recall that the phagocytes of all experimental tissue

samples possessed a fairly constant ultrastructural appearance; variability in morphology, on the other hand, is characteristic of cells undergoing degeneration. Furthermore, all membranes and organelles of the observed phagocytic cells were intact. The present description of the shape of this cell as either stellate or rounded is not inconsistent with the variability in morphology which has been shown to occur in mature histiocytes (Ham 1965). Lastly, micrographs in the present study demonstrated various stages in the phagocytosis by this cell of residual bodies and "dye-like" vacuoles. A phagocyte often appeared to lie within the cytoplasm of a normal cell. Although other investigators have interpreted such a relationship as the ingestion of a "degenerative body" by a normal cell (Bellairs 1961, Farbman 1968), such an ultrastructural appearance could be explained by a consideration of the plane of sectioning.

Control:

Neural tissue:

As has been substantiated by the observations of numerous investigators (Duncan 1957, Langman et al. 1966, Stensaas et al. 1968, Angevine et al. 1970), neural tissue of the 10-, 11-, and 12-day control embryos was composed of a layer of pseudo-stratified columnar epithelium. Although a few cytoplasmic processes were present, axons were not observed; such a description identified this layer as the ventricular zone, as has been characterized by Angevine and co-workers (1970). These investigators have delimited three additional embryonic neural tissue zones, the subventricular, intermediate, and marginal zones, but none of these zones were developed at this early gestation period.

These undifferentiated neural cells displayed the following morphological features. 1) Twelve-day cells exhibited a few cilia. Cilia of prenatal neurons have been described by Duncan (1957), Brightman (1961), Brightman et al. (1963), and Bunge et al. (1965). 2) The numerous, irregular microvilli seen were typically those which have been described in early cell stages of chick and rabbit neural cells (Duncan 1957, Tennyson et al. 1962, Fujita et al. 1964). 3) Embryonic terminal bars were evident (Duncan 1957, Bellairs 1959, Trelstad et al. 1966), but the complex cell interdigitations of fetal and adult rat brain (Brightman et al. 1963, Hirano et al. 1967) were not evident. 4) An abundance of free cytoplasmic ribosomes was characteristic both of these cells and those of embryonic tissues in general (Fujita et al. 1964, Meller et al. 1966). 5) Organelle disruption was occasionally encountered, as indicated by the presence of residual bodies. Such a phenomenon is part of the normal developmental processes of the neural tube and of other embryonic tissues (Levi-Montalcini 1964, Saunders 1966, Kelley 1970).

Gut:

The primitive embryonic rat gut is formed from a single layer of visceral endodermal cells noted in the 10-day embryonic stage. By the 11- to 12-day period, this layer had developed into a tube of simple columnar epithelium composed of cells displaying an irregular micro-villous border. These micro-villous borders have been shown to possess regularity in fetal rat stages (Hayward et al. 1964, Hayward 1967, Cornell et al. 1969). Dunn (1967) has interpreted the debris seen in the gut lumen to be dead cells, an interpretation which was confirmed in the present study. No evidence was found either of pinocytosis or

of cell interdigitations of a complex nature, both of which have been shown to be prominent features of fetal rat gut cells (Dunn 1967, Cornell et al. 1969). Hayward (1967) has interpreted the close spatial relationship between elements of the rough endoplasmic reticulum and mitochondria seen within cells of fetal rat hindgut to have been due to the high energy requirements of the endoplasmic reticulum. This relationship was also exhibited in the 11- and 12-day rat hindgut cells of the present study.

Myocardium:

The ultrastructure of 12-day rat myocardium was identical to those descriptions of Cedergren et al. (1964), Forssmann et al. 1970), Henningsen et al. (1970), and Chacko (1970).

Mesenchyme:

Those mesenchyme cells which were in some stage of mitotic division exhibited an organelle similar to elements of the rough endoplasmic reticulum. This organelle, called "paired cisternae", has been identified in human tumor cells (Hanaoka et al. 1970) and in human embryonic mesenchyme (Kelley 1970), tissues which display considerable evidence of mitotic activity. Hanaoka et al. (1970) has considered these elements to be remnants of nuclear envelopes which, after completion of mitosis, would separate and reform the rough endoplasmic reticulum. However, Kelley (1970) has suggested that these paired cisternae served as material for the restoration of the nuclear envelope. Although branching of the paired cisternae was observed in the present study, it was not possible to determine whether the members of the cisternal pair were fusing or were separating.

The ultrastructural morphology of the mesenchymal cells in general

was nondescript.

Extra-embryonic membranes:

The ultrastructural characteristics of the yolk sac cells of late embryonic and fetal stages of the rat have been described by Wislocki et al. (1955), Schultz et al. (1966), Lambson (1966), Connell (1967), and Carpenter et al. (1969).

The ultrastructural characteristics of the trophoblast cells of the fetal rat have been characterized by Jollie (1964), Enders (1965), and Connell (1967).

SUMMARY

Selection of an adequate fixative for embryonic tissues of the rat followed an exhaustive survey of a large number of preservatives commonly employed in electron microscopy. The fixative of choice, composed of formaldehyde and glutaraldehyde in a phosphate buffer, proved to be significantly superior to other trial fixatives.

Heavy depositions of fibrin polymers in areas adjacent to 10-day neural plates and within lumina of 11- and 12-day hindguts were positively correlated with high malformation rate probabilities in brain, spinal cord, vertebral axis, and hindgut areas. This correlation suggested that fibrin deposition was participant in the malformations to be expected in these areas.

Accumulations of glycogen were significantly more dense in experimental than in control 12-day myocardium, a tissue which was highly susceptible to the malforming effects of Trypan blue. Alpha and beta glycogen was detected within experimental 11- and 12-day hindgut endoderm cells. Such alterations in glycogen metabolism may have served to signal the presence of intra-cellular Trypan blue.

Residual bodies occurred with greater frequency in mesenchyme of 10-, 11-, and 12-day experimental embryos than in mesenchyme of comparable control embryos. Other studies have indicated that a high content of residual bodies indicates approaching cell death. Such a phenomenon in mesenchyme could have compromised adjacent epithelia, resulting in malformation.

Blue deposits of dye were described by light microscopy within the hindgut of experiment embryos and within 1 μ sections of experimental embryonic and extra-embryonic tissues. Ultrastructural examinations

of experimental tissues demonstrated the presence of "dye-like" vacuoles, the contents of which bore a morphologic similarity to known deposits of dye within maternal rat proximal convoluted tubules and visceral yolk sac placentae. Such structures add to the possibility that the site of action of Trypan blue is within the embryo.

REFERENCES

Anderson, E., Condon, W., & Sharp, D. A study of oogenesis and early embryogenesis in the rabbit, Oryctolagus cuniculus, with special reference to the structural changes of mitochondria. J. Morph., 1970, 130, 67-92.

Anderson, L. M., & Telfer, W. H. Trypan blue inhibition of yolk deposition. A clue to follicle cell function in the Cecropia moth. J. Embryol. Exp. Morph., 1970, 23, 35-52.

Anderson, R. G. W. The formation and structure of the basal body (centriole) from the Rhesus monkey oviduct. Unpublished doctor's dissertation. University of Oregon Medical School, 1970.

Angelici, D., & Pourtois, M. The role of acid phosphatase in the fusion of the secondary palate. J. Embryol. Exp. Morph., 1968, 20, 15-23.

Angevine, J. B. Jr., Bodian, D., Coulombre, A. J., Edds, M. V. Jr., Hamburger, V., Jacobson, M., Lyser, K. M., Prestige, M. C., Sidman, R. L., Varon, S., & Weiss, P. A. Embryonic vertebrate central nervous system: revised terminology. Anat. Rec., 1970, 166, 257-262.

Barber, A. N., & Geer, J. C. Studies on the teratogenic properties of Trypan blue and its components in mice. J. Embryol. Exp. Morph., 1964, 12, 1-14.

Battle, H. I., & Laale, H. W. Trypan blue-induced anomalies in embryos of the zebrafish (Brachydanio rerio). Anat. Rec., 1960, 138, 333. (Abstract)

Baudhuin, P., Hers, H. G., & Loeb, H. An electron microscopic and biochemical study of type II glycogenosis. Lab. Invest., 1964, 13, 1139-1152.

Beaudoin, A. R. Serum proteins during normal rat pregnancy and rat pregnancies insulted with a teratogen. Anat. Rec., 1963, 145, 205. (Abstract)

Beaudoin, A. R. The teratogenicity of Congo red in rats. Proc. Soc. Exp. Biol. Med., 1964, 117, 176-179.

Beaudoin, A. R. Serum proteins and disazo dye teratogenesis. Teratology, 1969, 2, 85-90.

Beaudoin, A. R., & Ferm, V. H. The effect of disazo dyes on protein metabolism in the pregnant rabbit. J. Exp. Zool., 1961, 147, 219-226.

Beaudoin, A. R., & Kahkonen, D. The effect of Trypan blue on the serum proteins of the fetal rat. Anat. Rec., 1963, 147, 387-396.

Beaudoin, A. R., & Pickering, M. J. Teratogenic activity of several synthetic compounds structurally related to Trypan blue. Anat. Rec., 1960, 137, 297-305.

Beaudoin, A. R., & Roberts, J. Serum proteins and teratogenesis. Life Sci., 1965, 4, 1353-1358.

Beaudoin, A. R., & Roberts, J. M. Teratogenic action of the thyroid stimulating hormone and its interaction with Trypan blue. J. Embryol. Exp. Morph., 1966, 15, 281-289.

Beck, F. Comparison of the different teratogenic effects of three commercial samples of Trypan blue. J. Embryol. Exp. Morph., 1961, 9, 673-677.

Beck, F., & Lloyd, J. B. An investigation of the relationship between foetal death and foetal malformation. J. Anat., 1963a, 97, 555-564.

Beck, F., & Lloyd, J. B. The preparation and teratogenic properties of pure Trypan blue and its common contaminants. J. Embryol. Exp. Morph., 1963b, 11, 175-184.

Beck, F., & Lloyd, J. B. Dosage-response curves for the teratogenic activity of Trypan blue. Nature, 1964, 201, 1136-1137.

Beck, F., & Lloyd, J. B. The teratogenic effects of azo dyes. In D. H. M. Woollam (Ed.) Advances in teratology. Vol. 1. London: Logos Press, 1966. pp. 131-194.

Beck, F., Lloyd, J. B., & Griffiths, A. Lysosomal enzyme inhibition by Trypan blue: a theory of teratogenesis. Science, 1967, 157, 1180-1182.

Beck, F., Spencer, B., & Baxter, J. S. Effect of Trypan blue on rat embryos. Nature, 1960, 187, 605-607.

Bellairs, R. The development of the nervous system in chick embryos, studied by electron microscopy. J. Embryol. Exp. Morph., 1959, 7, 94-115.

Bellairs, R. Cell death in chick embryos as studied by electron microscopy. J. Anat., 1961, 95, 54-60.

Berry, C. L. The effect of Trypan blue on the growth of the rat embryo in vivo. J. Embryol. Exp. Morph., 1970, 23, 213-218.

Bertini, F., & Sacerdote, F. Malformations caused in mouse embryos by a red dye contained in commercial Trypan blue. Teratology, 1970, 3, 371-376.

Biava, C. Identification and structural forms of human particulate glycogen. Lab. Invest., 1963, 12, 1179-1197.

Brambell, F. W. R., Hemmings, W. A., Henderson, M., & Kekwick, R. A. Electrophoretic studies of serum proteins of foetal rabbits. Proc. Roy. Soc. London (Biol.), 1953, 141, 300-314.

Brambell, F. W. R., & Mills, I. H. Studies on sterility and prenatal mortality in wild rabbits. II. The occurrence of fibrin in the yolk sac contents of embryos during and immediately after implantation. J. Exp. Biol., 1947, 23, 332-345.

Brenner, R. M. Renewal of oviduct cilia during the menstrual cycle of the rhesus monkey. Fertil. Steril., 1969, 20, 599-611.

Brightman, M. W. The fine structure of ciliated ependyma. Anat. Rec., 1961, 139, 210-211. (Abstract)

Brightman, M. W., & Palay, S. L. The fine structure of ependyma in the brain of the rat. J. Cell Biol., 1963, 19, 415-440.

Bruni, C. B., & Paluello, F. M. A biochemical and ultrastructural study of liver, muscle, heart and kidney in type II glycogenosis. Virchow Arch. (Zellpath.), 1970, 4, 196-207.

Bunge, R. P., Bunge, M. B., & Peterson, E. R. An electron microscope study of cultured rat spinal cord. J. Cell Biol., 1965, 24, 163-192.

Candiollo, L., & Filogamo, G. Lamellar bodies within the neuroblasts of the neural tube in the chick embryo. Z. Zellforsch., 1966, 69, 480-488.

Cardiff, R. D. A histochemical and electron microscopic study of skeletal muscle in a case of Pompe's disease (Glycogenosis II). Pediatrics, 1966, 37, 249-259.

Carlson, E. C., & Ollerich, D. A. Intranuclear tubules in trophoblast III of rat and mouse chorioallantoic placenta. J. Ultrastruct. Res., 1969, 28, 150-160.

Carpent, G. Absence d'action tératogène du bleu trypan chez des Rattes gestantes lorsque l'implantation est retardée par une lactation simultanée. Ann. Endocr. (Paris), 1962, 23, 630-633.

Carpenter, S. J., & Ferm, V. H. Uptake and storage of Thorotrast by the rodent yolk sac placenta: an electron microscopic study. Amer. J. Anat., 1969, 125, 429-456.

Cedergren, B., & Harary, H. I. In vitro studies on single beating rat heart cells. VI. Electron microscopic studies of single cells. J. Ultrastruct. Res., 1964, 11, 428-442.

Chacko, K. Ultrastructure of developing myocardium of rat embryos and cytochemical localization of nucleoside phosphatase (ATPase) activity. Unpublished doctor's dissertation. University of Oregon Medical School, 1970.

Christie, G. A. The teratogenic activity of Trypan blue, and its effect upon the thyro-hypophyseal axis in the rat. J. Anat., 1964, 98, 377-384.

Clark, E. L., & Clark, E. R. On the reaction of certain cells in the tadpole's tail toward vital dyes. Anat. Rec., 1918, 15, 231-256.

Clark, E. R., & Clark, E. L. The relation between the monocytes of the blood and the tissue macrophages in living amphibian larvae. Anat. Rec., 1928, 38, 8. (Abstract)

Clark, E. R., & Clark, E. L. Relation of monocytes of the blood to tissue macrophages. Amer. J. Anat., 1930, 46, 149-186.

Connell, R. S. Ultrastructural and cytochemical studies of the extra-embryonic membranes of the rat. Unpublished doctor's dissertation, University of Oregon Medical School, 1967.

Cornell, R., & Padykula, H. A. A cytological study of intestinal absorption in the suckling rat. Amer. J. Anat., 1969, 125, 291-316.

Cox, S. J. Energy metabolism in isolated embryonic rat heart. Unpublished doctor's dissertation, University of Oregon Medical School, 1970.

Critchfield, C., & Daniel, J. C., Jr. Teratogenic effects of Trypan blue on Coturnix quail when injected into the mother. Growth, 1965, 29, 301-309.

Cuddigan, B. J., & Kay, D. The fine structure of platelet fibrin. Brit. J. Haemat., 1968, 15, 177-180.

Dalton, A. J. A chrome-osmium fixative for electron microscopy. Anat. Rec., 1955, 121, 281. (Abstract)

Davis, H. W. Studies on the teratogenic mechanism of action of Trypan blue. Unpublished doctor's dissertation, University of Oregon Medical School, 1968.

Davis, H. W., & Gunberg, D. L. Trypan blue in the rat embryo. Teratology, 1968, 1, 125-134.

DeAngelis, V., & Nalbandian, J. Ultrastructure of mouse and rat palatal processes prior to and during secondary palate formation. Arch. Oral Biol., 1968, 13, 601-608.

de Duve, C., & Wattiaux, R. Functions of lysosomes. Ann. Rev. Physiol., 1966, 28, 435-492.

del Cerro, M. P., Snider, R. S., & Oster, M. L. Evolution of the extracellular space in immature nervous tissue. Experientia, 1968, 24, 929-930.

Dijkstra, J., & Gillman, J. Chromatographic separation of biologically active components from commercial Trypan blue. Nature, 1961, 191, 803-804.

Dossel, W. E. On the fixation of embryonic Avian tissue for electron microscopy. Anat. Rec., 1966, 154, 499-500. (Abstract)

Drochmans, P. Mise en évidence du glycogène dans la cellule hépatique par microscopie électronique. J. Biophys. Biochem. Cytol., 1960, 8, 553-558.

Drochmans, P. Morphologie du glycogène. Etude au microscope électronique de colorations négatives du glycogène particulaire. J. Ultrastruct. Res., 1962, 6, 141-163.

Duncan, D. Electron microscope study of the embryonic neural tube and notochord. Texas Rep. Biol. Med., 1957, 15, 367-377.

Dunn, J. S. The fine structure of the absorptive epithelial cells of the developing small intestine of the rat. J. Anat., 1967, 101, 57-68.

Enders, A. C. A comparative study of the fine structure of the trophoblast in several hemochorial placentas. Amer. J. Anat., 1965, 116, 29-68.

Ericsson, J. L. E. Mechanism of cellular autophagy. In J. T. Dingle and H. B. Fell (Eds.) Lysosomes in biology and pathology. Vol. II. Amsterdam: North Holland Publishing Company, 1969a. pp. 345-394.

Ericsson, J. L. E. Studies on induced cellular autophagy. I. Electron microscopy of cells with in vivo labelled lysosomes. Exp. Cell Res., 1969b, 55, 95-106.

Ericsson, J. L. E., Trump, B. F., & Weibel, J. Electron microscopic studies of the proximal tubule of the rat kidney. II. Cytosegresomes and cytosomes: their relationship to each other and the lysosome concept. Lab. Invest., 1965, 14, 1341-1365.

Evans, H. M., & Scott, K. On the differential reaction to vital dyes exhibited by the two great groups of connective-tissue cells. Contributions to Embryology, Carnegie Institute of Washington, 1920, 10, 1-56.

Fahrenbach, H. W. Personal communication. 1969.

Farbman, A. I. Electron microscope study of palate fusion in mouse embryos. Develop. Biol., 1968, 18, 93-116.

Ferm, V. H. Permeability of the rabbit blastocyst to Trypan blue. Anat. Rec., 1956, 125, 745-760.

Ferm, V. H. Teratogenic effects of Trypan blue on hamster embryos. J. Embryol. Exp. Morph., 1958, 6, 284-287.

Ferm, V. H. Relative effect of teratogenic and non-teratogenic azo dyes on adrenal weight. Anat. Rec., 1959, 133, 379-380. (Abstract)

Fisher, E. H., & Stein, E. A. Alpha amylases. In P. Boyer (Ed.) The enzymes. Vol. 4. New York: Academic Press, 1960. pp. 313-343.

Forssmann, W. G., & Girardier, L. A study of the T system in rat heart. J. Cell Biol., 1970, 44, 1-19.

Fouts, J. R., Kamm, J. J., & Brodie, B. B. Enzymatic reduction of prontosil and other azo dyes. J. Pharmacol. Exp. Ther., 1957, 120, 291-300.

Fox, H. Tissue degeneration: an electron microscopic study of the pronephros of Rana temporaria. J. Embryol. Exp. Morph., 1970, 24, 139-157.

Fox, M. H., & Goss, C. M. Syndrome of cardiac aberrations associated with malformation of the primitive cardiac loop. Anat. Rec., 1955, 121, 294-295. (Abstract)

Fox, M. H., & Goss, C. M. Experimental production of a syndrome of congenital cardiovascular defects in rats. Anat. Rec., 1956, 124, 189-208.

Fox, M. H., & Goss, C. M. Experimentally produced malformations of the heart and great vessels in rat fetuses. Atrial and caval abnormalities. Anat. Rec., 1957, 129, 309-332.

Fox, M. H., & Goss, C. M. Experimentally produced malformations of the heart and great vessels in rat fetuses. Transposition complexes and aortic arch abnormalities. Amer. J. Anat., 1958, 102, 65-92.

Fraser, F. C., & Fainstat, T. D. Production of congenital defects in the offspring of pregnant mice treated with cortisone. Pediatrics, 1951, 8, 527-533.

Fujita, H., & Fujita, S. Electron microscopic studies on the differentiation of the ependymal cells and the glioblast in the spinal cord of domestic fowl. Z. Zellforsch., 1964, 64, 262-272.

Garancis, J. C., Panares, R. R., Good, T. A., & Kuzma, J. F. Type III glycogenosis. A biochemical and electron microscopic study. Lab. Invest., 1970, 22, 468-477.

Geber, W. F. Comparative teratogenicity of isoproterenol and Trypan blue in the fetal hamster. Proc. Soc. Exp. Biol. Med., 1969, 130, 1168-1170.

Gilbert, C., & Gillman, J. The morphogenesis of Trypan blue induced defects of the eye. S. Afr. J. Med. Sci., 1954, 19, 147-154.

Gillman, J., Gilbert, C., Gillman, T., & Spence, I. A preliminary report on hydrocephalus, spina bifida and other congenital anomalies in the rat produced by Trypan blue: the significance of these results in the interpretation of congenital malformations following maternal rubella. S. Afr. J. Med. Sci., 1948, 13, 47-90.

Gillman, J., Gilbert, C., Spence, I., & Gillman, T. A further report on congenital anomalies in the rat produced by Trypan blue. S. Afr. J. Med. Sci., 1951, 16, 125-135.

Gillman, J., Gillman, T., & Gilbert, C. Reticulosis and reticulum - cell tumours of the liver produced in rats by Trypan blue with reference to hepatic necrosis and fibrosis. S. Afr. J. Med. Sci., 1949, 14, 21-83.

Glücksmann, A. Cell deaths in normal vertebrate ontogeny. Biol. Rev., 1951, 26, 59-86.

Goldmann, E. E. Die äussere und innere Sekretion des gesunden Orangismus im lichte der vitalen Färbung. Beitr. Klin, Chir., 1909, 64, 192-265.

Goldstein, D. J. Trypan blue induced anomalies in the genito-urinary system of rats. S. Afr. J. Med. Sci., 1957, 22, 13-22.

Greenhouse, G. Trypan blue induced teratogenesis and enzymes in the mouse yolk sac. Anat. Rec., 1969, 163, 191. (Abstract)

Greenhouse, G., & Hamburgh, M. Analysis of Trypan blue induced teratogenesis in Rana pipiens embryos. Teratology, 1968, 1, 61-74.

Grobstein, C. Role of connective tissue in embryologic development. Second International Conference on Congenital Malformation, 1963, 224-232.

Gunberg, D. L. Spina bifida and herniation of hindbrain in the offspring of Trypan blue injected rats. Anat. Rec., 1954, 118, 387. (Abstract)

Gunberg, D. L. Spina bifida and the Arnold-Chiari malformation in the progeny of Trypan blue injected rats. Anat. Rec., 1956, 126, 343-368.

Gunberg, D. L. Some effects of exogenous hydrocortisone on pregnancy in the rat. Anat. Rec., 1957, 129, 133-154.

Gunberg, D. L. Variations in the teratogenic effects of Trypan blue administered to pregnant rats of different strain and substrain origin. Anat. Rec., 1958, 130, 310. (Abstract)

Gunberg, D. L. Further studies of the effects of Trypan blue on cultured rat embryos. Teratology, 1969, 2, 261. (Abstract)

Hall, C. E. Electron microscopy of fibrinogen and fibrin. J. Biol. Chem., 1949, 179, 857-864.

Ham, A. W. Histology. Philadelphia: J. B. Lippincott Company, 1965. (Page 231)

Hamburgh, M. Malformations in mouse embryos induced by Trypan blue. Nature, 1952, 169, 27.

Hamburgh, M. The embryology of Trypan blue induced abnormalities in mice. Anat. Rec., 1954, 119, 409-428.

Hamburgh, M., & Callahan, V. Differences in teratogenic response and in capacity to repair in embryos of two inbred strains of mice. Experientia, 1967, 23, 449-452. (Abstract)

Hamburgh, M., Nebel, L., & Greenhouse, G. Penetration and uptake of Trypan blue in the yolk sac placenta of the mouse. Amer. Zool., 1966, 6, 581-582. (Abstract)

Hanaoka, H., & Friedman, B. Paired cisternae in human tumor cells. J. Ultrastruct. Res., 1970, 32, 323-333.

Harm, H. Der Einfluss von Trypanblau auf die Nachkommenschaft trächtiger Kaninchen. Z. Naturforsch. (B), 1954, 9B, 536-540.

Hartwell, J. L., & Fieser, L. F. Coupling of o-tolidine and Chicago acid. Org. Syn., 1936, 16, 12-17.

Hayward, A. F. Changes in fine structure of developing intestinal epithelium associated with pinocytosis. J. Anat., 1967, 102, 57-70.

Hayward, A. F., & Dunn, J. S. Electron microscopy of developing jejunal epithelium in the rat. J. Anat., 1964, 98, 681. (Abstract)

Henningsen, B., & Schiebler, T. H. Zur Frühentwicklung der herzeigenen Strombahn. Elektronenmikroskopische Untersuchung an der Ratte. Zeit. Anat. Entwicklungsgesch., 1970, 130, 101-114.

Herman, L., & Kauffman, S. L. The fine structure of embryonic mouse neural tube with special reference to cytoplasmic microtubules. Develop. Biol., 1966, 13, 145-162.

Hirano, A., & Zimmerman, H. M. Some new cytological observations of the normal rat ependymal cell. Anat. Rec., 1967, 158, 293-302.

Hoar, R. M., & Salem, A. J. Time of teratogenic action of Trypan blue in Guinea pigs. Anat. Rec., 1961, 141, 173-182.

Hommes, O. R. Trypan blue in the rabbit. Acta. Morph. Neerl. Scand., 1958, 2, 28-37.

Horn, R. G., Hawiger, J., & Collins, R. D. Electron microscopy of fibrin-like precipitate formed during the paracoagulation reaction between soluble fibrin monomer complexes and protamine sulphate. Brit. J. Haemat., 1969, 17, 463-466.

Hug, G., Garancis, J. C., Schubert, W. K., & Kaplan, S. Glycogen storage disease, types II, III, VIII, IX. Amer. J. Dis. Child., 1966, 111, 457-474.

Hug, G., & Schubert, W. K. Lysosomes in type II glycogenosis. Changes during administration of extract from Aspergillus niger. J. Cell Biol., 1967, 35, C1-C6.

Izquierdo, L., & Vial, J. D. Electron microscope observations on the early development of the rat. Z. Zellforsch., 1962, 56, 157-179.

Jensh, R. P., & Brent, R. L. An analysis of the growth retarding effects of Trypan blue in the albino rats. Anat. Rec., 1967, 159, 453-458.

Jollie, W. P. Fine structural changes in placental labyrinth of the rat with increasing gestational age. J. Ultrastruct. Res., 1964, 10, 27-47.

Kaplan, S., & Johnson, E. M. Teratogenic effects of direct injection of aqueous and protein-bound Trypan Blue into the bloodstream of 3-day chick embryos. Teratology, 1970, 3, 269-272.

Karasaki, S., & Nigam, V. N. An electron microscope study of glycogen formation in Novikoff Ascites-Hepatoma cells. J. Nat. Cancer Inst., 1969, 43, 1197-1200.

Karges, H. E., & Kühn, K. The cross striation pattern of the fibrin fibril. Europ. J. Biochem., 1970, 14, 94-97.

Karnovsky, M. J. A formaldehyde-glutaraldehyde fixative of high osmolality for use in electron microscopy. J. Cell Biol., 1965, 27, 137A-138A. (Abstract)

Karrer, H. E. Electron-microscopic study of glycogen in chick embryo liver. J. Ultrastruct. Res., 1960, 4, 191-212.

Kay, D., & Cuddigan, B. J. The fine structure of fibrin. Brit. J. Haemat., 1967, 13, 341-347.

Kelley, R. O. An electron microscopic study of mesenchyme during development of interdigital spaces in man. Anat. Rec., 1970, 168, 43-54.

Koenig, H., & Nayyar, R. Localization and effects of Trypan blue in the nervous system. A light and electron microscope study. J. Cell Biol., 1969, 43, 71A. (Abstract)

Lambson, R. O. An electron microscopic visualization of transport across rat visceral yolk sac. Amer. J. Anat., 1966, 118, 21-52.

Lane, B. P., & Europa, D. L. Differential staining of ultrathin sections of epon-embedded tissues for light microscopy. J. Histochem. Cytochem., 1965, 13, 579-582.

Langman, J., Guerrant, R. L., & Freeman, B. G. Behavior of neuroepithelial cells during closure of the neural tube. J. Comp. Neurol., 1966, 127, 399-412.

Latta, J. S., & Busby, L. F. The reaction of the chick embryo and its membranes to Trypan blue. Amer. J. Anat., 1929, 44, 171-198.

Leak, L. V., & Burke, J. F. The ultrastructure of human embryonic myocardium. Anat. Rec., 1964, 149, 623-650.

Levi-Montalcini, R. Growth control of nerve cells by a protein factor and its antiserum. Science, 1964, 143, 105-110.

Lillie, R. D. Histopathologic technic and practical histochemistry. New York: McGraw-Hill Book Company, 1965.

Lloyd, J. B., & Beck, F. The identification of some acid disazo dyes by paper electrophoresis of their reduction products. Stain Techn., 1964, 39, 7-12.

Lloyd, J. B., & Beck, F. Teratogenesis. In J. T. Dingle and H. B. Fell (Eds.) Lysosomes in biology and pathology. Vol. 1. Amsterdam: North-Holland Publishing Company, 1969. (pages 433-449)

Lloyd, J. B., Beck, F., Griffiths, A., & Parry, L. M. The mechanism of action of acid bisazo dyes. In P. N. Campbell (Ed.) The interaction of drugs and subcellular components in animal cells. Boston: Little, Brown and Company, 1968. (pages 171-202)

Luft, J. H. Permanganate - a new fixative for electron microscopy. J. Biophys. Biochem. Cytol., 1956, 2, 799-802.

Majno, G., & Palade, G. E. Studies on inflammation. I. The effect of histamine and serotonin on vascular permeability: an electron microscopic study. J. Biophys. Biochem. Cytol., 1961, 11, 571-606.

Maunsbach, A. B. The influence of different fixatives and fixation methods on the ultrastructure of rat kidney proximal tubule cells. I. Comparison of different perfusion fixation methods and of glutaraldehyde, formaldehyde and osmium tetroxide fixatives. J. Ultrastruct. Res., 1966a, 15, 242-282.

Maunsbach, A. B. The influence of different fixatives and fixation methods on the ultrastructure of rat kidney proximal tubule cells. II. Effects of varying osmolality, ionic strength, buffer system and fixative concentration of glutaraldehyde solutions. J. Ultrastruct. Res., 1966b, 15, 283-309.

McLoughlin, C. B. The importance of mesenchymal factors in the differentiation of chick epidermis. I. The differentiation in culture of the isolated epidermis of the embryonic chick and its response to excess vitamin A. J. Embryol. Exp. Morph., 1961a, 9, 370-384.

McLoughlin, C. B. The importance of mesenchymal factors in the differentiation of chick epidermis. II. Modification of epidermal differentiation by contact with different types of mesenchyme. J. Embryol. Exp. Morph., 1961b, 9, 385-409.

Meller, K., Eschner, J., & Glees, P. The differentiation of endoplasmic reticulum in developing neurons of the chick spinal cord. Z. Zellforsch., 1966, 69, 189-197.

Millonig, G. Further observations on a phosphate buffer for osmium solutions in fixation. Proc. 5th Intern. Conf. Electron Micro., 1962, 2, P8. (Abstract)

Monie, I. W., Takacs, E., & Warkany, J. Transposition of the great vessels and other cardiovascular abnormalities in rat fetuses induced by Trypan blue. Anat. Rec., 1966, 156, 175-190.

Mulherkar, L. The effects of Trypan blue on chick embryos cultured in vitro. J. Embryol. Exp. Morph., 1960, 8, 1-5.

Murakami, U. Artificial induction of pesudoencephaly, short-tail, taillessness, myelencephalic blebs and some fissure formations (phenocopies) of the mouse. Nagoya J. Med. Sci., 1952, 15, 185-194.

Murphy, D. P. Heredity counseling. The obstetrician and congenital malformations in brothers and sisters. Eugen. Quart., 1956, 3, 161-164.

Myers, L. Experimentally induced anomalies of the internal ears of albino rat embryos. S. Afr. J. Sci., 1955, 51, 214-216.

Nebel, L., & Hamburgh, M. Observations on the penetration and uptake of Trypan blue in embryonic membranes of the mouse. Z. Zellforsch., 1966, 75, 129-137.

Padykula, H. A., & Richardson, D. A correlated histochemical and biochemical study of glycogen storage in the rat placenta. Amer. J. Anat., 1963, 112, 215-242.

Palade, G. E. A study of fixation for electron microscopy. J. Exp. Med., 1952, 95, 285-298.

Pease, D. C. Histological techniques for electron microscopy. New York: Academic Press, 1964. (pages 51-53)

Perry, M. M. Identification of glycogen in thin sections of amphibian embryos. J. Cell. Science, 1967, 2, 257-264.

Ramamurty, P. S. On the contribution of the follicle epithelium to the deposition of yolk in the oocyte of Panorpa communis (Mecoptera). Exp. Cell Res., 1968, 33, 601-605.

Reinius, S. Ultrastructure of blastocyst attachment in the mouse. Z. Zellforsch., 1967, 77, 257-266.

Revel, J. P. Electron microscopy of glycogen. J. Histochem. Cytochem., 1964, 12, 104-114.

Revel, J. P., Napolitano, L., & Fawcett, D. W. Identification of glycogen in electron micrographs of thin tissue sections. J. Biophys. Biochem. Cytol., 1960, 8, 575-590.

Reynolds, E. S. The use of lead citrate at high pH as an electron-opaque stain in electron microscopy. J. Cell Biol., 1963, 17, 208-212.

Richardson, K. C., Jarett, L., & Finke, E. H. Embedding in epoxy resins for ultrathin sectioning in electron microscopy. Stain Techn., 1960, 35, 313-324.

Rudolph, R., & Weiss, E. Intracytoplasmatische „Glykogenablagerungen, lamelläre Strukturen und virus-ähnliche Einschlüsse in Mastzellentumoren des Hundes. Eine elektronenmikroskopische Untersuchung. Z. Krebsforsch., 1969, 72, 343-349.

Ruggeri, A. Ricerche ultrastrutturali sulla distribuzione del glicogeno nelle cellule dell'embrione di pollo in rapporto alla presenza delle inclusioni vitelline. Z. Zellforsch., 1969, 101, 463-476.

Sander, K., & Vollmar, H. Vital staining of insect eggs of incorporation of Trypan blue. Nature, 1967, 216, 174-175.

Saunders, J. W., Jr. Death in embryonic systems. Science, 1966, 154, 604-612.

Schlafke, S., & Enders, A. C. Observations on the fine structure of the rat blastocyst. J. Anat., 1963, 97, 353-360.

Schlafke, S., & Enders, A. C. Cytological changes during cleavage and blastocyst formation in the rat. J. Anat., 1967, 102, 13-32.

Schnürer, L. B. Maternal and foetal responses to chronic stress in pregnancy. Acta Endocr. Suppl., 1963, 80, 1-96.

Schultz, P. W., Reger, J. F., Schultz, R. L. Effects of Triton WR-1339 on the rat yolk sac placenta. Amer. J. Anat., 1966, 119, 199-234.

Scott, G. B. D. The effects of Trypan blue on the formation of thrombi in the generalized Shwartzman reaction. Brit. J. Exp. Path., 1963, 44, 317-325.

Scott, G. B. D. Trypan blue and the generalized Shwartzman reaction. The nature and formation of fibrinoid material in the pulmonary arteries. Brit. J. Exp. Path., 1968, 49, 251-256.

Smiley, G. R., & Dixon, A. D. Fine structure of midline epithelium in the developing palate. J. Cell Biol., 1966, 31, 162A. (Abstract)

Smith, W. N. A. The site of action of Trypan blue in cardiac teratogenesis. Anat. Rec., 1963, 147, 507-524.

Smith, W. N. A. Influence of Trypan blue on resorption of rat embryos. Nature, 1963, 200, 699-700. (Abstract)

Snell, G. D., & Stevens, L. C. Early embryology. In E. L. Green (Ed.) Biology of the laboratory mouse. New York: McGraw-Hill Book Company, 1966. (pages 205-246)

St. Krzyzowska-Gruca, & Schiebler, T. H. Experimentelle Untersuchungen am Dottersackepithel der Ratte. Z. Zellforsch., 1967, 79, 157-171.

Stecher, P. G. (Ed.) The Merck index of chemicals and drugs. Rahway, N. J.: Merck and Company, Inc., 1960. (page 460)

Steiner, J. W., & Carruthers, J. S. Studies on the fine structure of the terminal branches of the biliary tree. I. The morphology of normal bile canaliculi, bile pre-ductules (Ducts of Hering) and bile ductules. Amer. J. Path., 1961, 38, 639-660.

Stensaas, L. F., & Stensaas, S. S. An electron microscope study of cells in the matrix and intermediate laminae of the cerebral hemisphere of the 45 mm rabbit embryo. Z. Zellforsch., 1968, 91, 341-365.

Stéphan, F., & Sutter, B. Action du bleu trypan sur la différenciation du mésoderme axial chez l'embryon de poulet. C. R. Soc. Biol. (Paris), 1960, 154, 1620-1622.

Stéphan, F., & Sutter, B. Réaction de l'embryon de poulet au bleu trypan. J. Embryol. Exp. Morph., 1961, 9, 410-421.

Stewart, G. J., & Niewiarowski, S. Nonenzymatic polymerization of fibrinogen by protamine sulfate. An electron microscopic study. Biochim. Biophys. Acta, 1969, 194, 462-469.

Still, W. J. S., & Boult, E. H. Electron microscopic appearance of fibrin in thin sections. Nature, 1957, 179, 868-869.

Sumi, S. M. The extracellular space in the developing rat brain: its variation with changes in osmolarity of the fixative, method of fixation and maturation. J. Ultrastruct. Res., 1969, 29, 398-425.

Sweney, L. R., & Shapiro, B. L. Histogenesis of Swiss white mouse secondary palate from nine and one-half days to fifteen and one-half days in utero. I. Epithelial-mesenchymal relationships - light and electron microscopy. J. Morph., 1970, 130, 435-450.

Takada, M. Electron microscopic observations on the passage of electrolyte solutions and Trypan blue fluid through the walls of venules and capillaries of the venous side. Nagoya Med. J., 1963, 9, 113-124.

Telfer, W. H., & Anderson, L. M. Functional transformations accompanying the initiation of a terminal growth phase in the Cecropia moth oocyte. Dev. Biol., 1968, 17, 512-535.

Tennyson, V. M. The fine structure of the axon and growth cone of the dorsal root neuroblast of the rabbit embryo. J. Cell Biol., 1970, 44, 62-79.

Tennyson, V. M., & Pappas, G. D. An electron microscope study of ependymal cells of the fetal, early postnatal and adult rabbit. Z. Zellforsch., 1962, 56, 595-618.

Trelstad, R. L., Revel, J. P., & Hay, E. D. Tight junctions between cells in the early chick embryo as visualized with the electron microscope. J. Cell Biol., 1966, 31, C6-C10.

Trump, B. F. Electron microscopic study of the uptake of Trypan blue by the cells of the rat nephron. Anat. Rec., 1960, 136, 293. (Abstract)

Trump, B. F. An electron microscope study of the uptake, transport and storage of colloidal materials by the cells of the vertebrate nephron. J. Ultrastruct. Res., 1961, 5, 291-310.

Trump, B. F., & Bulger, R. E. New ultrastructural characteristics of cells fixed in a glutaraldehyde-osmium tetroxide mixture. Lab. Invest., 1966, 15, 368-379.

Tuchmann-Duplessis, H., & Mercier-Parot, L. Influence du bleu trypan et de l'azobleu sur la développement de l'embryon du rat. C. R. Assn. Anat., 1955, 42, 1326-1330.

Tuchmann-Duplessis, H., & Mercier-Parot, L. A propos de malformations produites par le bleu trypan. Biol. Med. (Paris), 1959, 48, 238-251.

Turbow, M. M. Trypan blue induced teratogenesis of rat embryos cultivated in vitro. J. Embryol. Exp. Morph., 1966, 15, 387-395.

Vye, M. V., & Fischman, D. A. The morphological alteration of particulate glycogen by en bloc staining with uranyl acetate. J. Ultrastruct. Res., 1970, 33, 278-291.

Waddington, C. H., & Carter, T. C. A note on abnormalities induced in mouse embryos by Trypan blue. J. Embryol. Exp. Morph., 1953, 1, 167-180.

Warkany, J., Wilson, J. G., & Geiger, J. F. Myeloschisis and myelomeningocele produced experimentally in the rat. J. Comp. Neurol., 1958, 109, 35-64.

Watson, M. L. Staining of tissue sections for electron microscopy with heavy metals. J. Biophy. Biochem. Cytol., 1958a, 4, 475-478.

Watson, M. L. Staining of tissue sections for electron microscopy with heavy metals. II. Application of solutions containing lead and barium. J. Biophy. Biochem. Cytol., 1958b, 4, 727-730.

Weber, R. Ultrastructural changes in regressing tail muscles of Xenopus larvae at metamorphosis. J. Cell Biol., 1964, 22, 481-487.

Wechsler, W. Elektronenmikroskopischer Beitrag zur Differenzierung des Ependyms am Ruckenmark von Huhnerembryonen. Z. Zellforsch., 1966, 74, 423-442.

Wessels, N. K., & Evans, J. Ultrastructural studies of early morphogenesis and cytodifferentiation in the embryonic mammalian pancreas. Develop. Biol., 1968, 17, 413-446.

West, E. W., Todd, W. R., Mason, H. S., & Van Bruggen, J. T. Textbook of biochemistry. New York: The Macmillan Company, 1966. (pages 402 and 586)

White, J. G., Krivit, W., & Vernier, R. Ultrastructural investigation of the fibrin clot utilizing ferritin-labelled anti-human fibrinogen antibody. Blood, 1964, 24, 443-450.

White, J. G., Krivit, W., & Vernier, R. L. The platelet-fibrin relationship in human blood clots: an ultrastructural study utilizing ferritin-conjugated anti-human fibrinogen antibody. Blood, 1965, 25, 241-257.

Wilson, J. G. Influence of severe hemorrhagic anemia during pregnancy on development of the offspring in the rat. Proc. Soc. Exp. Biol. Med., 1953, 84, 66-69.

Wilson, J. G. Influence on the offspring of altered physiologic states during pregnancy in the rat. Ann. N. Y. Acad. Sci., 1954, 57, 517-525.

Wilson, J. G. Teratogenic activity of several azo dyes chemically related to Trypan blue. Anat. Rec., 1955, 123, 313-334.

Wilson, J. G., Beaudoin, A. R., & Free, J. H. Studies on the mechanism of teratogenic action of Trypan blue. Anat. Rec., 1959, 133, 115-128.

Wilson, J. G., Shepard, T. H., & Gennaro, J. F. Studies on the site of teratogenic action of C^{14}-labelled Trypan blue. Anat. Rec., 1963, 145, 300. (Abstract)

Wislocki, G. Experimental studies on fetal absorption. I. The vitally stained fetus. II. The behavior of the fetal membranes and placenta of the cat toward colloidal dyes injected into the maternal blood-stream. Contrib. to Embryol., Carnegie Inst. Wash., 1920, 11, 45-60.

Wislocki, G. B. Further experimental studies on fetal absorption. III. The behavior of the fetal membranes and placenta of the guinea-pig toward Trypan blue injected into the maternal blood-stream. IV. The behavior of the placenta and fetal membranes of the rabbit toward Trypan blue injected into the maternal blood-stream. Contr. to Embryol., Carnegie Inst. Wash., 1921, 13, 89-101.

Wislocki, G. B., & Dempsey, E. W. Electron microscopy of the placenta of the rat. Anat. Rec., 1955, 123, 33-64.

Wislocki, G. B., & Padykula, H. A. Histochemistry and electron microscopy of the placenta. In W. C. Young (Ed.) Sex and internal secretions. Baltimore: The Williams and Wilkins Co., 1961, Vol II. (pages 883-957)

Yamada, T., Whallon, J., Tomizawa, T., Shimoda, S., & Shichijo, K. Further studies on the mechanism of action of Trypan blue and related dyes in suppressing thyroid activity in the rat. Metabolism, 1965, 14, 281-290.

Zettergvist, H. The ultrastructural organization of the columnar absorbing cells of the mouse jejunum. Unpublished doctor's dissertation, Karolinska Institutet, Stockholm, 1956.

ABBREVIATIONS FOR FIGURES 3-98

a	- amniotic membrane	mf	- myofibril
ac	- amniotic cavity	ms	- mesothelial cell
al	- allantois	mv	- microvilli
bm	- basal laminae	mvb	- multivesicular body
c	- centriole	my	- mesenchyme
ce	- coelomic mesothelium	n	- nucleus
cf	- cytoplasmic fragments	ne	- nuclear envelope
ch	- chromatin	nl	- neural tube lumen
co	- chorionic trophoblast	no	- notochord
cp	- cytoplasmic process	np	- neural plate
ctc	- connective tissue cell	pc	- phagocytic cell
cts	- connective tissue space	pci	- paired cisternae
d	- debris or desmosome	r	- ribosomes
de	- distal endoderm	rb	- residual body
dv	- "dye-like" vacuole or dye vacuole	rer	- rough endoplasmic reticulum
ec	- extra-embryonic coelom	st	- spindle tubules
f	- fibrin	t	- trophoblast
frbc	- fetal red blood cell	ul	- uterine lumen
gl	- gut lumen	v	- vacuole or vesicle
gly	- glycogen	V	- vacuole
Go	- Golgi complex	va	- vascular endothelium
ic	- intra-embryonic coelom	ve	- visceral endoderm
id	- intercalated disc	vs	- vascular space
is	- intercellular space	ys	- yolk sac placenta
m	- mitochondria	ysc	- yolk sac cavity
me	- mesoderm	Z	- z band

Figure 1. Approximation of a 9-day rodent conceptus (Snell et al. 1966).

This illustration demonstrates the inverse relationship between visceral yolk sac (proximal endoderm) and embryonic ectoderm. The developing embryonic mass pushes into its own yolk sac, resulting in an inversion of the germ layers.

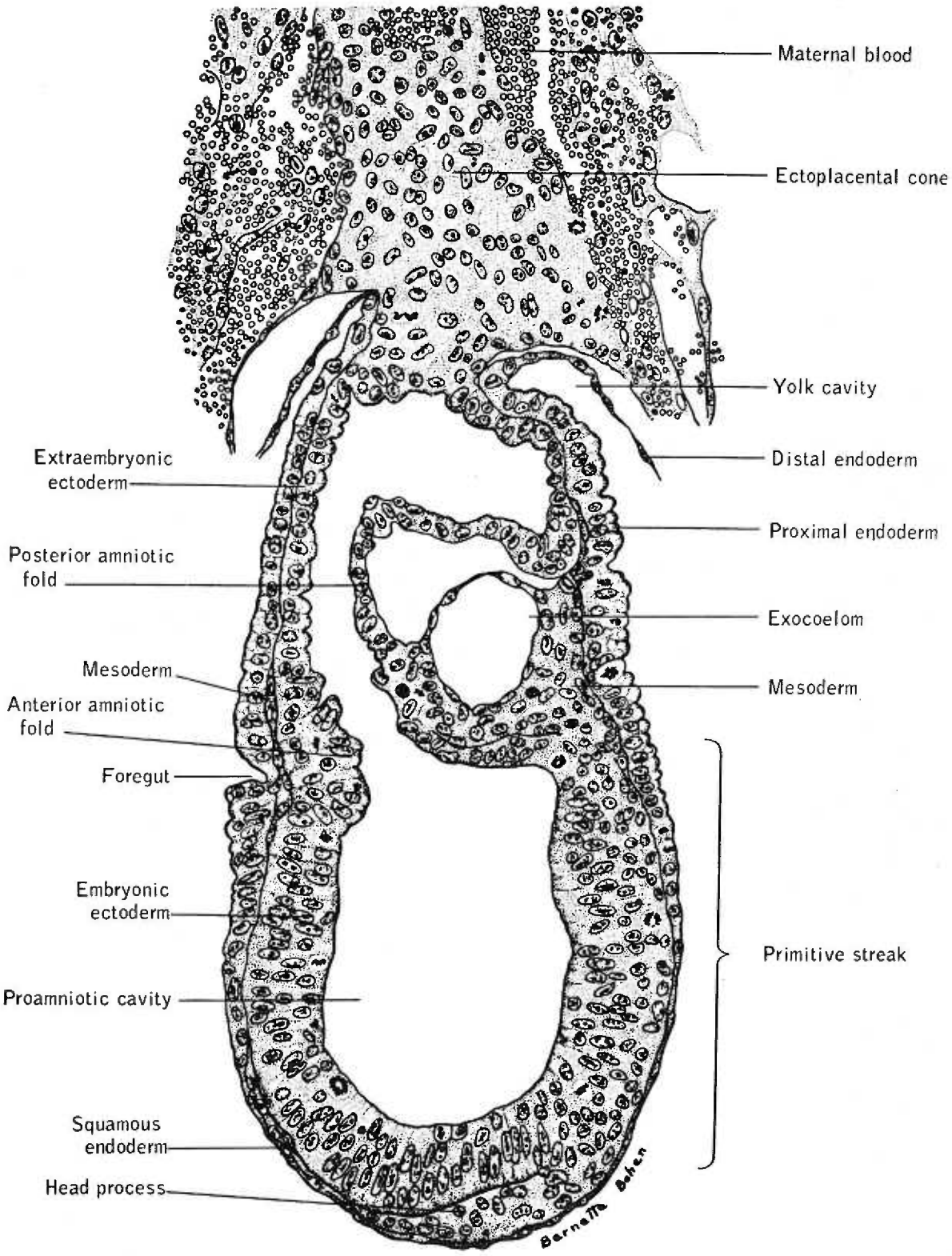
Maternal blood
Ectoplacental cone
Yolk cavity
Distal endoderm
Extraembryonic ectoderm
Proximal endoderm
Posterior amniotic fold
Exocoelom
Mesoderm
Mesoderm
Anterior amniotic fold
Foregut
Embryonic ectoderm
Primitive streak
Proamniotic cavity
Squamous endoderm
Head process

Figure 2. Approximation of a 10-day rodent embryo (Snell et al. 1966).

This illustration demonstrates the visceral yolk sac surrounding the developing embryo. Two major cavities, the extra-embryonic coelom and the amniotic cavity, are separated by the amnion. The amnion is formed of a layer of ectoderm lining the amniotic cavity, and a layer of mesoderm lining the extra-embryonic coelom. The chorion, adjacent to the ectoplacental cone, eventually participates in the formation of the definitive chorio-allantoic placenta. At this stage, ectoderm forms a flattened neural plate in this dorsi-flexed embryo.

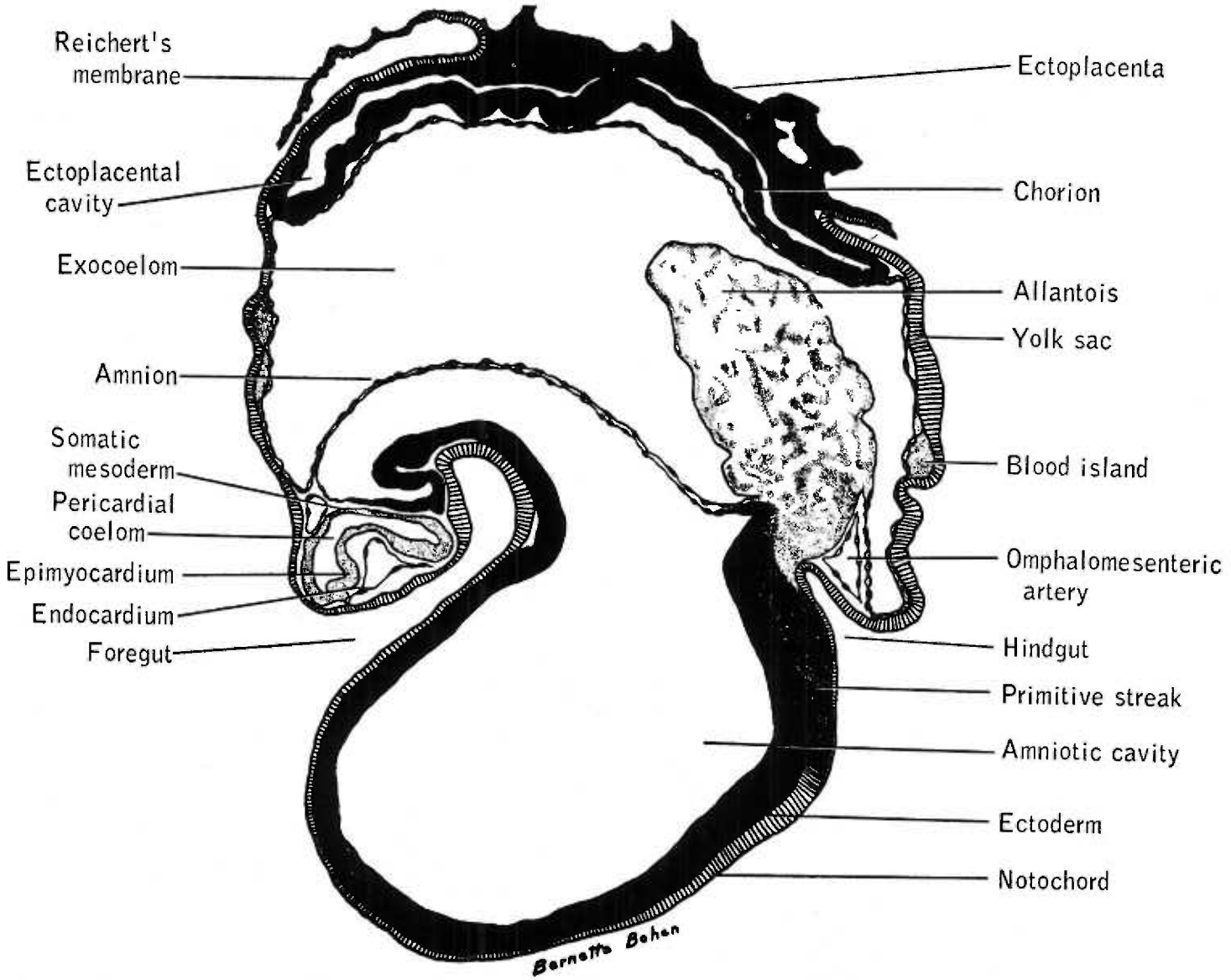
Reichert's membrane
Ectoplacenta
Ectoplacental cavity
Chorion
Exocoelom
Allantois
Yolk sac
Amnion
Somatic mesoderm
Blood island
Pericardial coelom
Omphalomesenteric artery
Epimyocardium
Endocardium
Hindgut
Foregut
Primitive streak
Amniotic cavity
Ectoderm
Notochord
Bernette Behen

Figure 3. Ten-day neural plate, experimental.

Fibrin polymers (f) occupy the amniotic cavity (ac). The neurectoderm cells below contain a few small deposits of glycogen (gly). Several "dye-like" vacuoles (dv) contain a homogeneous, electron-dense material which is surrounded by a clear peripheral area. Inter-cellular space (is).

x12,000

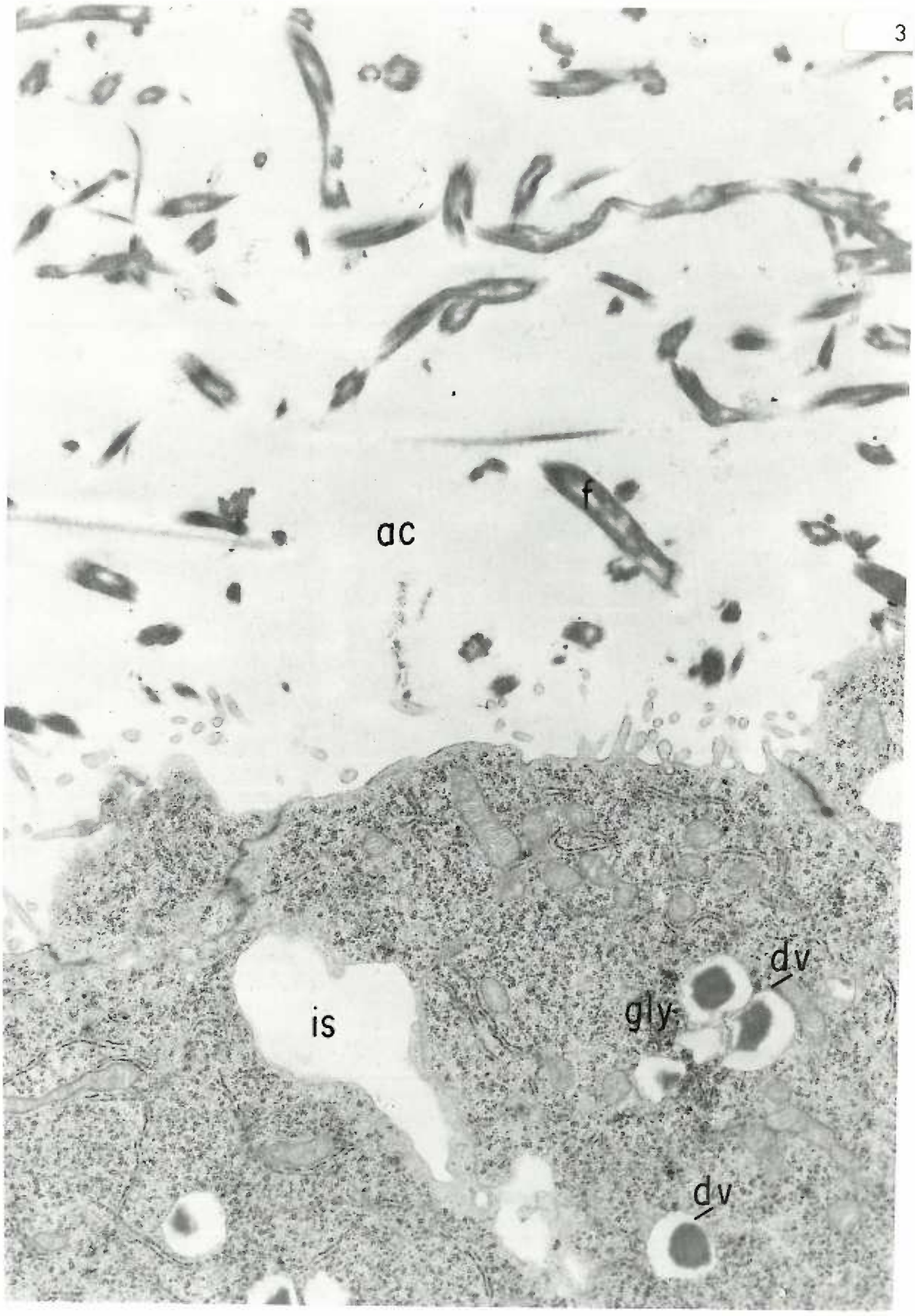
ac
f
is
gly
dv
dv

Figure 4. Ten-day neural plate, experimental.

Numerous fibrin polymers (f) occupy the amniotic cavity (ac). One polymer (arrow) exhibits the 230 Å axial periodicity characteristic of fibrin. Each polymer in cross section exhibits an electron-dense sheath of 400-600 mμ which encloses a central lumen of 150 mμ. Glycogen (gly) and "dye-like" vacuoles (dv) are prominent in the neurectoderm cells. Multivesicular body (mv).

x20,000

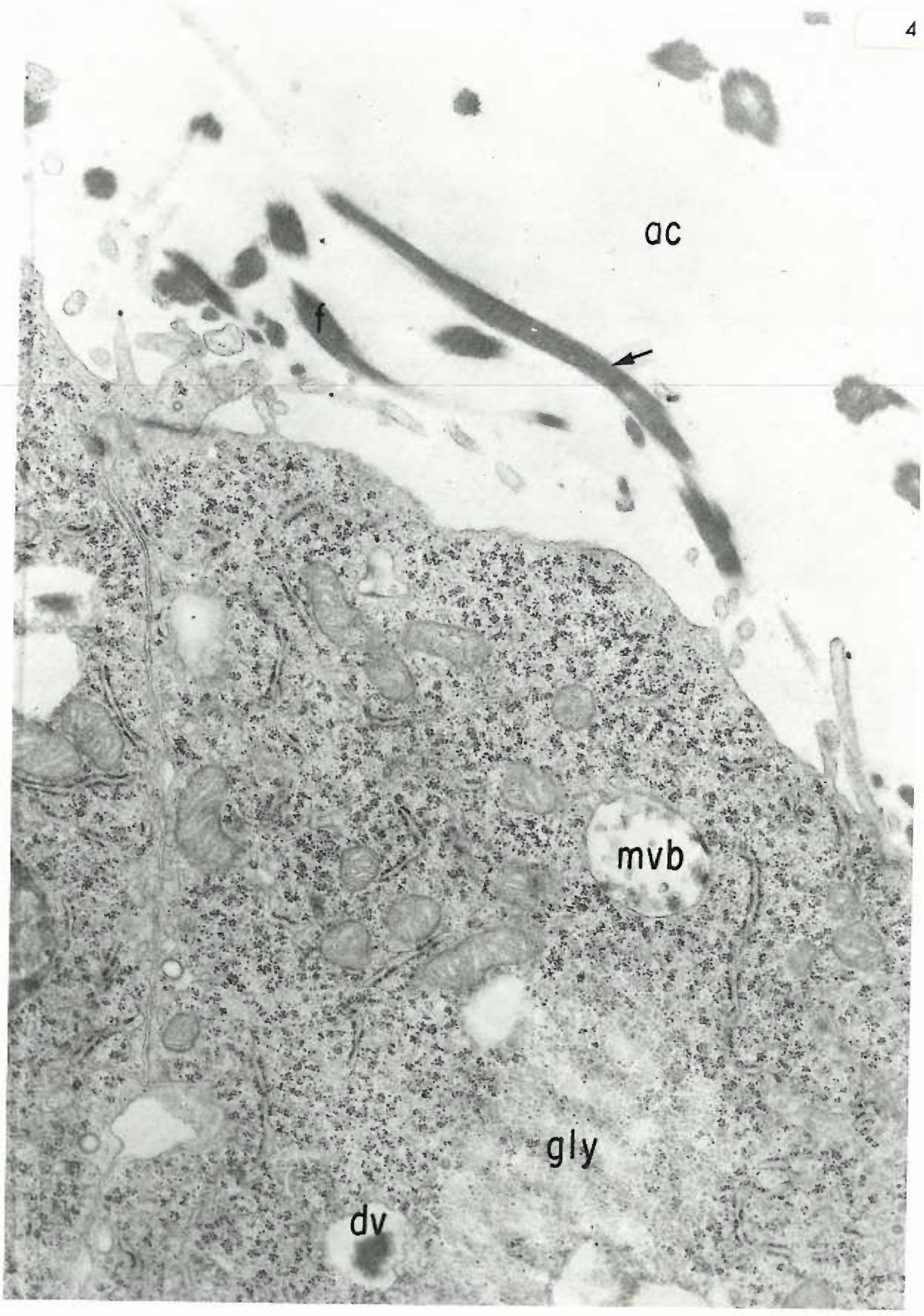
ac
f
mvb
gly
dv

Figure 5. Ten-day neural plate, experimental.

A tangential section of neural plate ectoderm shows a portion of the amniotic cavity (ac) into which microvilli project. Another portion of the amniotic cavity contains strands of a fibrous material (f) similar to fibrin polymers. Small clumps of glycogen (gly) are scattered throughout the cytoplasm. Several "dye-like" vacuoles (dv) are in evidence; one lies near a large, heterogeneous residual body (rb).

x20,000

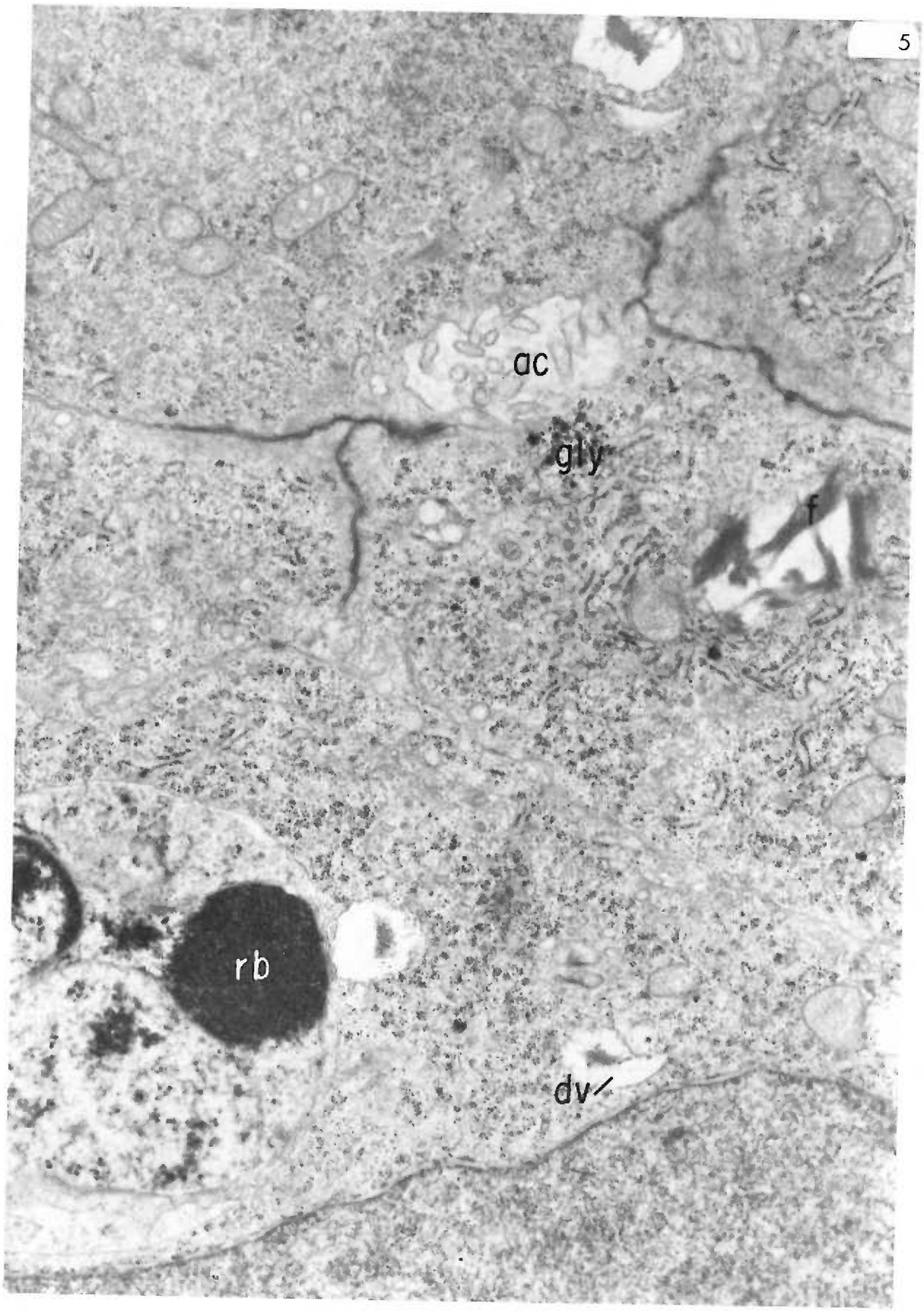
ac
gly
f
rb
dv

Figure 6. Ten-day neural plate, experimental.

Small microvilli project from this neurectoderm cell into the amniotic cavity (ac). A 1 μ "dye-like" vacuole (dv) is surrounded by clusters of glycogen particles (gly).

x54,000

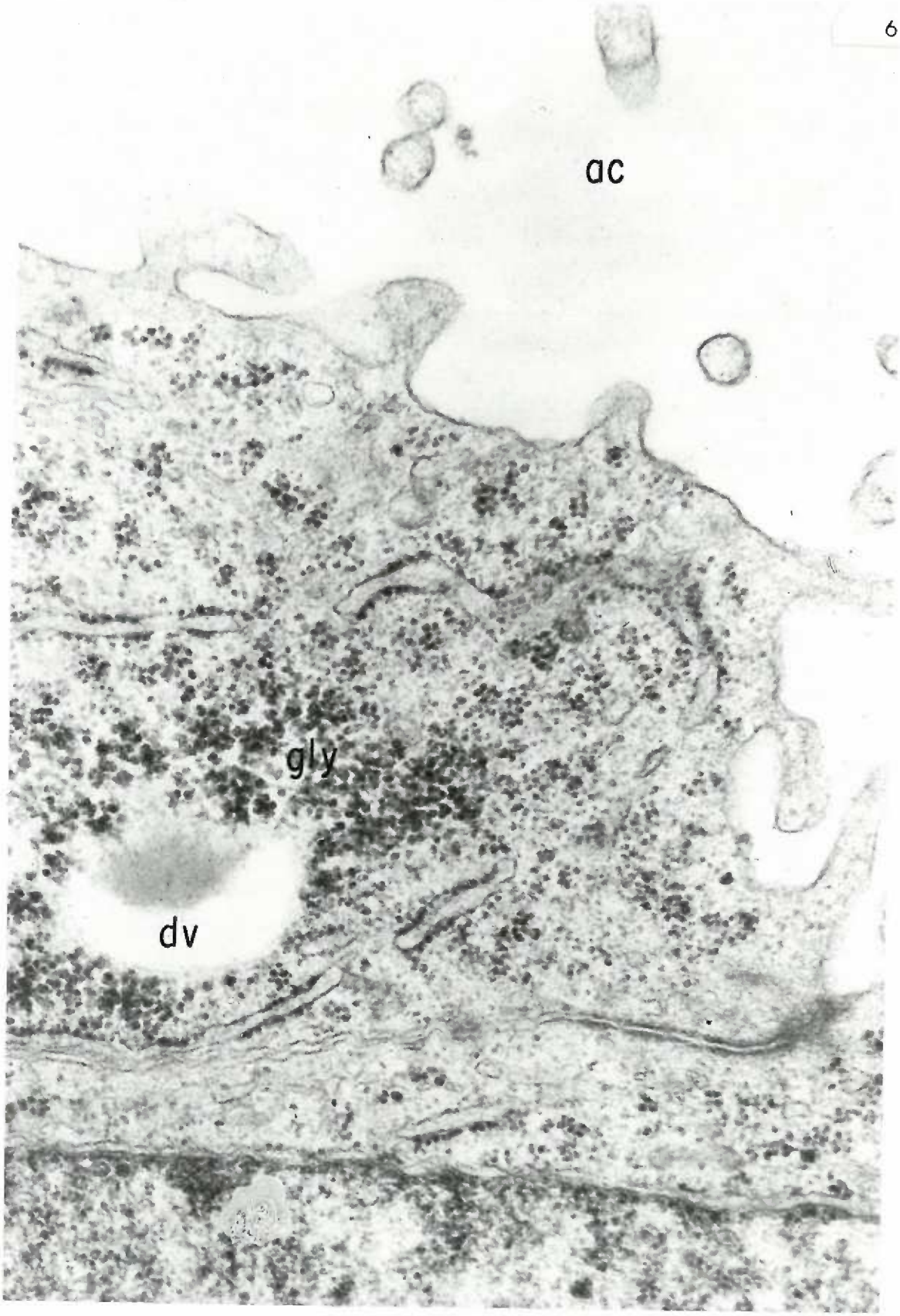
ac
gly
dv

Figure 7. Ten-day neural plate, experimental.
Several of the "dye-like" vacuoles seen in this micrograph are adjacent to small accumulations of glycogen (gly). The residual body (rb) adjacent to a "dye-like" vacuole contains some glycogen particles (arrow). Multivesicular body (mvb); amniotic cavity (ac).

x20,000

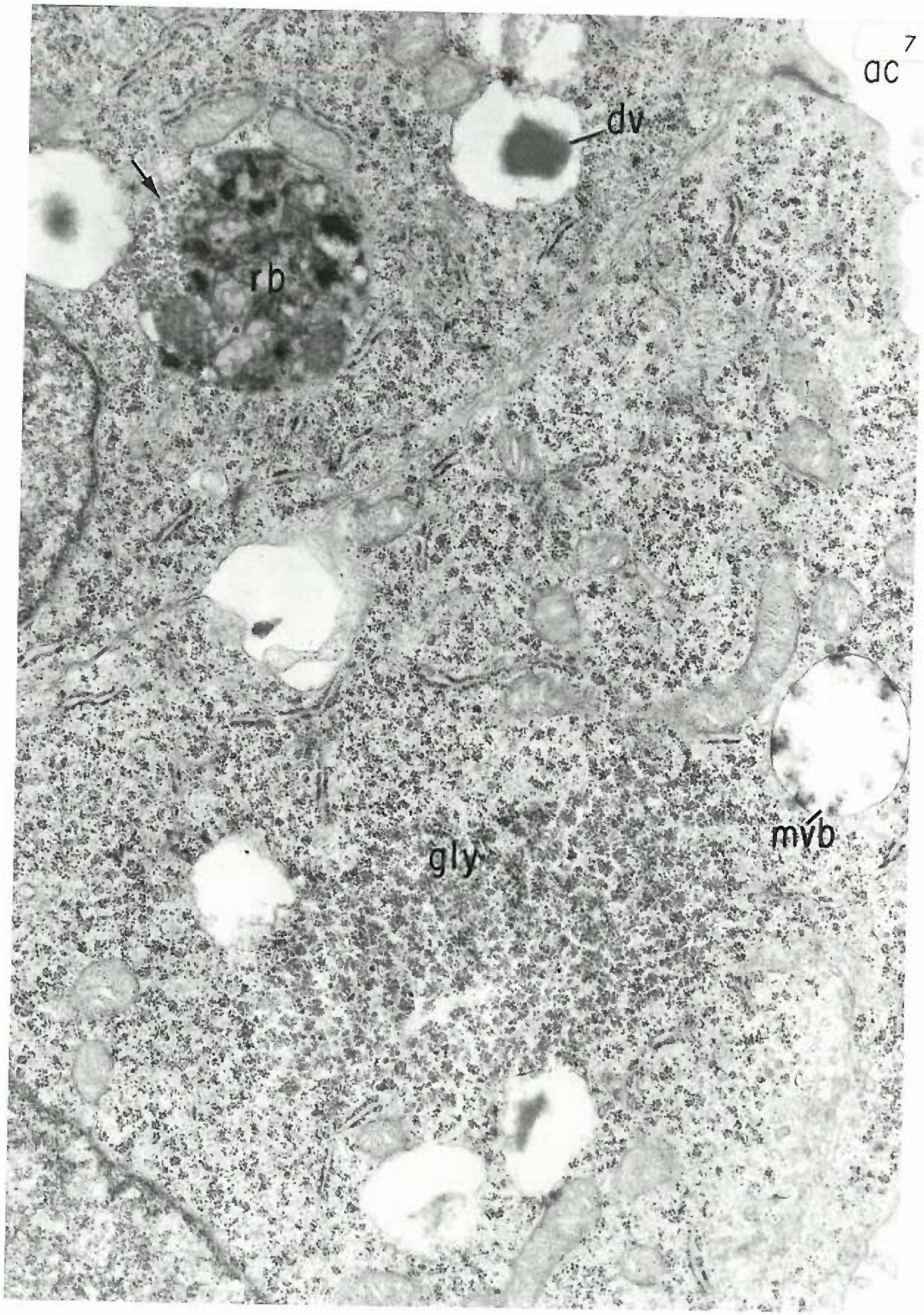
ac
dv
rb
gly
mvb

Figure 8. Ten-day neural plate, experimental.
Several "dye-like" vacuoles (dv) are clustered in the cytoplasm of the neurectoderm cells. Amniotic cavity (ac).

x20,000

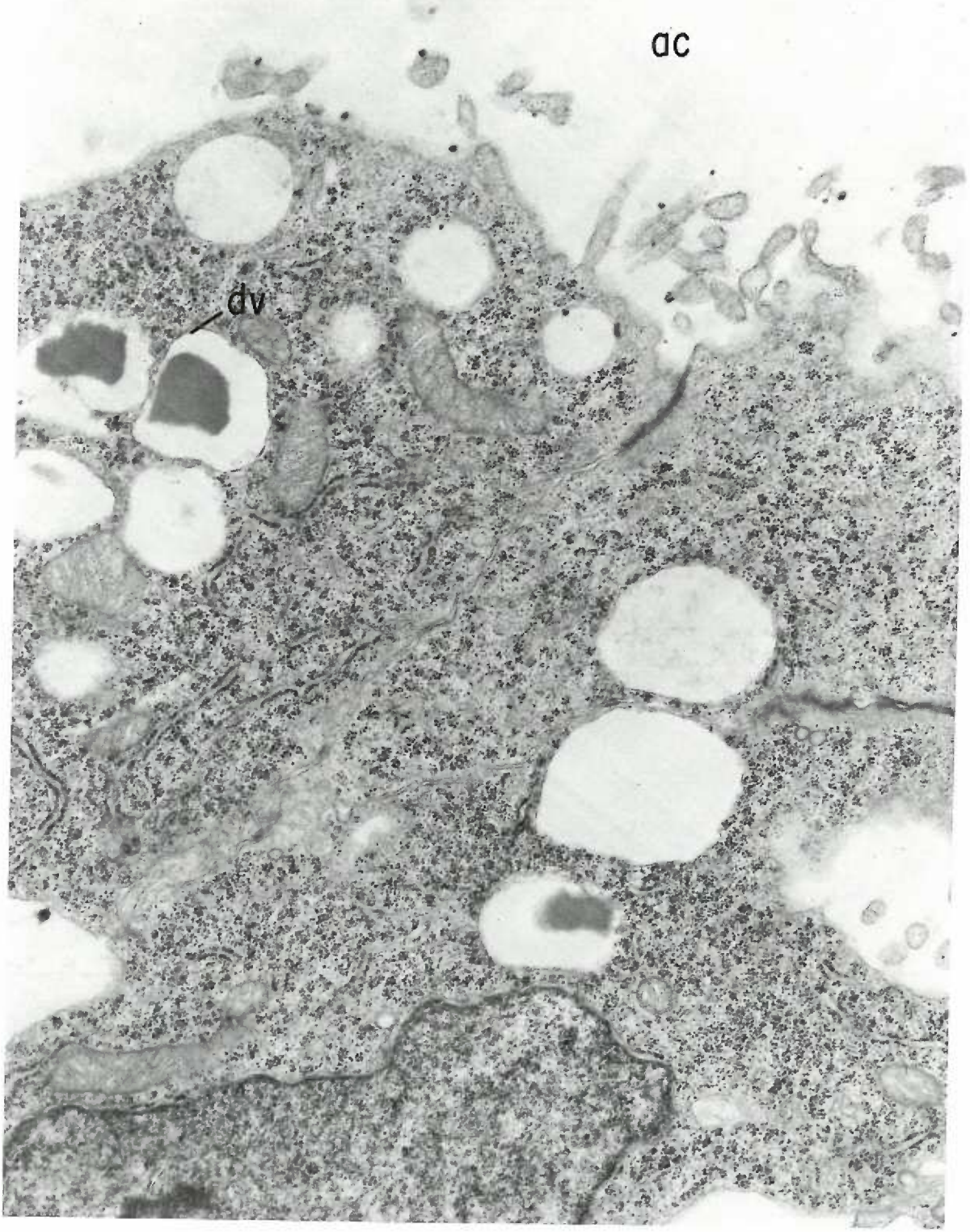
ac
dv

Figure 9. Ten-day neural plate, experimental. Neurectoderm cells bordering the amniotic cavity (ac) exhibit a Golgi complex (Go), a multi-vesicular body (mvb), and a centriole (arrow). Some of the "dye-like" vacuoles (dv) lie adjacent to deposits of glycogen (gly). Residual body (rb).

x20,000

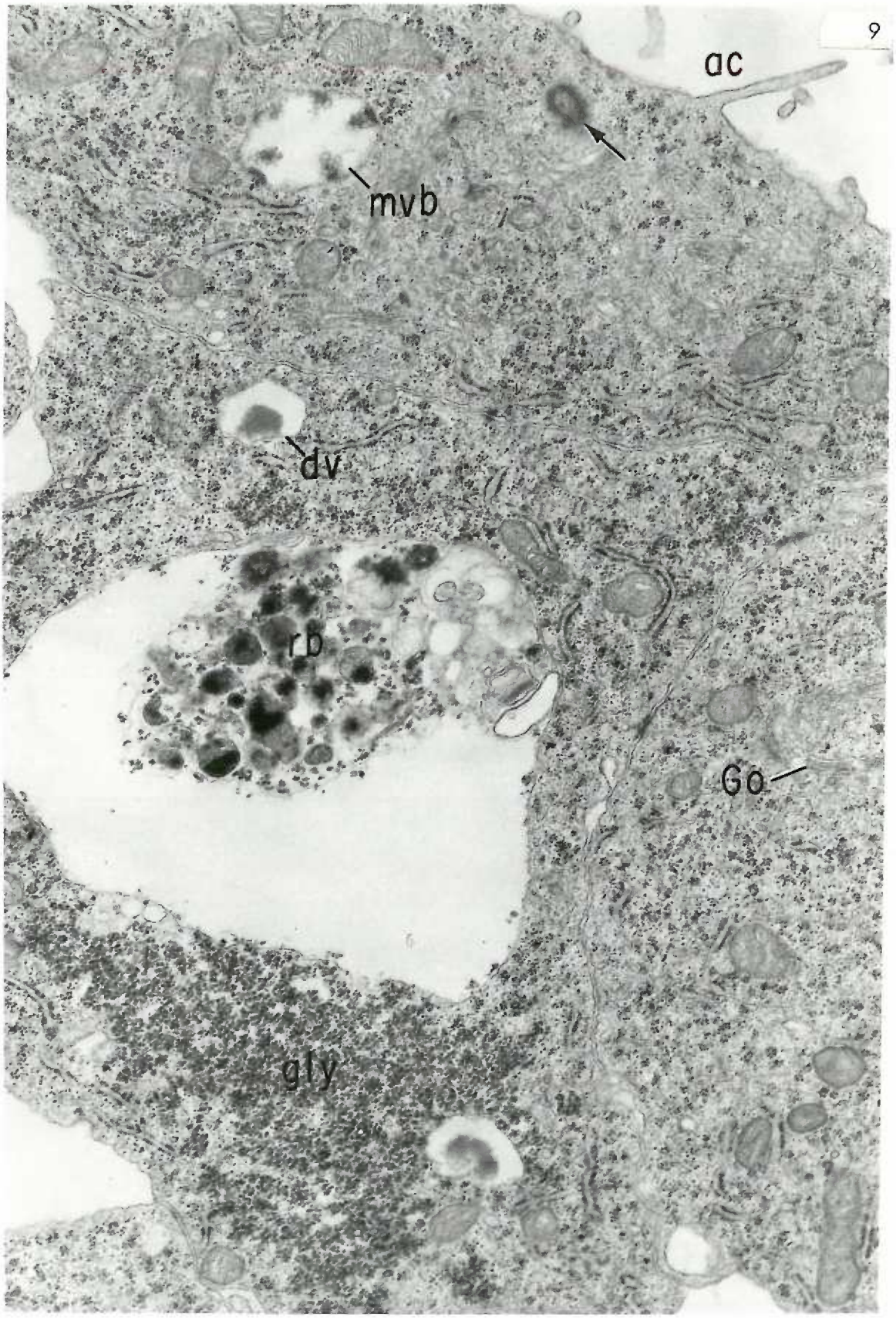
ac
mvb
dv
rb
Go
gly

Figure 10. Ten-day neural plate, experimental.
The neurectoderm cells of the neural plate (np) contain small vacuoles with dark centers and clear peripheral areas (arrows). These vacuoles coincide with the morphology of the "dye-like" vacuoles seen with the electron microscope (Figures 7, 8, 9). Mesenchyme (my); amniotic cavity (ac). Richardson's stain.

x400

Figure 11. Ten-day neural plate, control.
The neurectoderm cells of the neural plate (np) exhibit none of the "dye-like" vacuoles seen in Figure 10, above. Mesenchyme (my); amniotic cavity (ac). Richardson's stain.

x400

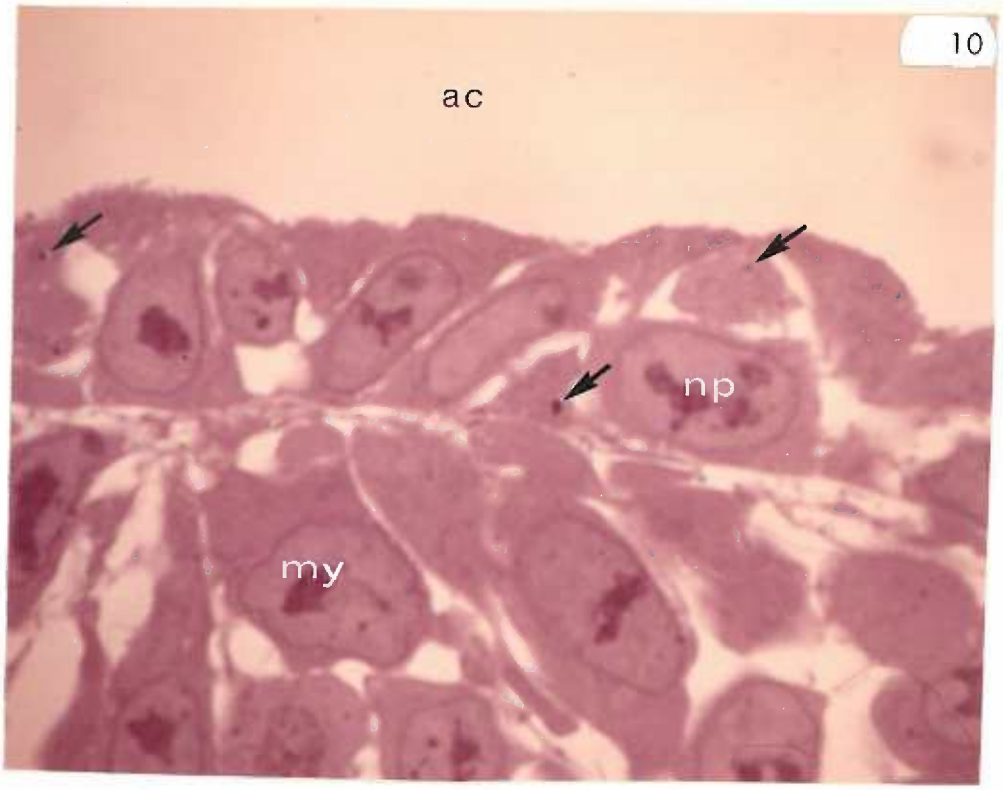
10
ac
np
my

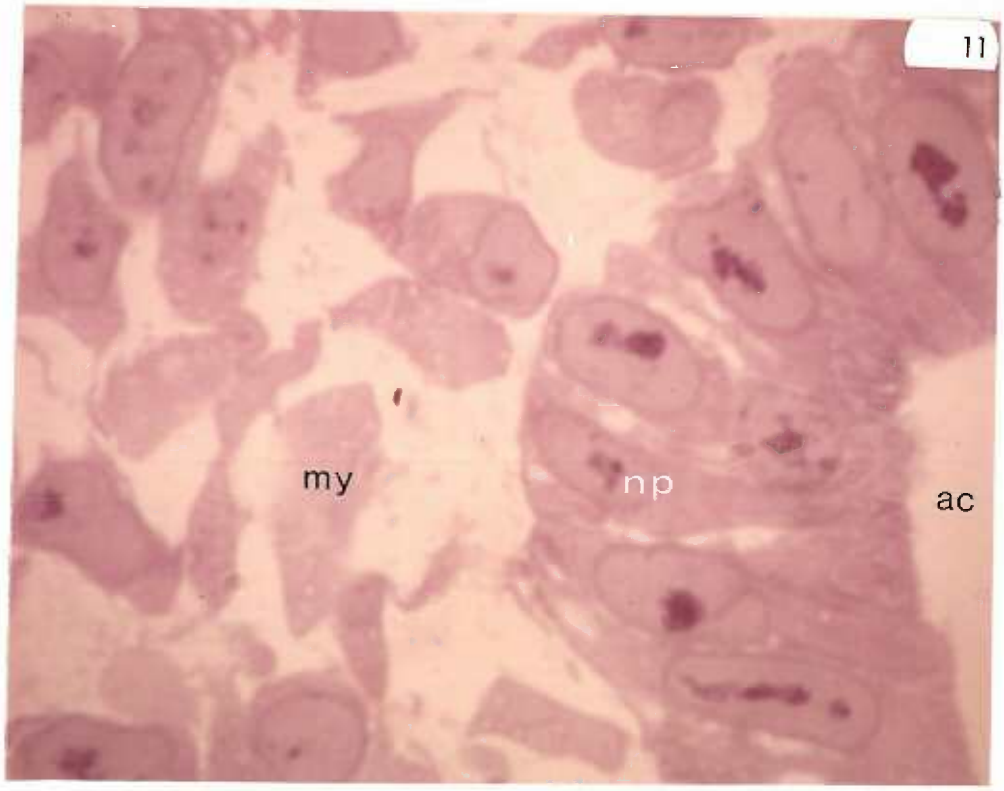
11
my
np
ac

Figure 12. Ten-day neural plate, experimental.

A large residual body (rb) lies adjacent to a small residual body. Both contain an electron-dense, floccular material. One possible "dye-like" vacuole (dv) is present in the large residual body. Nucleus (n).

x20,000

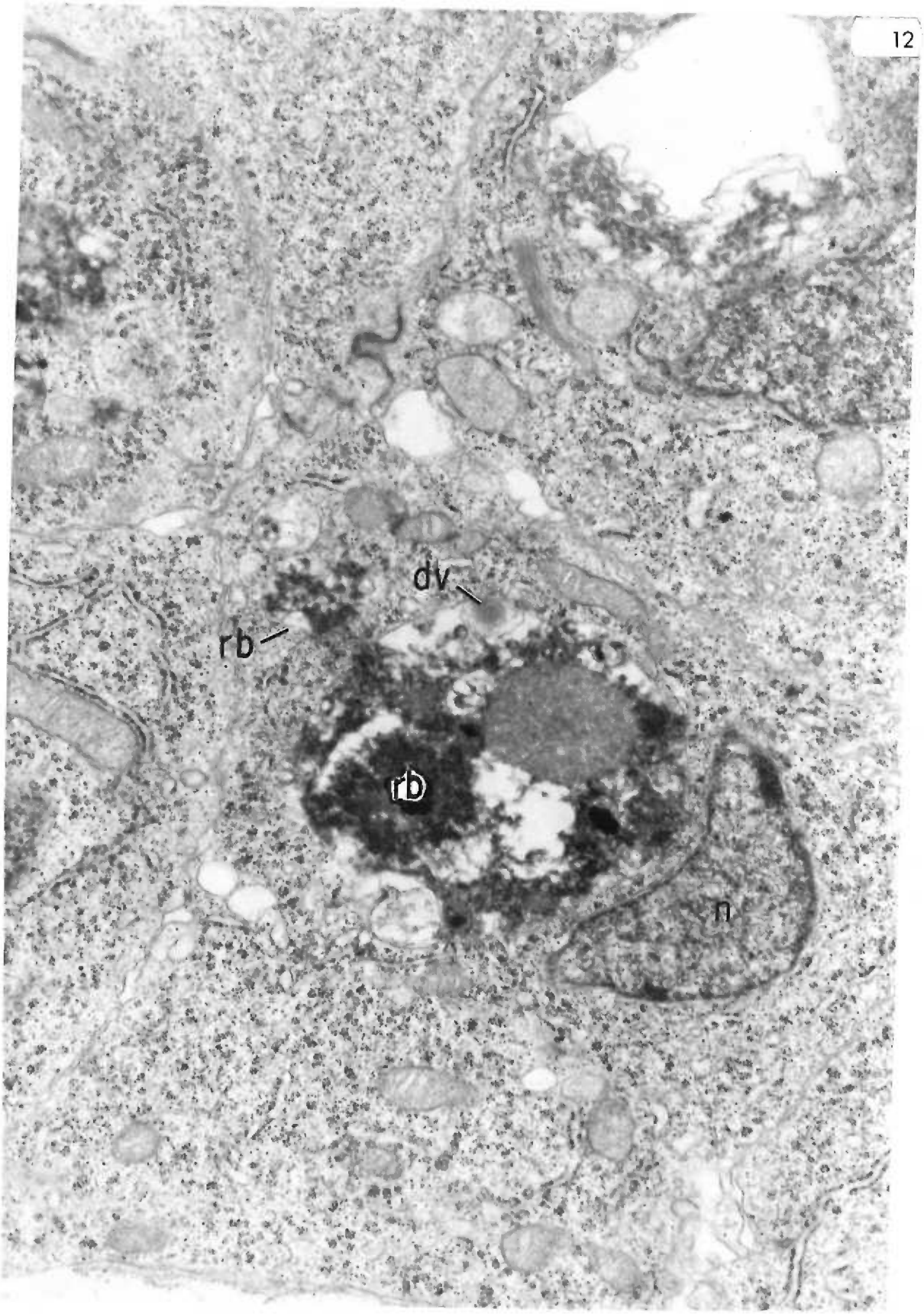
12
dv
rb
rb
n

Figure 13. Eleven-day neural tube, experimental.

This constricted neural tube lumen (nl) contains polyribosomes (arrow). Two "dye-like" vacuoles (dv) lie adjacent to the nucleus (n) of a neurectoderm cell. A large phagocytic cell (pc) contains a "dye-like" vacuole (dv).

x20,000

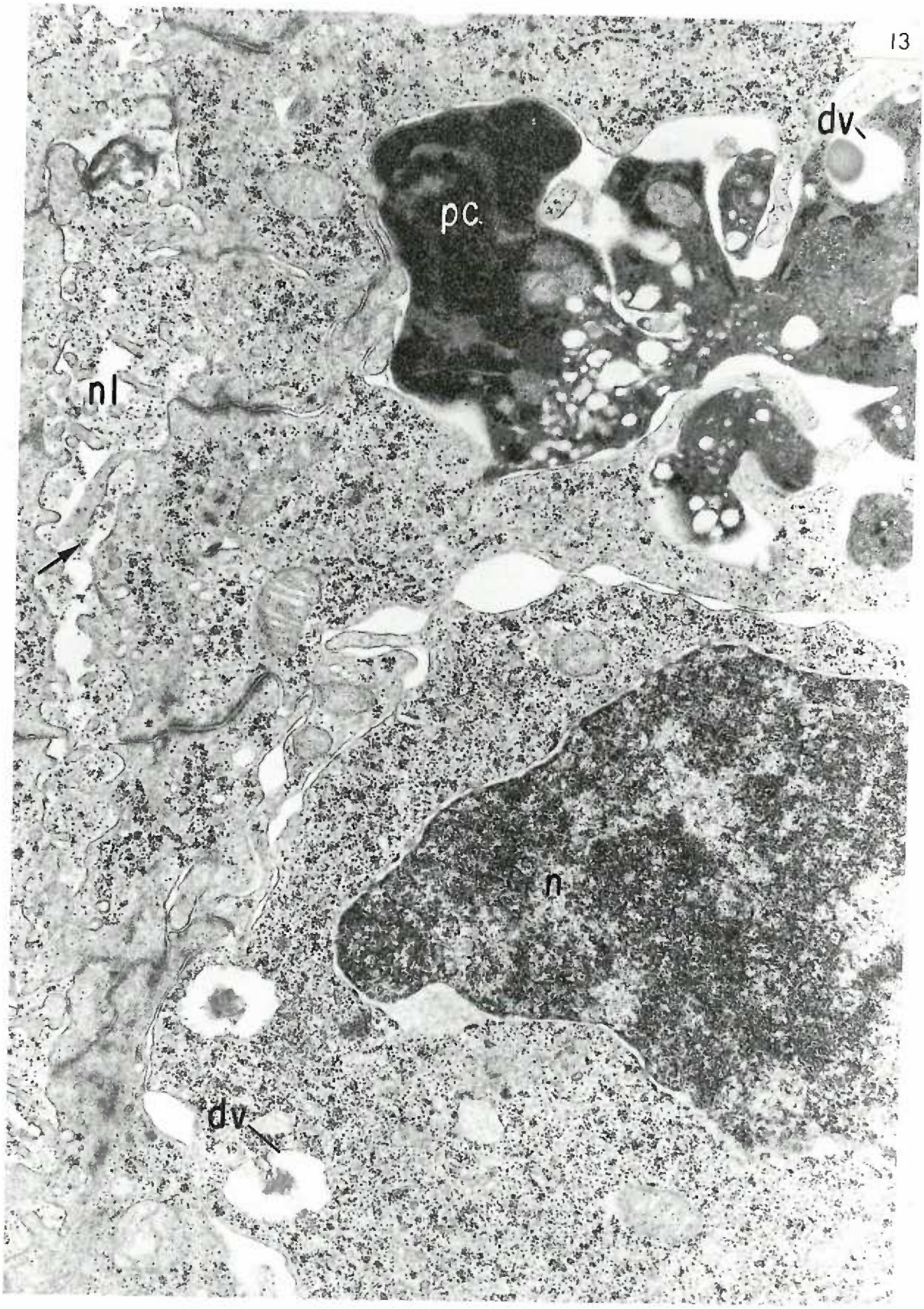
dv
pc
nl
n
dv

Figure 14. Eleven-day neural tube, experimental.

An electron-dense phagocytic cell (pc) between two neurectoderm cells demonstrates segments of nuclear substance (n). The cytoplasm of this phagocyte contains numerous free ribosomes (r), mitochondria (m), and strands of rough endoplasmic reticulum (rer). Other portions of cytoplasm (arrows) are probably pseudopodia. A single "dye-like" vacuole (dv) lies within the phagocytic cell cytoplasm. The large inter-cellular space (is) appears to be partly artifactual.

x20,000

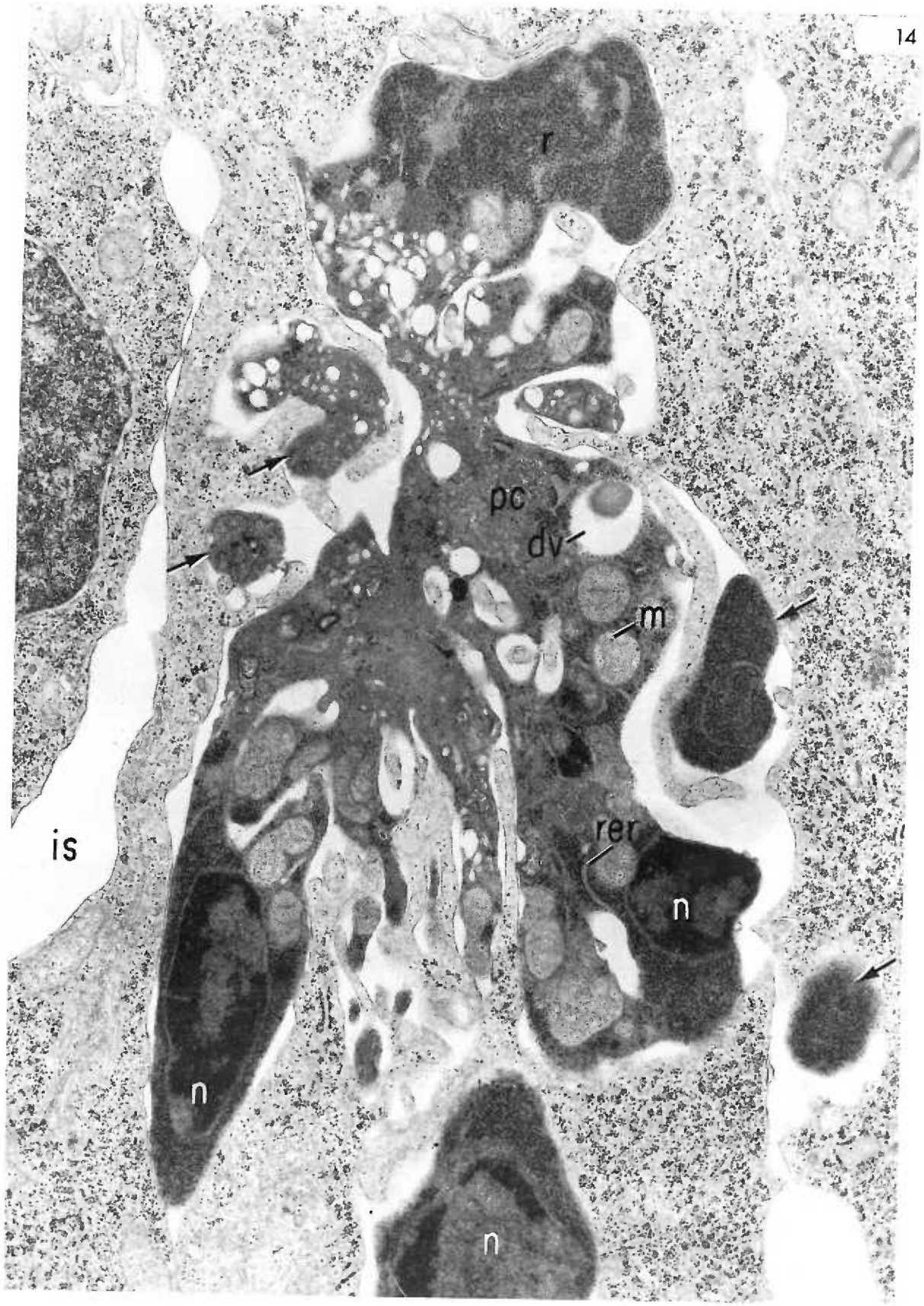
r
pc
dv
m
is
rer
n
n
n

Figure 15. Eleven-day neural tube, experimental.
The neurectoderm cells exhibit three "dye-like" vacuoles (arrows), two of which lie within a large residual body (rb). Inter-cellular space (is); neural tube lumen (nl).

x20,000

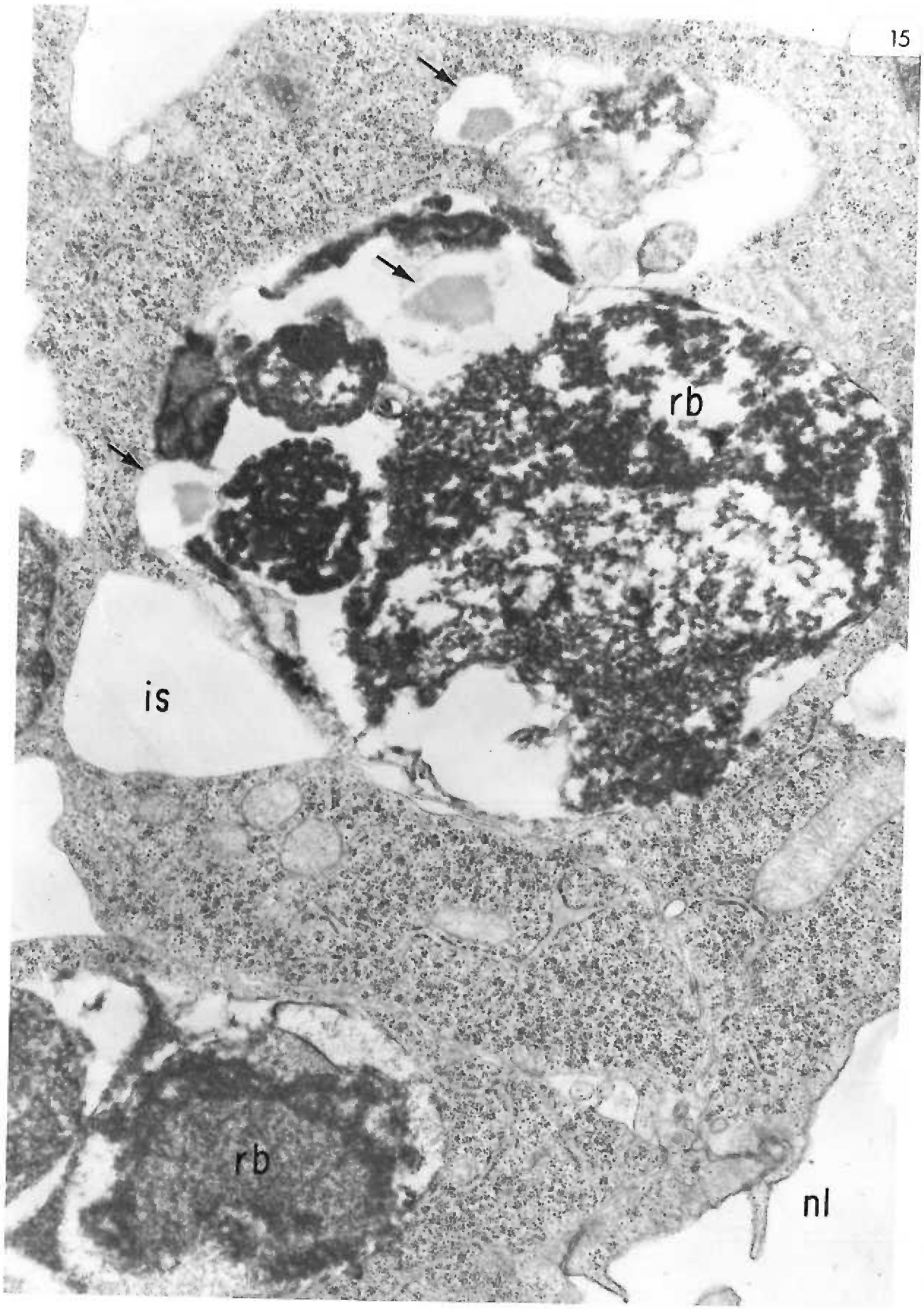
rb
is
rb
nl

Figure 16. Ten-day neural plate, control.

A large, heterogeneous residual body (rb) appears to lie within the cytoplasm of a neurectoderm cell. The residual body is filled with floccular and granular material of high electron-density. Mitochondrial remnants (arrows).

x40,000

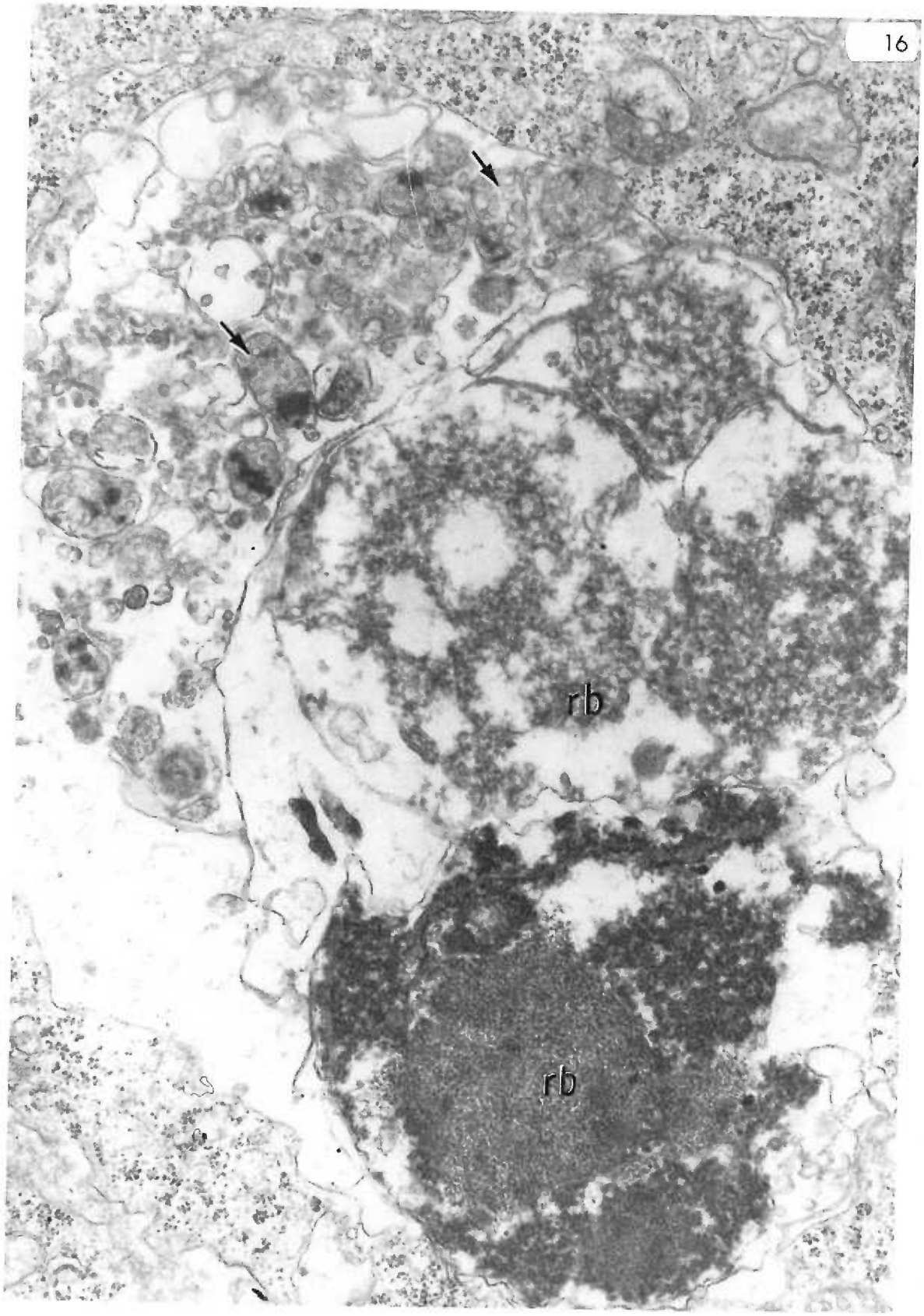
16
rb
rb

Figure 17. Ten-day neural plate, control.

A cell undergoing mitosis displays a condensation of chromatin material (ch). Neurectoderm cells bordering the amniotic cavity (ac) are connected by terminal bars (arrows). Intercellular space (is).

x12,000

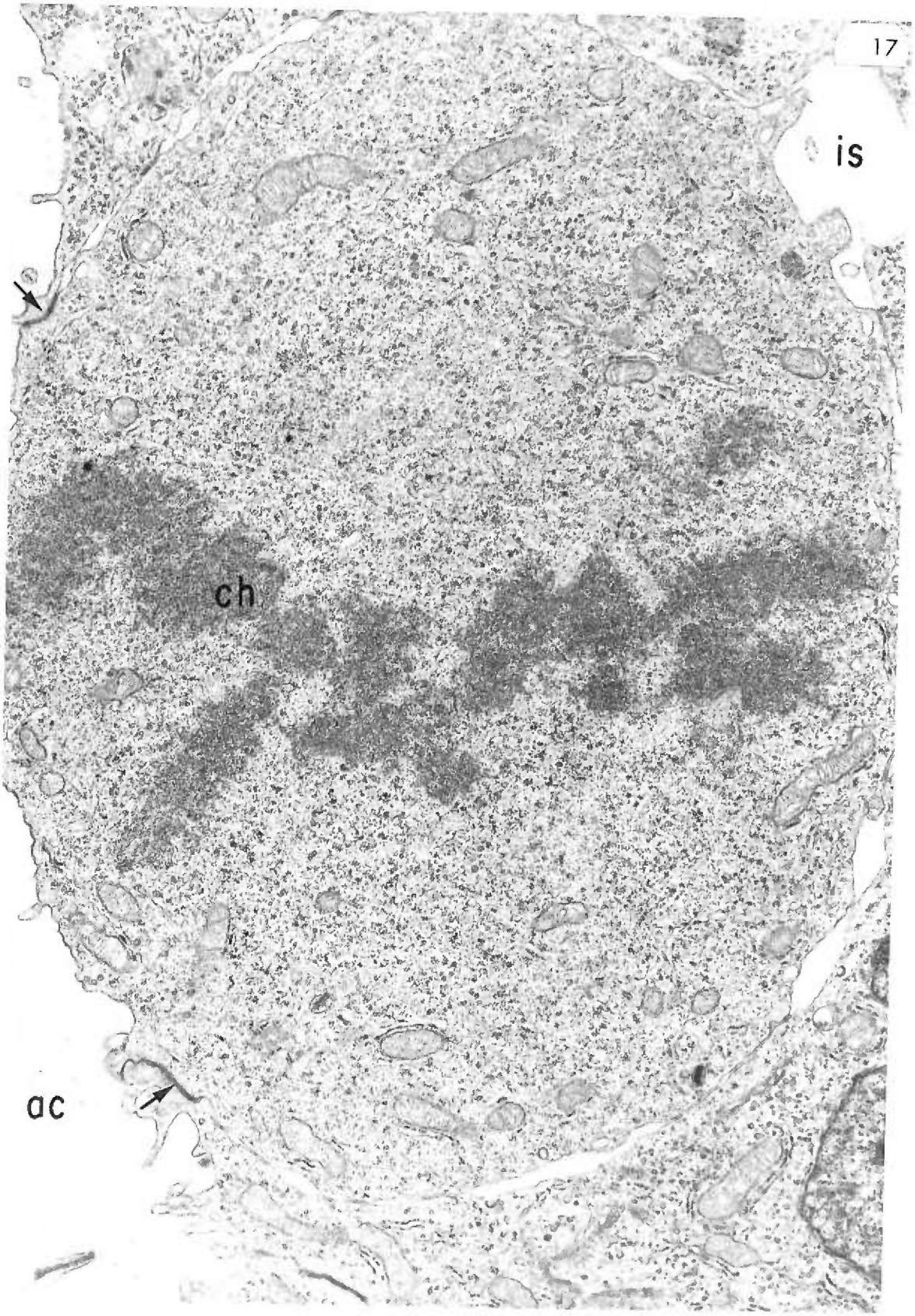
17
is
ch
ac

Figure 18. Eleven-day neural tube, control.

A mitotic figure is seen in this cell bordering the neural tube lumen (nl). The cytoplasmic processes (cp) seen extending toward the lumen will later develop into neuronal processes. The neurectoderm cells are connected at the luminal surface by terminal bars (arrows) and at the lateral surfaces by desmosomes. Chromatin (ch); intercellular space (is); centriole (c); nucleus (n).

x12,000

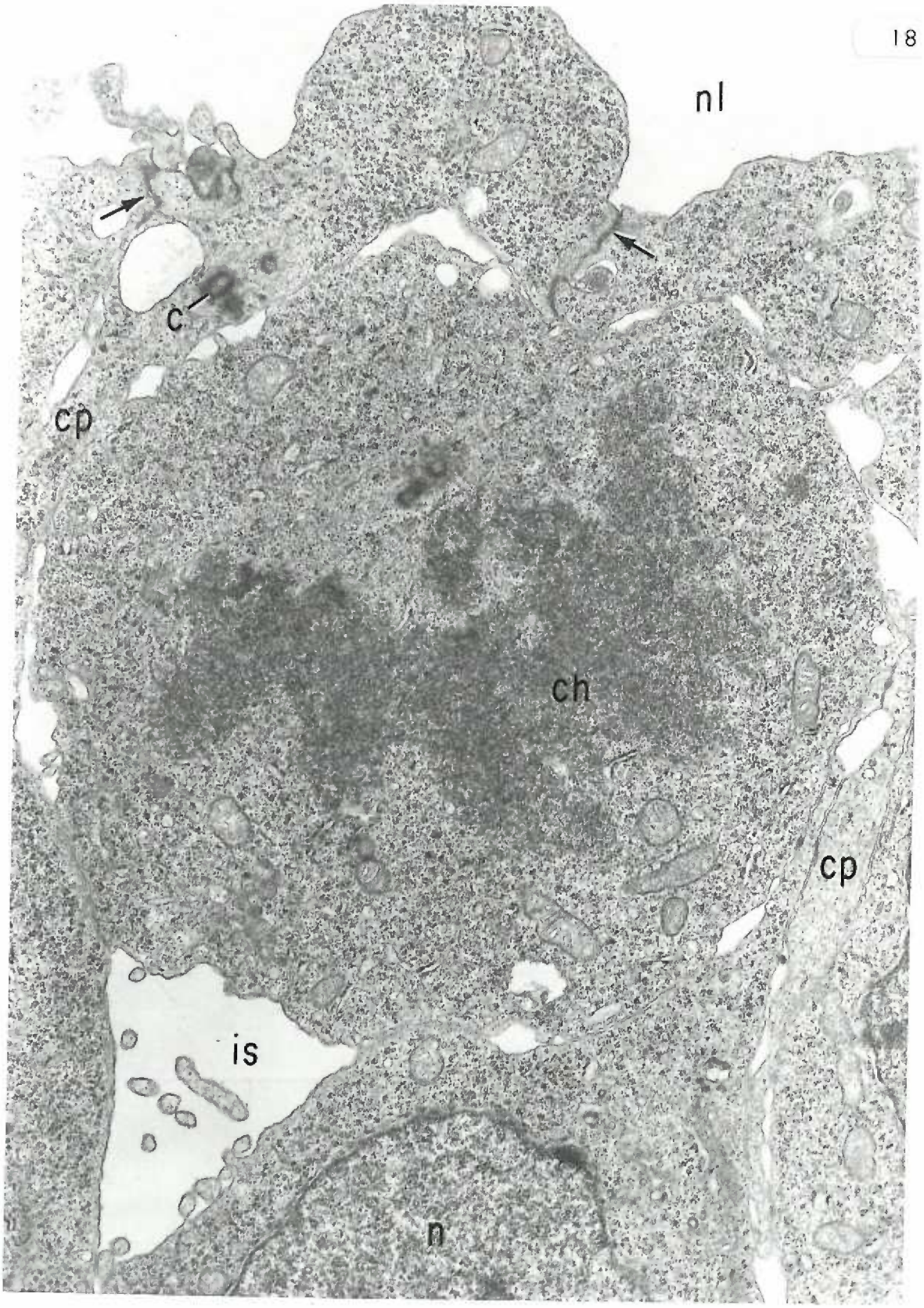
nl
c
cp
ch
cp
is
n

Figure 19. Twelve-day neural tube, control.
Adjacent to the nucleus (n) of a neurectoderm cell is an organelle (pci) that is composed of a central, smooth membrane situated between two ribosome-bound membranes. Neurectoderm cells bordering the luminal surface of the neural tube are connected by terminal bars (arrows). Mitochondria (m).

x29,000

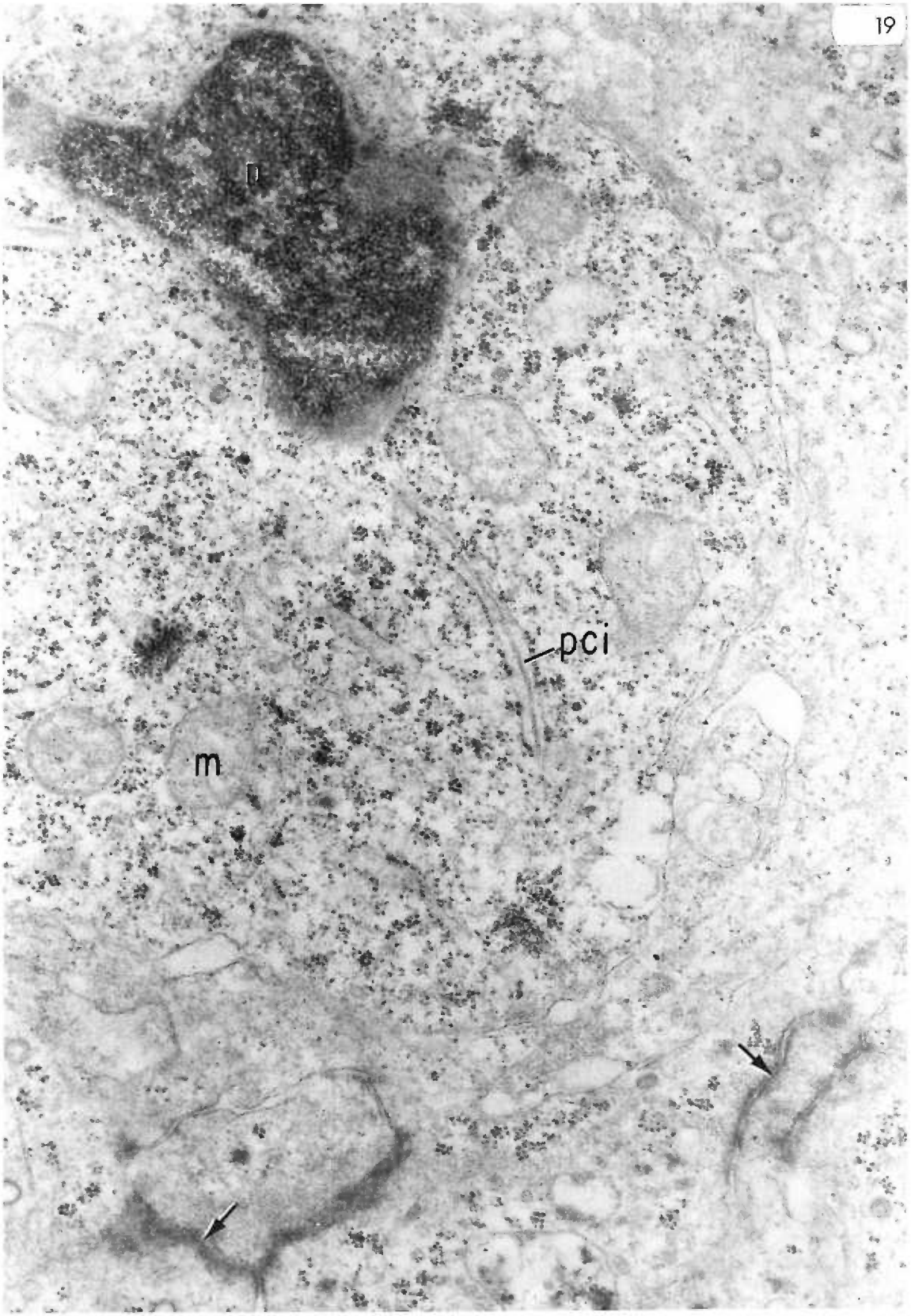
19
n
pci
m

Figure 20. Twelve-day myocardium, experimental. Extensive accumulations of glycogen particles (gly) fill the cytoplasm of a myocardial cell. A small cluster (arrow) of material of high electron density, similar to glycogen rosettes, is located in the extracellular space (arrow).

x29,000

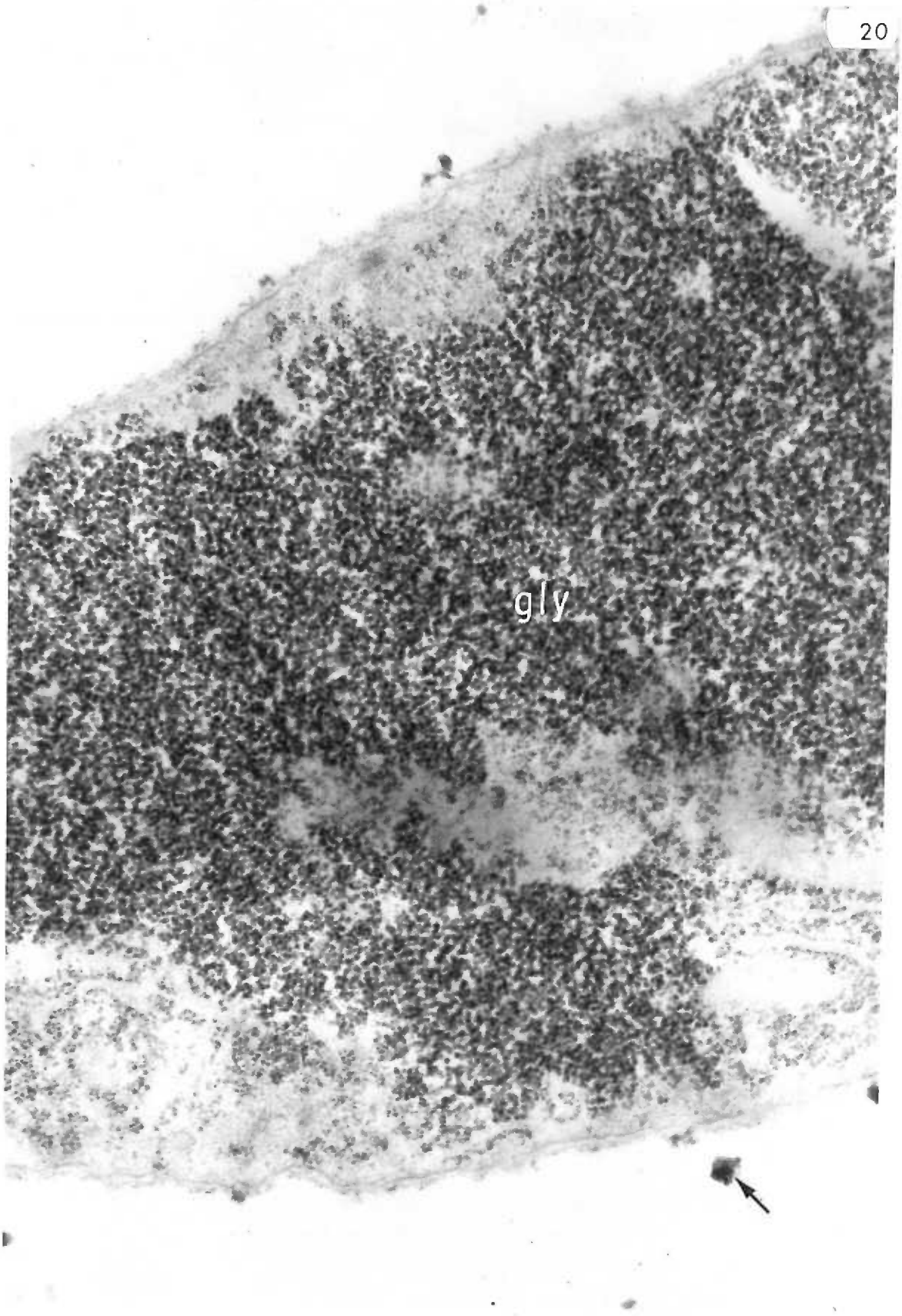
20
gly

Figure 21. Twelve-day myocardium, experimental.

The elongated mitochondria (m) and rough endoplasmic reticulum (rer) exhibit poorly defined membranes. Some myofibrillae (mf) are seen adjacent to intra-cellular deposits of glycogen (gly). Some extra-cellular glycogen particles (arrow) coat the membrane of this myocardial cell.

x29,000

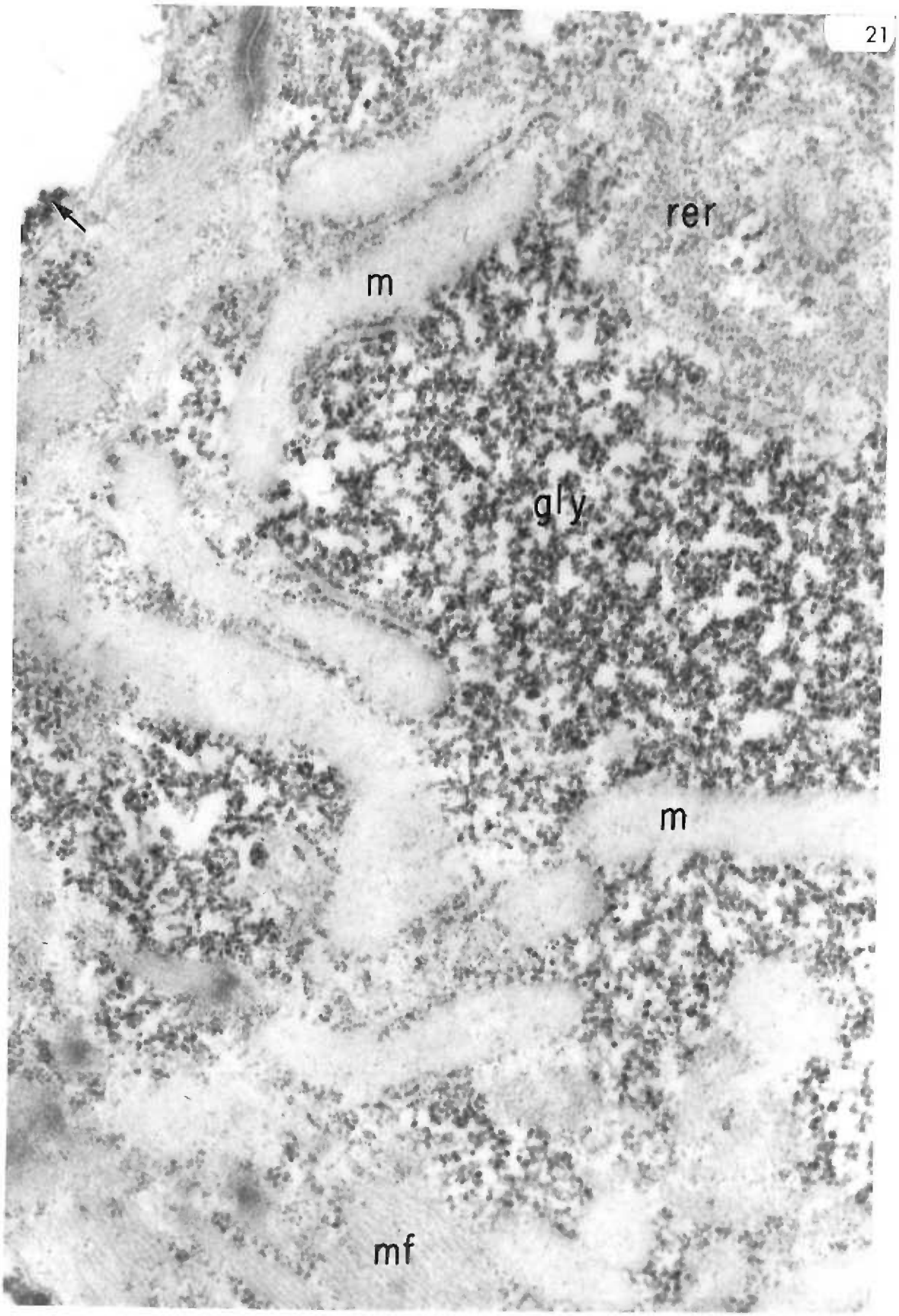
21
rer
m
gly
m
mf

Figure 22. Twelve-day myocardium, experimental.

A thick lamina of glycogen (arrows) adheres to the outer surface of the membranes of two adjacent myocardial cells. These glycogen particles are identical to those inside the cells (gly). Mitochondria (m) and myofibrils (mf) are poorly defined. Intercalated disc (id).

x29,000

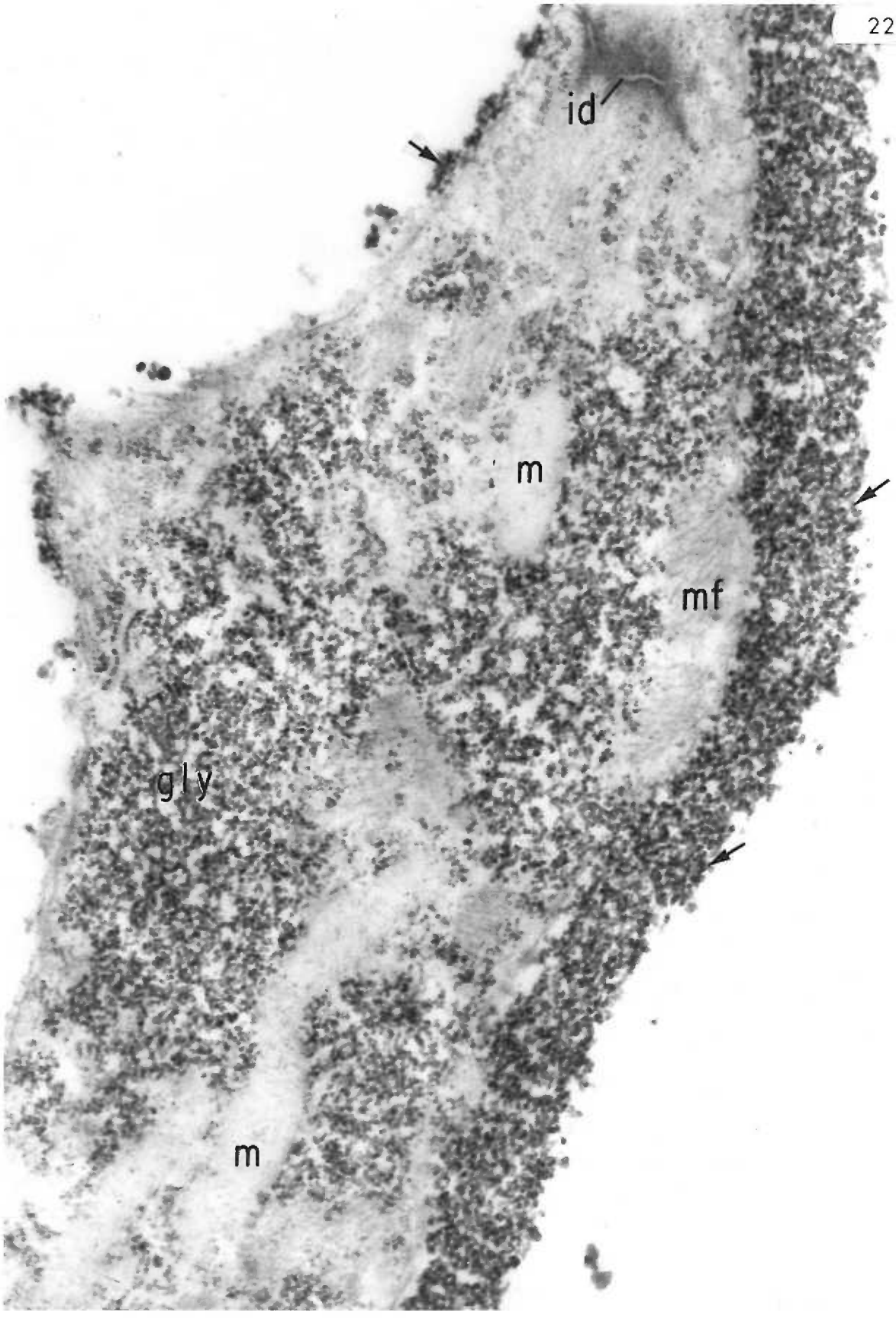
id
m
mf
gly
m

Figure 23. Twelve-day myocardium, experimental.
Large demi-lunes of glycogen particles (gly) coat the limiting membranes of myocardial cells. Additional accumulations of glycogen (gly) occur within the cytoplasm among myofibrillae (mf) and poorly defined mitochondria (m). Intercellular space (is).

x29,000

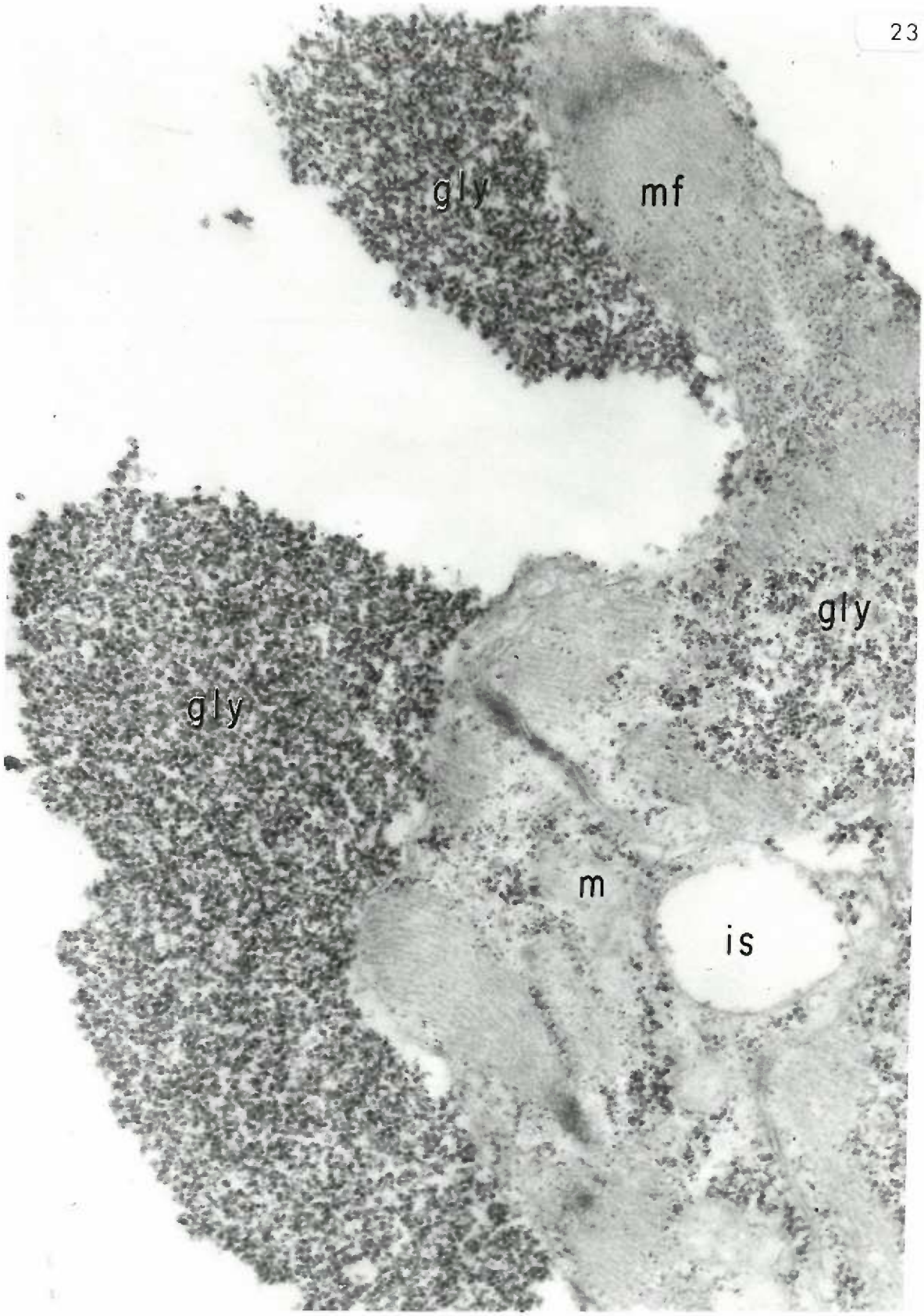
gly
mf
gly
gly
m
is

Figure 24. Twelve-day myocardium, experimental.
Numerous sites of positive reaction exist in both extra- and intra-cellular loci (arrows). These sites of PAS-positive response coincide with extra- and intra-cellular glycogen deposits observed with the electron microscope (Figures 22, 23). Periodic acid-Schiff stain.

x400

Figure 25. Twelve-day myocardium, control.
A few PAS-positive sites (arrow) are observed in intra-cellular loci. Periodic acid-Schiff stain.

x400

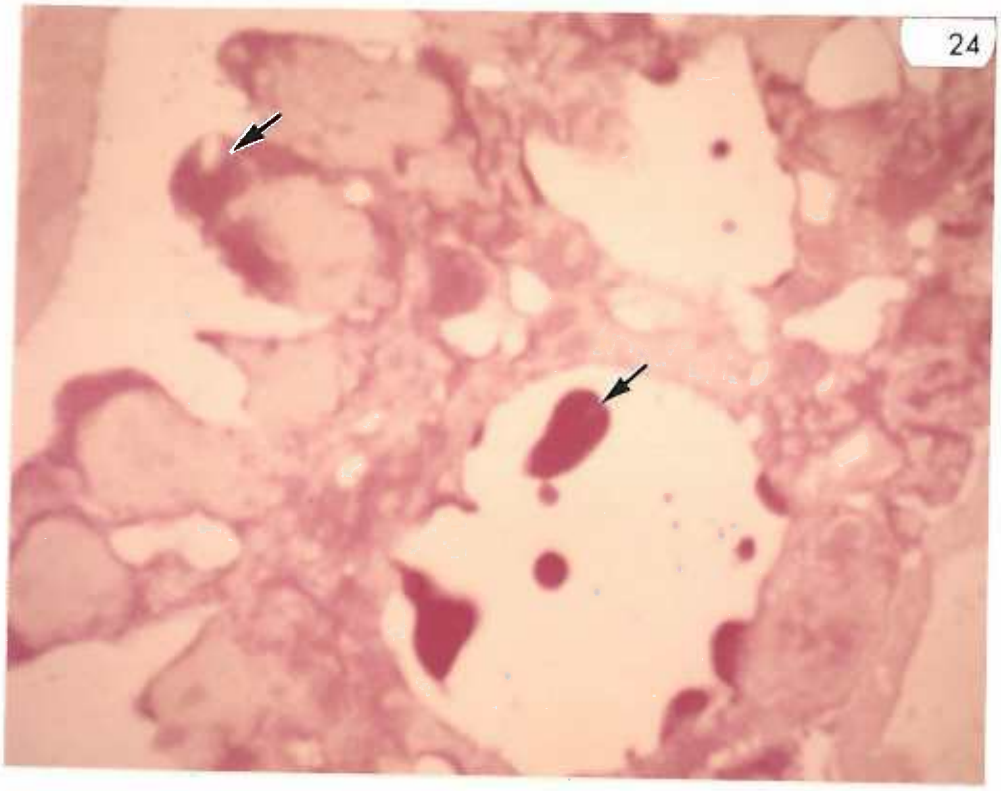
24

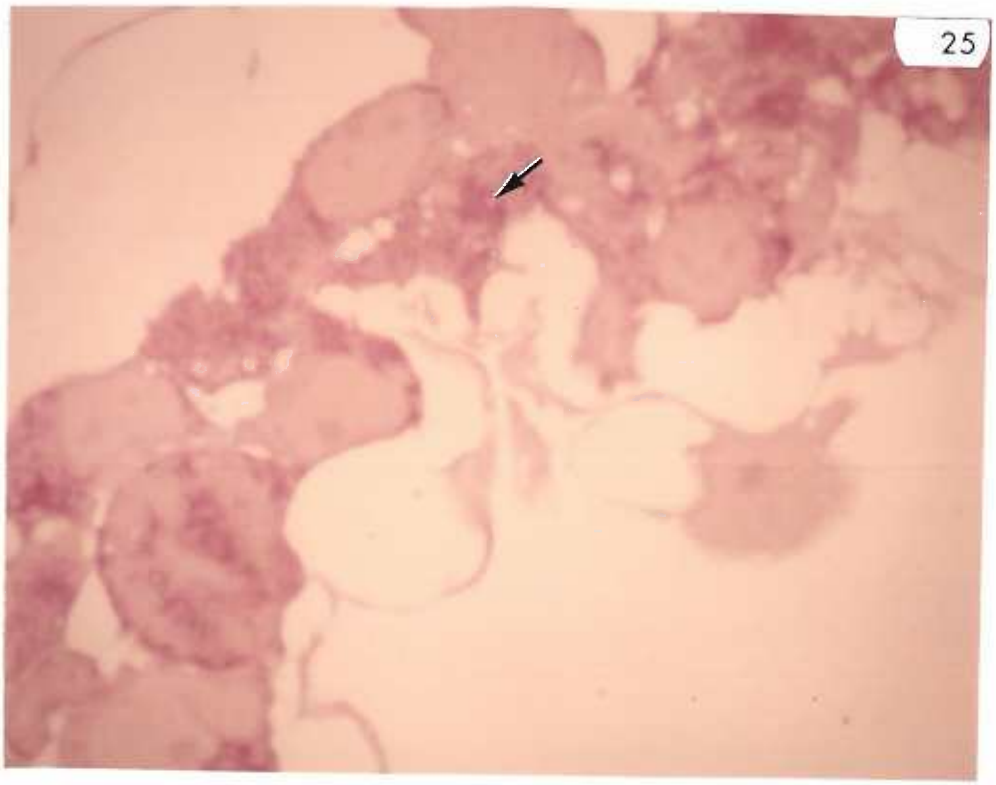
25

Figure 26. Twelve-day myocardium, control.

Several myocardial cells join to form a cord of cells. Desmosomes (d) and intercalated discs (id) connect these cells. Myofibrillae (mf) exhibiting prominent Z bandings (z) appear to attach to the intercalated discs. Mitochondria (m).

x20,000

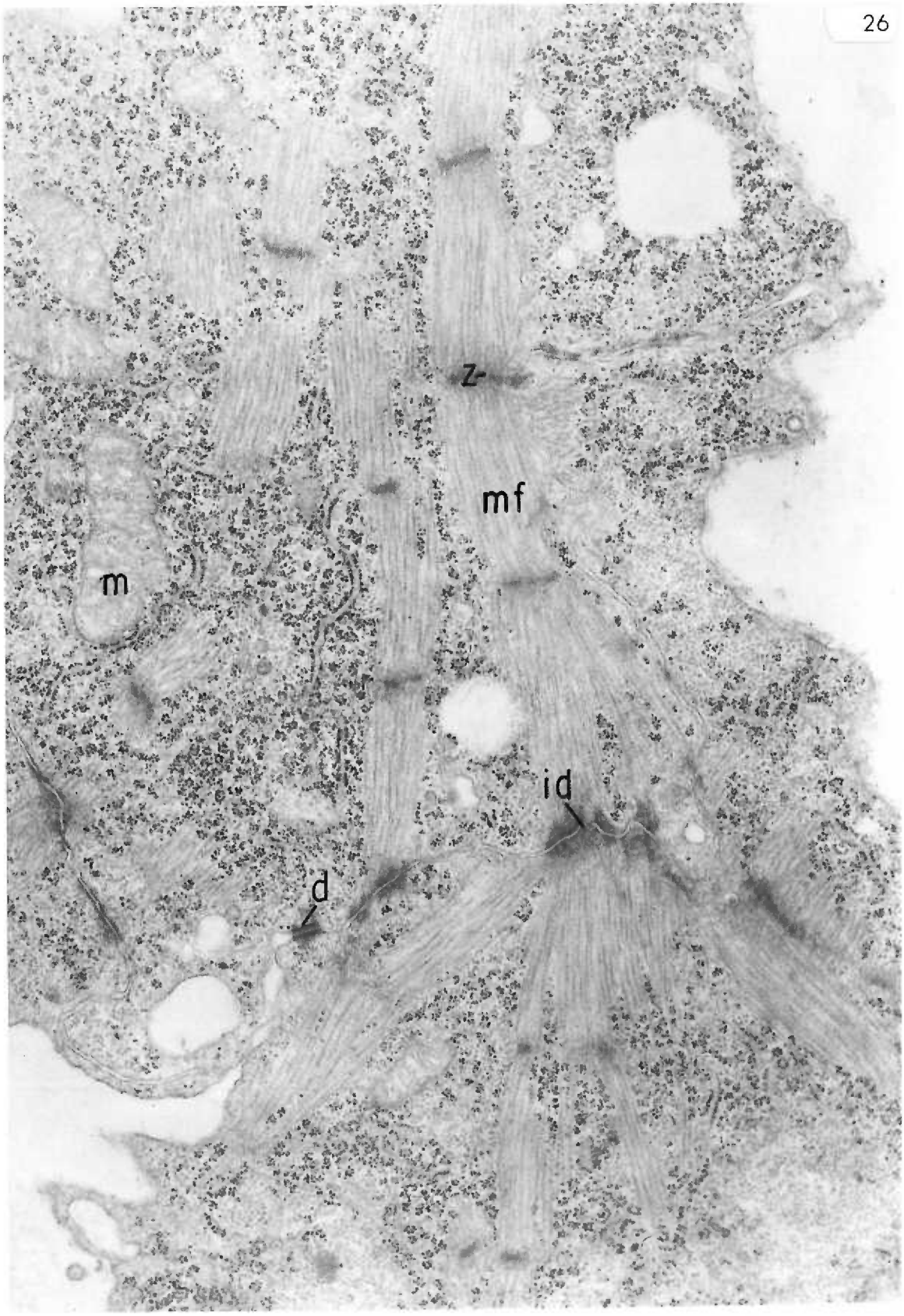
z
mf
m
id
d

Figure 27. Twelve-day myocardium, control.

Two myocardial cells are attached by a desmosome (d) and an intercalated disc (id). Numerous myofibrillae (mf) are apparent in the cytoplasm. Glycogen particles (arrow) appear less electron-dense than the slightly smaller polyribosomes. Mitochondria (m); Z banding (z); glycogen (gly).

x29,000

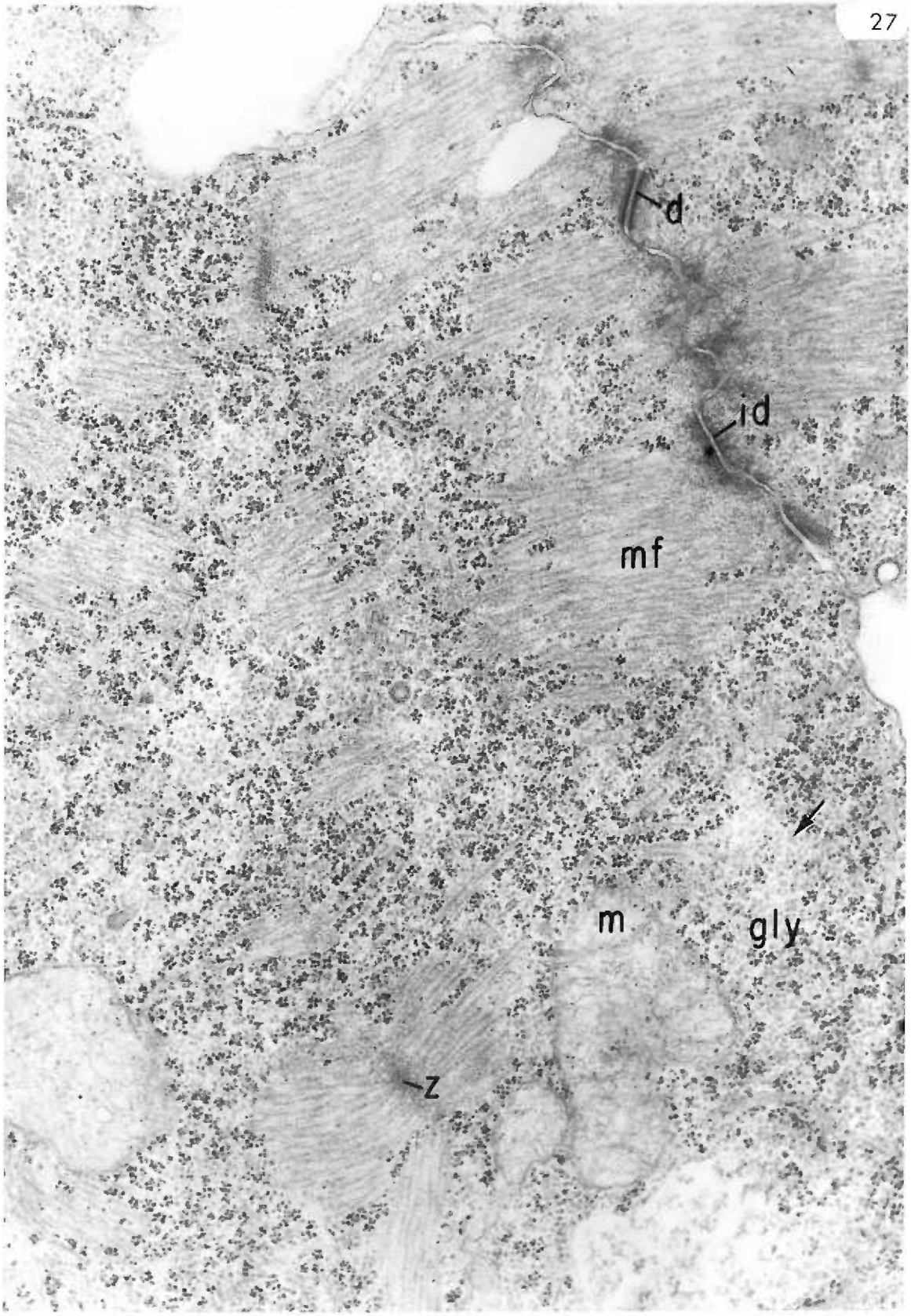
d
id
mf
m
gly
z

Figure 28. Ten-day visceral endoderm of the presumptive gut, experimental.

Irregular microvilli project from the surface of the visceral endoderm cells (ve) into the yolk sac cavity (ysc). A cluster of "dye-like" vacuoles (dv) lies in the apical cytoplasm of one cell. Part of a splanchnic mesoderm cell (me) lies beneath the endoderm.

x12,000

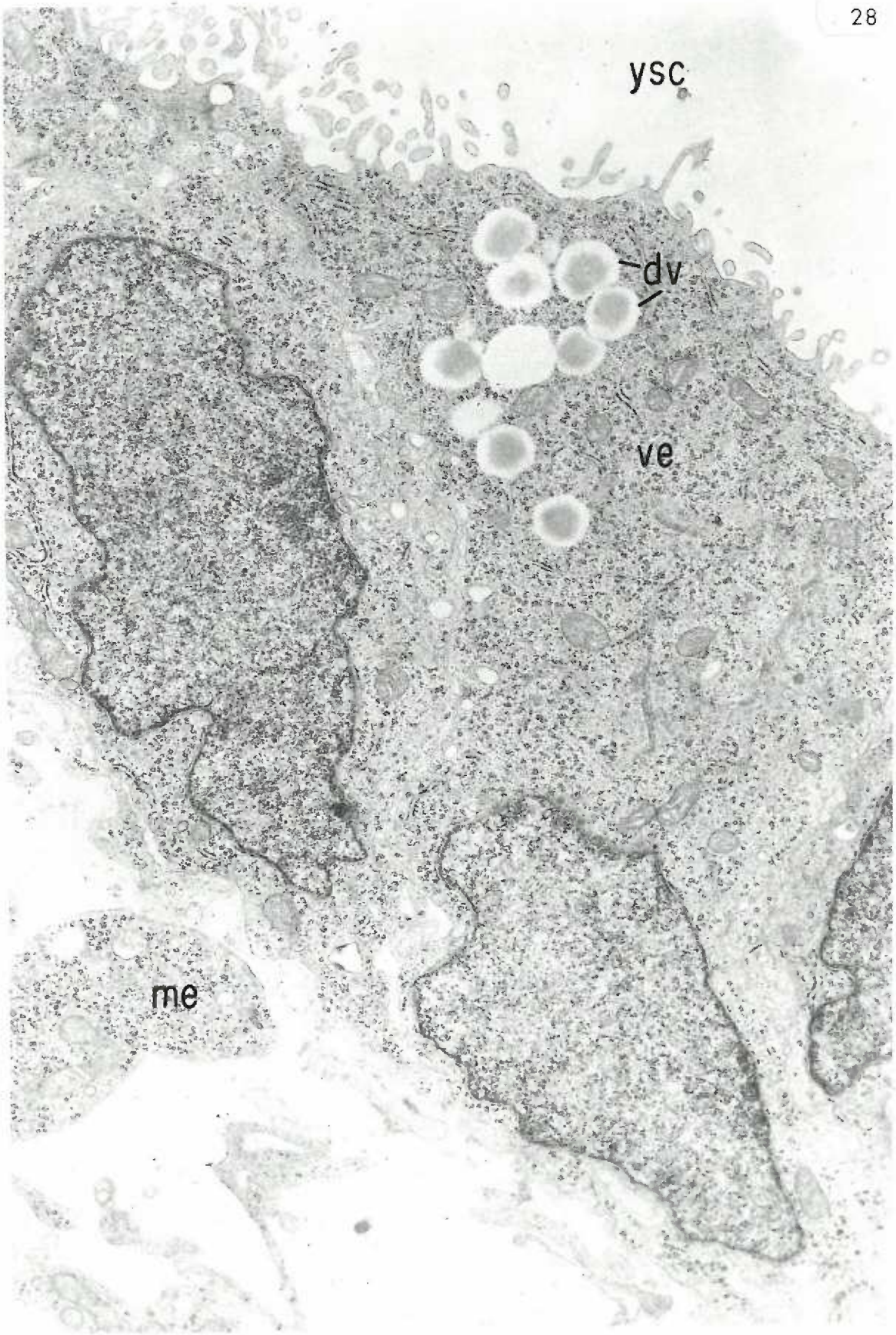
ysc
dv
ve
me

Figure 29. Ten-day visceral endoderm of the presumptive gut, experimental.

Beneath a single cell layer of visceral endoderm cells (ve) is a splanchnic mesoderm cell (me) which lines the intra-embryonic coelom (ic). Three "dye-like" vacuoles (dv) are seen as a cluster in the visceral endoderm border of the yolk sac cavity (ysc).

x29,000

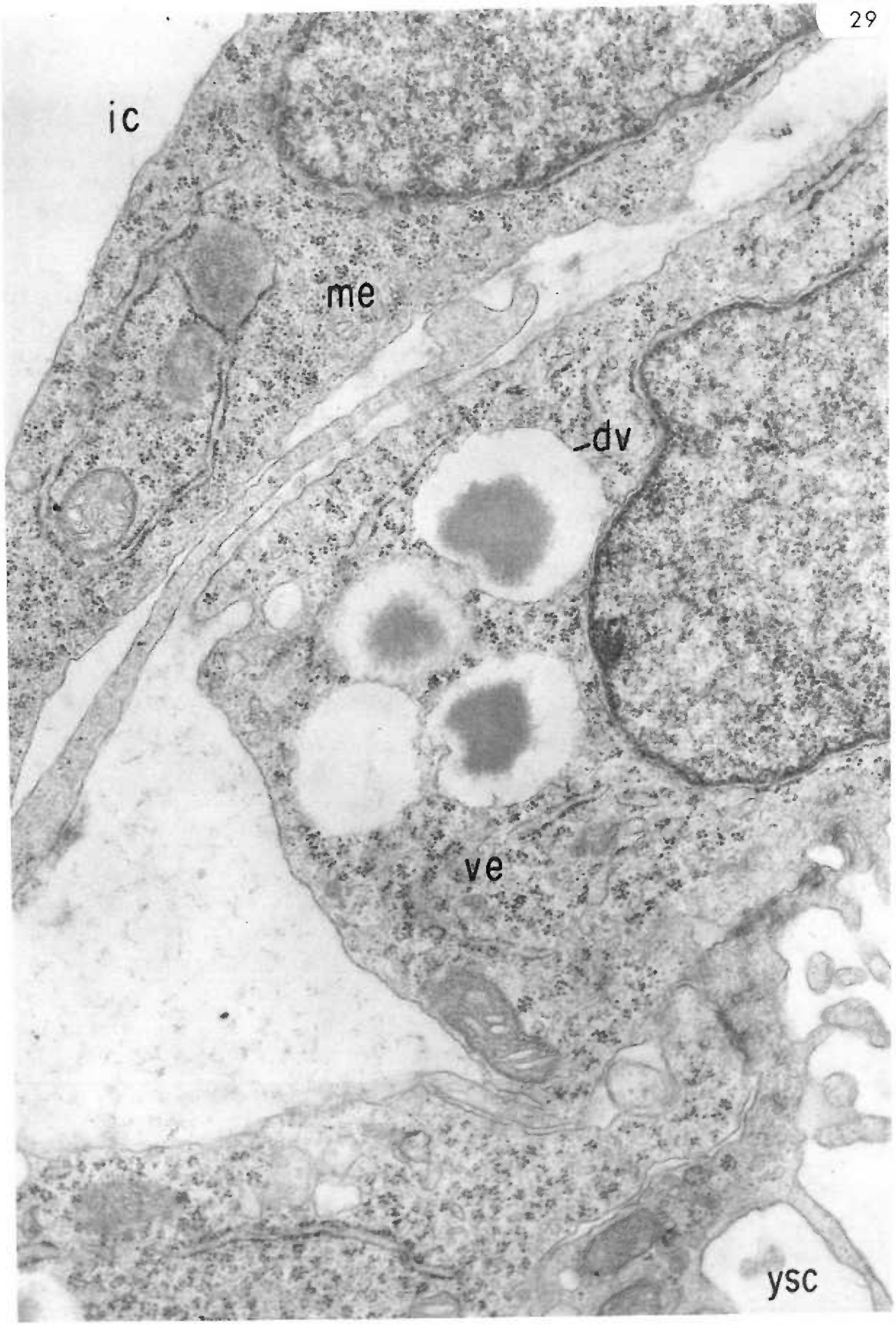
ic
me
dv
ve
ysc

Figure 30. Ten-day visceral endoderm of presumptive gut, experimental.

Portions of two splanchnic mesoderm cells (me) separate the visceral endodern (ve) from the intra-embryonic coelom (ic). Several "dye-like" vacuoles (dv) are visible in the cytoplasm of the mesoderm cells.

x29,000

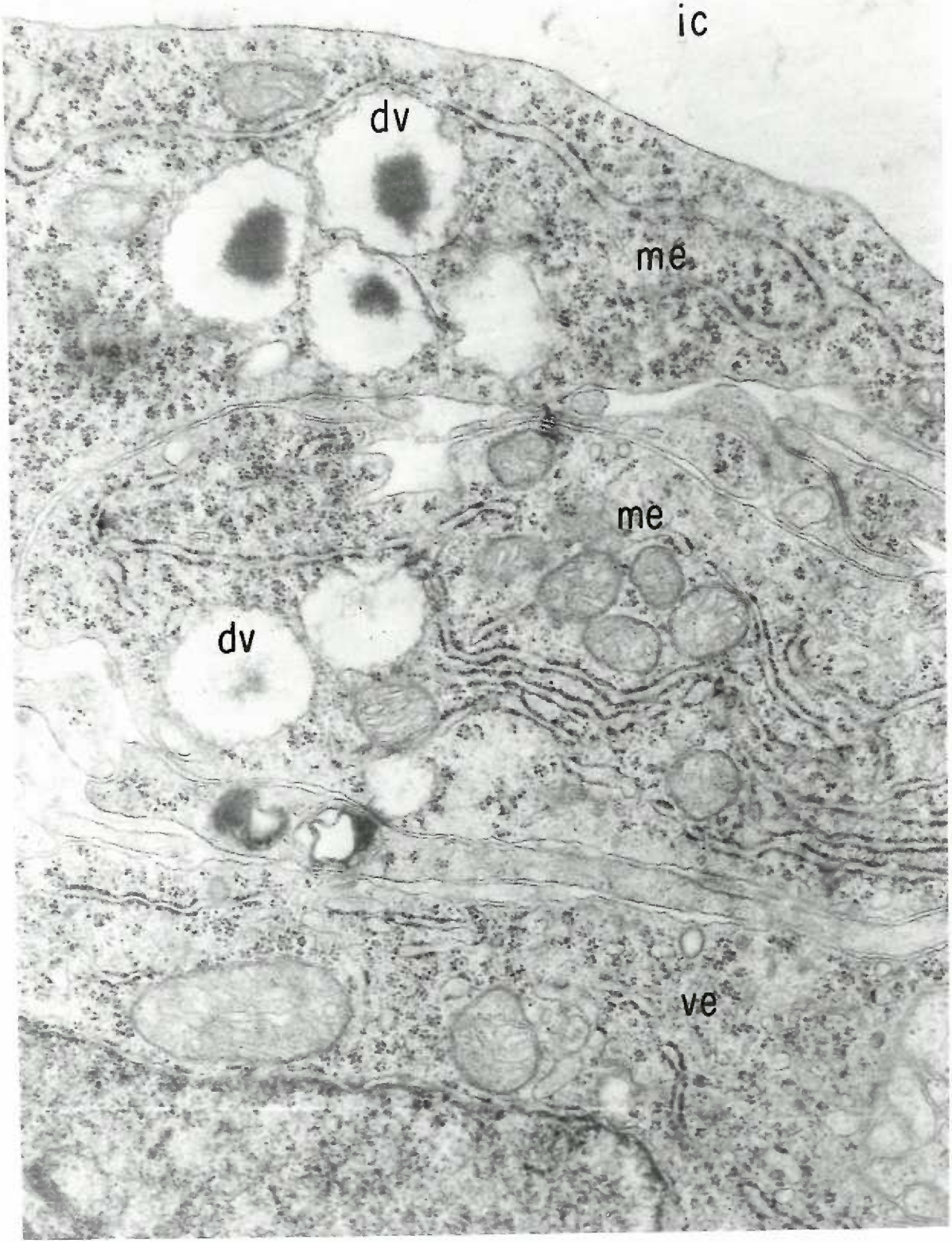
ic
dv
me
me
dv
ve

Figure 31. Ten-day visceral endoderm of presumptive gut, experimental.

Numerous vacuoles (arrows) with darkly stained centers and clear peripheral areas are exhibited within the cells of the visceral endoderm (ve). Such vacuoles coincide morphologically with the "dye-like" vacuoles observed in electron micrographs (Figures 28, 29, 30). Mesenchyme (my); yolk sac cavity (ysc). Richardson's stain.

x400

Figure 32. Ten-day visceral endoderm of presumptive gut, control.

No vacuoles of the "dye-like" morphology are present in these control visceral endoderm cells (ve). Mesenchyme (my); yolk sac cavity (ysc). Richardson's stain.

x400

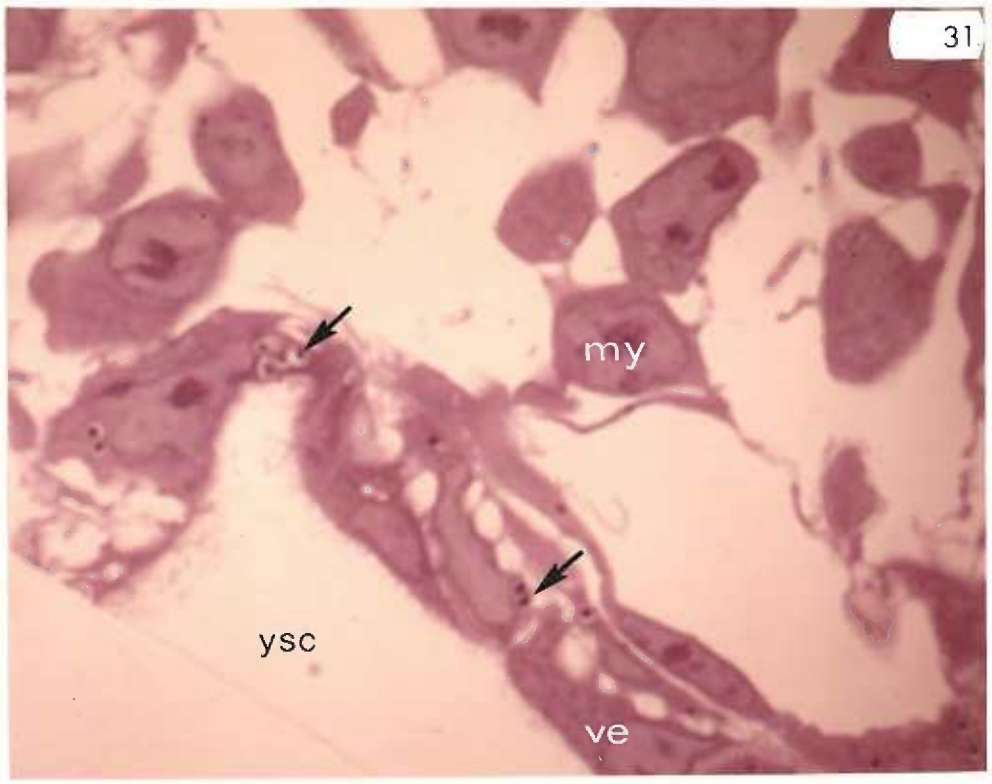
31
my
ysc
ve

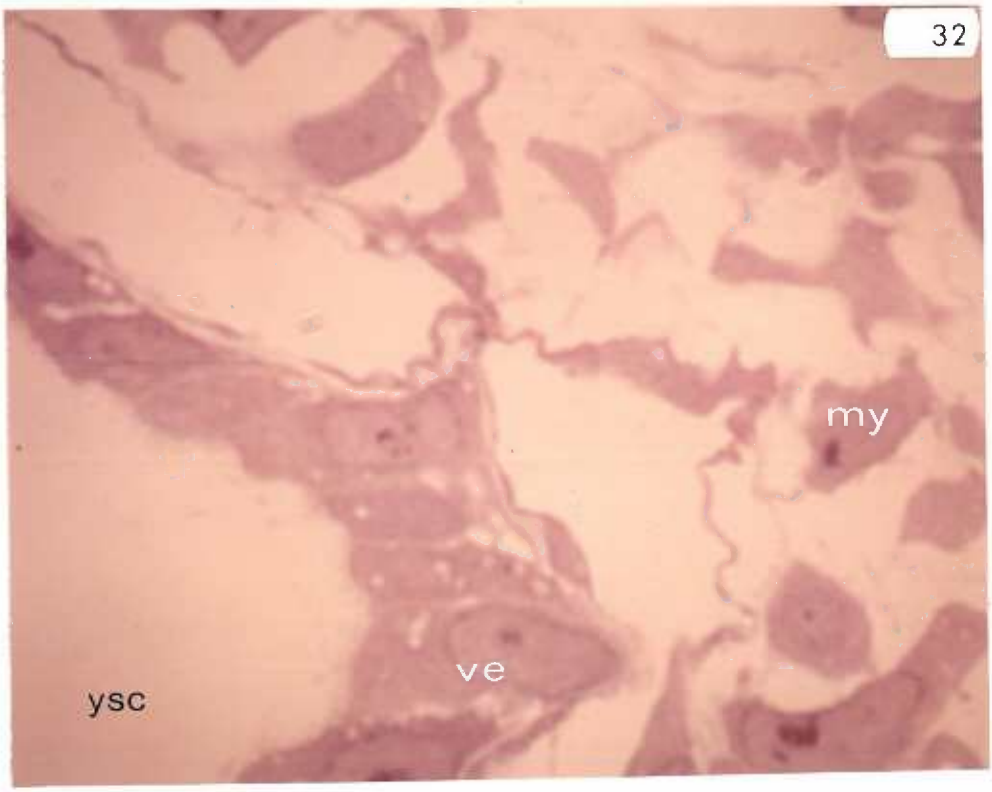
32
my
ve
ysc

Figure 33. Eleven-day hindgut, experimental.

The gut lumen (gl) contains polymers of fibrin (f) sectioned at various angles. The 230 Å periodicity characteristic of fibrin is clearly visible in one longitudinal view of a fibrin strand (double arrows). A transverse view of the fibrin polymer shows the electron-dense outer sheath and the central pale area (arrow).

x20,000

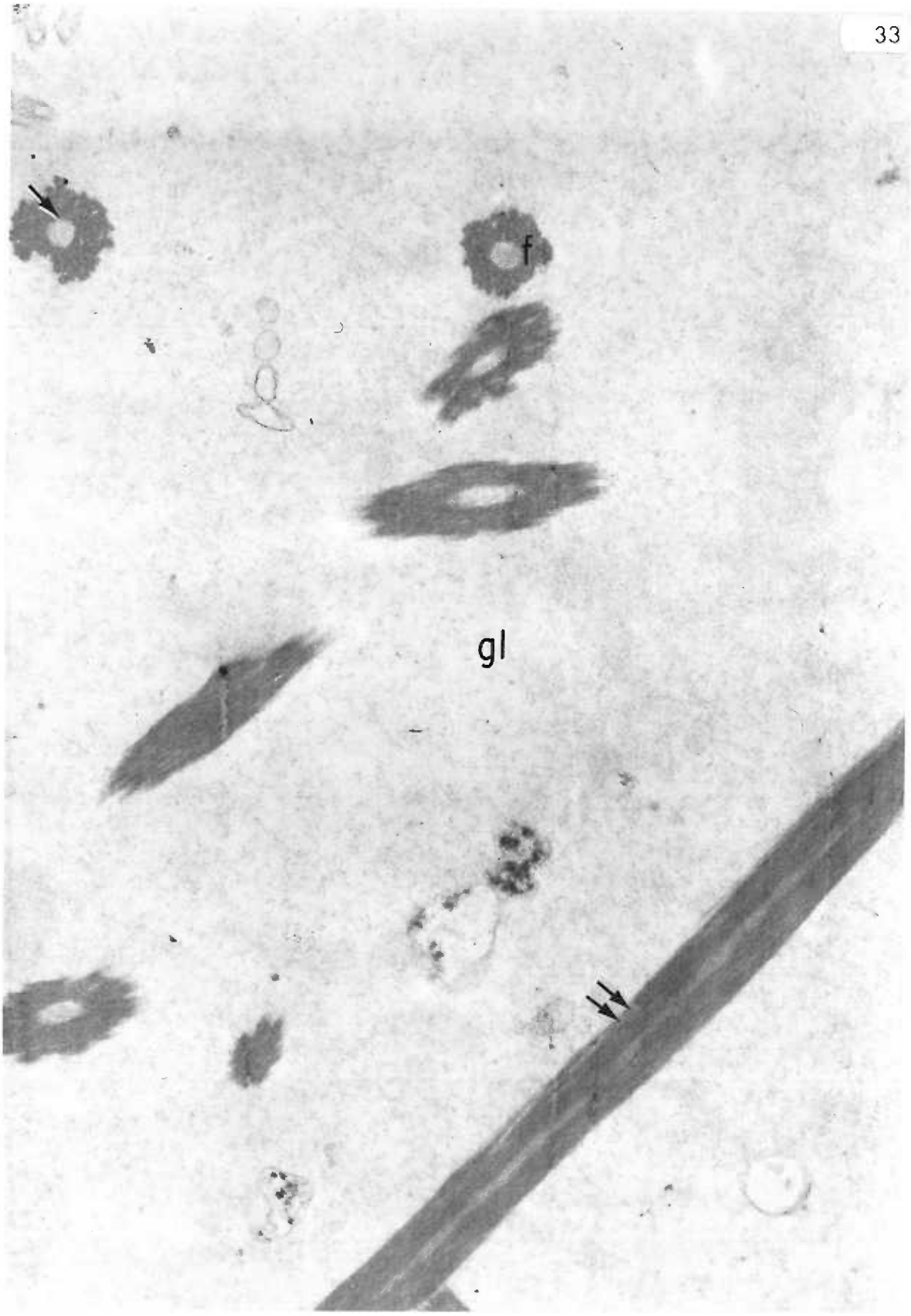
f
gl

Figure 34. Eleven-day hindgut, experimental.

A large fibrin polymer of 900 mμ diameter lies in the gut lumen (gl) near an epithelial cell. The axial periodicity of 230 Å is clearly visible (double arrows). The central 400 Å pale area of this polymer is filled with an electron-dense, granular material (arrow). Intercellular space (is).

x20,000

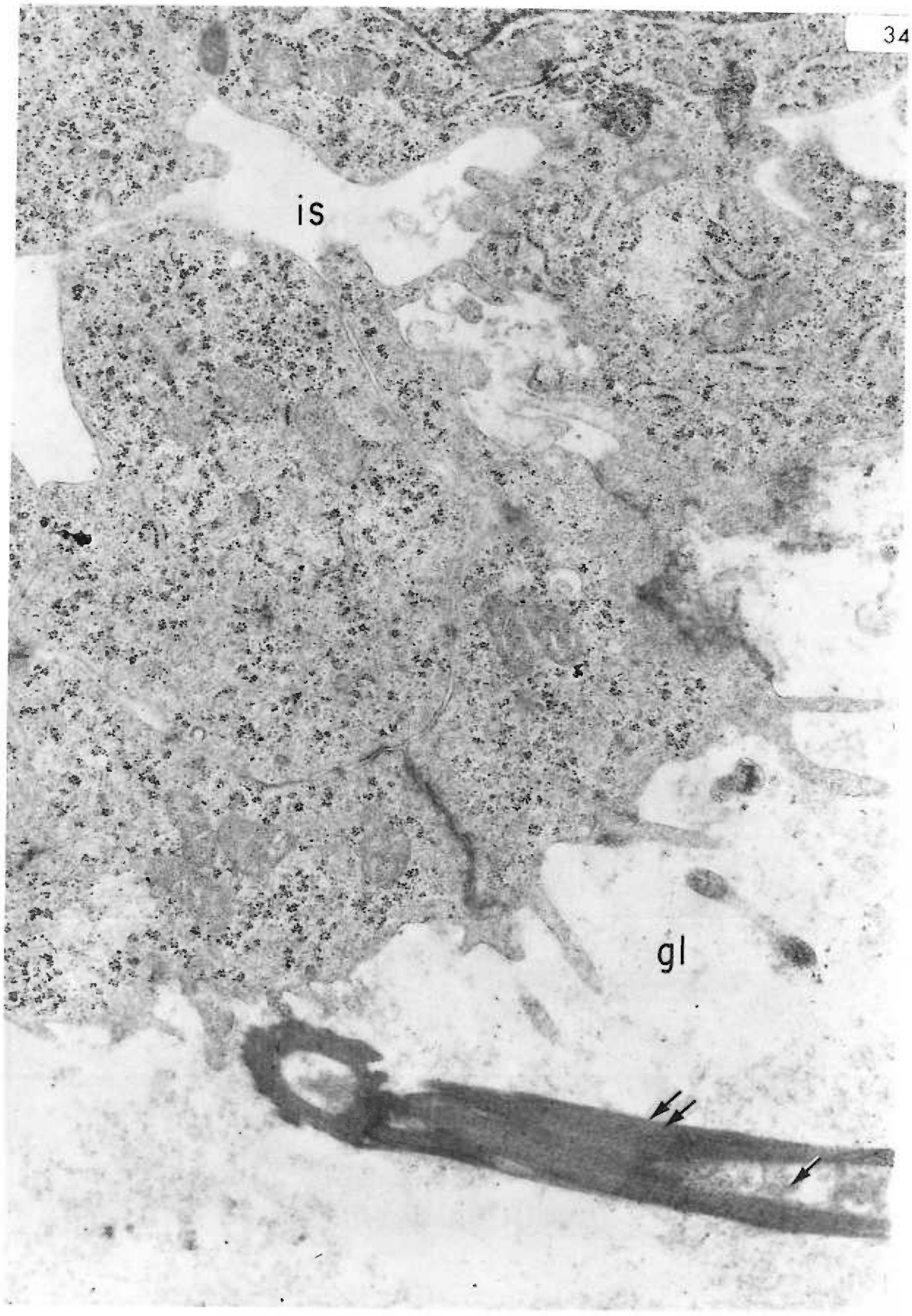
is
gl

Figure 35. Eleven-day hindgut, experimental.
Numerous aggregations of glycogen (gly) fill the ctyoplasm of the gut epithelial cells. A few, large alpha glycogen rosettes (arrows) of high electron density are scattered throughout the cell matrix; additional rosettes (double arrow) occur in the intercellular space (is).

x29,000

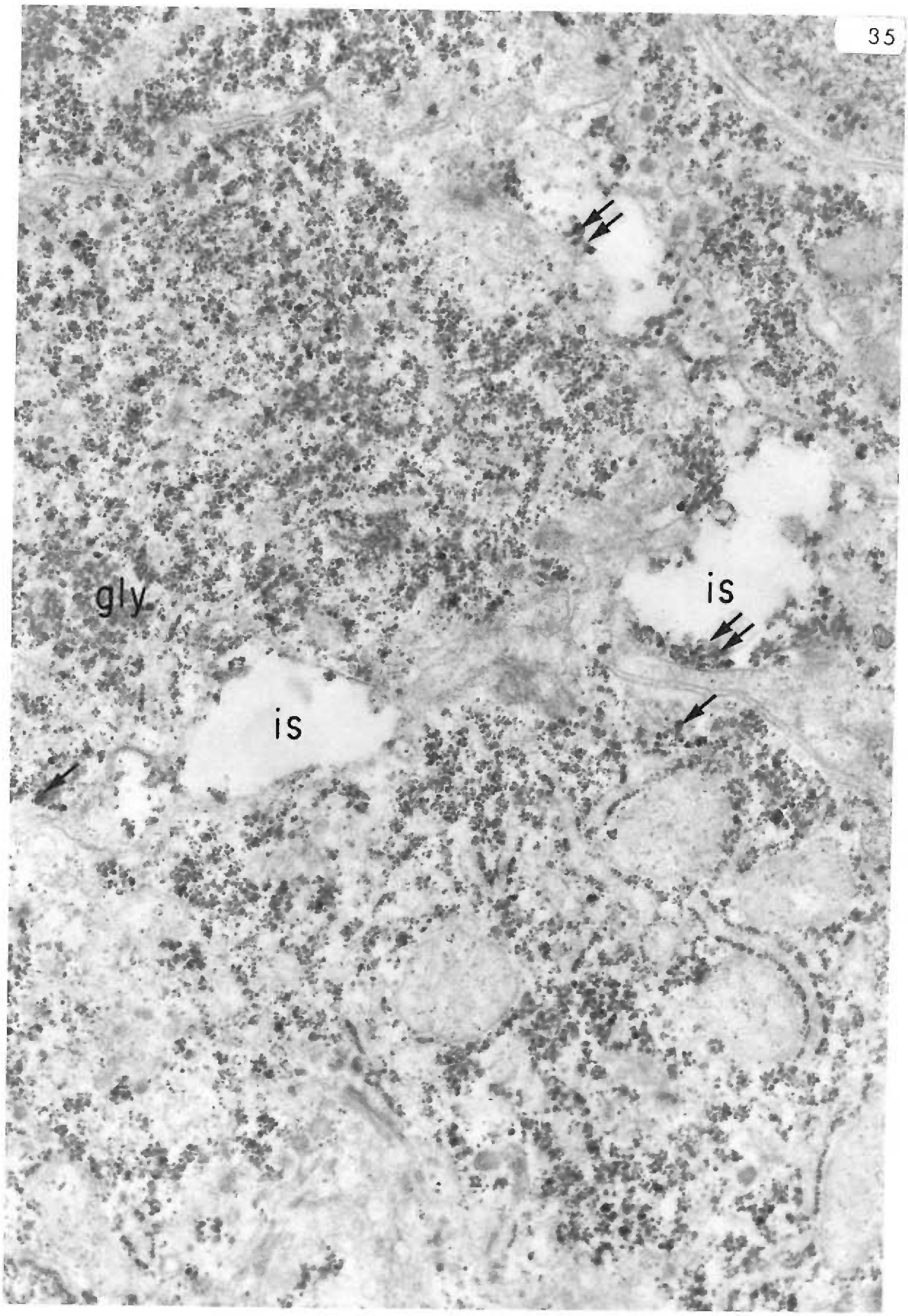
gly
is
is

Figure 36. Eleven-day hindgut, experimental.

An endoderm cell contains three "dye-like" vacuoles (dv) in its cytoplasm. These vacuoles exhibit a dense, homogeneous material which is surrounded by a clear peripheral area.

x40,000

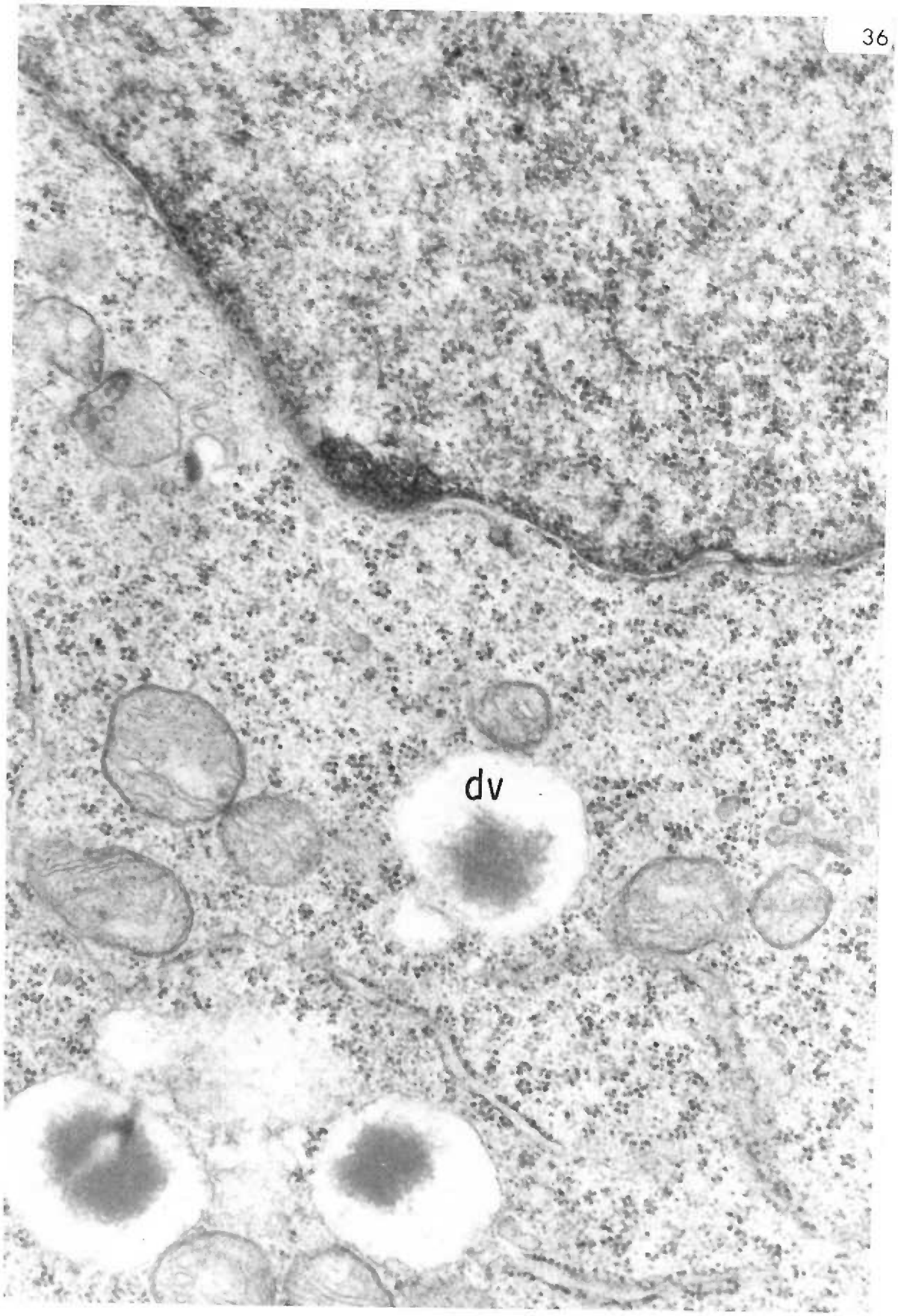
dv

Figure 37. Twelve-day hindgut, experimental.

The gut lumen (gl) contains a number of fibrin strands (f) in transverse section. One large polymer shows a central area (arrow) containing a fine granular material. A few of the fibrin strands do not exhibit a pale central area. Debris (d).

x20,000

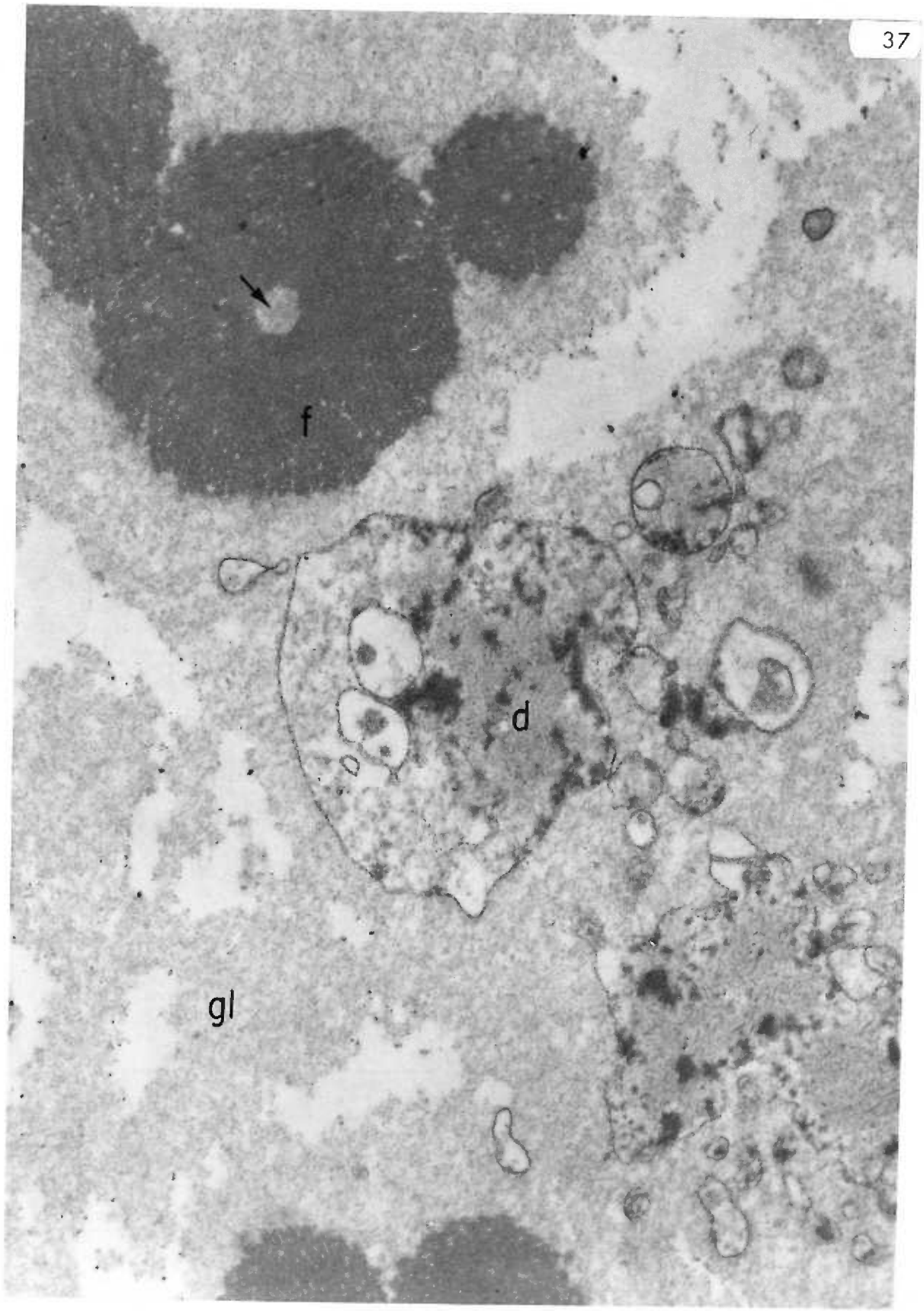
f
d
gl

Figure 38. Twelve-day hindgut, experimental.

Large accumulations of glycogen (gly) fill the cytoplasm of the endoderm cells. Cytoplasmic organelles are usually seen at the periphery of such extensive deposits.

x29,000

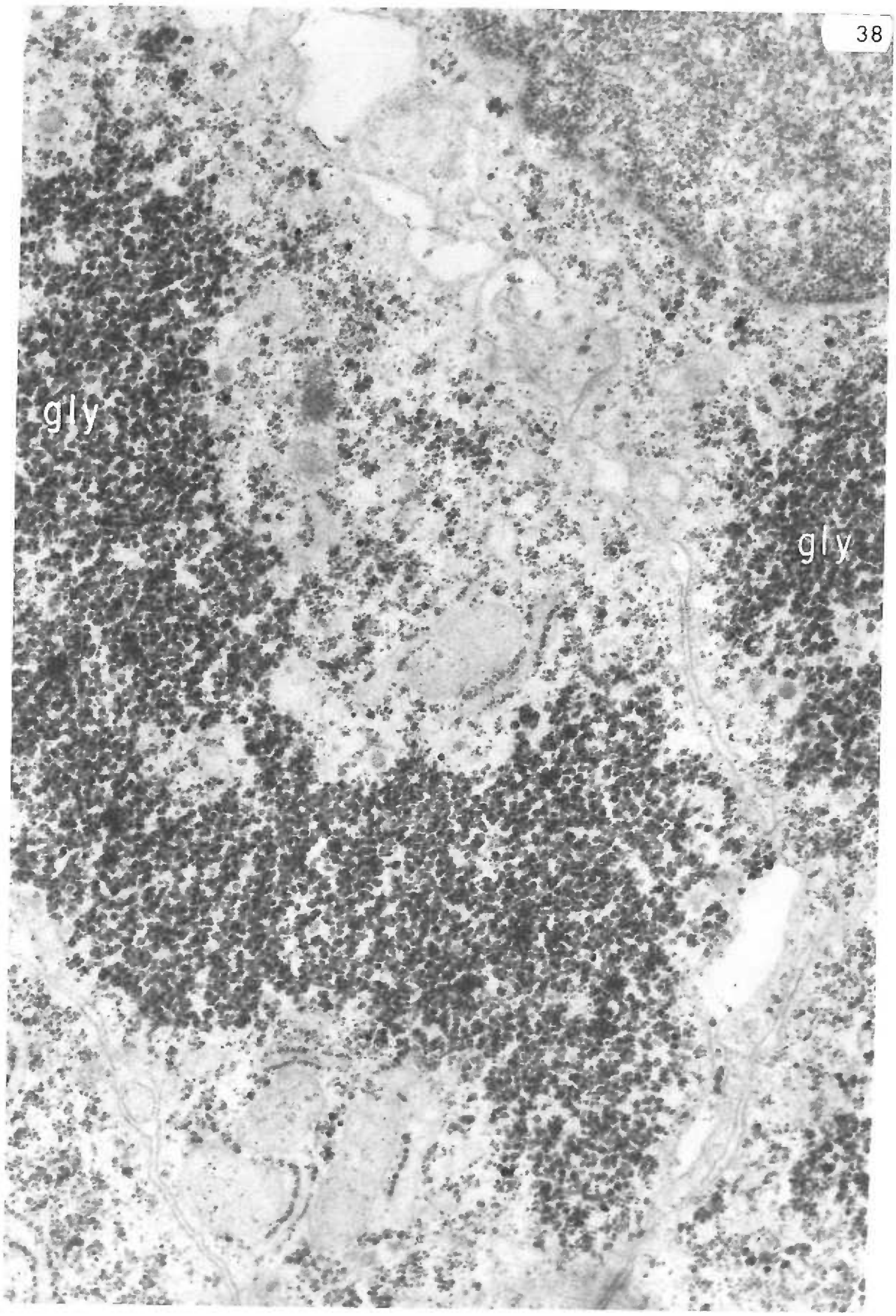
38
gly
gly

Figure 39. Twelve-day hindgut, experimental.

Scattered deposits of glycogen (gly) fill the cytoplasm of the gut endoderm cells. Some electron-dense alpha rosettes of glycogen (arrows) are visible. Mitochondria (m) and rough endoplasmic reticulum have poorly defined membranes. Gut lumen (gl).

x29,000

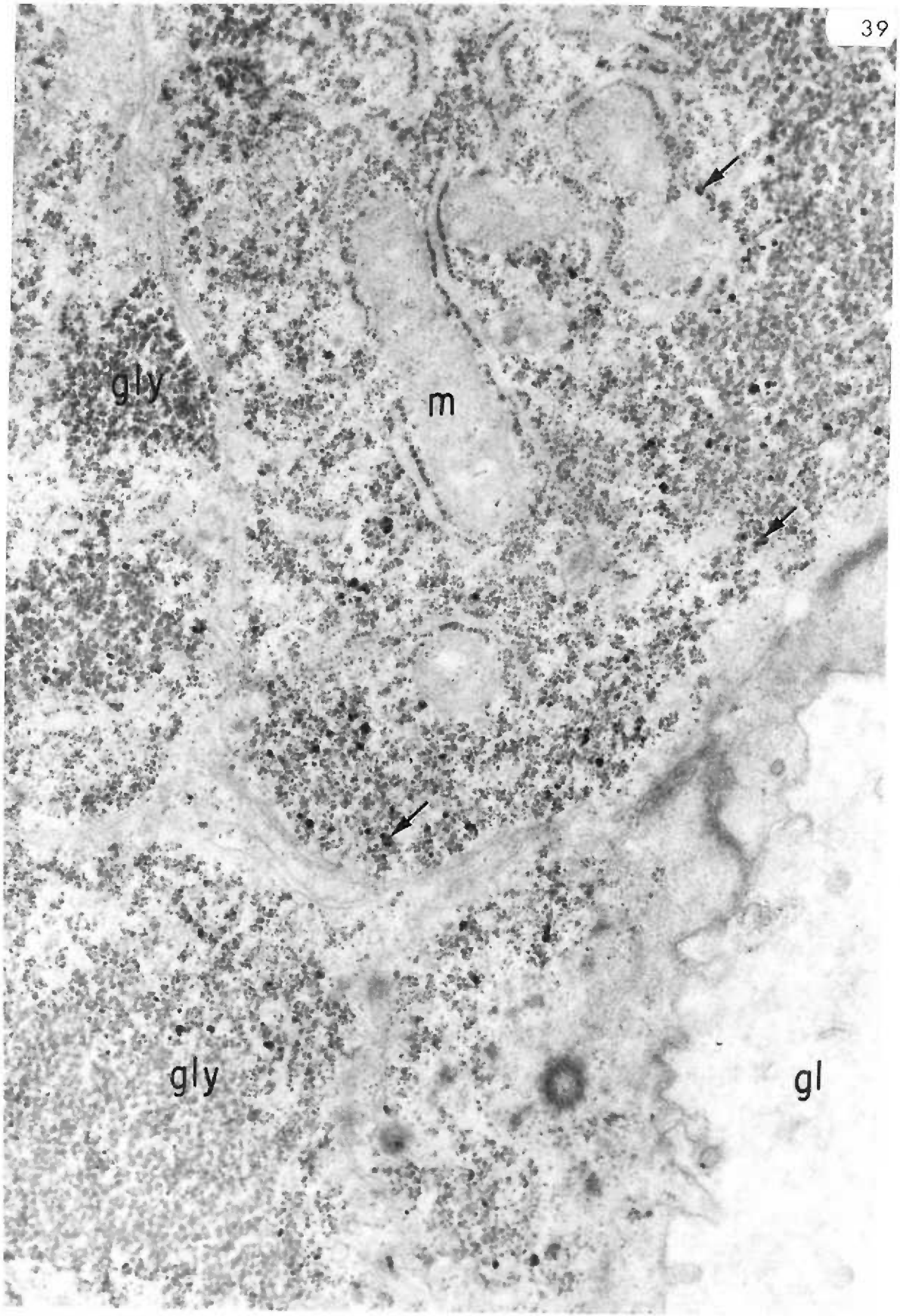
gly
m
gly
gl

Figure 40. Twelve-day hindgut, experimental.

A large glycogen deposit (gly) lies at the edge of the epithelial cell adjacent to the intercellular space (is). Alpha rosettes (arrows) of glycogen appear in the intercellular space.

x40,000

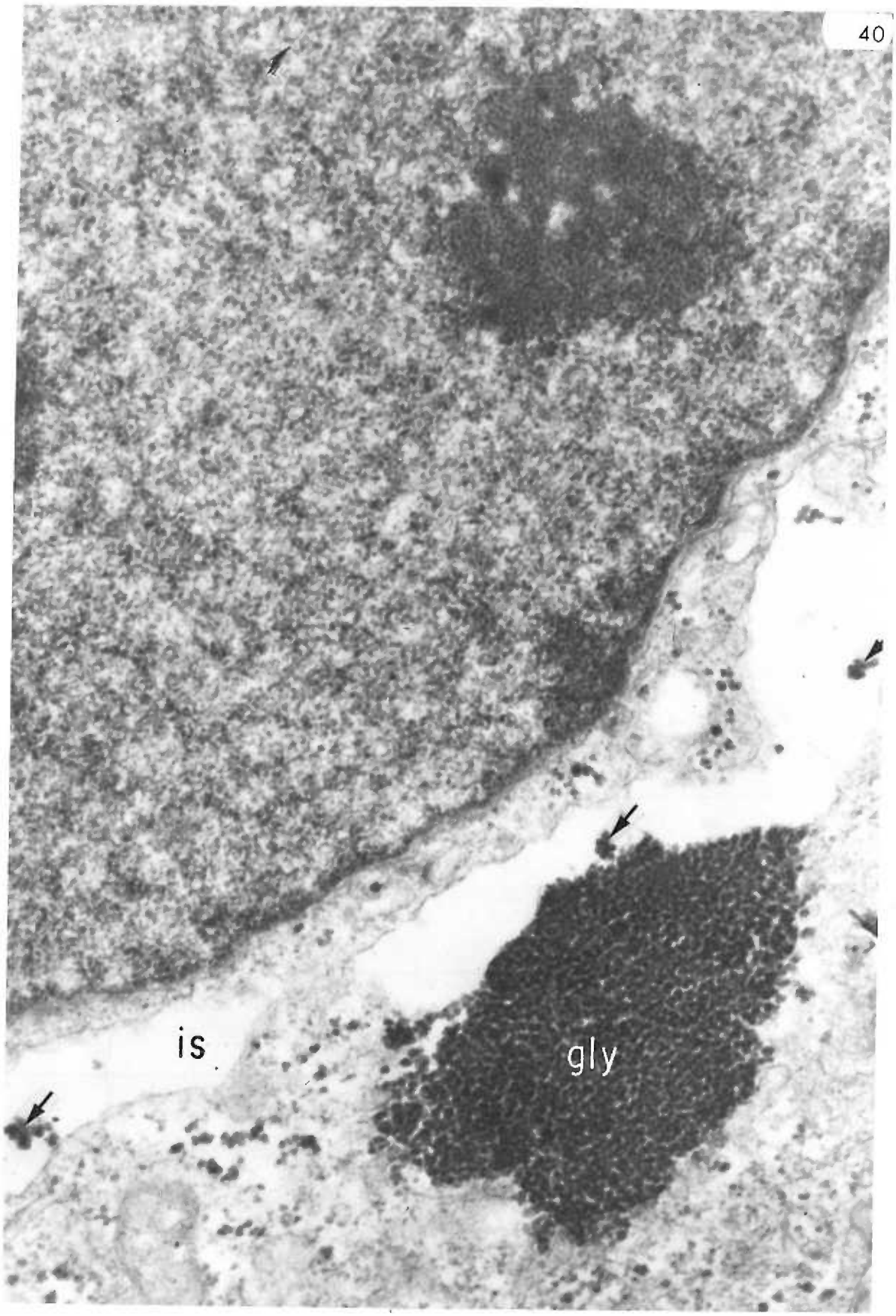
is
gly

Figure 41. Twelve-day hindgut, experimental.
The endoderm cells surrounding the gut lumen (gl) exhibit sites of intensely positive-PAS reaction (arrows) which correspond in morphology to glycogen deposits observed in electron micrographs (Figures 38, 39). Additional sites of positive reaction occur in the notocord (no). Periodic acid-Schiff stain.

x400

Figure 42. Twelve-day hindgut, control.
A generalized PAS-positive reaction is seen in the endoderm cells surrounding the gut lumen (gl). No intensely positive-PAS reaction sites are present. Periodic acid-Schiff stain.

x400

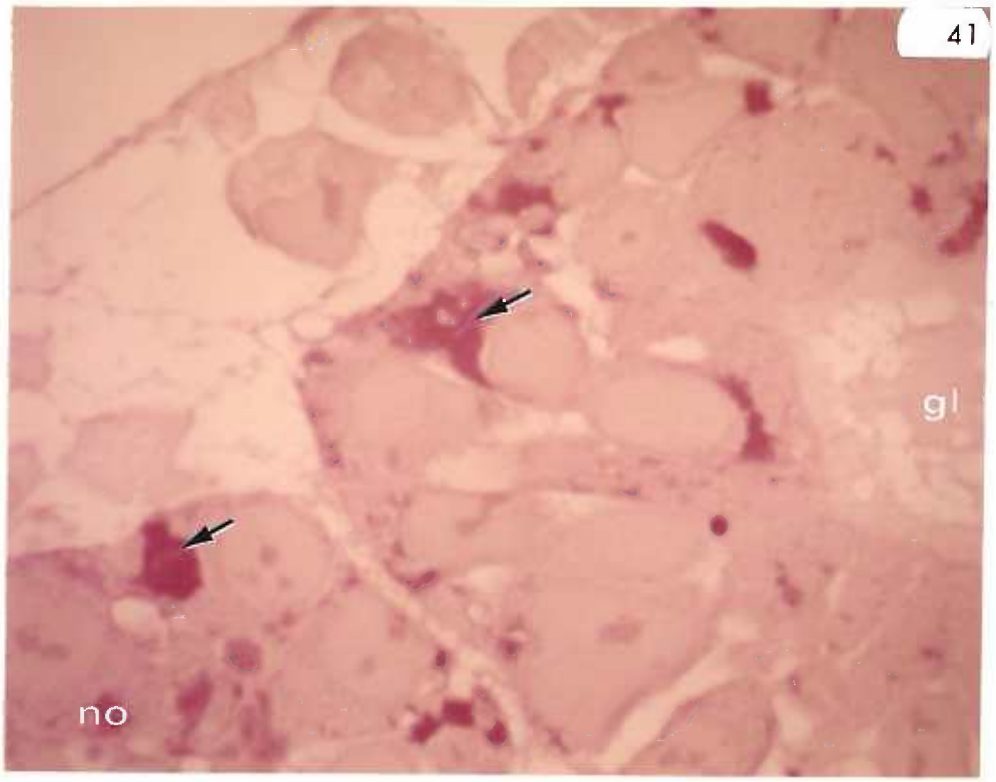
41
gl
no

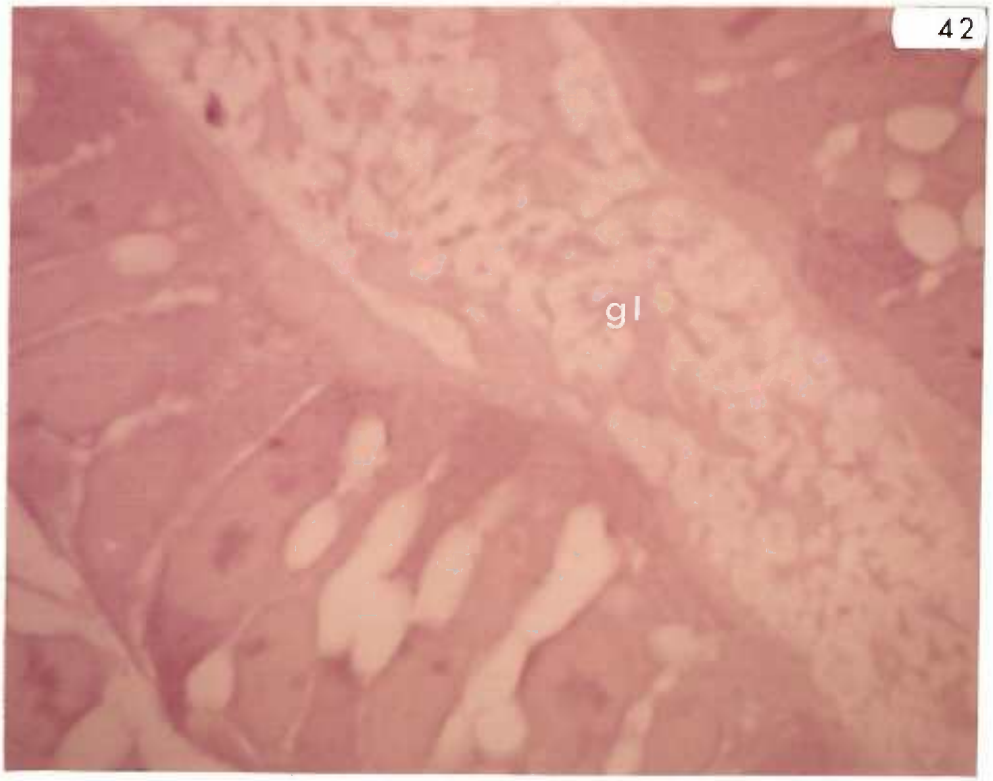
42
gl

Figure 43. Twelve-day hindgut, experimental.

Only a few glycogen particles are present in the cell cytoplasm following alpha-amylase digestion. Ribosomes are still bound to elements of the endoplasmic reticulum (arrows). Golgi complex (Go). Alpha-amylase digestion.

x29,000

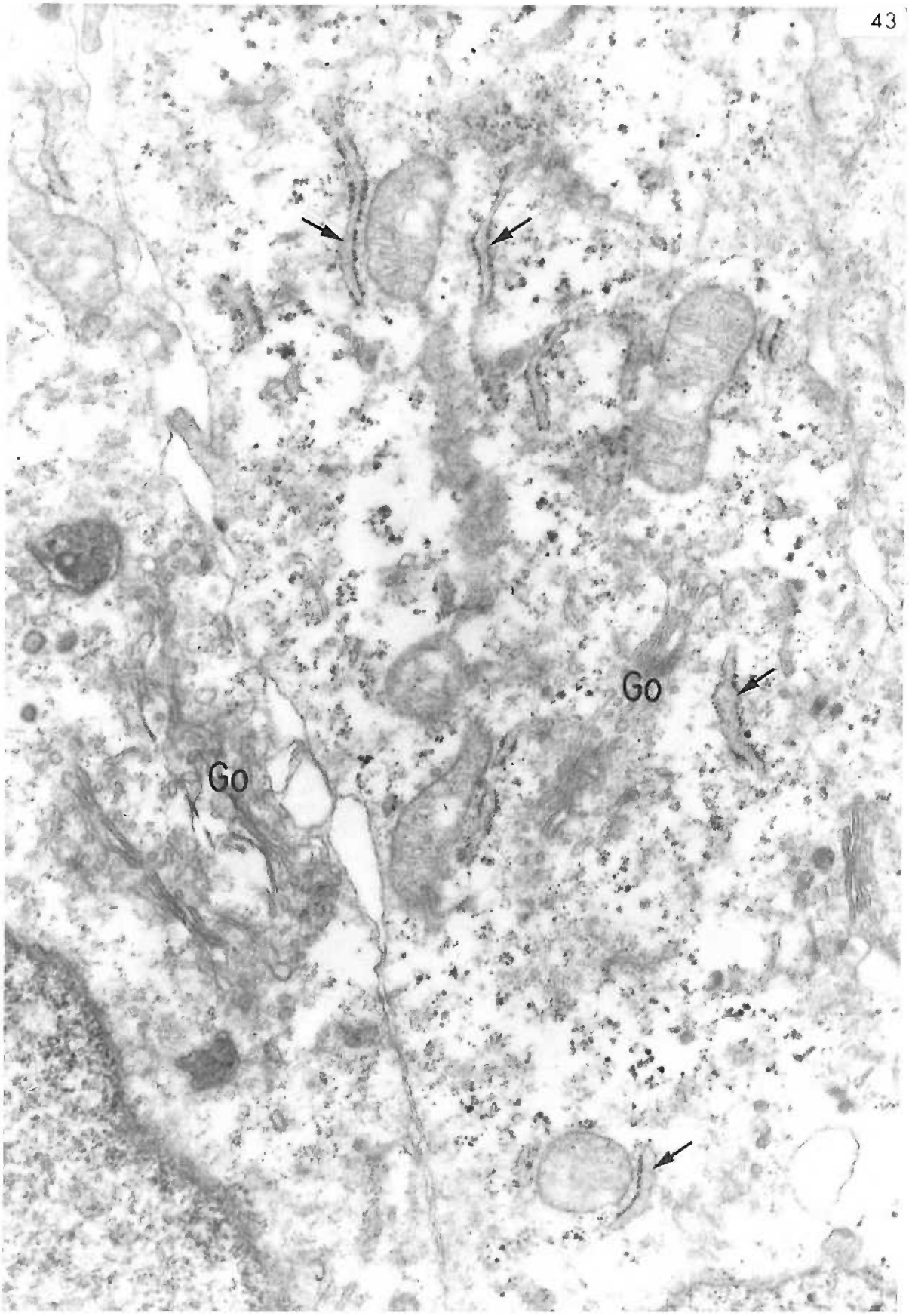
Go
Go

Figure 44. Twelve-day hindgut, experimental.

Following alpha-amylase digestion, no glycogen particles are present in the cytoplasm of the gut endoderm. Free and bound ribosomes (rer) are present. Mitochondria (m); Golgi complex (Go); gut lumen (gl). Alpha-amylase digestion.

x29,000

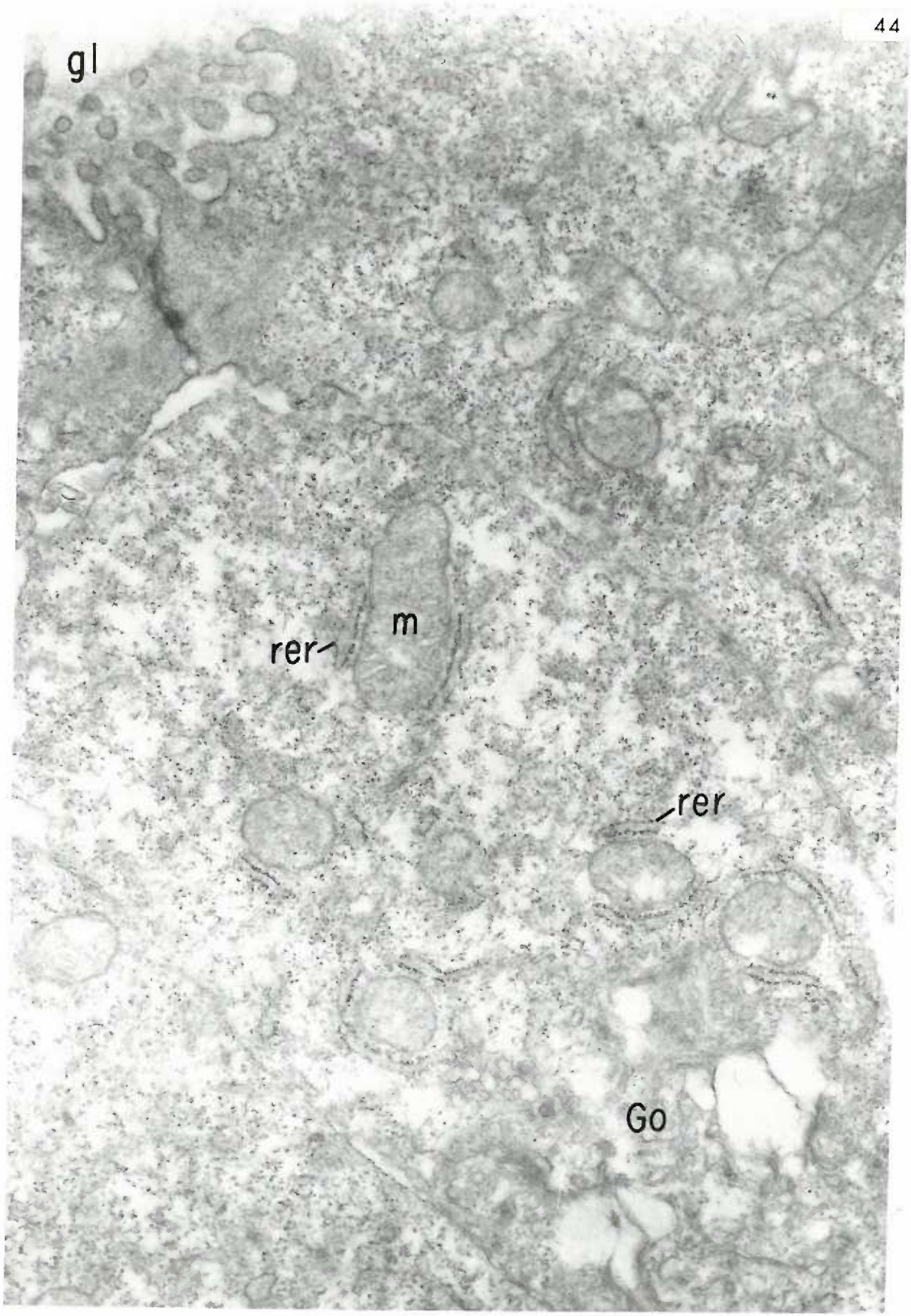
gl
m
rer
rer
Go

Figure 45. Twelve-day hindgut, experimental.

Glycogen particles (gly) remain in this endoderm cell following digestion in pancreatic ribonuclease. Some large alpha glycogen deposits (arrow) are visible. Elements of rough endoplasmic reticulum (rer) lack ribosomes. Free ribosomes are also absent. Ribonuclease digestion.

x54,000

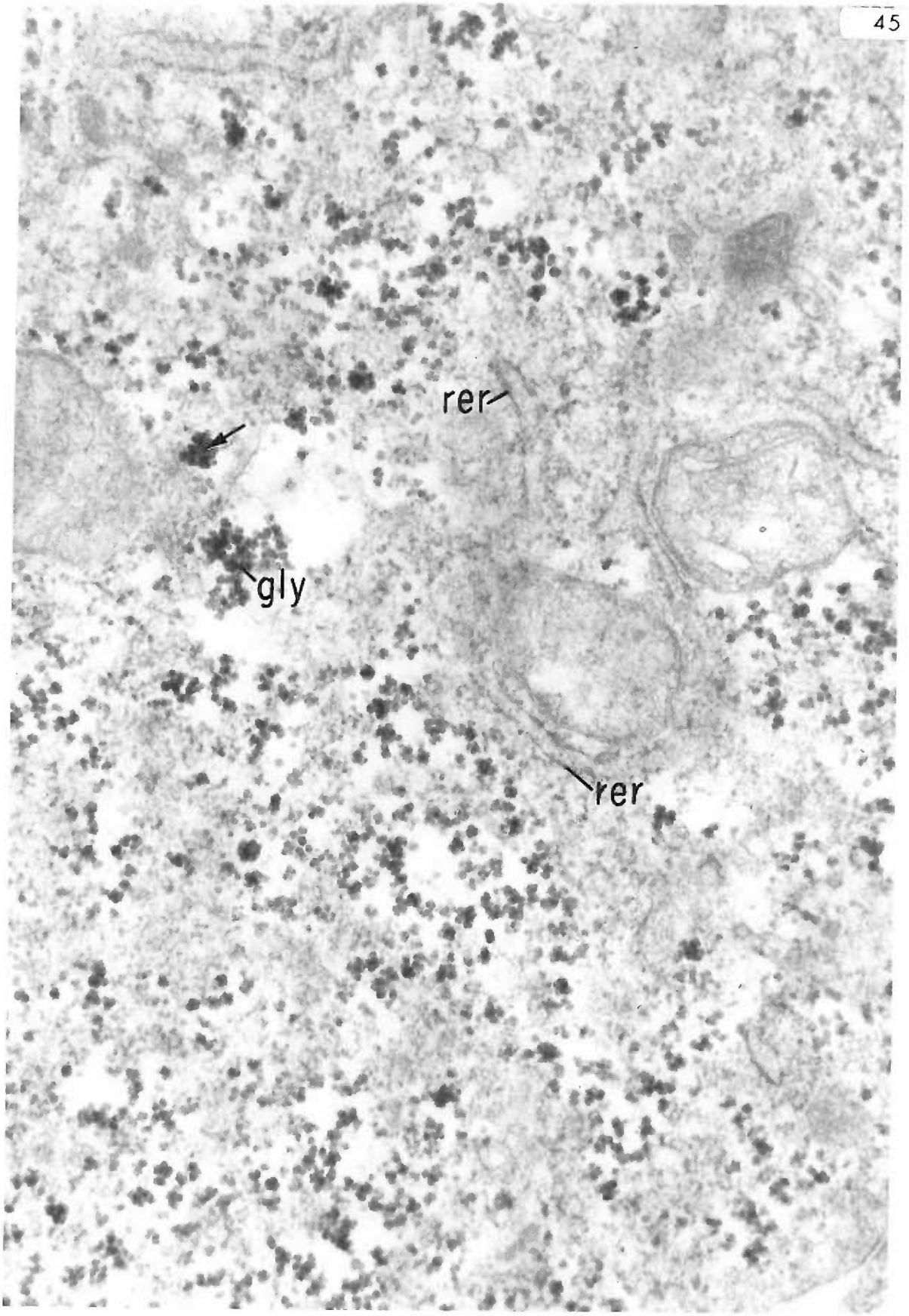
rer
gly
rer

Figure 46. Twelve-day hindgut, experimental.

Large alpha rosettes of glycogen (arrow) exist in the endoderm cell following ribonuclease digestion. Additional glycogen (gly) particles are evident in a neighboring cell. Intercellular space (is); gut lumen (gl). Ribonuclease digestion.

x29,000

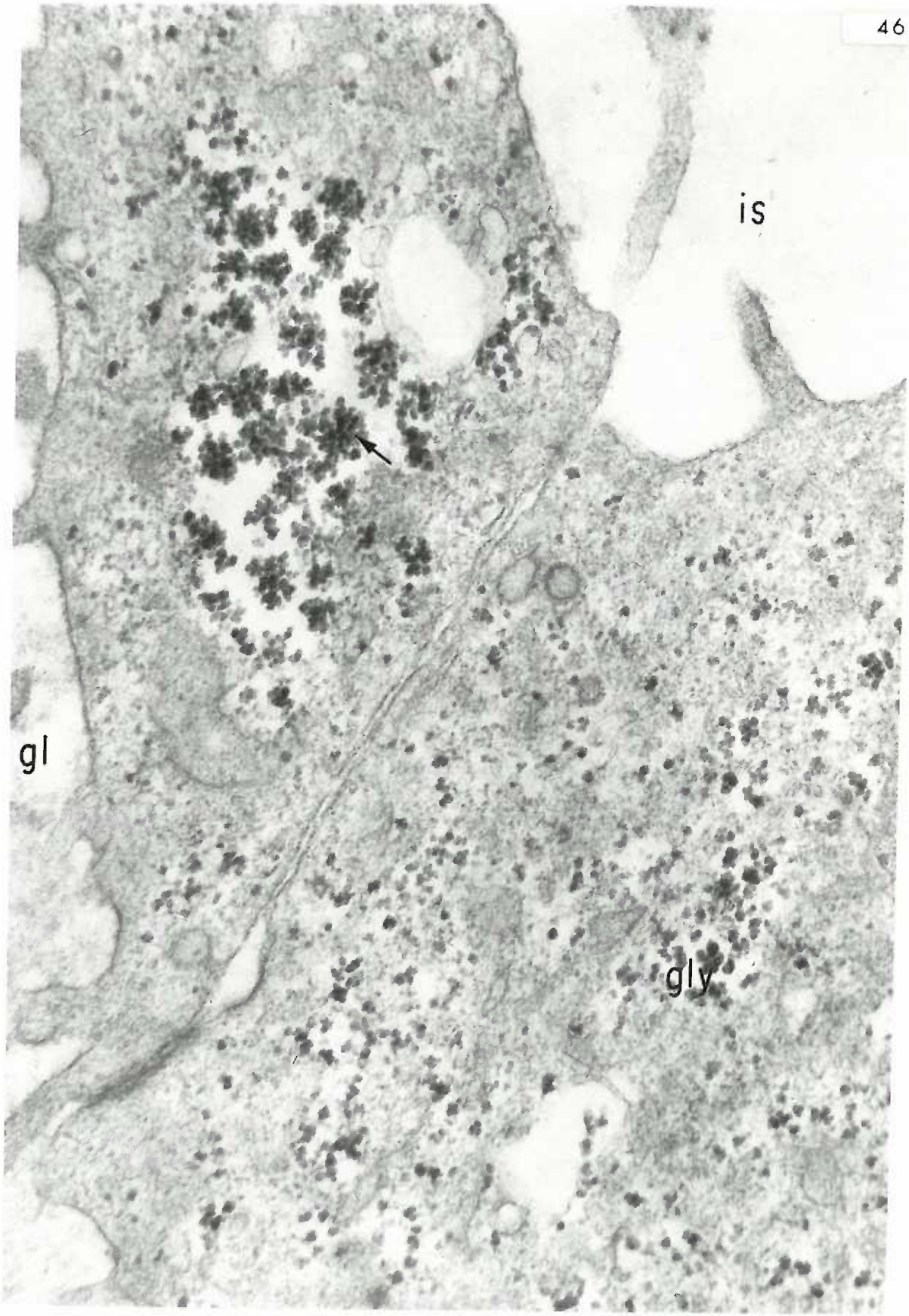
is
gl
gly

Figure 47. Twelve-day hindgut, experimental.

An endoderm cell in some phase of mitosis exhibits condensed chromatin material (ch). Also visible is a "dye-like" vacuole (dv) which is surrounded by glycogen particles (gly).

x40,000

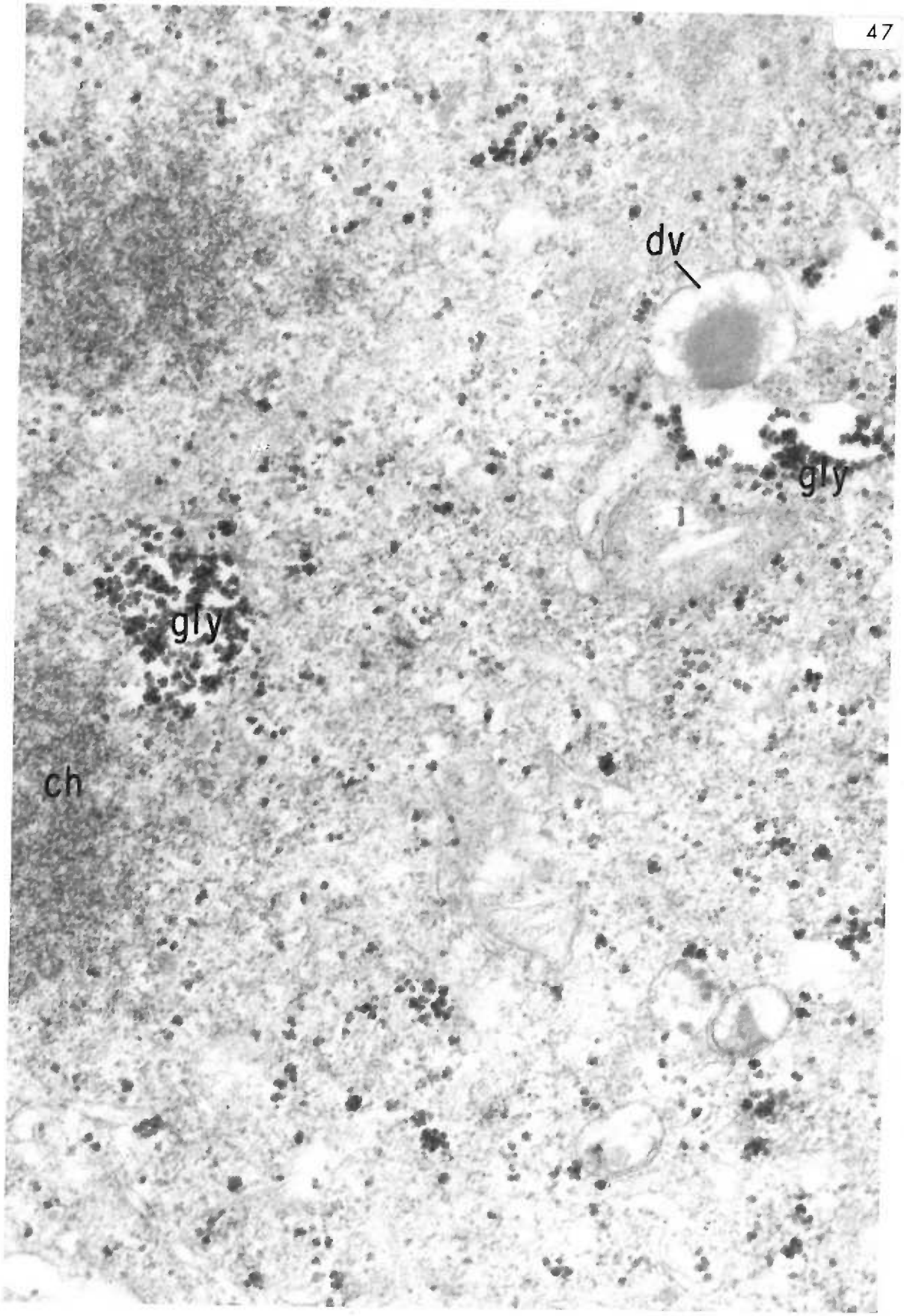
dv
gly
gly
ch

Figure 48. Twelve-day hindgut, experimental.
Following treatment with sodium hydrosulfite, a "dye-like" vacuole (dv) within a mesenchymal cell (my) exhibits a core of material more granular and less compact than it appears before such treatment. Nuclear chromatin material (arrow) is also more granular in appearance after such treatment. Intercellular space (is). Sodium hydrosulfite exposure.

x29,000

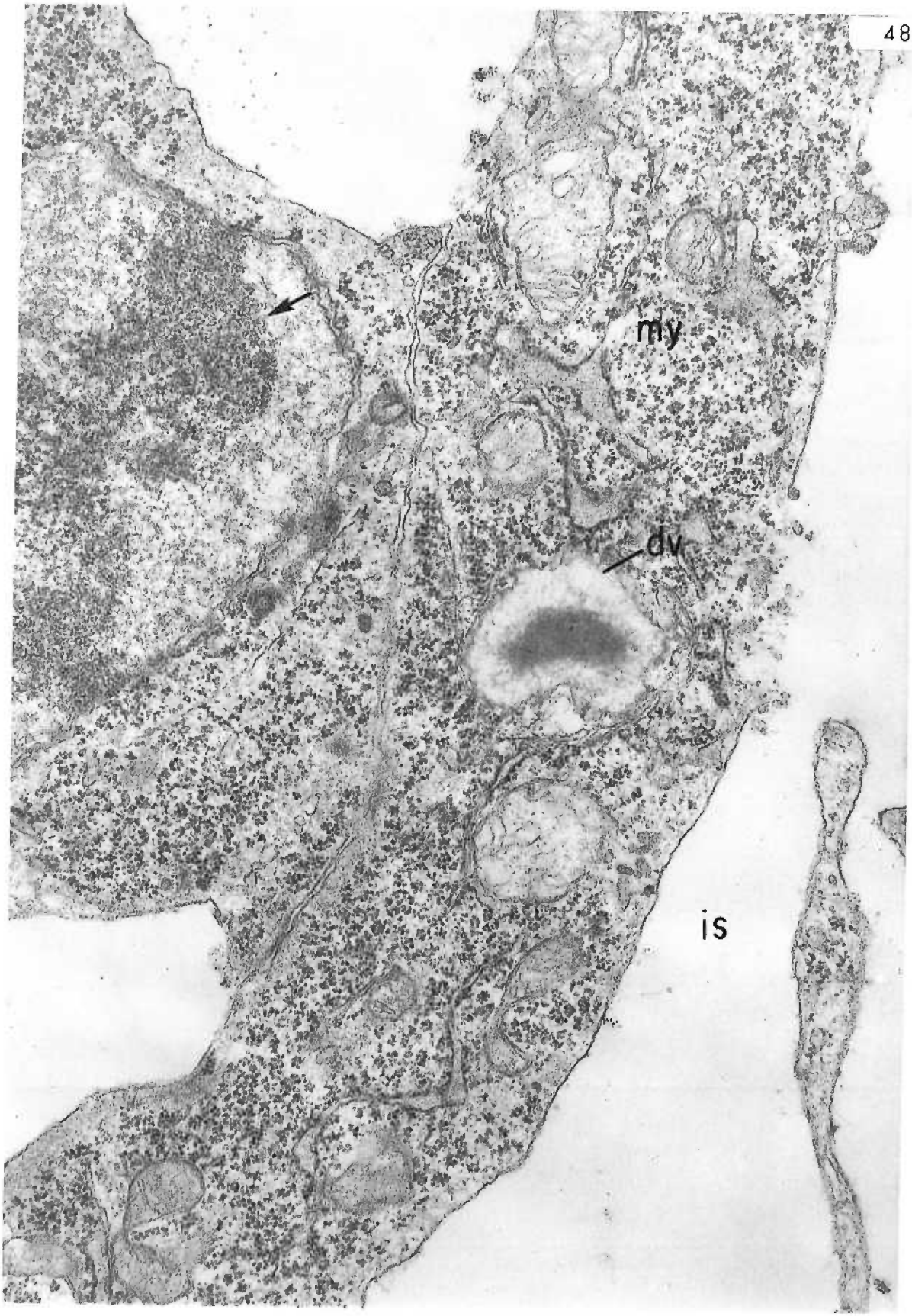
my
dv
is

Figure 49. Ten-day visceral endoderm of the presumptive gut, control.

The visceral endoderm (ve) exhibits microvilli (mv) which project into the yolk sac cavity (ysc). A single cell layer of splanchnic mesoderm (me) separates the visceral endoderm from the intra-embryonic coelom (ic). Intercellular space (is).

x29,000

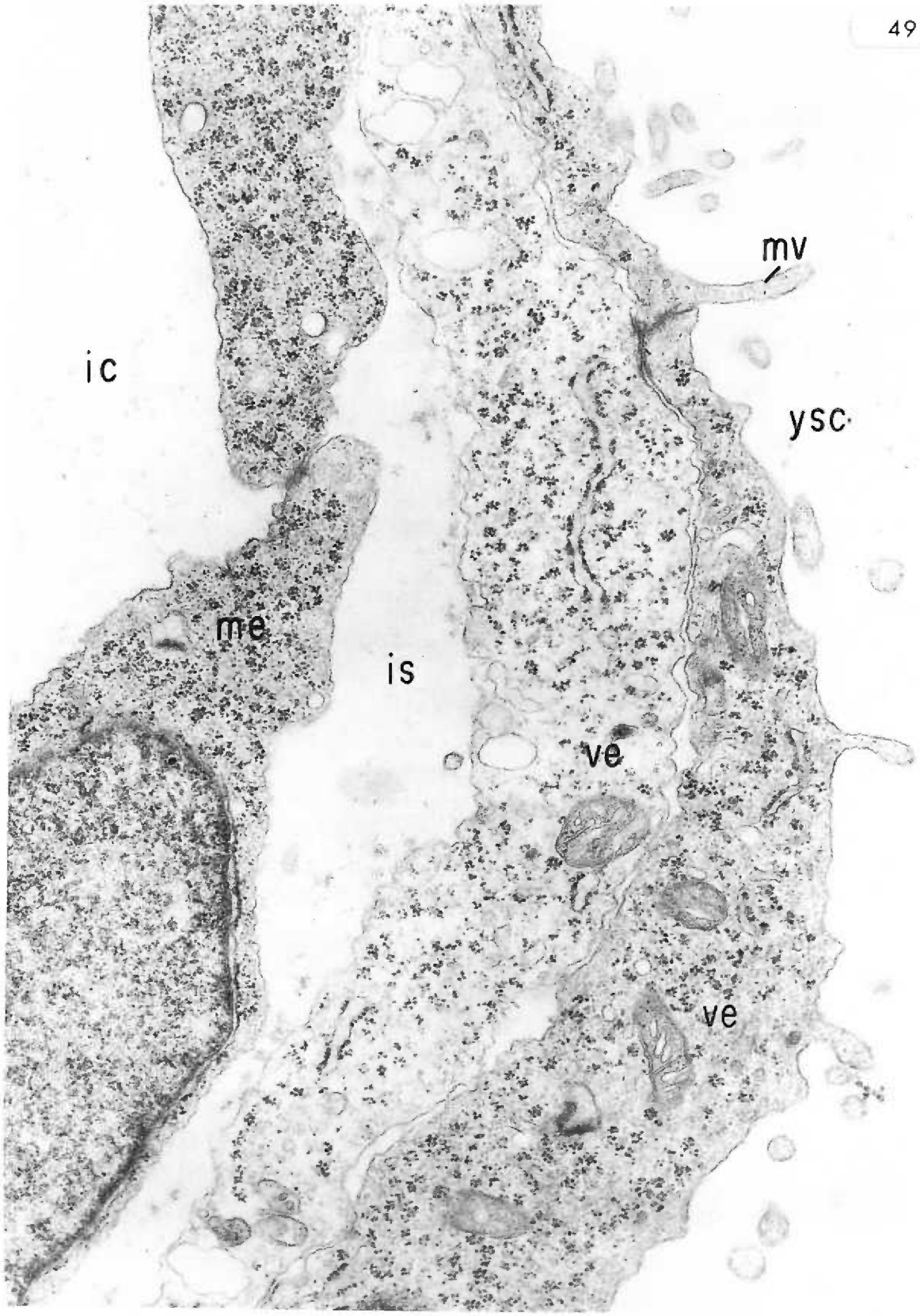
mv
ic
ysc
me
is
ve
ve

Figure 50. Eleven-day hindgut, control.

The hindgut epithelial cells display irregular microvillous projections into the gut lumen (gl). These cells contain large nuclei (n) with nuclear pores (arrows).

x12,000

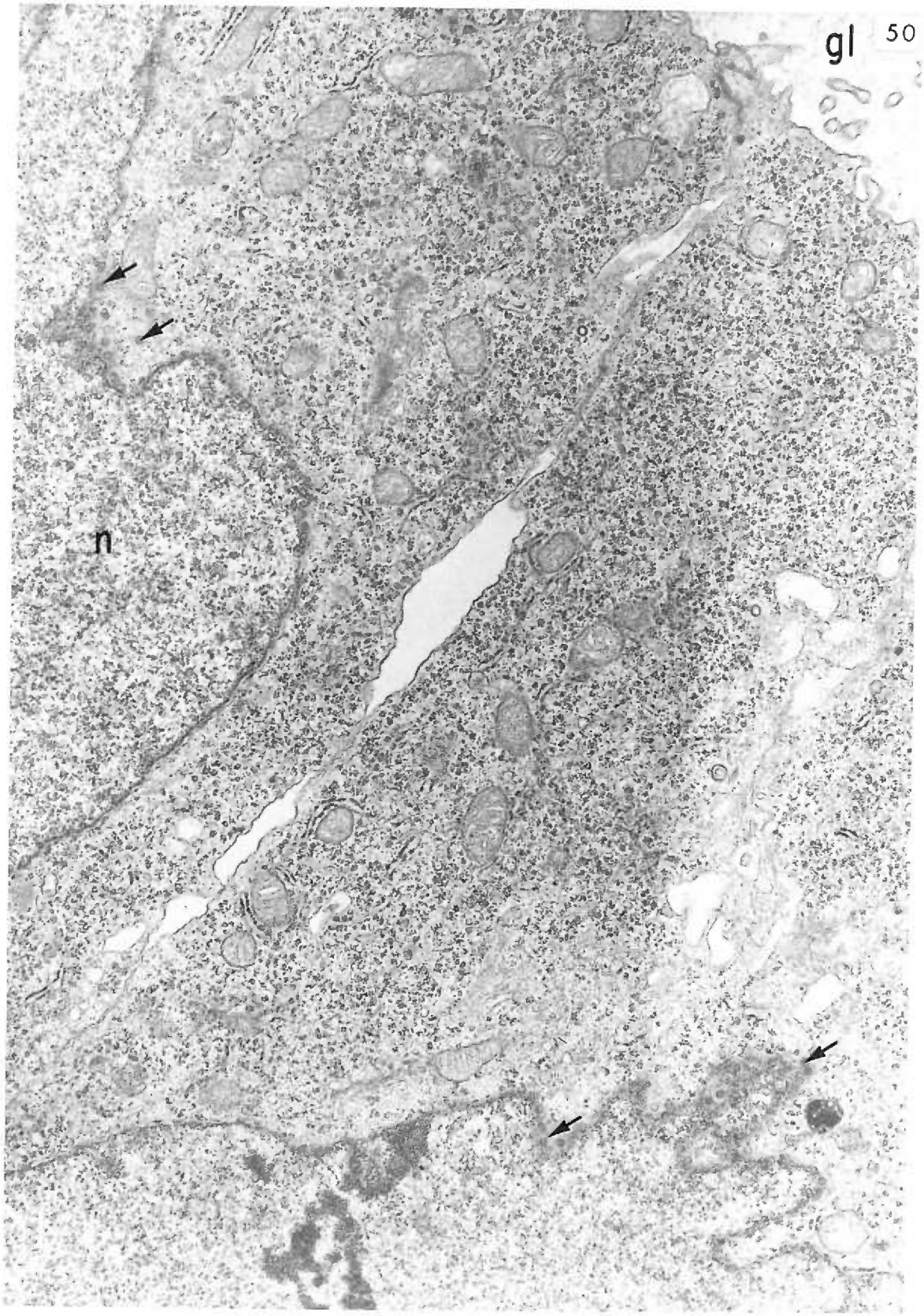
gl
50
n

Figure 51. Twelve-day hindgut, control.

Cellular debris (d) fills the gut lumen (gl). A degenerating cell projecting into the lumen exhibits a membranous junction (arrow) with a viable endoderm cell. Cross-sections of two fibrin-like structures (f) are visible.

x29,000

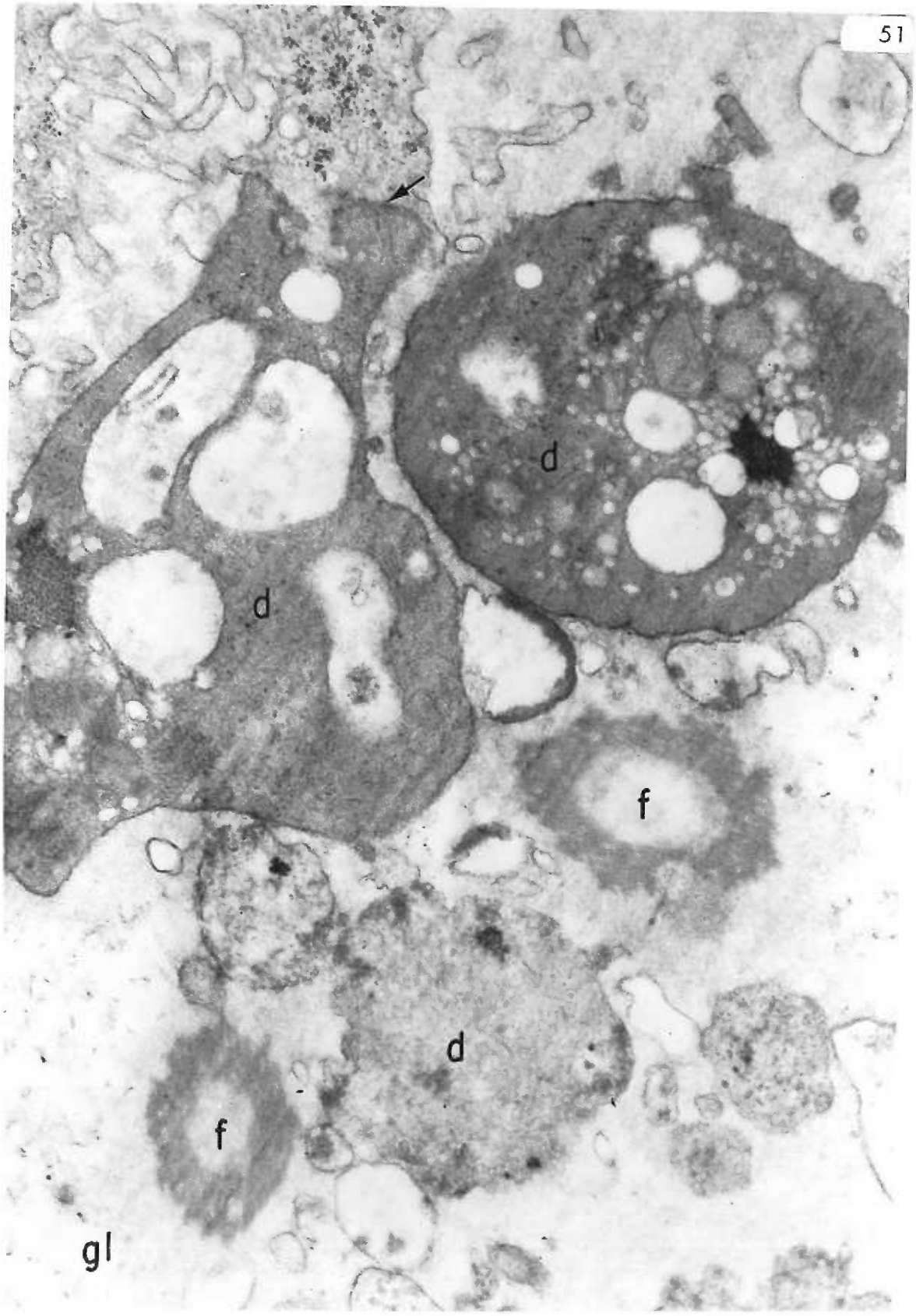
51
d
d
f
d
f
gl

Figure 52. Twelve-day hindgut, control.

The gut lumen (gl) is lined with a layer of simple columnar epithelium. Cellular debris (d) and a fine coagulum fill the lumen, into which microvilli (mv) project. Terminal bars (arrows) connect neighboring epithelial cells near their luminal ends. Some degree of interdigitation occurs between contiguous membranes. Long, oval mitochondria (m) are seen adjacent to strands of rough endoplasmic reticulum (rer).

x29,000

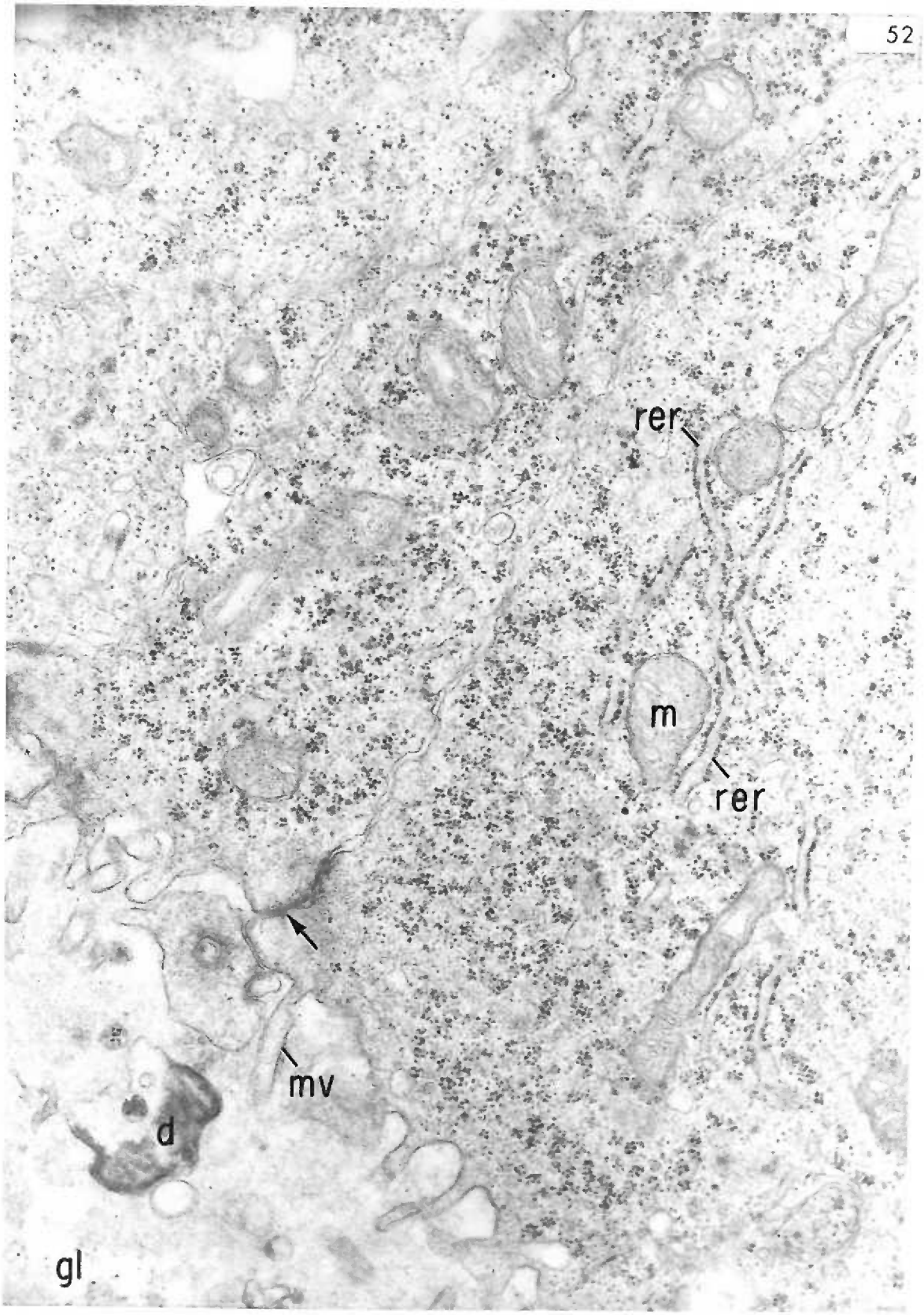
rer
m
rer
mv
d
gl

Figure 53. Eleven-day mesenchyme, experimental. Adjacent mesenchyme cells contain large deposits of pale, glycogen-like material (gly). Large residual bodies (rb) lie within two cells. Nucleus (n); intercellular space (is). Uranyl acetate stain.

x20,000

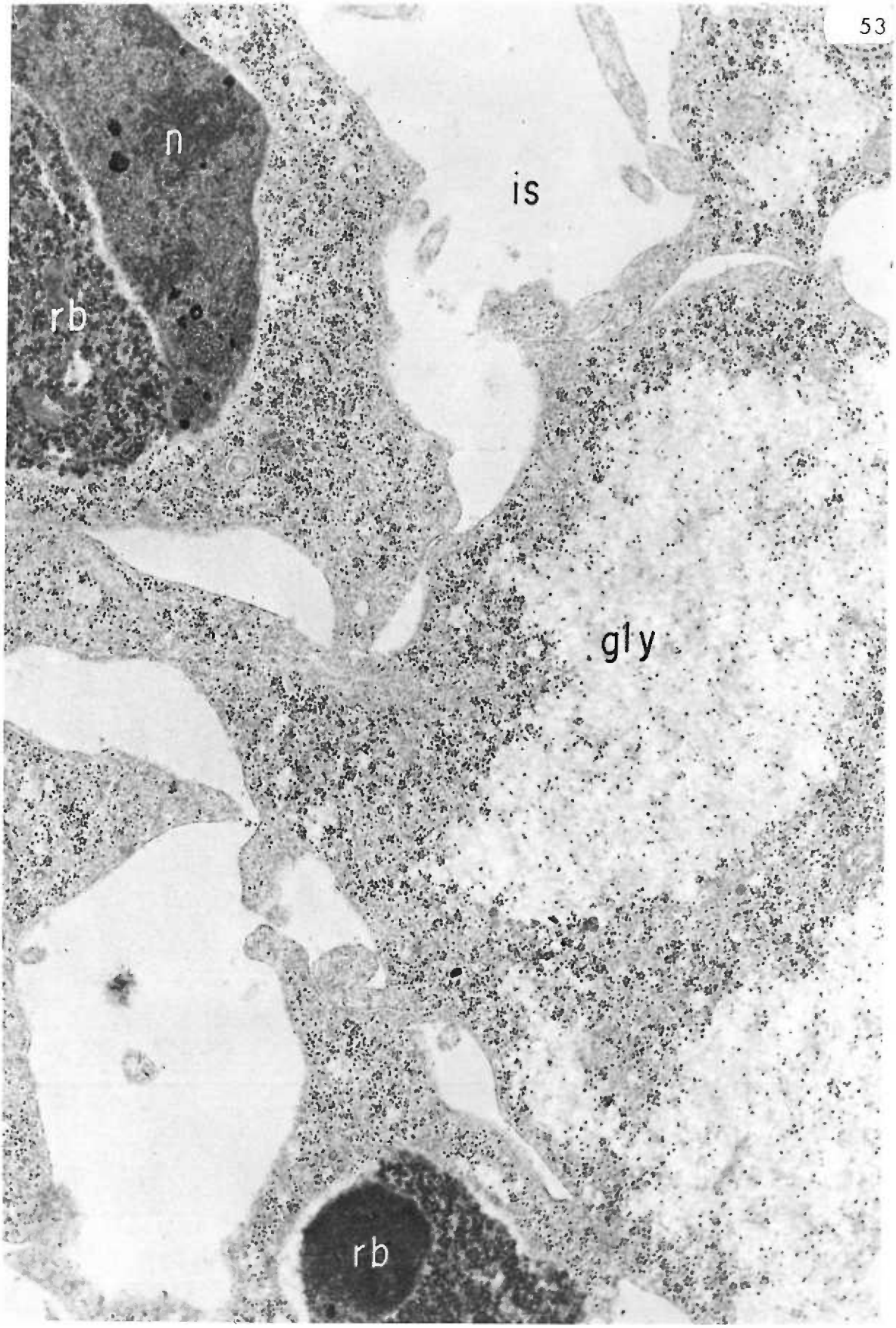
n
is
rb
gly
rb

Figure 54. Eleven-day mesenchyme, experimental. Mesenchyme cells contain large residual bodies (rb) with heterogeneous contents. A possible "dye-like" vacuole (dv) lies within one residual body. Two accumulations of glycogen-like (gly) material almost fill the remaining cytoplasm. Uranyl acetate stain.

x20,000

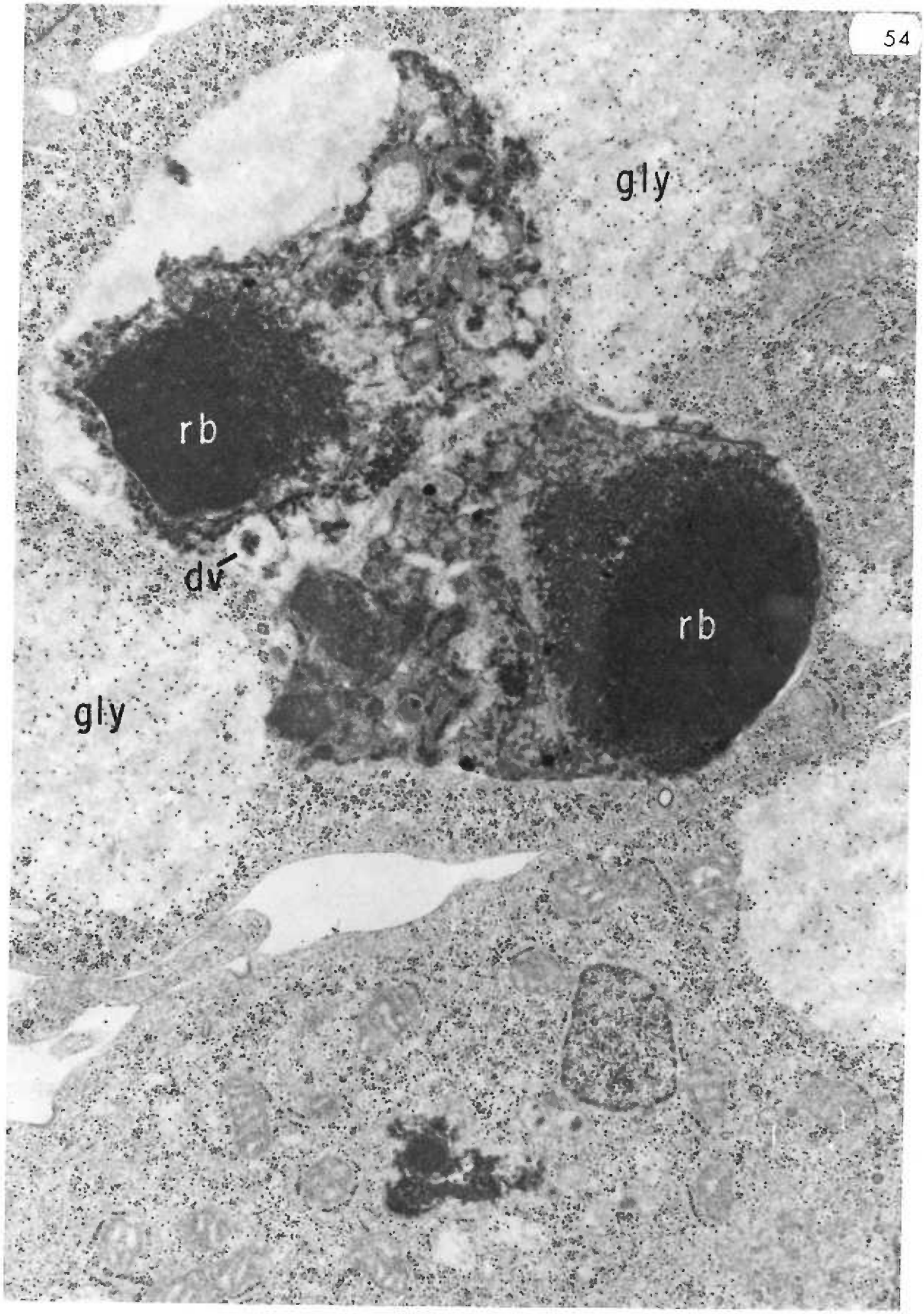
gly
rb
dv
rb
gly

Figure 55. Eleven-day mesenchyme, experimental.
The mesenchymal cells (my) exhibit residual bodies (rb) which contain a floccular material of high electron density. A group of "dye-like" vacuoles (dv) lies between two residual bodies. Nucleus (n); intercellular space (is).

x20,000

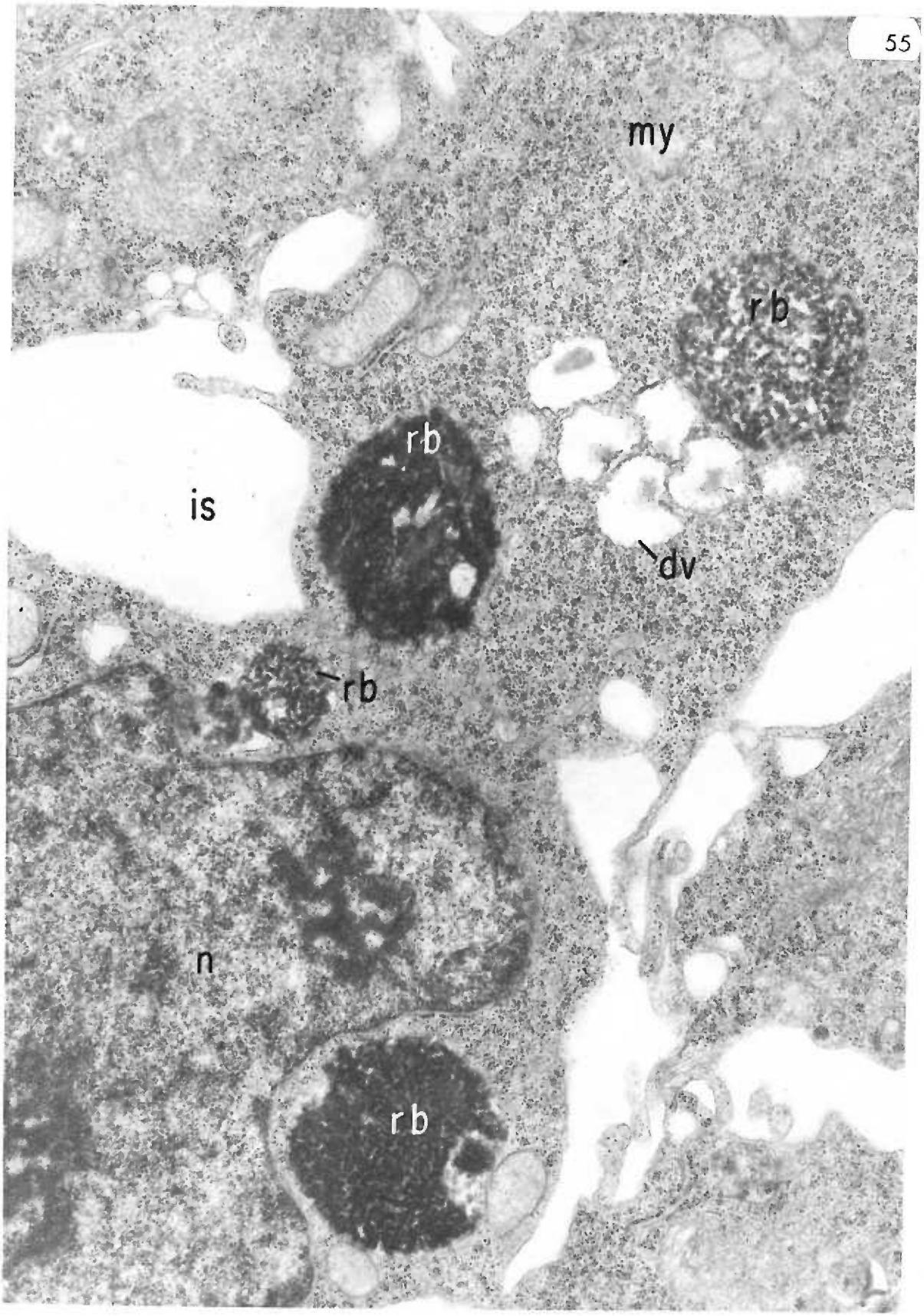
my
rb
rb
is
dv
rb
n
rb

Figure 56. Twelve-day mesenchyme, experimental.
Several mesenchyme cells (my) exhibit large residual bodies (rb) which contain electron-dense floccular materials. The stellate-shaped mesenchymal cells are separated by large intercellular spaces (is).

x12,000

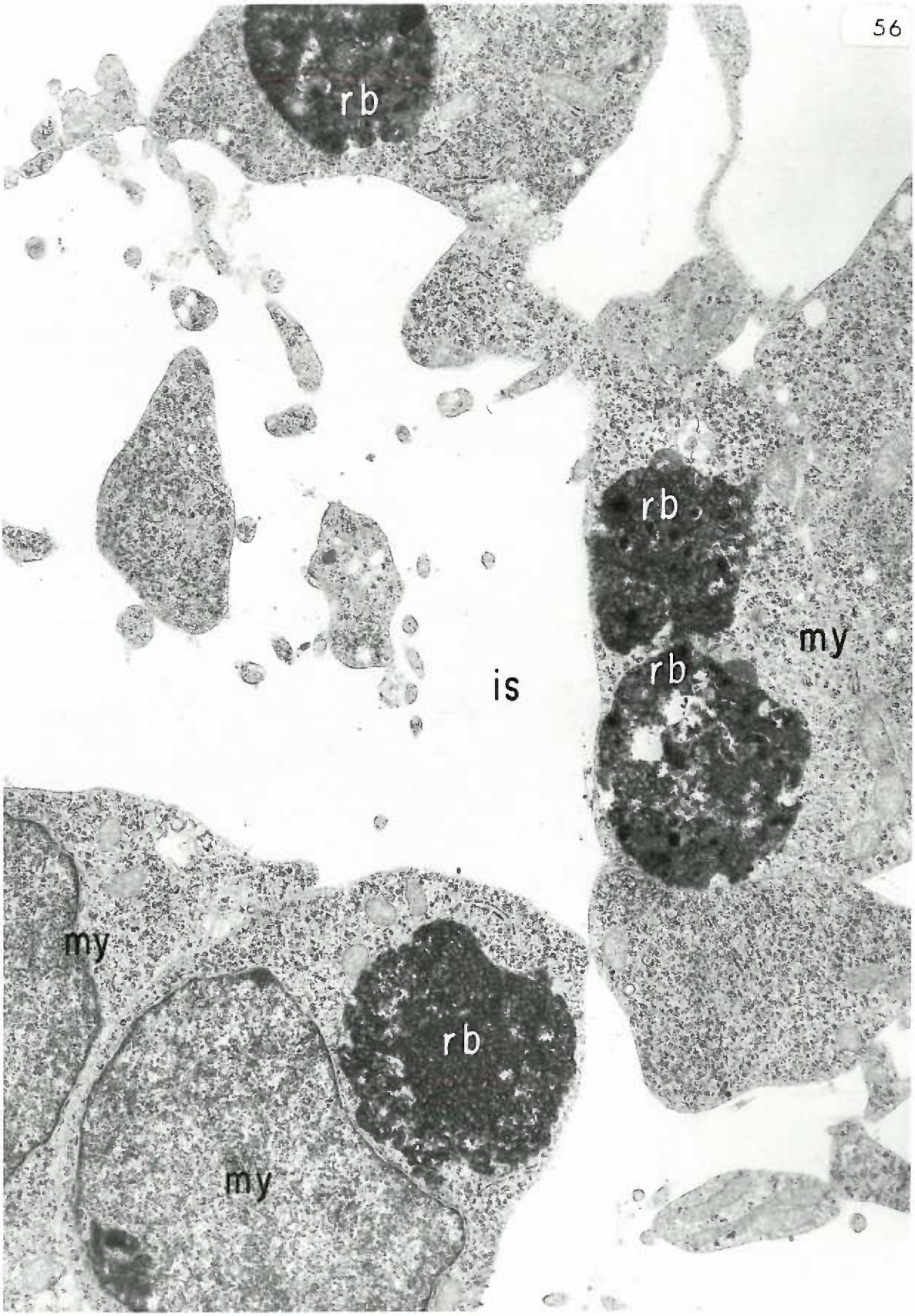
rb
rb
my
rb
is
my
rb
my

Figure 57. Eleven-day mesenchyme, experimental.
A phagocytic cell situated among several mesenchymal cells (my) exhibits three portions of nuclear material (n). Each portion of the nucleus is surrounded by a lighter staining nuclear envelope (ne) which resembles the membranous component of the rough endoplasmic reticulum (rer). The high number of ribosomes appears to account for the electron-dense appearance of the cytoplasm. A small mass of glycogen-like material (gly) lies within the cytoplasm of the phagocytic cell. Residual body (rb); phagocytic cell (pc); intercellular space (is). Uranyl acetate stain.

x12,000

Figure 58. Eleven-day mesenchyme, experimental.
A serial section of Figure 57 illustrates (see at upper left) a pseudopodium of a phagocytic cell adjacent to a residual body (rb). The glycogen-like material (gly) fills a larger portion of the phagocyte cytoplasm than it did in Figure 57. Part of another phagocytic cell (pc) lies in the intercellular space (is). Rough endoplasmic reticulum (rer); mesenchyme (my); nucleus (n); nuclear envelope (ne). Uranyl acetate stain.

x12,000

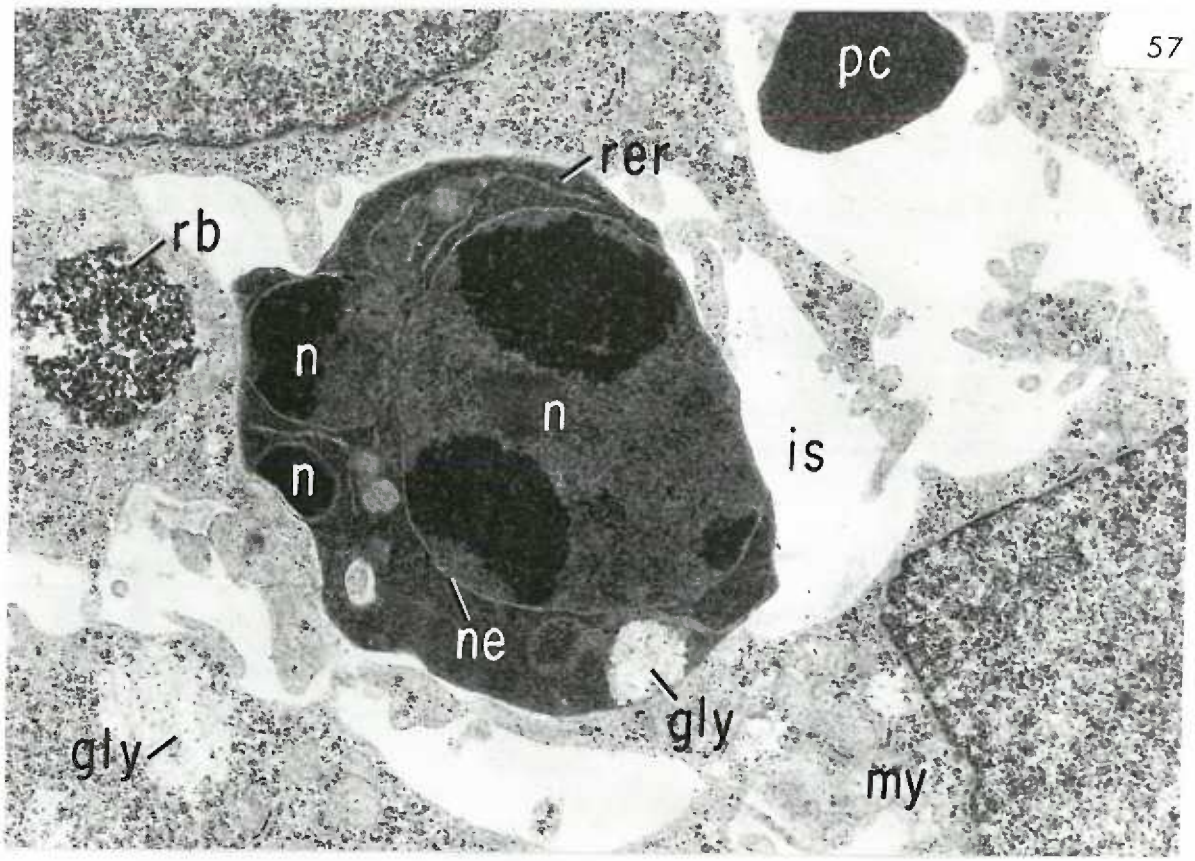
57
pc
rer
rb
n
n
n
is
ne
gly
gly
my

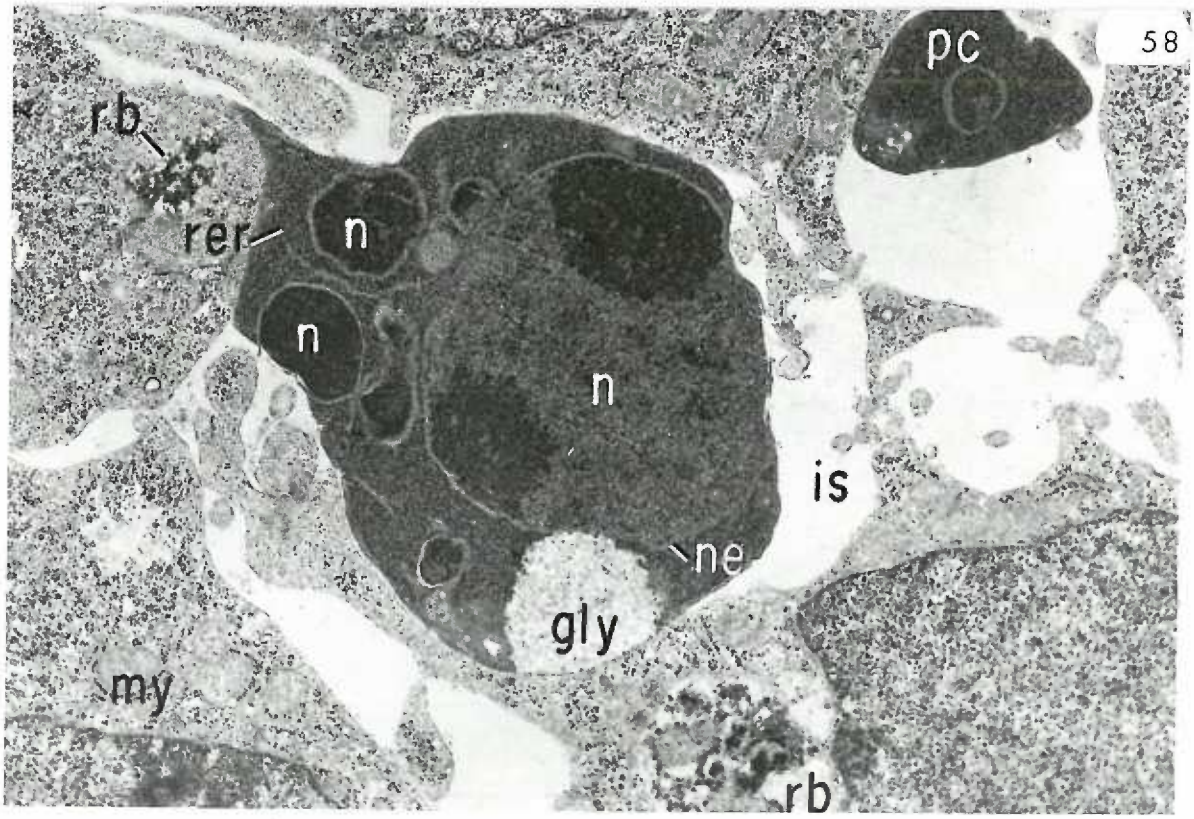
58
pc
rb
rer
n
n
n
is
ne
gly
my
rb

Figure 59. Eleven-day mesothelium, experimental. Mesothelial cells (ce) line the intra-embryonic coelom (ic), which contains a large cytoplasmic fragment (cf). An attenuated phagocytic cell (pc) lying between adjacent mesothelial cells exhibits numerous pseudopodia (arrows). Nuclear portions (n) are surrounded by light staining nuclear envelopes. Oval mitochondria (m) are scattered in the cytoplasm of the phagocytic cell. Two large residual bodies (rb) are encircled by pseudopodia (arrows) of the phagocyte. Rough endoplasmic reticulum (rer).

x20,000

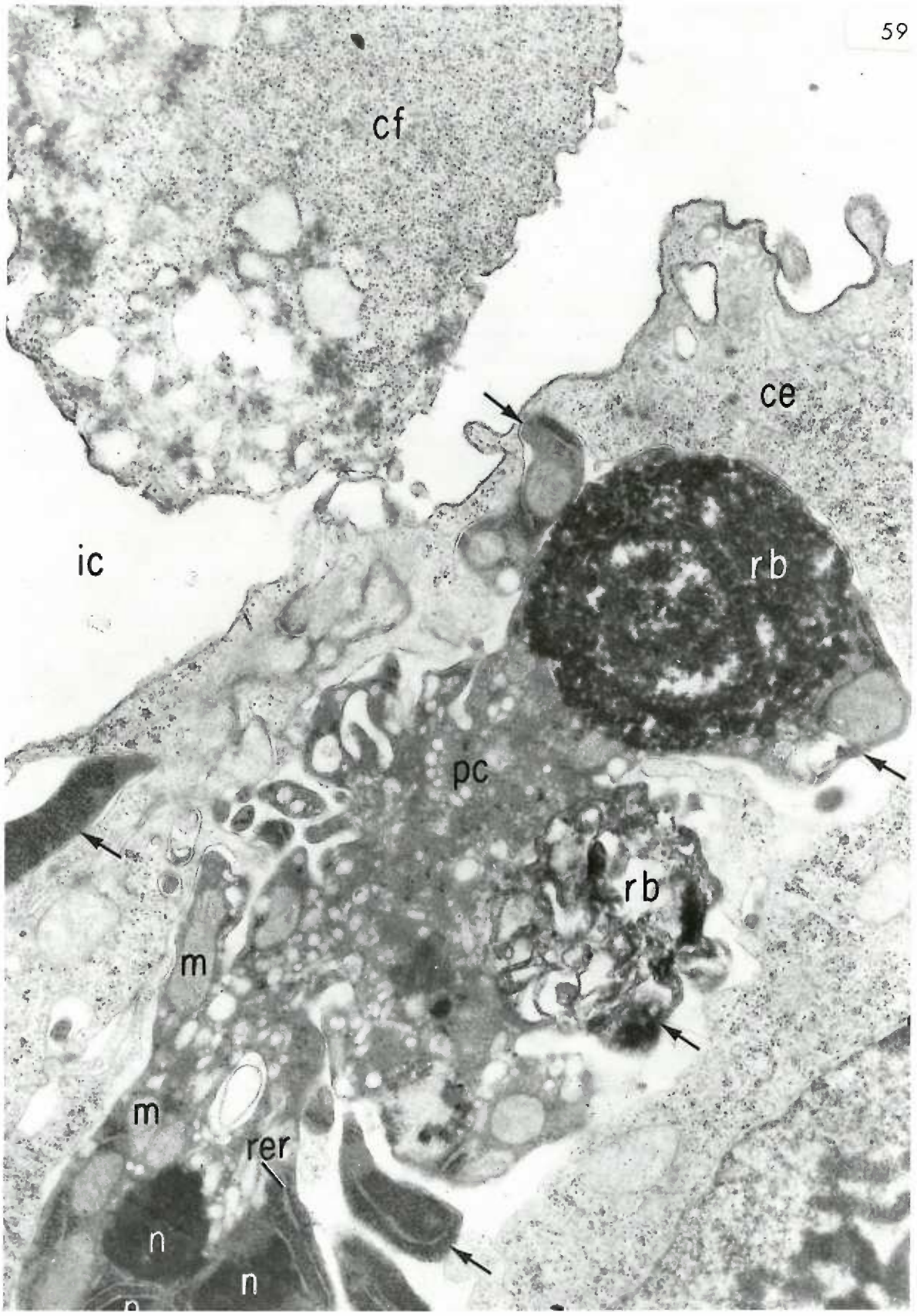
cf
ce
ic
rb
pc
rb
m
m
rer
n
n

Figure 60. Twelve-day mesenchyme, experimental.

Mesenchyme cells (my) bracket a portion of a phagocytic cell (pc). Scattered profiles of rough endoplasmic reticulum (rer), a portion of a nucleus (n), a large residual body (rb), and two "dye-like" vacuoles (dv) are visible in the phagocytic cell cytoplasm. Additional "dye-like" vacuoles cluster in the cytoplasm of a mesenchyme cell.

x40,000

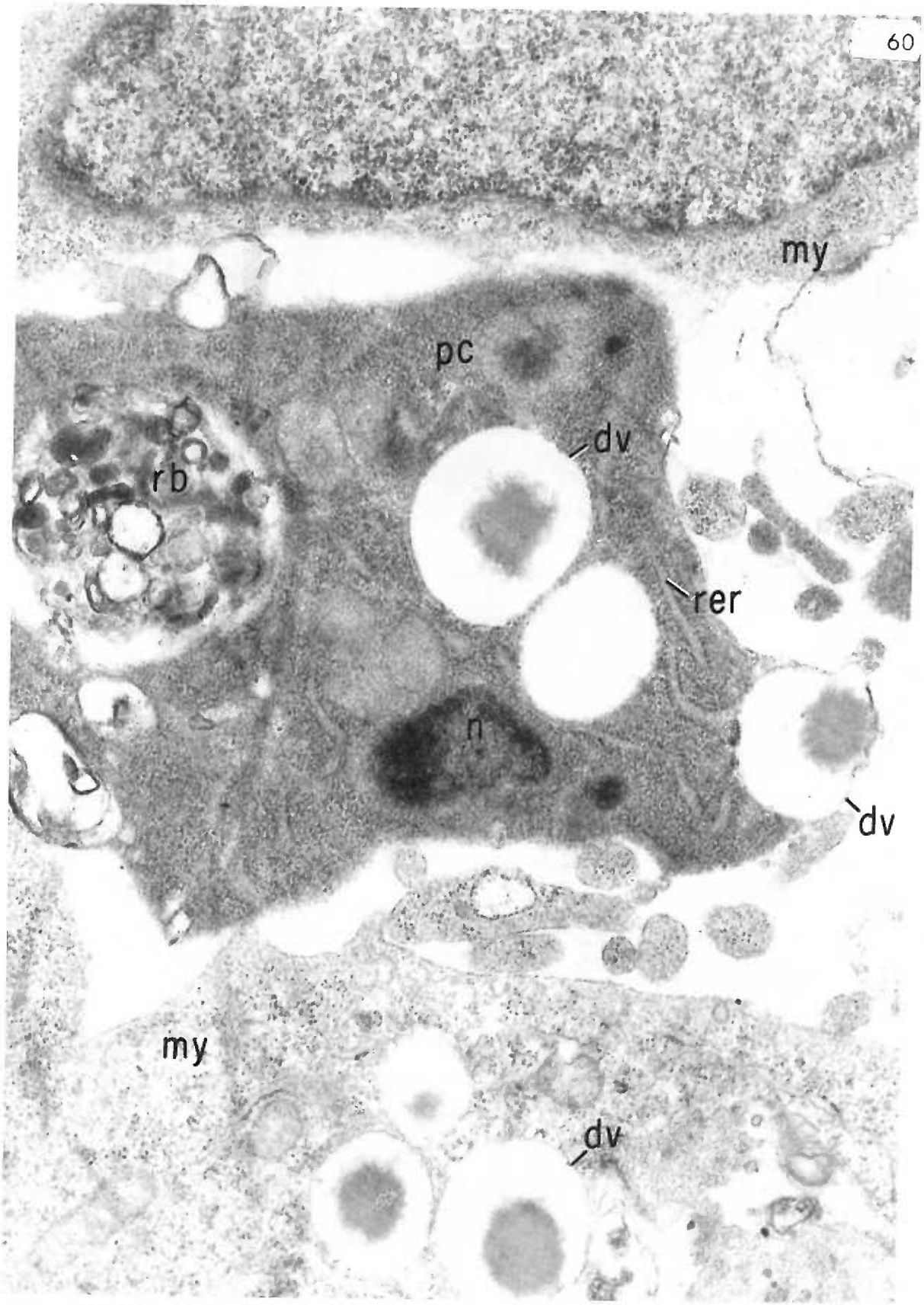
60
my
pc
dv
rb
rer
n
dv
my
dv

Figure 61. Twelve-day mesenchyme, control.

A mesenchyme cell exhibits numerous profiles of rough endoplasmic reticulum (er). An extensive Golgi complex (Go) is flanked by oval mitochondria (m). The oval-shaped nucleus is surrounded by a nuclear envelope (ne). A junction joins contiguous portions of two adjacent mesenchyme cells (arrows). Numerous polyribosomes are evident.

x20,000

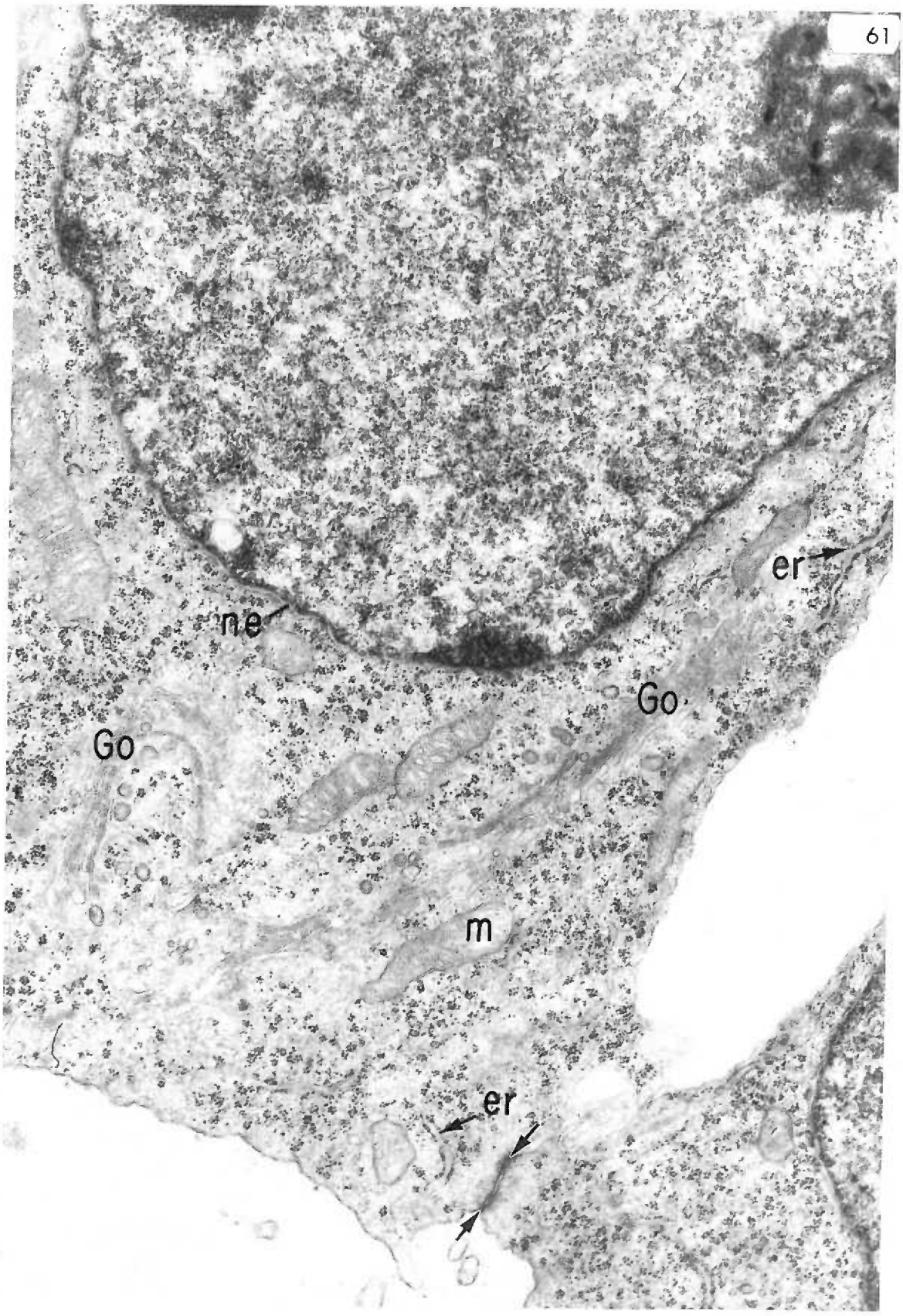
61
er
ne
Go
Go
m
er

Figure 62. Twelve-day mesenchyme, control.

This mesenchyme cell is completing mitosis; the chromatin material (ch) is re-forming. Numerous profiles of paired cisternae (pci) appear in the cytoplasm. One of the paired cisternae (see top of figure) possessing three membranes is branched at one end (arrow) into two normal-appearing elements of rough endoplasmic reticulum. Other paired cisternae with four membranous laminae (see bottom of figure) attach to a chromatin mass. Intercellular space (is).

x29,000

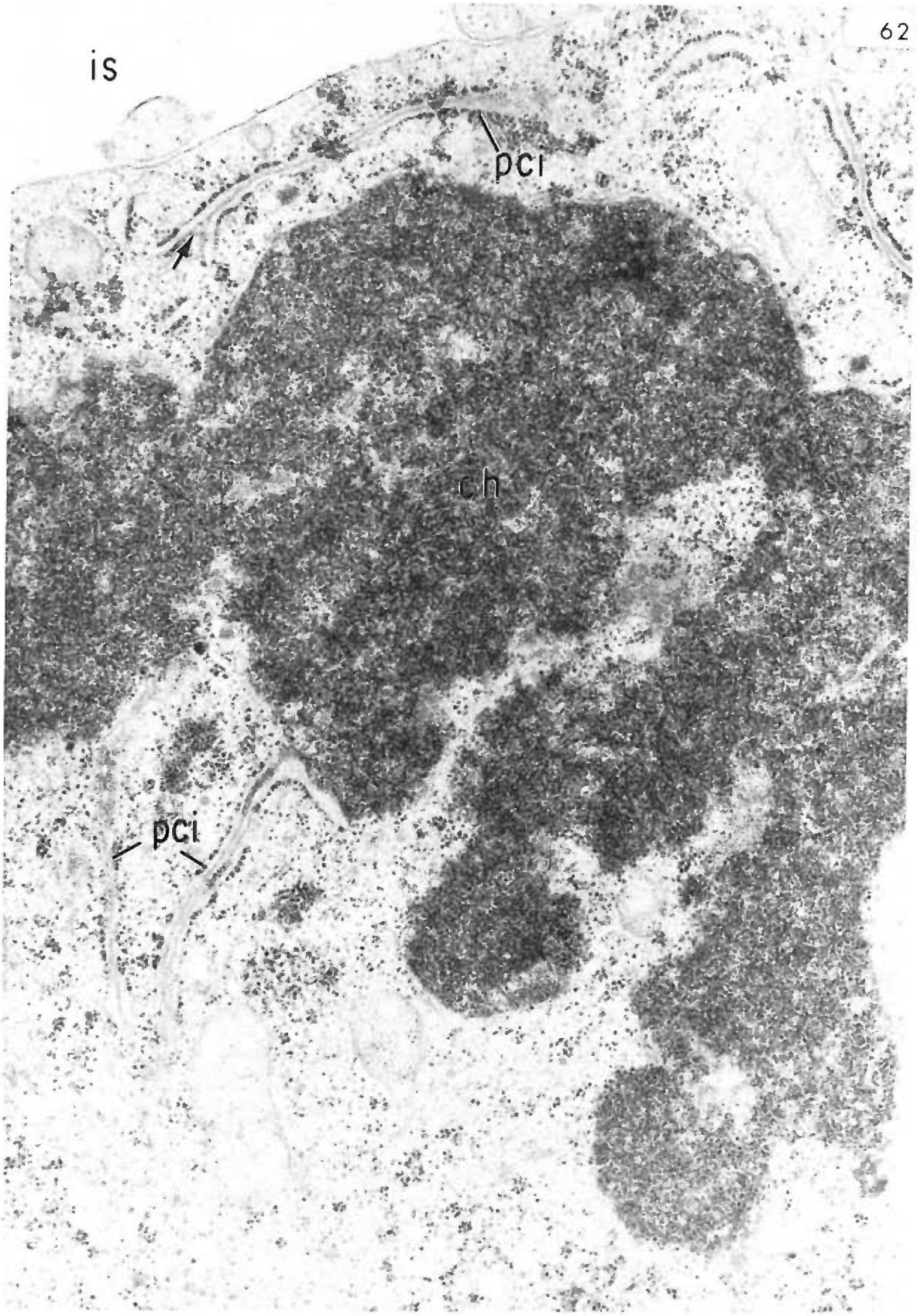
is
pci
ch
pci

Figure 63. Nine-day visceral yolk sac, experimental. A visceral yolk sac cell exhibits large vacuoles (dv) of high electron density which contain a homogeneous material thought to be Trypan blue. Nucleus (n); yolk sac cavity (ysc).

x29,000

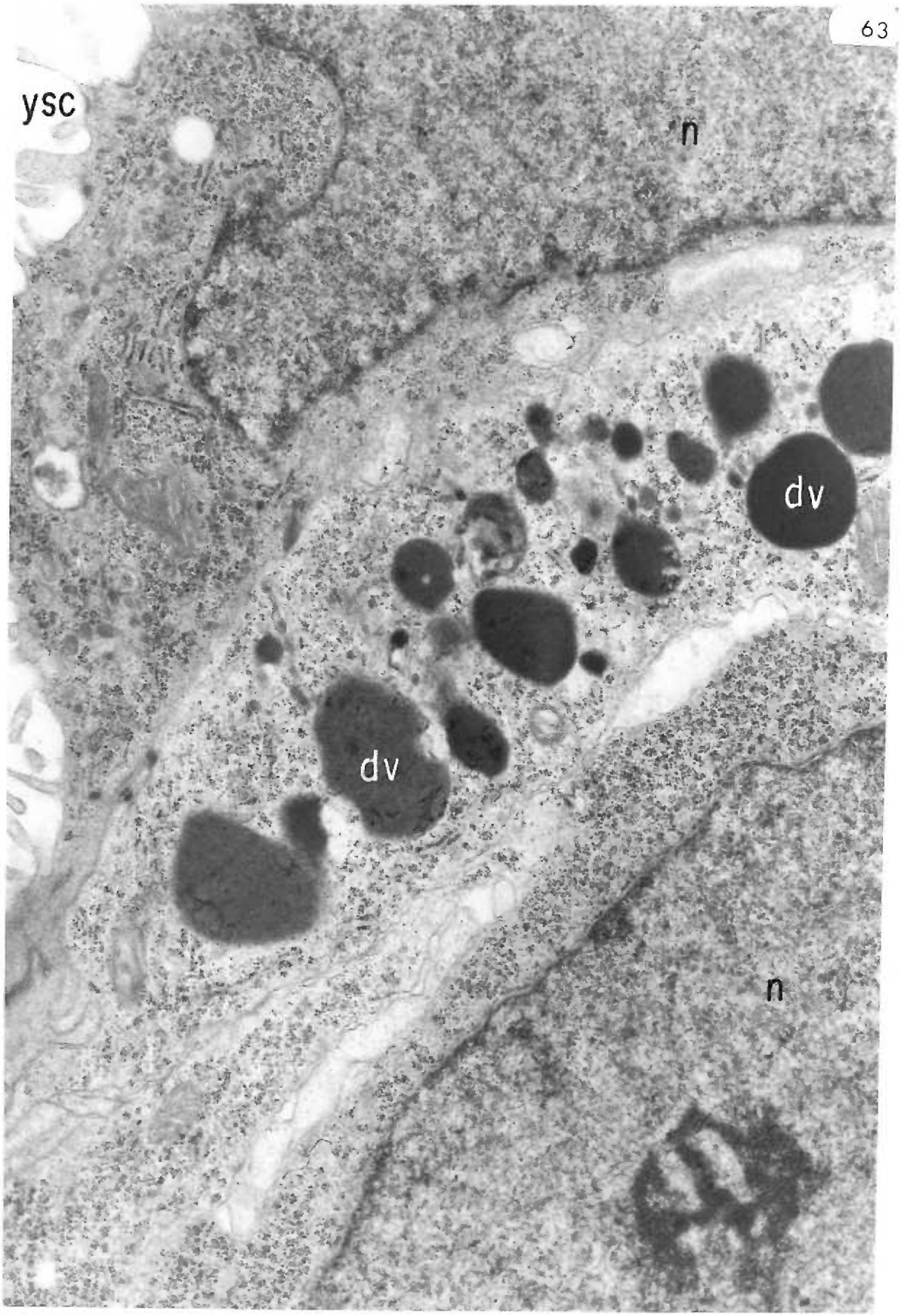
ysc
n
dv
dv
n

Figure 64. Nine-day visceral yolk sac, experimental. Small, apical vesicles (v) exhibiting a fuzzy inner lining are formed from invaginations between adjacent microvilli. Larger, supra-nuclear vacuoles are either segregating or combining; each vacuole contains a material of different electron density (arrows). Yolk sac cavity (ysc); mitochondria (m).

x20,000

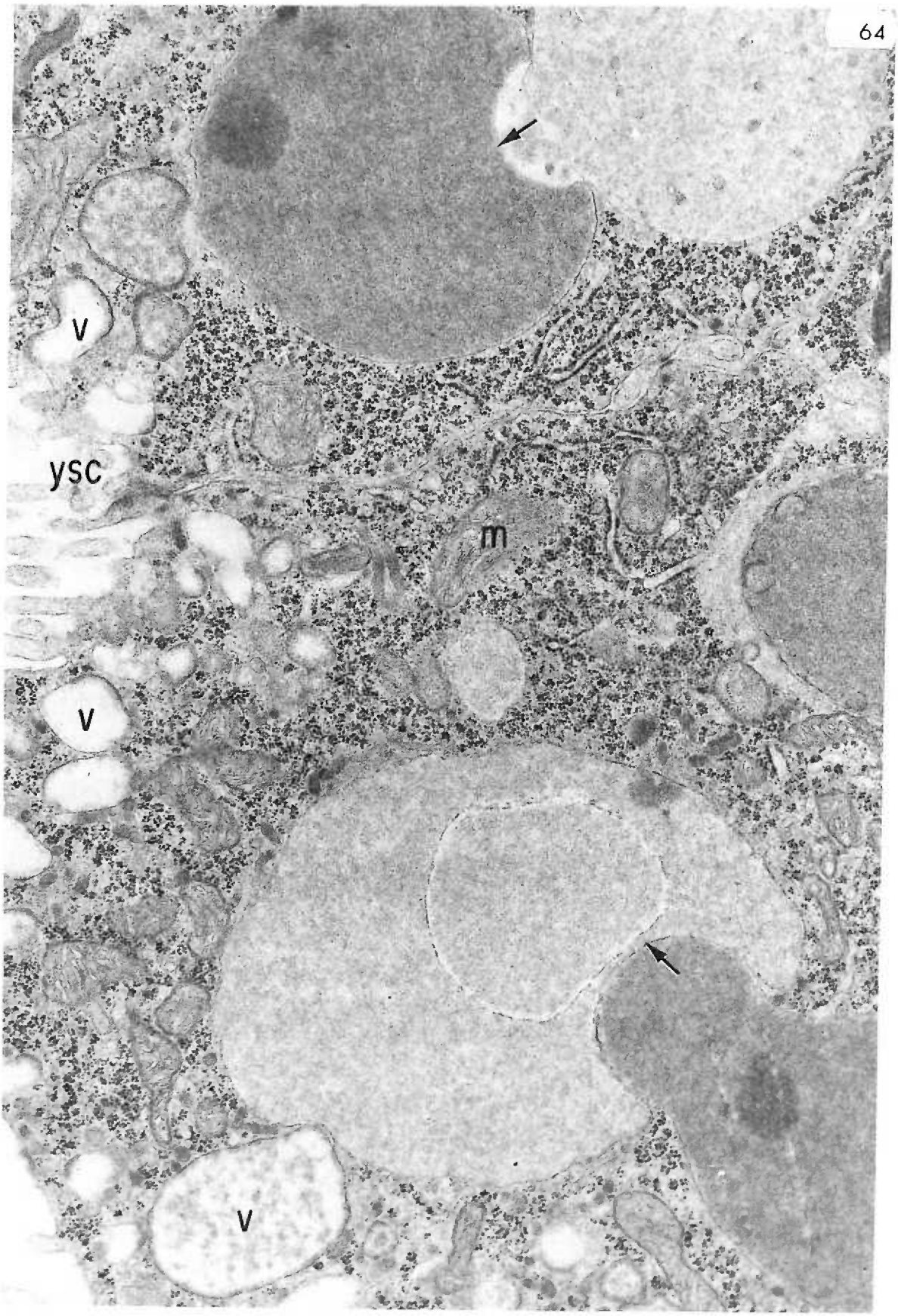
64
v
ysc
m
v
v

Figure 65. Nine-day visceral yolk sac, experimental. Numerous, dark blue vacuoles (arrows) fill the supra-nuclear cytoplasm of the visceral yolk sac cells (ys). Many of the smaller vacuoles stain as intensely blue as the larger vacuoles. Yolk sac cavity (ysc). Richardson's stain.

x400

Figure 66. Nine-day visceral yolk sac, experimental. The visceral yolk sac contains large and small supra-nuclear vacuoles (arrows) which show a blue hue. The light microscope examination of this tissue reveals a bright blue coloration in these vacuoles. Unstained.

x400


65
ysc
ys

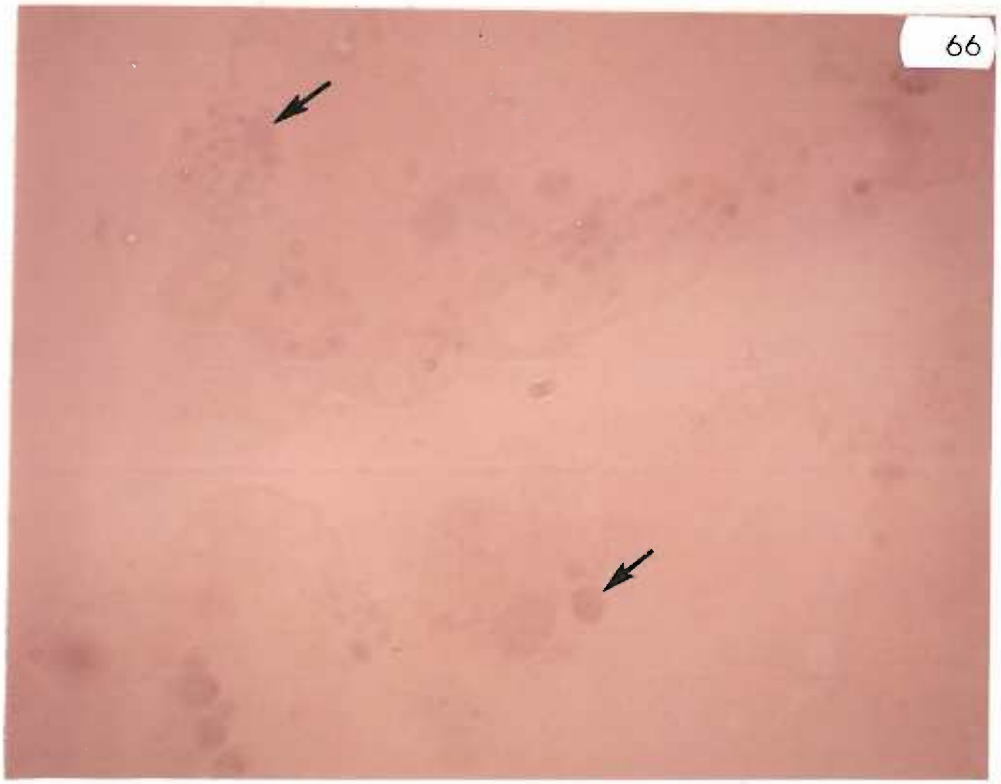
66

Figure 67. Ten-day visceral yolk sac, experimental. Well-developed microvilli project from the endoderm cells into the yolk sac cavity (ysc). The large supra-nuclear vacuoles (dv) contain a homogeneous, electron-dense material which is probably Trypan blue. Smaller, apical vacuoles (v) contain a dense, floccular material. A mesothelial cell (ms) separates the yolk sac from the extra-embryonic coelom (ec). Nucleus (n).

x12,000

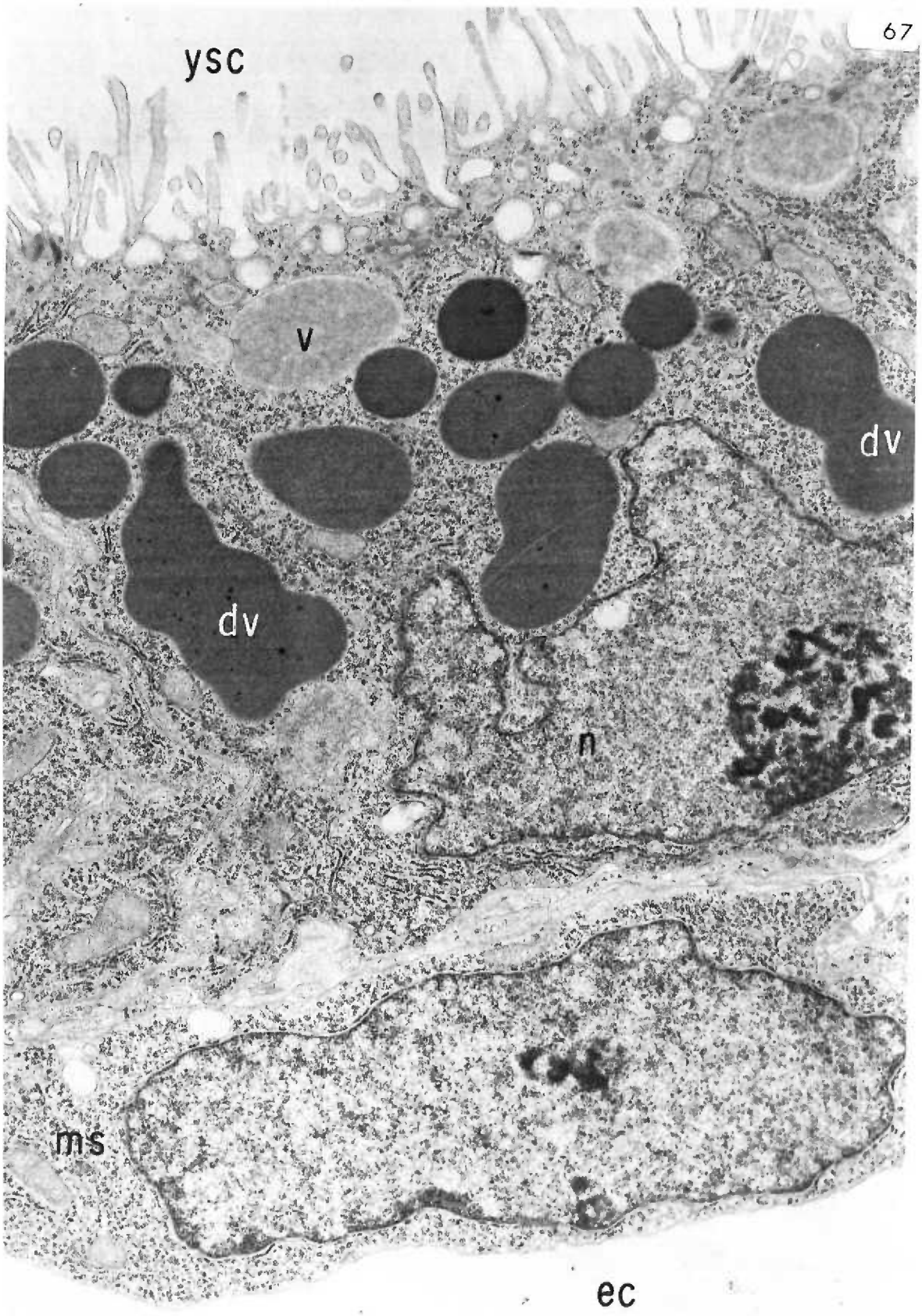
ysc
v
dv
dv
n
ms
ec

Figure 68. Eleven-day visceral yolk sac, experimental. The endoderm cells exhibit a heterogeneous population of vacuoles. Only an occasional electron-dense, homogeneous vacuole (dv) is exhibited. Other vacuoles (v) contain a dense, floccular material, while still others exhibit a spicular material (s). Small globules of electron-dense material (arrows) lie within the larger vacuoles. Yolk sac cavity (ysc).

x20,000

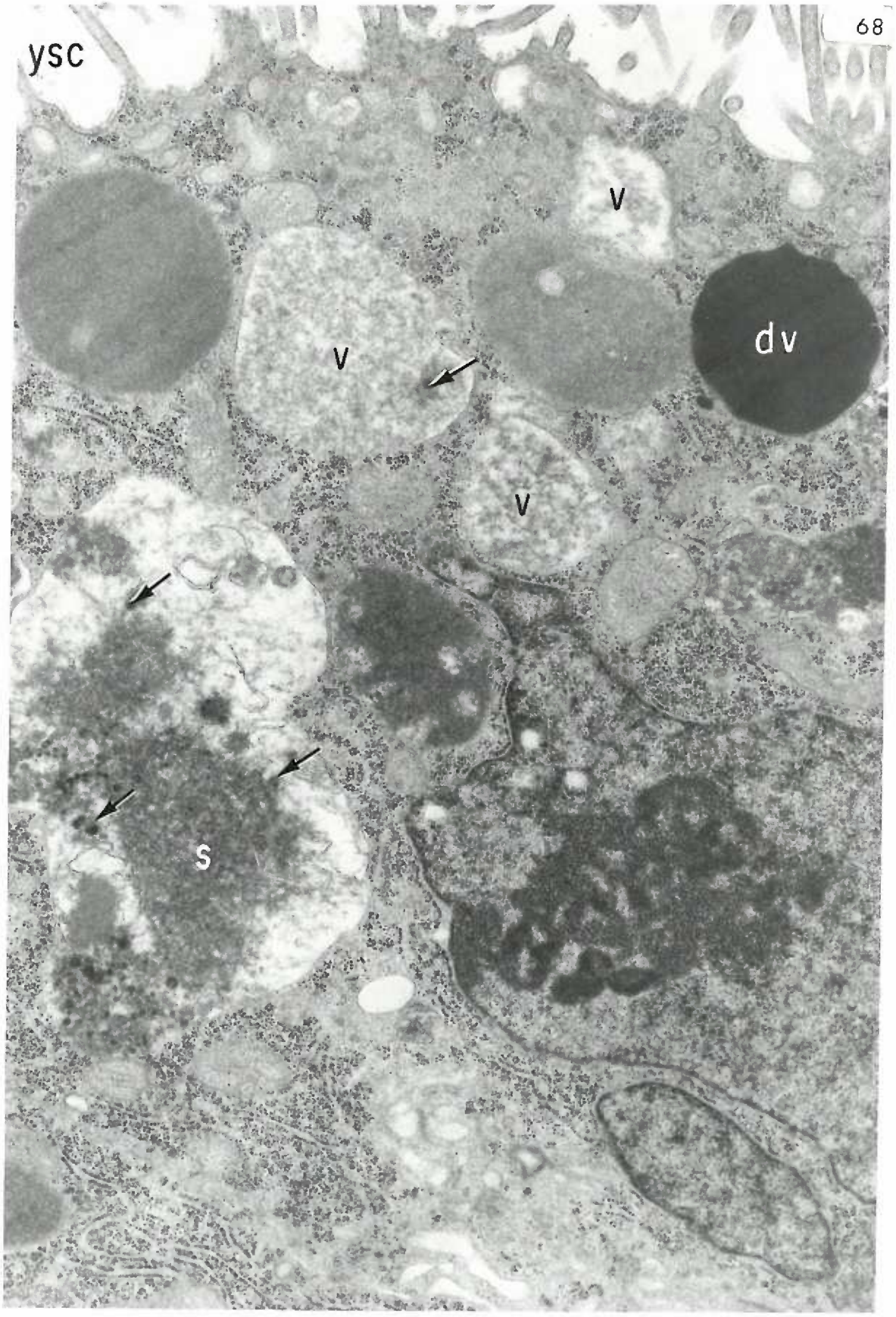
ysc
v
dv
v
v
s

Figure 69. Twelve-day visceral yolk sac, experimental. A vacuole (dv) of high electron-density contains a homogeneous material which is possibly Trypan blue. Other vacuoles (v) contain some condensed, floccular material or spicules (s). A few electron-dense globules of material (arrows) are evident within other vacuoles. Yolk sac cavity (ysc).

x20,000

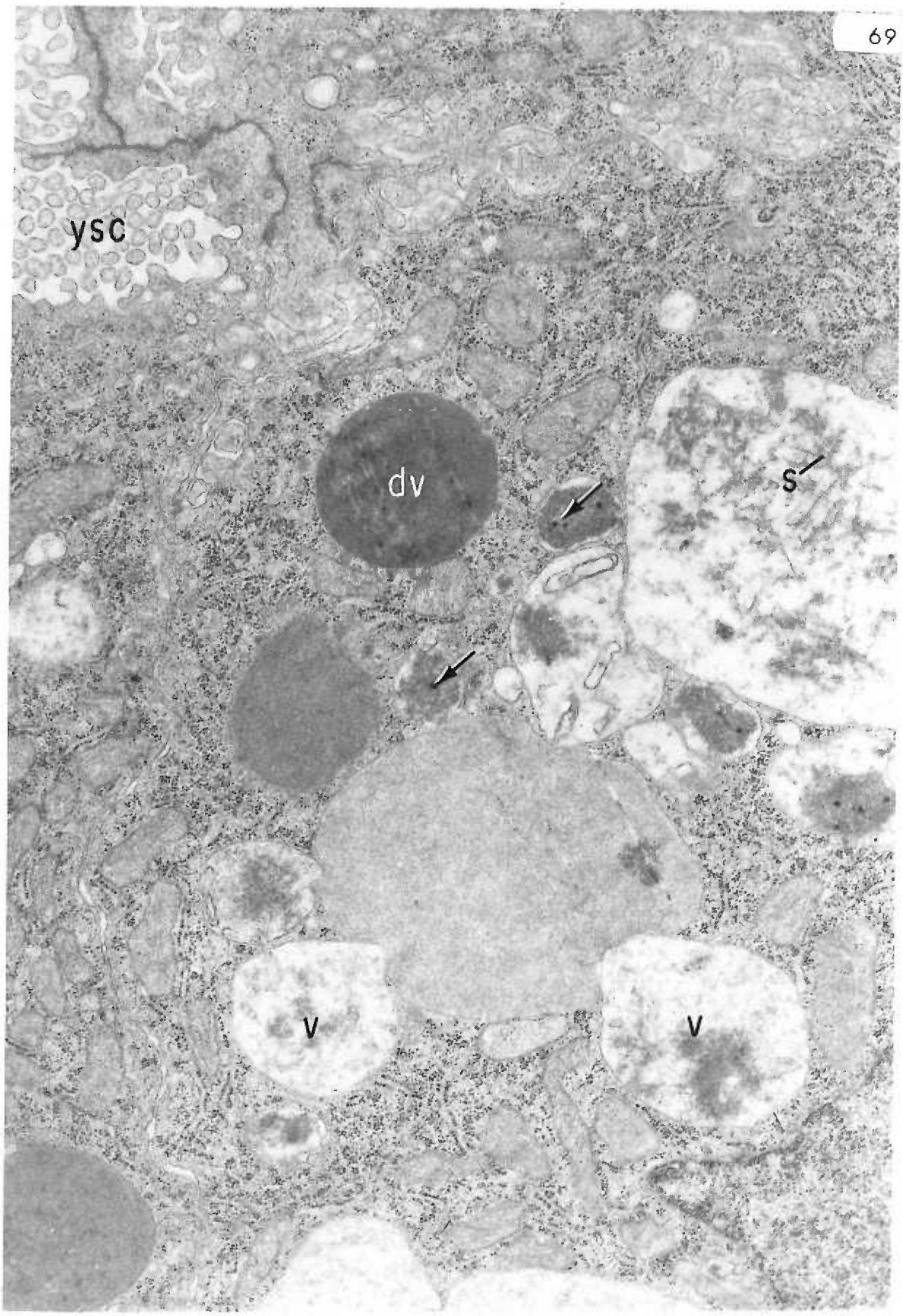
ysc
dv
s
v
v

Figure 70. Twelve-day visceral yolk sac, experimental. A large mass of debris (d) lying free in the yolk sac cavity (ysc) may be of cellular origin. Several vacuoles of very electron-dense material (dv) may contain Trypan blue. Yolk sac endoderm (ys).

x9,000

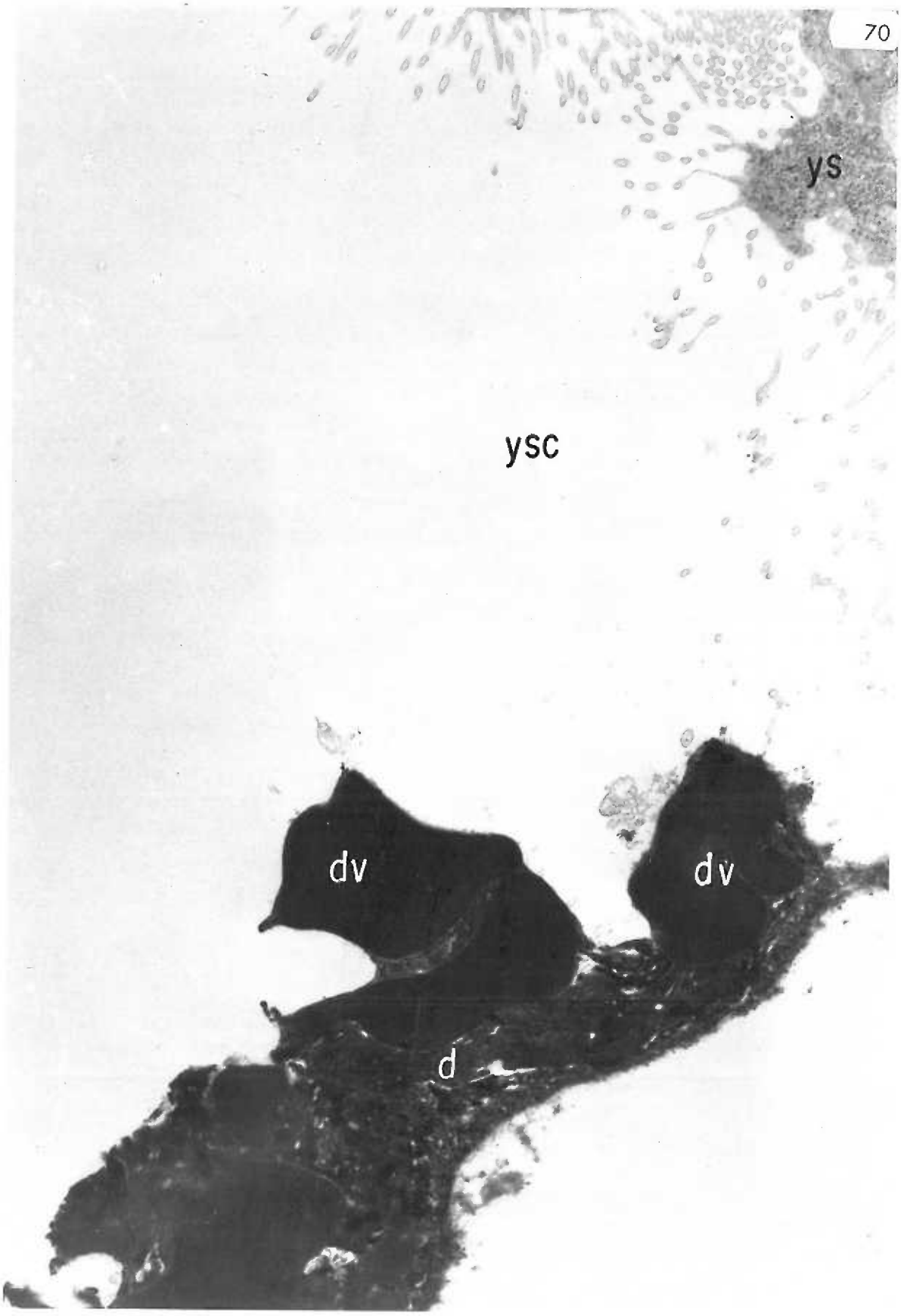
ys
ysc
dv
dv
d

Figure 71. Eleven-day visceral yolk sac, experimental. A layer of mesothelial cells (ms) separates the attenuated vascular endothelium (va) from the extra-embryonic coelom (ec). A fetal red blood cell (frbc) lies in the vascular lumen. A mesothelial cell contains two "dye-like" vacuoles (dv).

x20,000

Figure 72. Twelve-day visceral yolk sac, experimental. A "dye-like" vacuole (dv) with a dense center occupies the cytoplasm of a mesothelial cell (ms). Yolk sac endoderm (ys); connective tissue space (cts); extra-embryonic coelom (ec).

x20,000

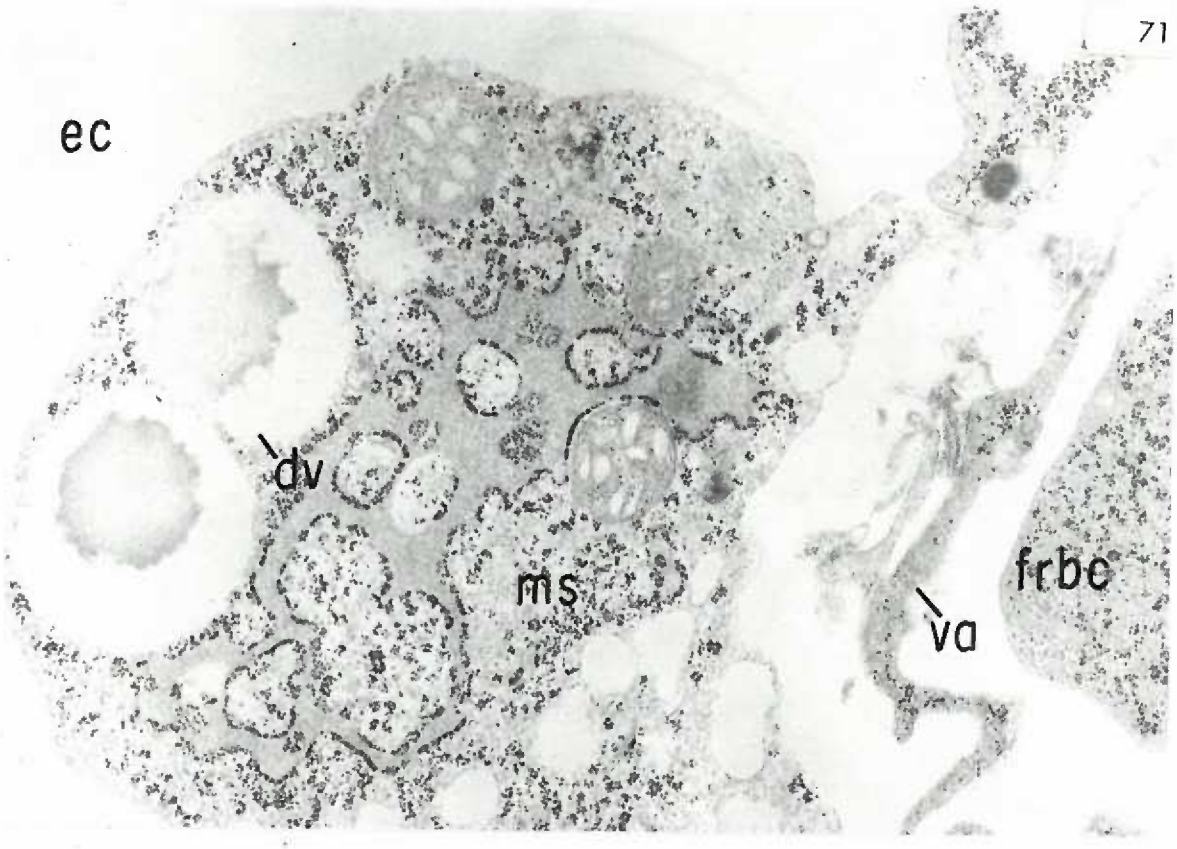
71
ec
dv
ms
va
frbc

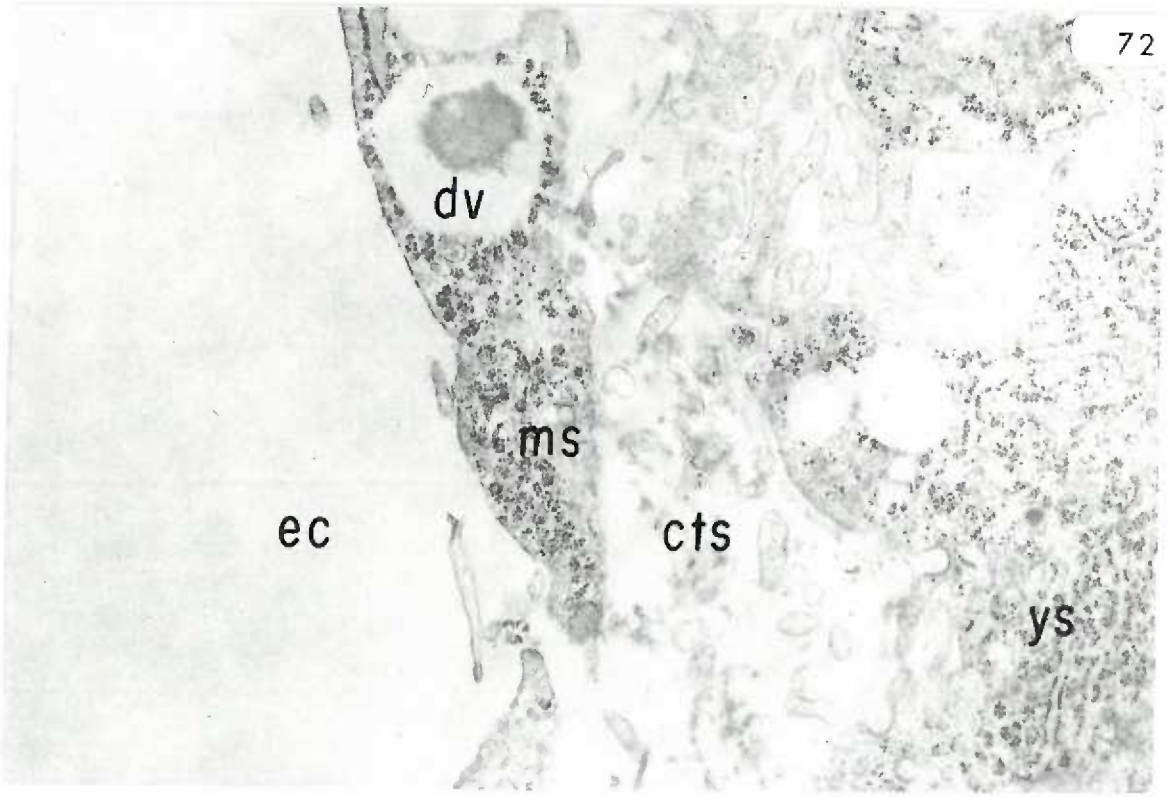
72
dv
ms
ec
cts
ys

Figure 73. Nine-day visceral yolk sac, control.

The phagocytic activities of this 9-day visceral yolk sac are demonstrated by the presence of small fuzzy vesicles or caveolae (arrows) which form between the bases of adjacent microvilli. These vesicles coalesce to form apical vacuoles (v) which contain a granular material of moderate electron-density. Larger supra-nuclear vacuoles (V) contain a granular material and membranous profiles (double arrows). Yolk sac cavity (ysc).

x20,000

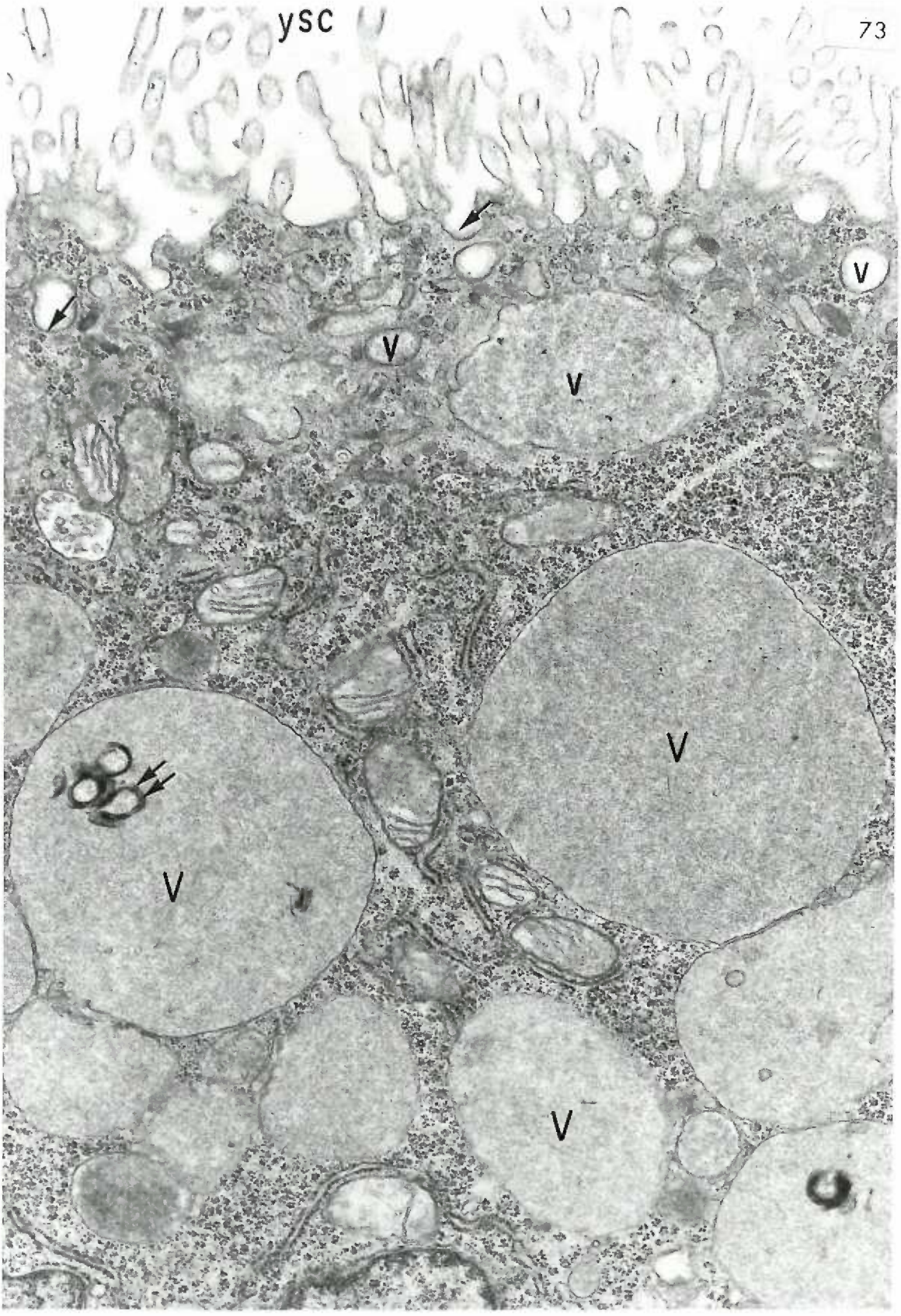
ysc
V
V
V
V
V
V
V

Figure 74. Ten-day visceral yolk sac, control.

This 10-day visceral yolk sac exhibits numerous caveolae (arrows) and supra-nuclear vacuoles (v). A mesothelial cell layer underlies the visceral yolk sac; in this tangential section, the mesothelium appears to be formed of several cell layers (ms). Yolk sac cavity (ysc).

x12,000

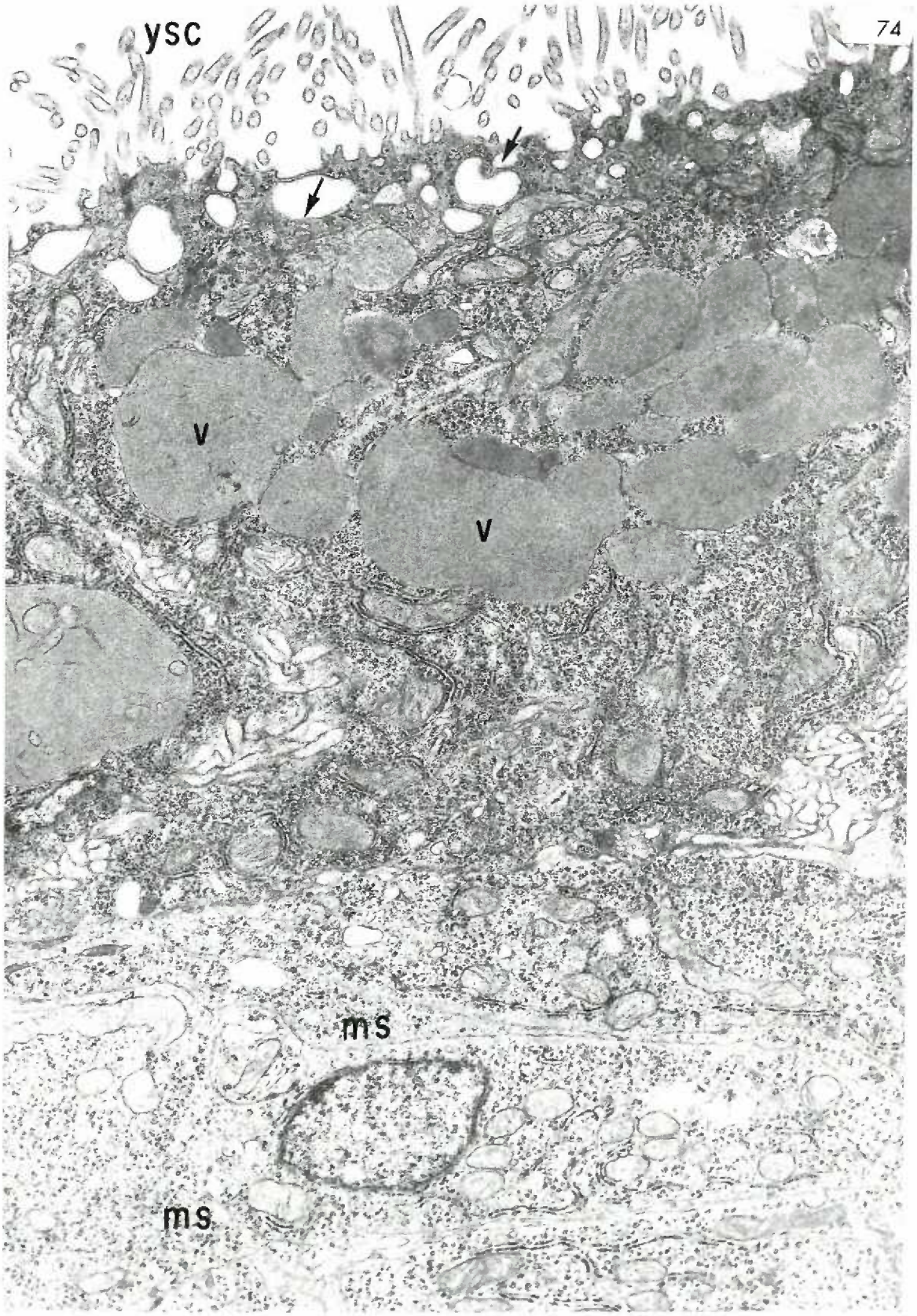
ysc
v
v
ms
ms

Figure 75. Eleven-day visceral yolk sac, control.

A heterogeneous population of vacuoles fills the supra-nuclear cytoplasm of the visceral yolk sac cells. Some vacuoles contain a fine, floccular material (v); larger vacuoles (V) contain a dense, granular substance. Caveolae (arrows); yolk sac cavity (ysc).

x12,000

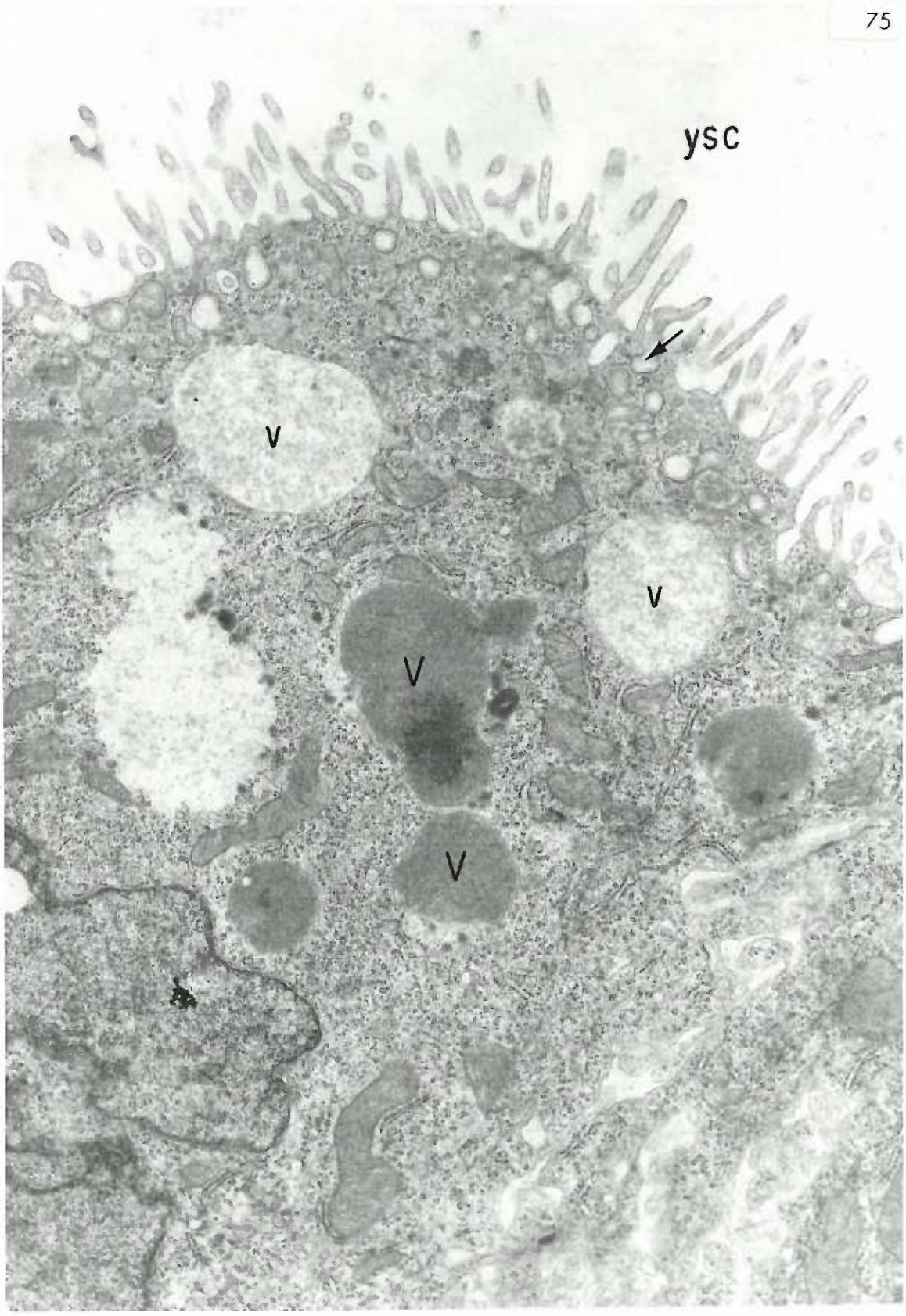
ysc
v
v
V
V

Figure 76. Twelve-day visceral yolk sac, control.
The visceral yolk sac cells exhibit several absorption vacuoles (v) in their supra-nuclear cytoplasm. A connective tissue cell (ctc) in the connective tissue space is separated from the extra-embryonic coelom (ec) by a layer of mesothelium (ms). Yolk sac cavity (ysc).

x12,000

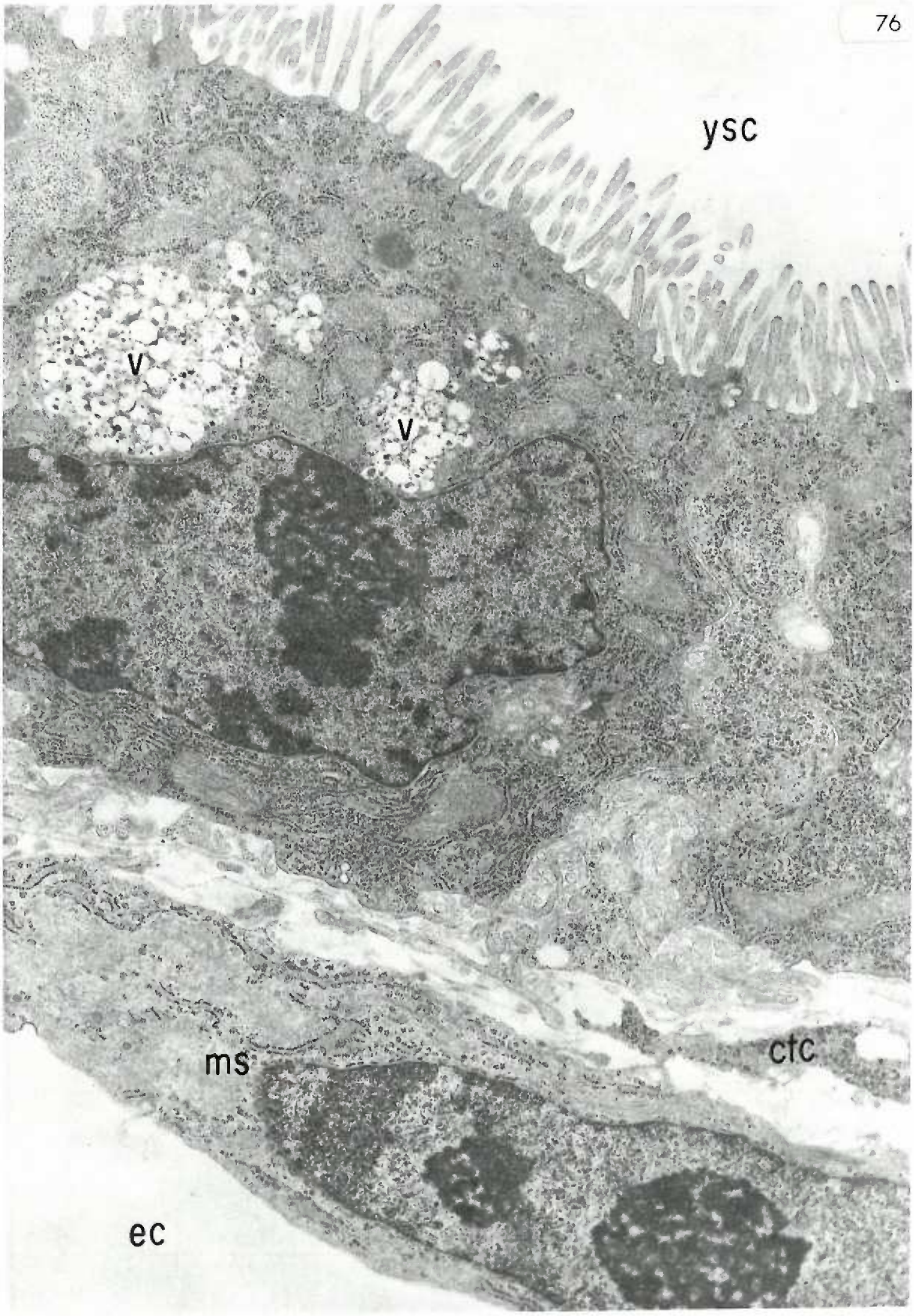
ysc
v
v
ms
ctc
ec

Figure 77. Eleven-day visceral yolk sac, control. "Foot-like" processes form inter-digitations extending from the basal ends of the yolk sac cells (ys). A vitelline vessel exhibits an attenuated endothelium (va). The extra-embryonic coelom (ec) is separated from the vascular endothelium by a layer of mesothelium (ms). Vascular space (vs).

x20,000

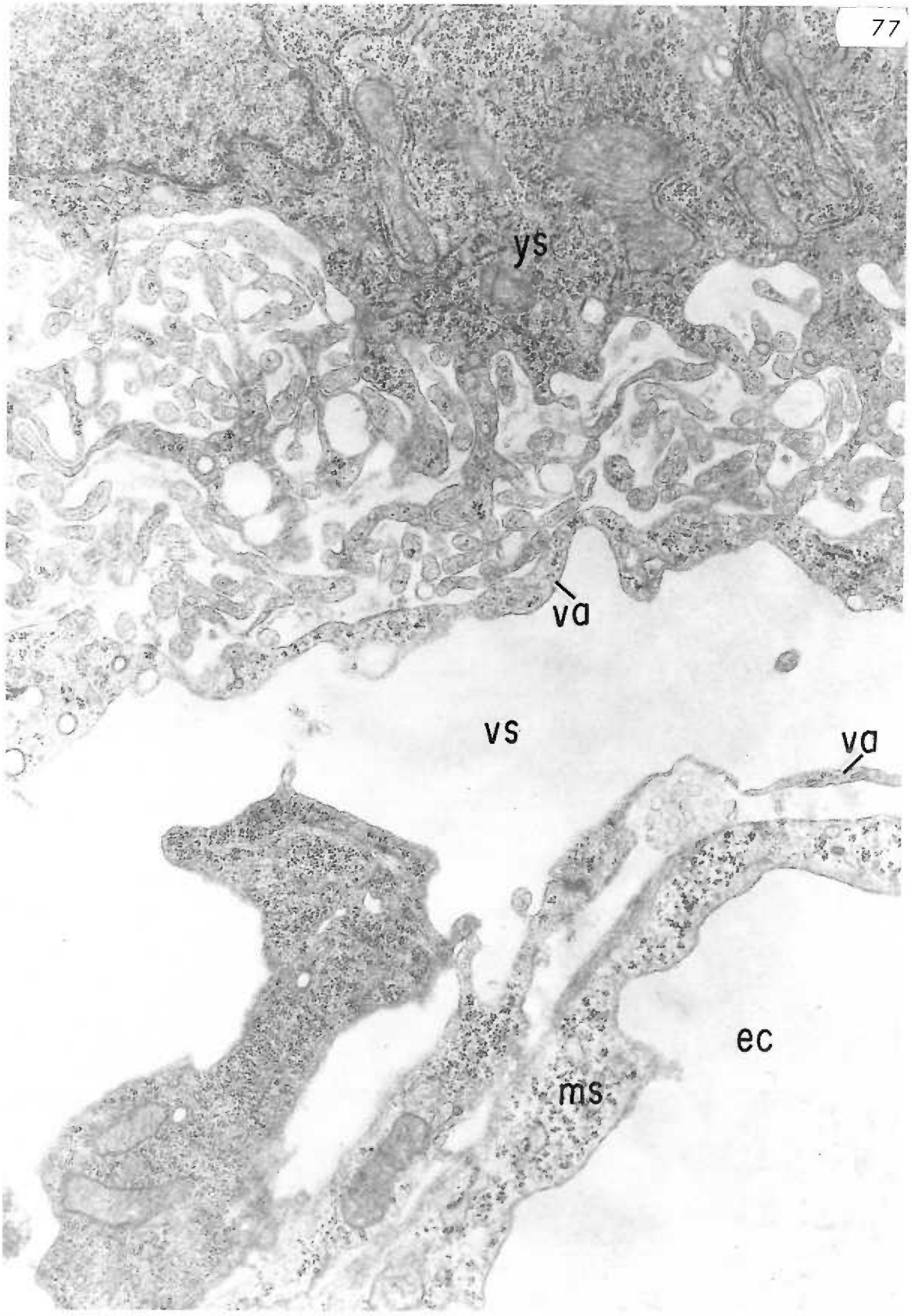
ys
va
vs
va
ec
ms

Figure 78. Ten-day trophoblast, junctional zone, experimental. The trophoblast cells in the junctional zone contain numerous, electron-dense vacuoles (v). Two vacuoles (dv) resemble those of the "dye-like" morphology. Nucleus (n).

x12,000

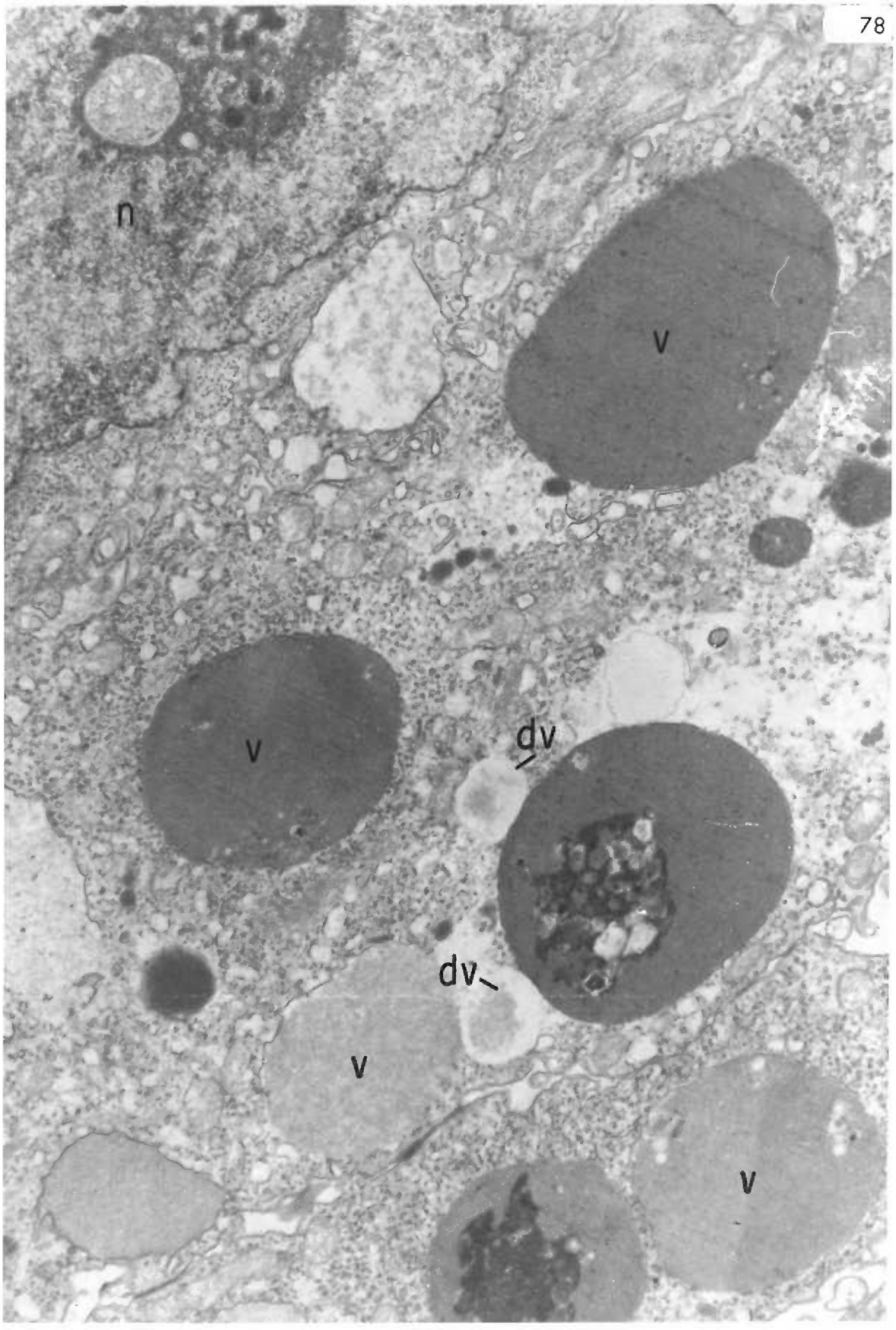
n
v
v
dv
dv
v
v

Figure 79. Ten-day trophoblast, junctional zone, experimental. The trophoblast cells contain vacuoles (arrows) which contain a dark-staining material surrounded by a clear peripheral area. These vacuoles coincide morphologically with those observed with the electron microscope (Figure 78). Richardson's stain.

x400

Figure 80. Ten-day trophoblast, junctional zone, control. The trophoblast cells contain large vacuoles (arrows) which coincide morphologically with the large vacuoles normally observed in this tissue with the electron microscope (Figure 85). Richardson's stain.

x400

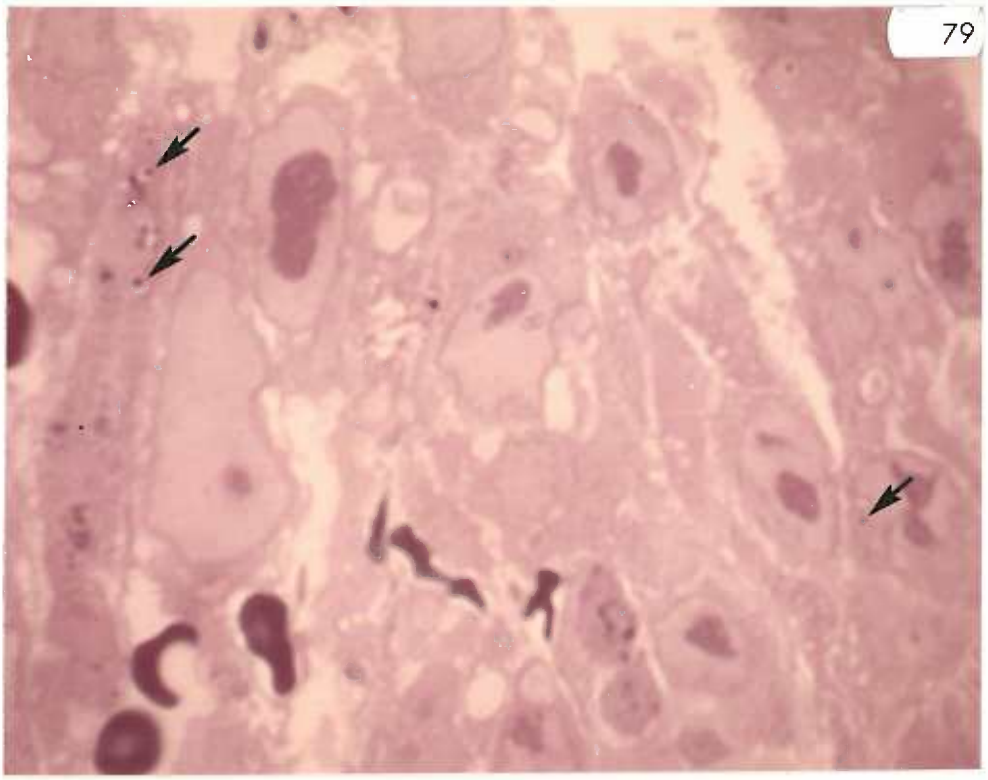
79

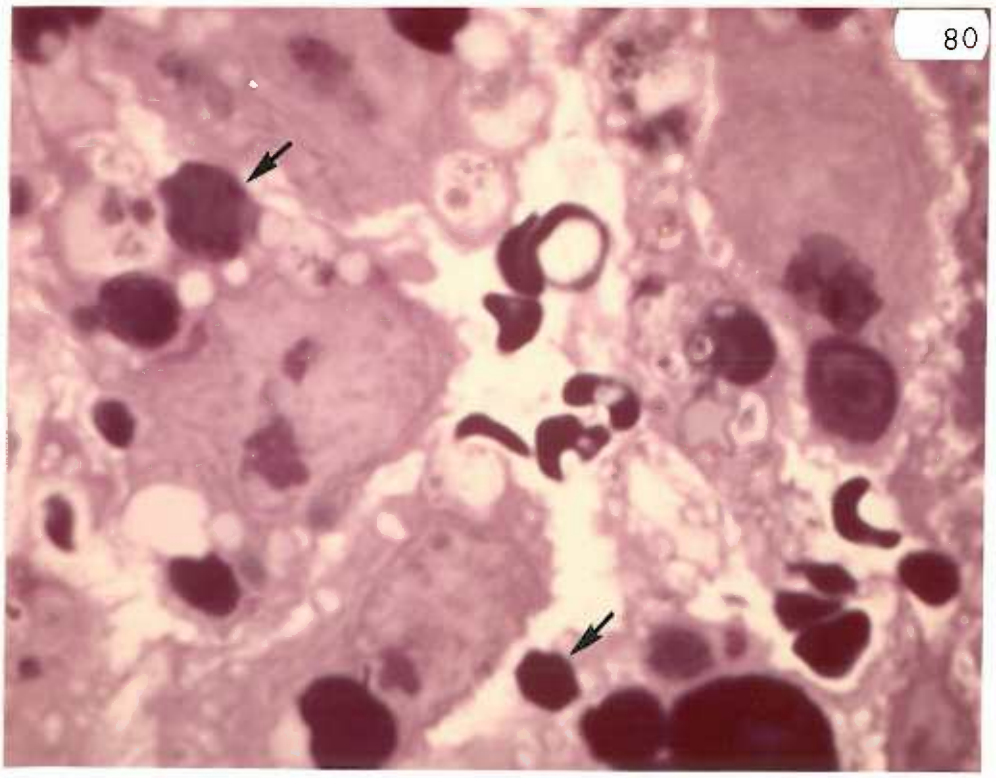
80

Figure 81. Ten-day chorionic trophoblast, experimental. A cluster of "dye-like" vacuoles (dv) lies in the cytoplasm of a chorionic trophoblast cell (co). Many vacuoles (v) filled with a floccular material of moderate electron-density are apparent in the yolk sac endoderm (ys). Nucleus (n); yolk sac cavity (ysc).

x20,000

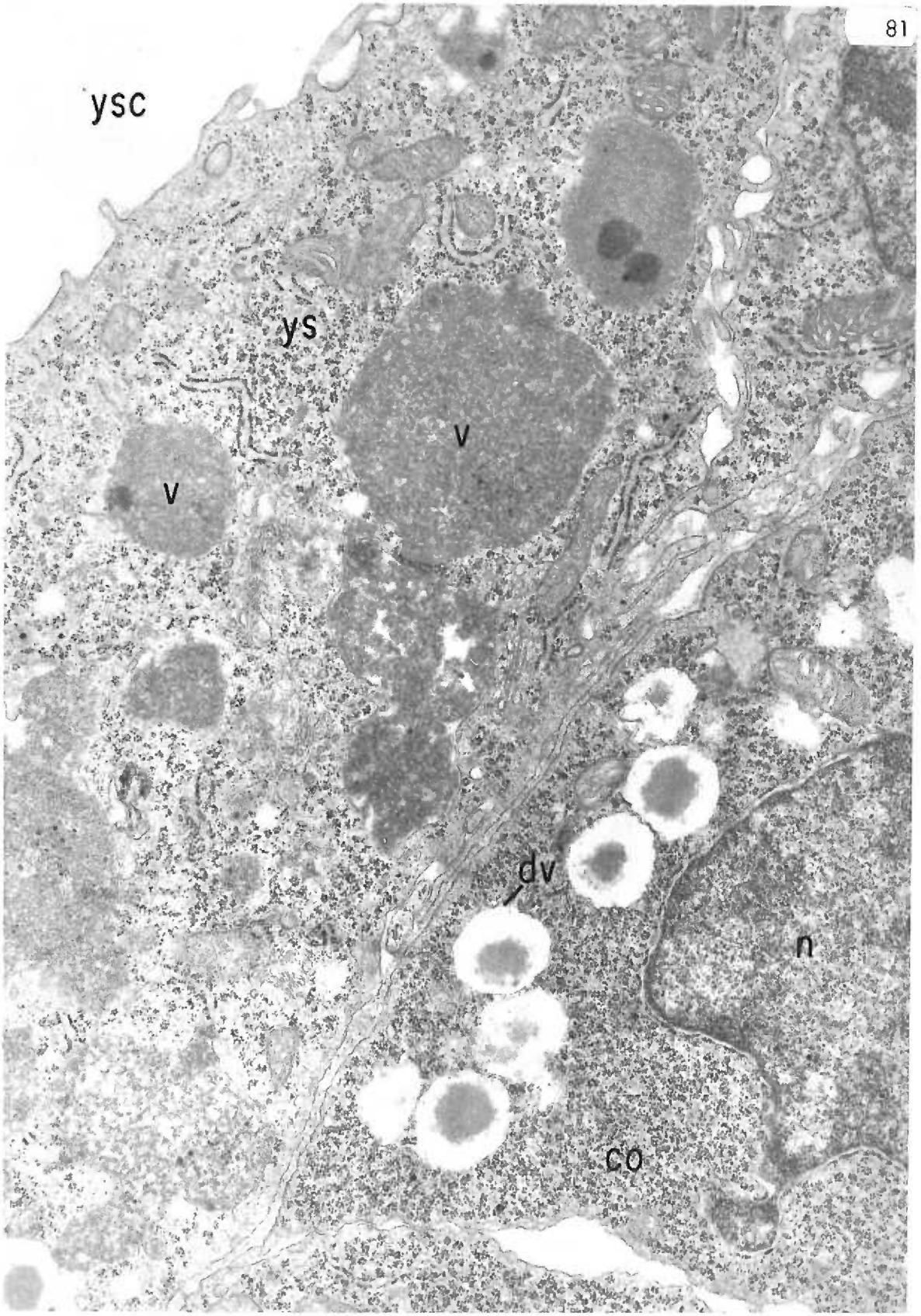
ysc
ys
v
v
dv
n
co

Figure 82. Ten-day chorionic trophoblast, experimental. Cells of the chorionic trophoblast (co) lie adjacent to the yolk sac endoderm (ys). Two "dye-like" vacuoles (dv) are visible in the yolk sac endoderm. Larger vacuoles (v) contain small globules of electron-dense material (arrows).

x20,000

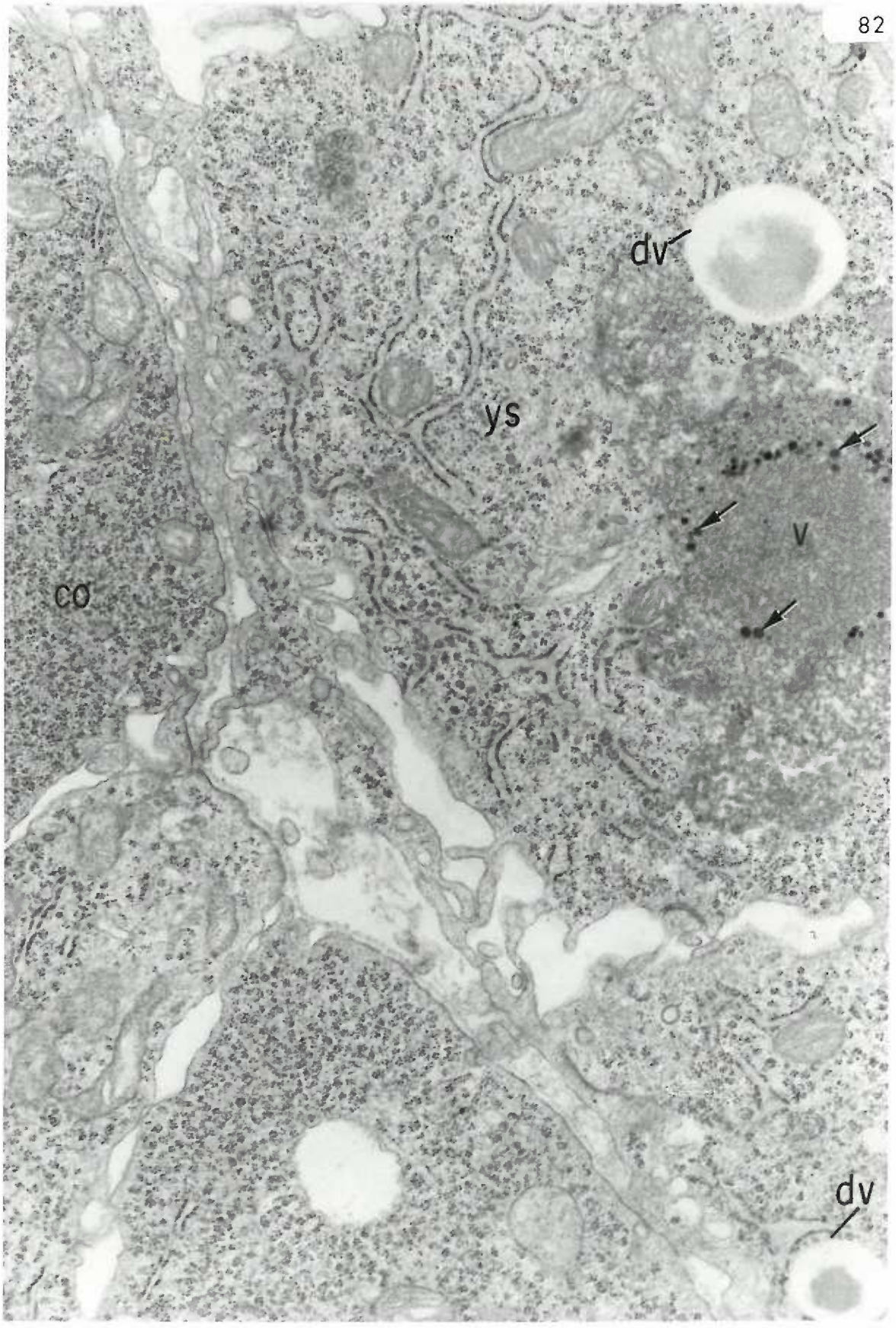
dv
ys
v
co
dv

Figure 83. Ten-day chorionic trophoblast, experimental. Small "dye-like" vacuoles (arrows) are clustered in the chorionic trophoblast cells (co), the visceral yolk sac endoderm (ys), and the distal endoderm cells (de). These "dye-like" vacuoles exhibit dark blue centers and clear peripheral areas. Trophoblast (t); yolk sac cavity (ysc); uterine lumen (ul). Richardson's stain.

x400

Figure 84. Ten-day chorionic trophoblast, control. Many small, clear vacuoles (arrow) are evident within the chorionic trophoblast cells (co). "Dye-like" vacuoles (see Figure 83) are not present in these cells. Yolk sac cavity (ysc); yolk sac endoderm (ys); extra-embryonic coelom (ec). Richardson's stain.

x400

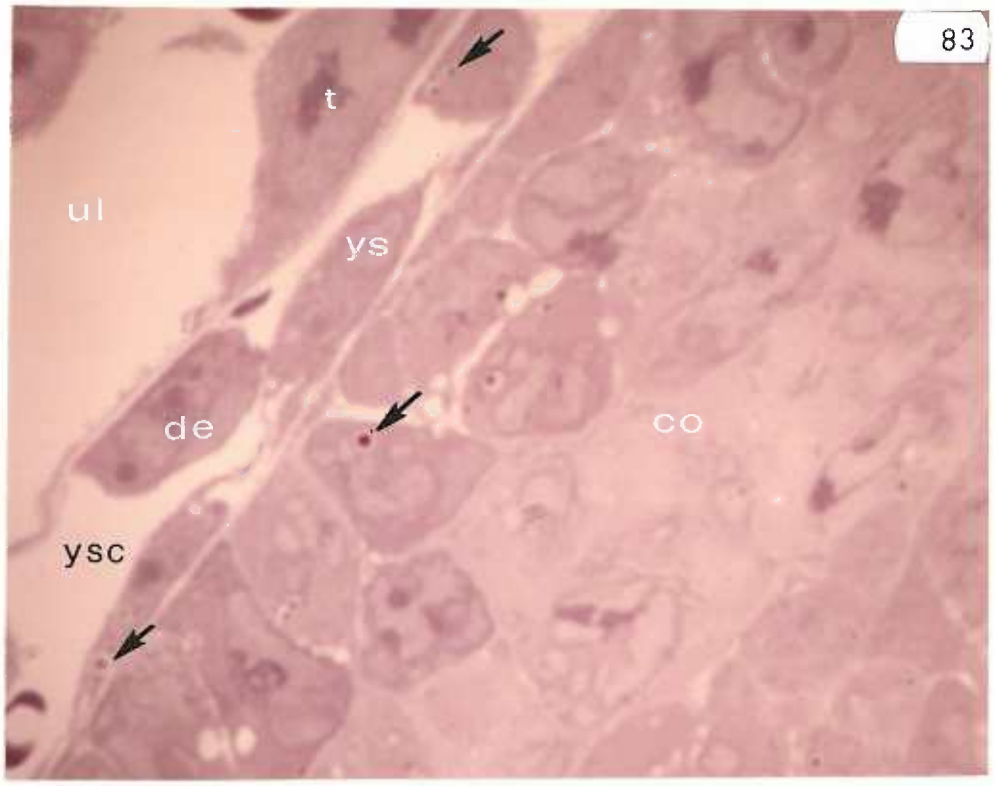
83
t
ul
ys
de
co
ysc


84
ec
ys
co
ysc

Figure 85. Ten-day trophoblast, junctional zone, control. A trophoblast cell contains two large vacuoles (v) containing membranous elements and a dense, granular material.

x29,000

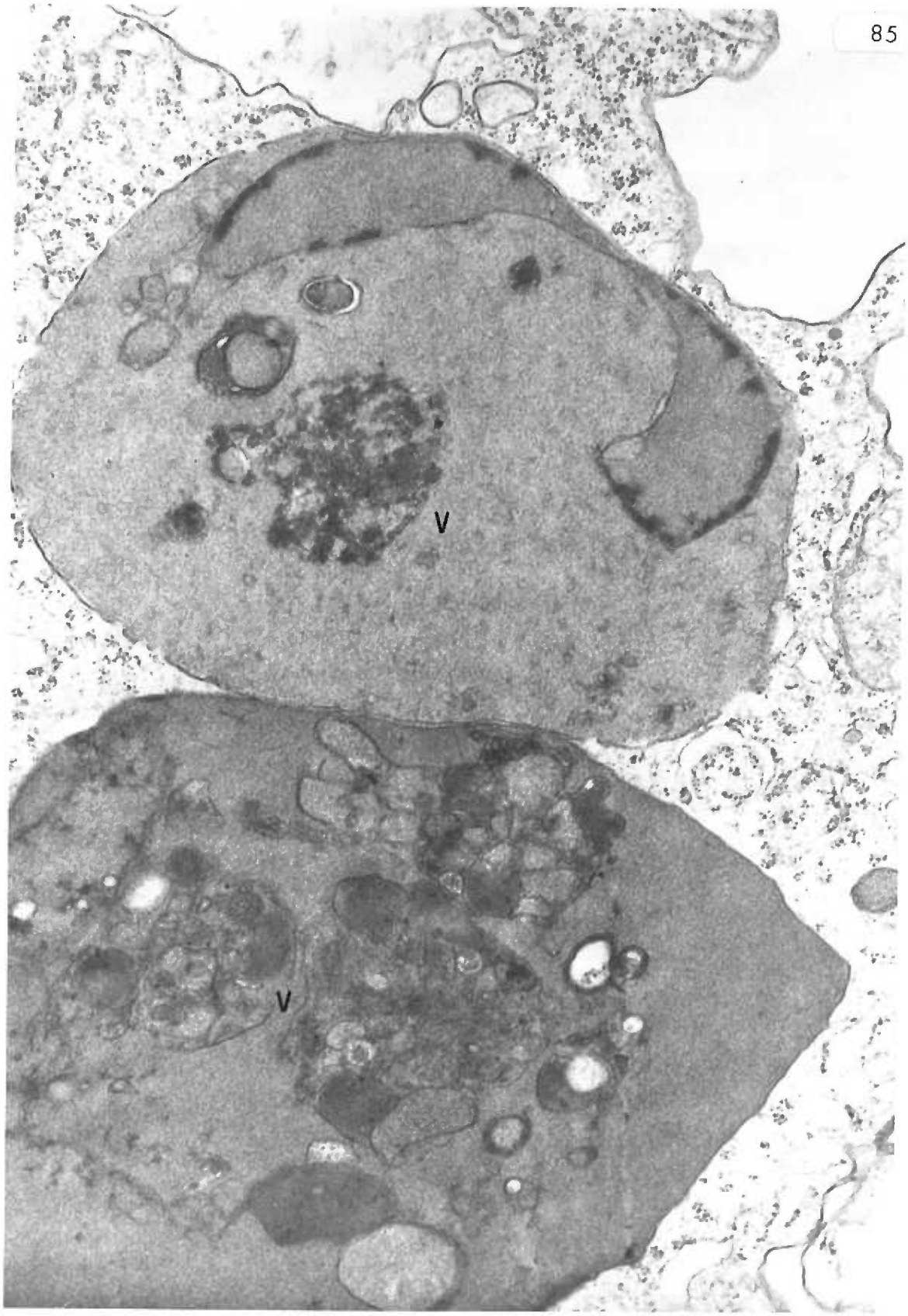
V
V

Figure 86. Ten-day chorionic trophoblast, control.

These chorionic trophoblast cells (co) contain numerous polyribosomes and mitochondria (m). A nucleus (n) shows several projections (arrows) into the cytoplasm. Centriole (c).

x12,000

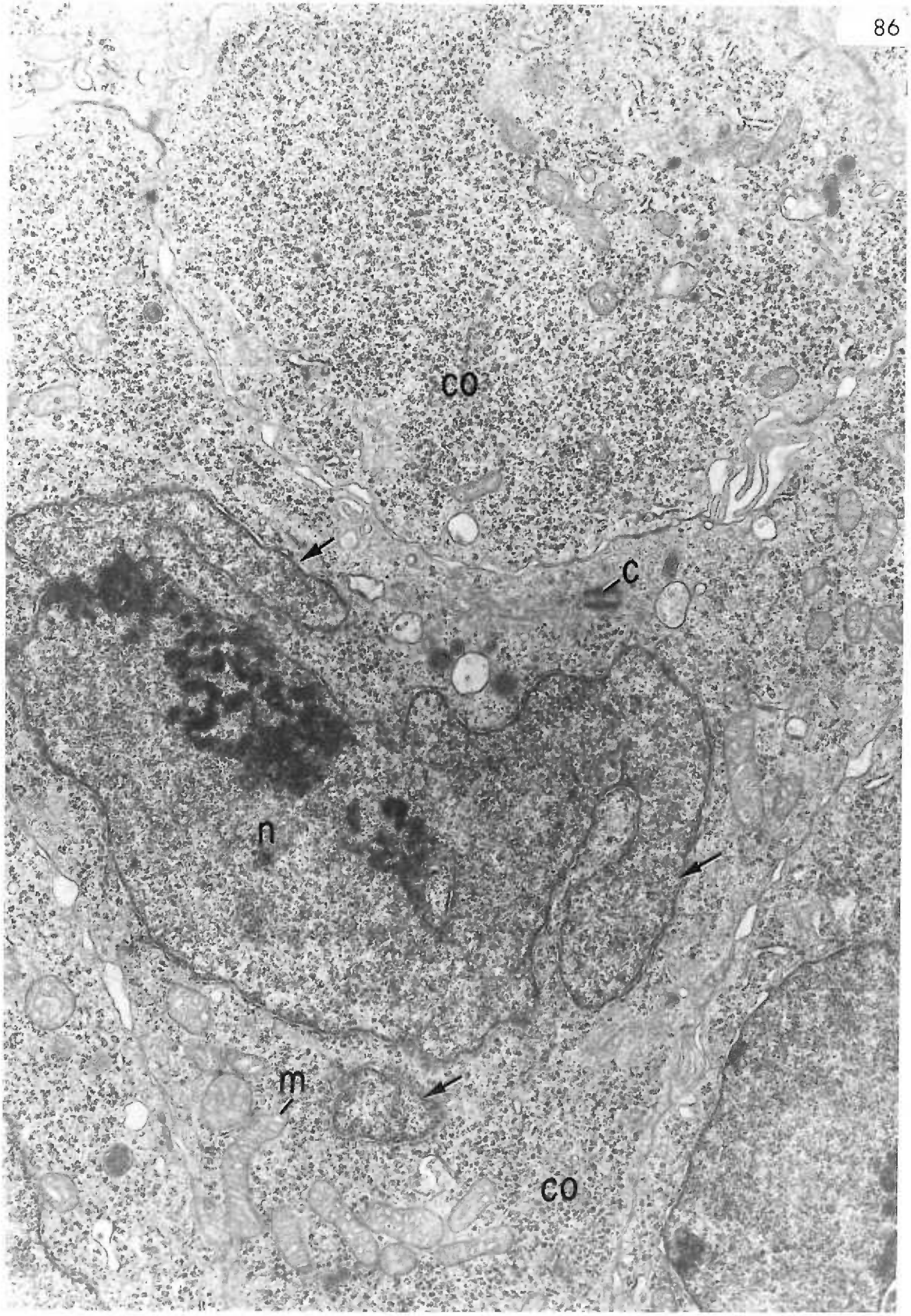
co
c
n
m
co

Figure 87. Ten-day amnion, experimental.

Three "dye-like" vacuoles (dv) are clustered in the amnion. The bi-laminar amnion exhibits a layer of ectoderm (a_1) which lines the amniotic cavity (ac) and a layer of mesoderm (a_2) which lines the extra-embryonic coelom (ec). The visceral yolk sac (ys) contains large vacuoles (dv) which probably contain Trypan blue. The visceral yolk sac is separated from the extra-embryonic coelom by a layer of mesothelium (ms).

x12,000

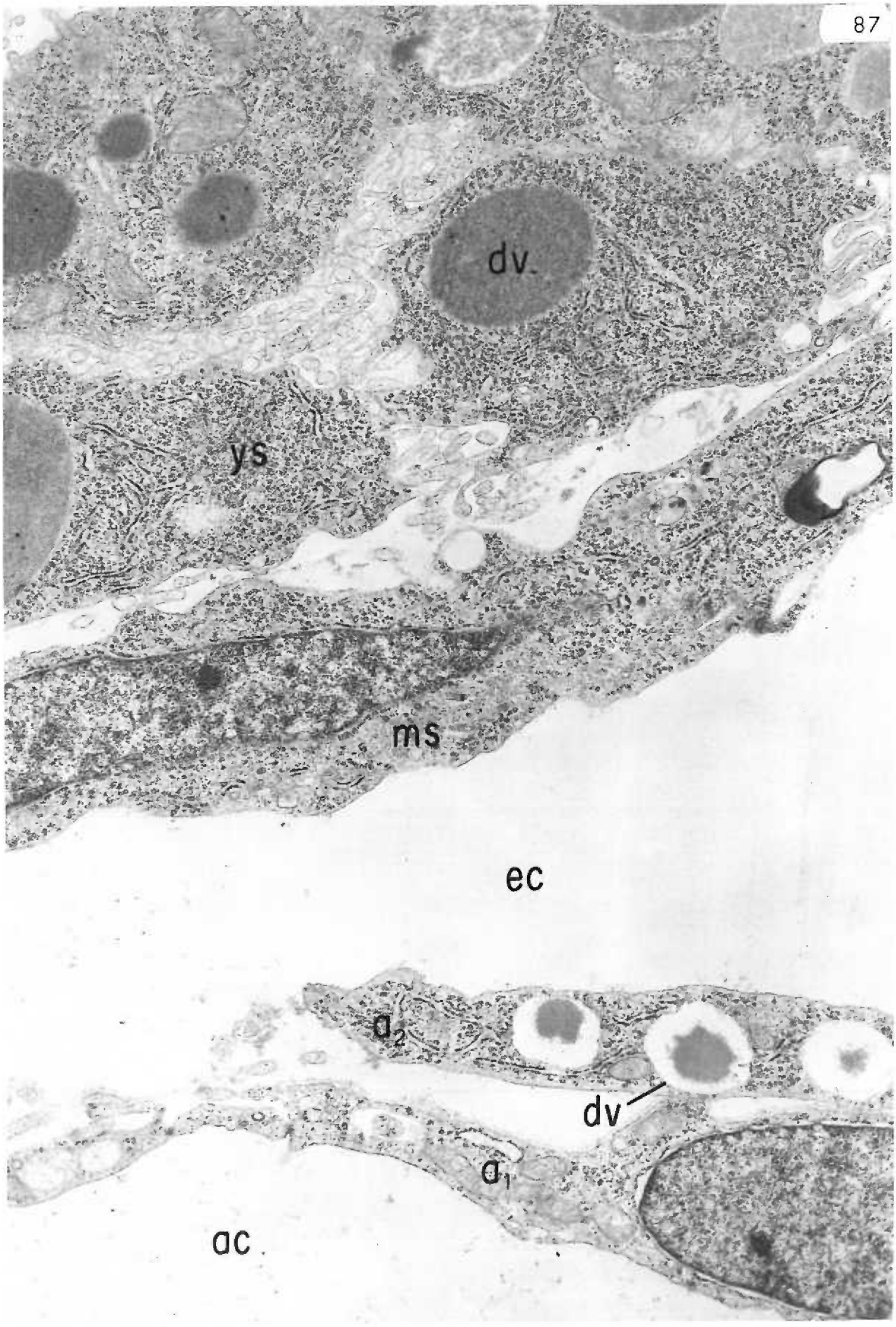
dv
ys
ms
ec
a_2
dv
a_1
ac

Figure 88. Ten-day amnion, experimental.
A portion of the amnion (a) contains several "dye-like" vacuoles (dv). A phagocytic cell (pc) displays unattached segments of pseudopodia (arrows). Extra-embryonic coelom (ec).

x20,000

Figure 89. Ten-day amnion, experimental.
A serial section of Figure 88 demonstrates "dye-like" vacuoles (dv). Portions of a phagocytic cell (pc) and its cytoplasmic extensions (arrows) are visible. Extra-embryonic coelom (ec); amnion (a).

x20,000

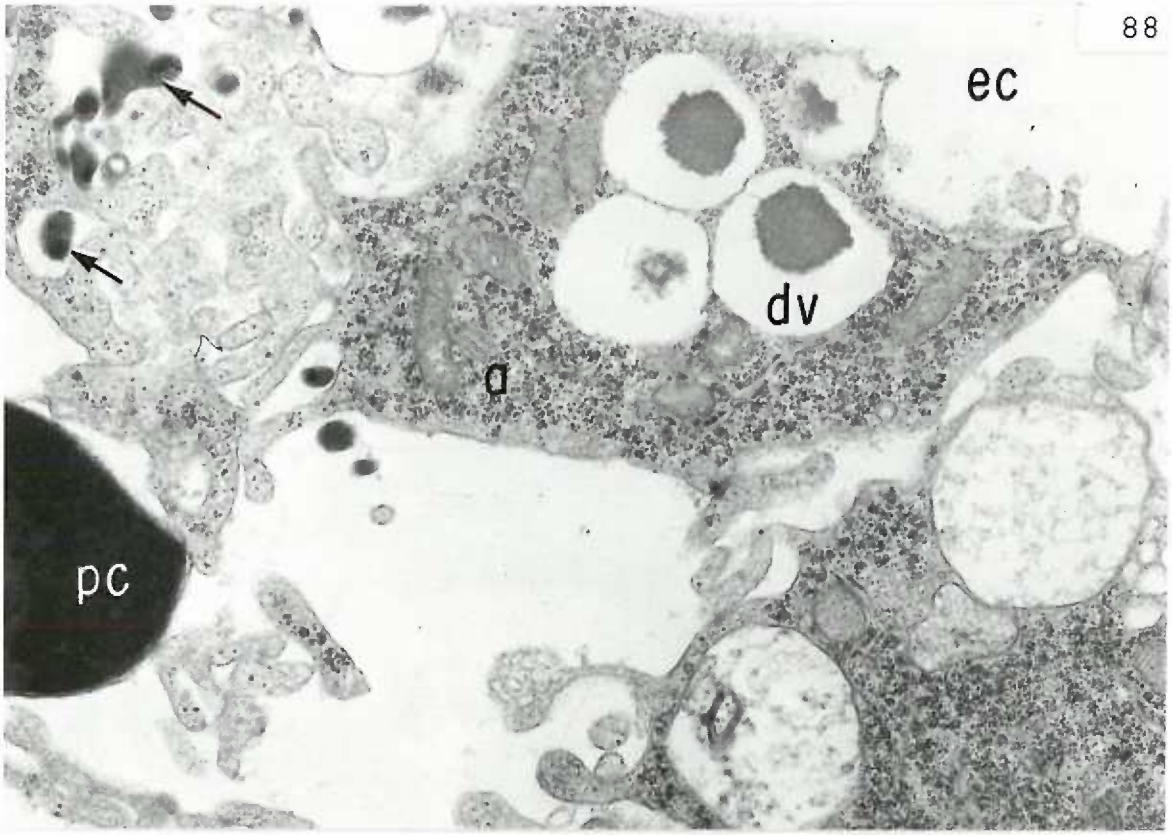
88
ec
dv
a
pc

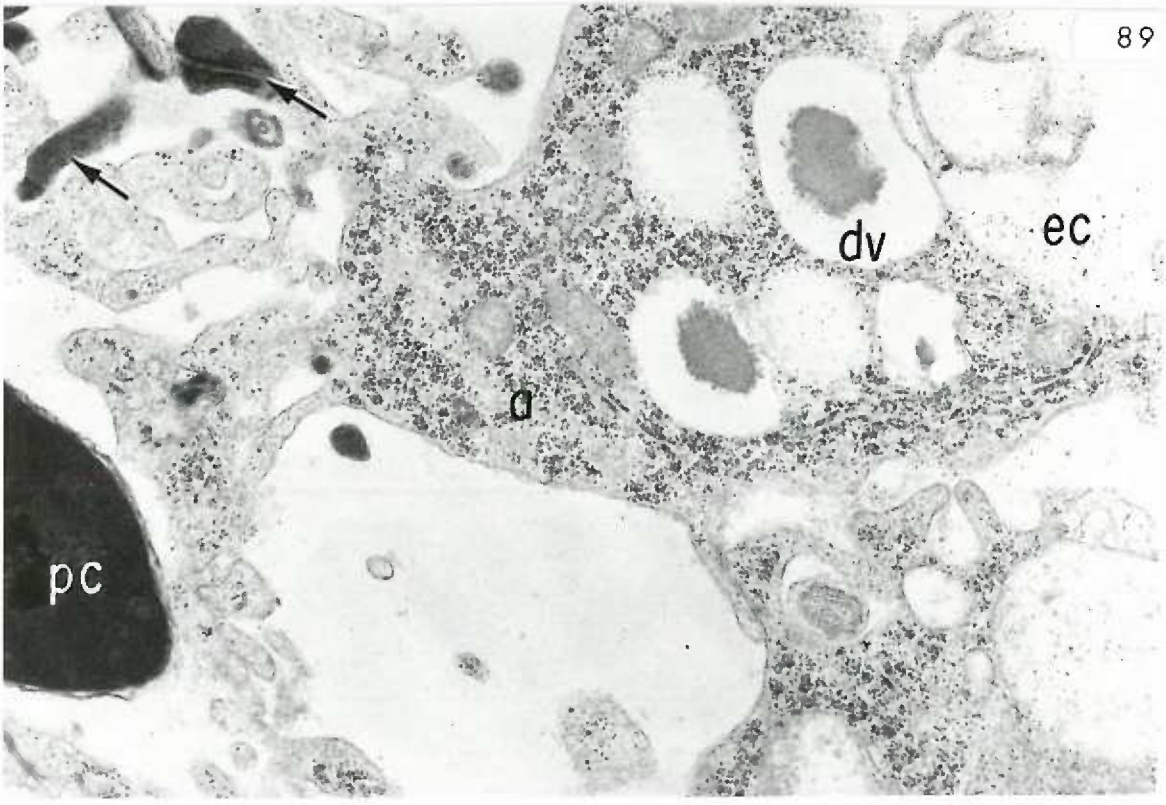
89
dv
ec
a
pc

Figure 90. Ten-day amnion, experimental.

Cells of the bi-laminar amnion (a) contain clusters of "dye-like" vacuoles (arrows). Allantois (al); amniotic cavity (ac). Richardson's stain.

x400

Figure 91. Ten-day amnion, control.

The cells of the amnion (a) do not contain "dye-like" vacuoles. Amniotic cavity (ac). Richardson's stain.

x400

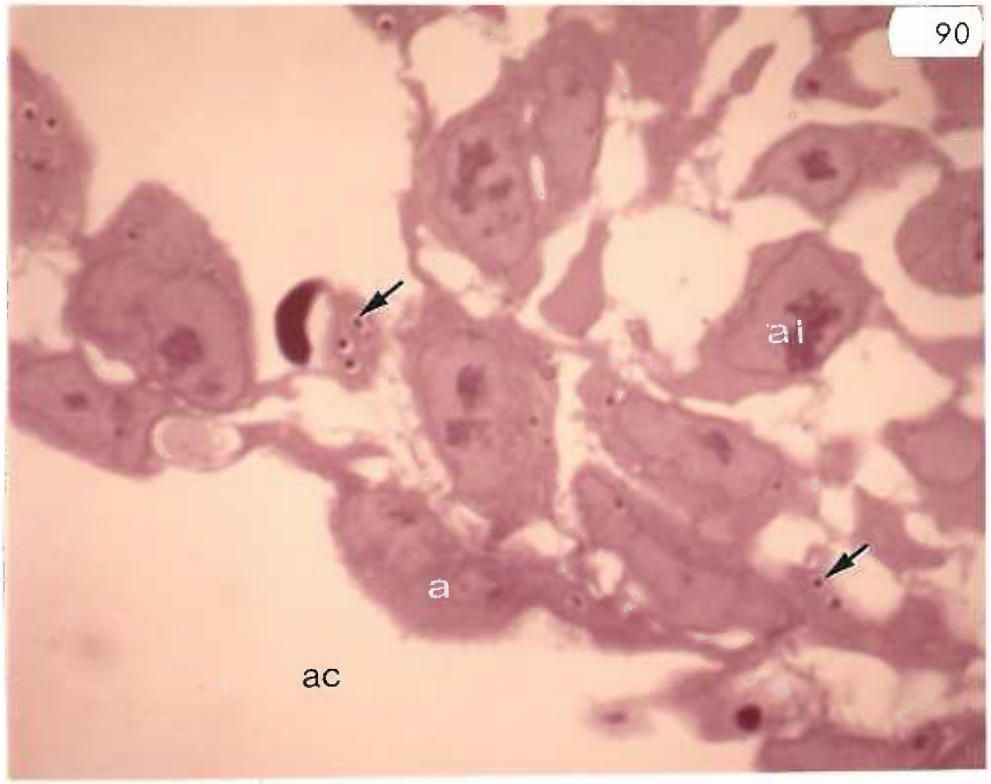
90
ai
a
ac

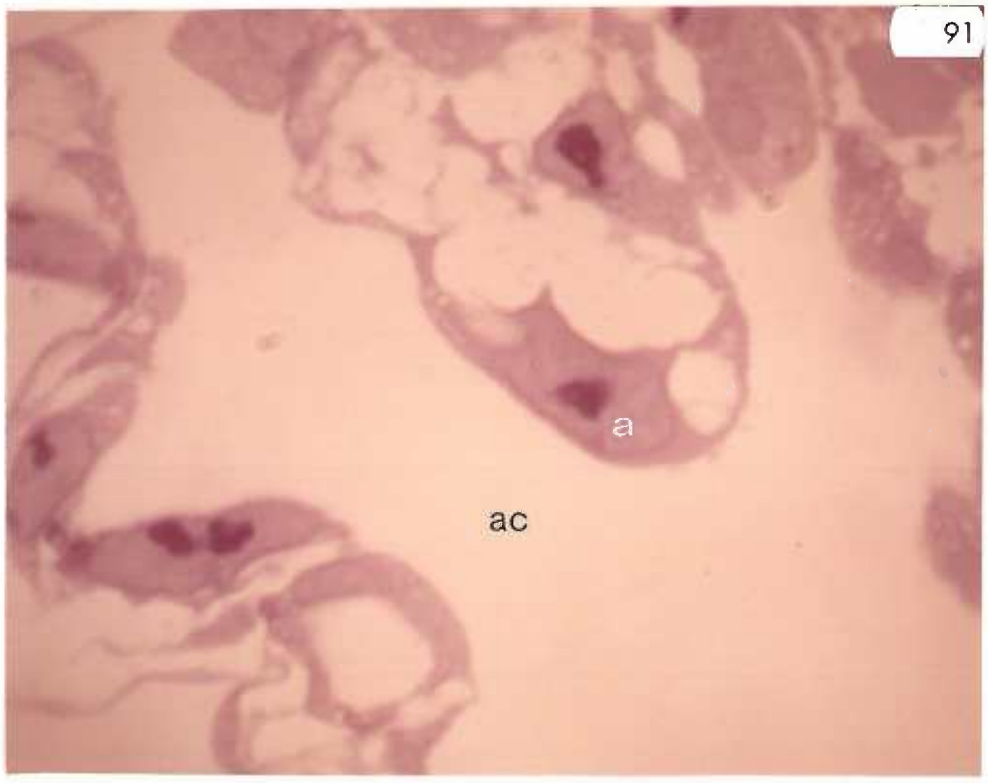
91
a
ac

Figure 92. Ten-day amnion, experimental.

Cytoplasmic portions (arrows) of high electron-density belong to a phagocytic cell (pc). One portion of this phagocytic cell contains strands of light-staining rough endoplasmic reticulum (rer). Amnion (a); residual body (rb).

x12,000

Figure 93. Ten-day amnion, experimental.

A serial section of Figure 92 illustrates additional portions of a phagocytic cell (pc). Pseudopodia (arrows) appear as separate entities in the extra-cellular space. Amnion (a); residual body (rb).

x12,000

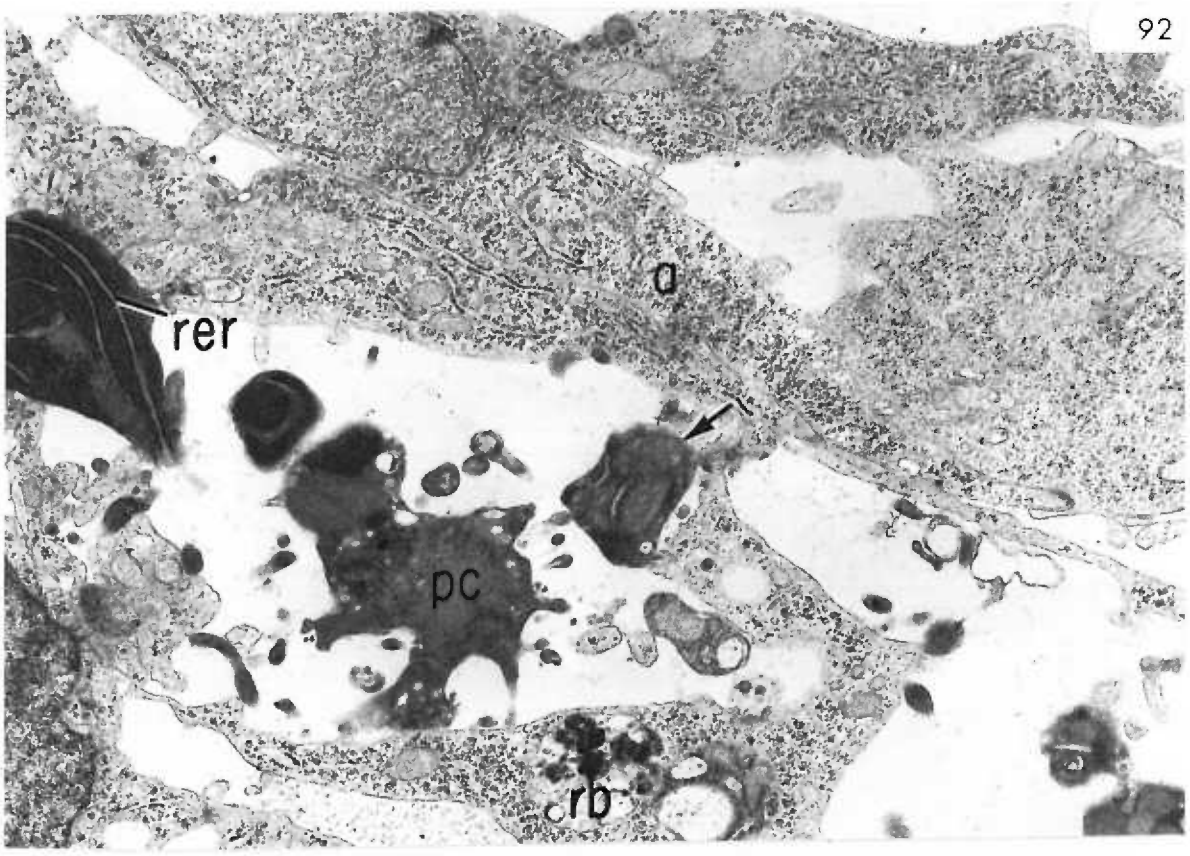
92
rer
g
pc
rb

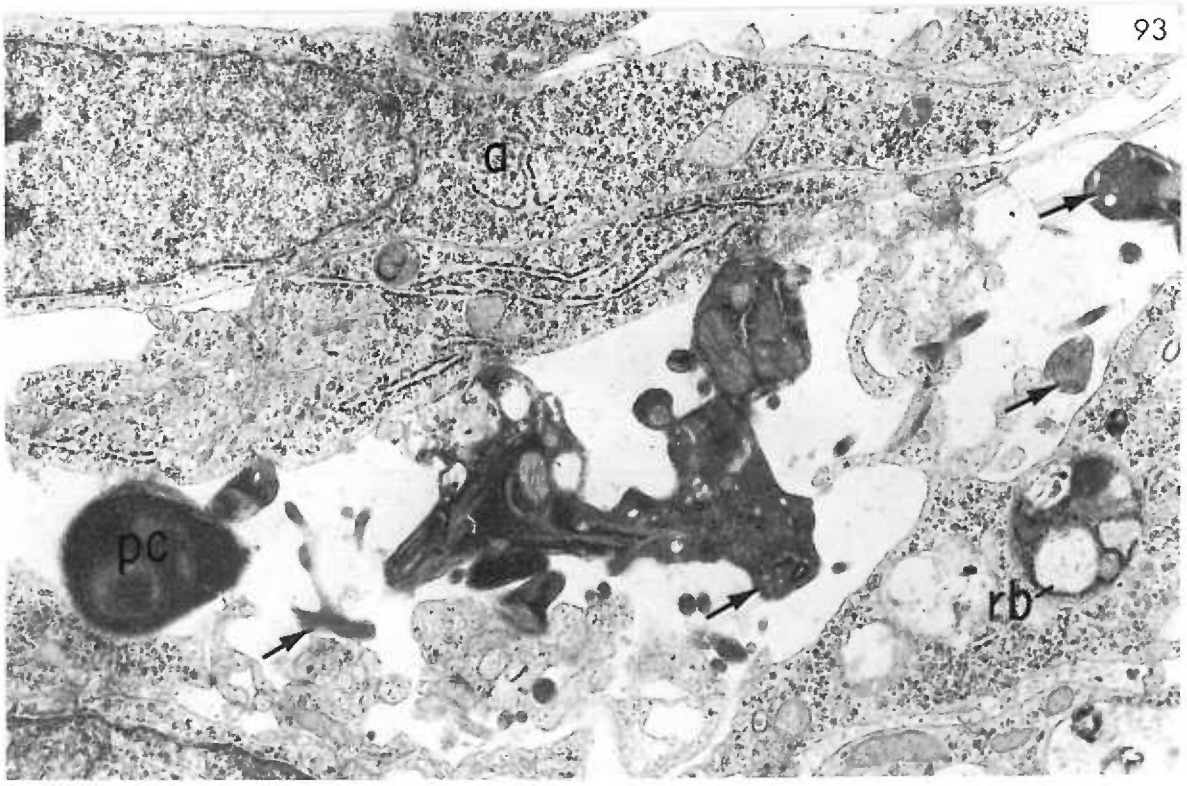
93
g
pc
rb

Figure 94. Ten-day amnion, control.

A folded amnion is composed of an ectodermal layer (a_1) lining the amniotic cavity (ac) and a mesodermal layer (a_2) lining the extra-embryonic coelom (ec). A dense protein-like material fills the amniotic cavity and the extra-embryonic coelom. Neural plate cells (np).

x12,000


a1
a2
ec
a2
a1
ac
np

Figure 95. Maternal kidney, proximal convoluted tubules, experimental.

Large vacuoles (dv) exhibit very electron-dense contents thought to be Trypan blue. These coincide in size and position to blue vacuoles seen in 1 μ sections viewed with the light microscope (Figure 96). Nucleus (n); mitochondria (m).

x20,000

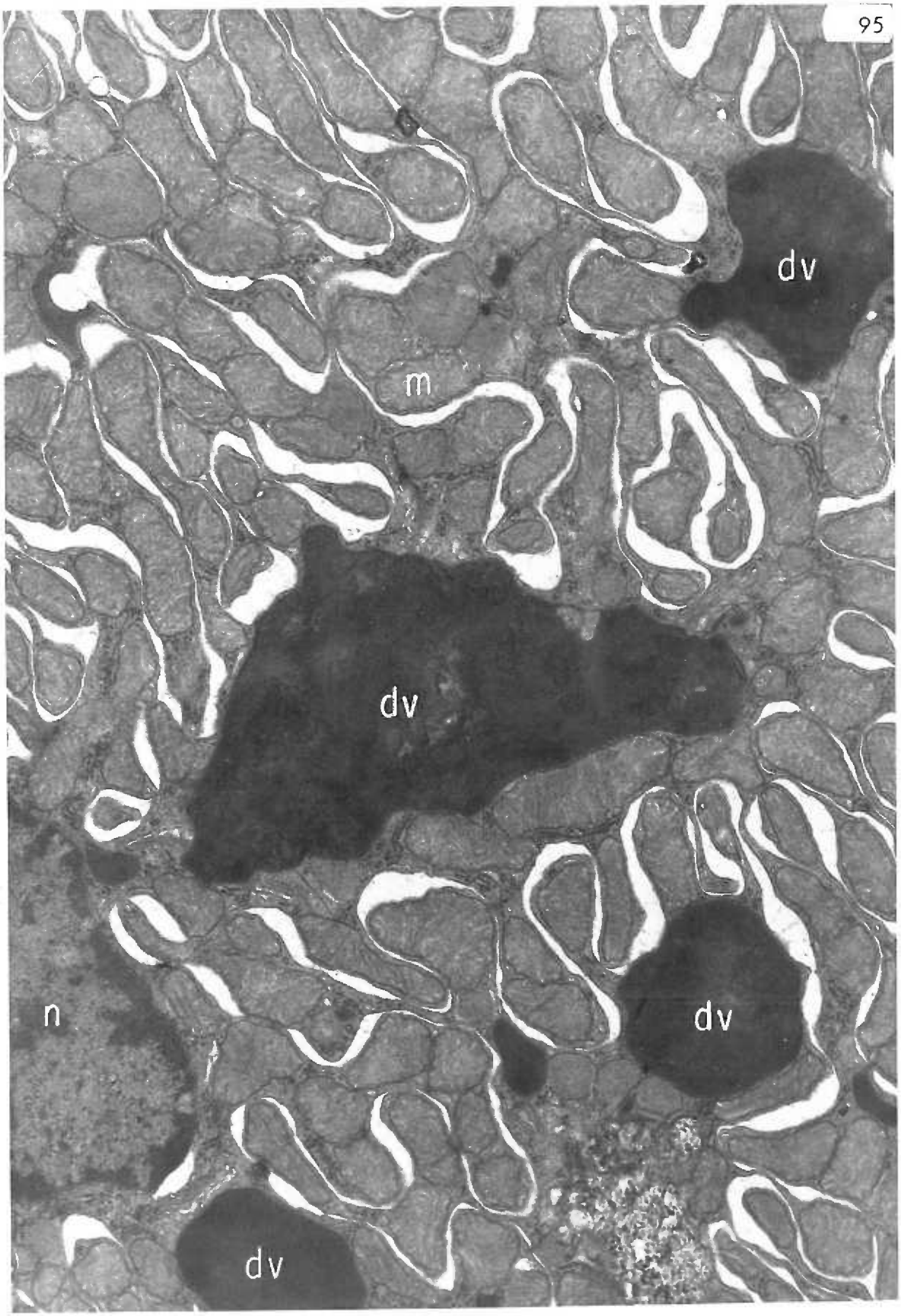
95
dv
m
dv
n
dv
dv

Figure 96. Maternal kidney, proximal convoluted tubules, experimental.

Cells of the proximal convoluted tubules exhibit large, dark bodies (arrow) in the basal cytoplasm which appear blue when examined by light microscopy. These vacuoles coincide in size and position with possible dye deposits seen ultrastructurally (Figure 95). Unstained 1 μ sections.

x400

Figure 97. Maternal kidney, proximal convoluted tubules, control.

A few refractile bodies (arrow) lie within the cytoplasm of these control proximal convoluted tubule cells. These probably correspond to the residual bodies seen ultrastructurally (Figure 98). Unstained 1 μ sections.

x400


96


97

Figure 98. Maternal kidney, proximal convoluted tubules, control.

The cells contain numerous residual bodies (rb) and oval mitochondria (m). Basal lamina (bm); connective tissue cell (ctc).

x12,000


ctc
rb
m
bm
rb

APPENDIX

Table 1

Osmium Tetroxide Fixation[+]

Additives:	Fixative A*
Palade's osmium* (Palade: 1952)	
Dalton's osmium* (Dalton: 1955)	
Sjostrand's osmium* (Zetterqvist: 1956)	
Millonig's osmium* (Millonig: 1962)	
osmium	2.0 %
s-collidine	0.1 M
$CaCl_2$	0.05 M
$MgCl_2$	0.05 M
(Fahrenbach: 1969)	
osmium	2.0 %
s-collidine	0.2 M
$CaCl_2$	0.01 M
$MgCl_2$	0.01 M
HCl	9.0 %
(Fahrenbach: 1969)	

*Fixation time: 1 hour
[+]All concentrations are final. Aqueous mixtures only.

Table 2

Osmium Tetroxide-Glutaraldehyde Fixation

Additives:	Fixative A	Fixative B	Procedure*:
osmium*	1.0 %		Combine+: 2 volumes Fixative A
glutaraldehyde		50.0 %	1 volume Fixative B
s-collidine		0.063 M	5 volumes buffer
(Trump: 1966)			
osmium *	5.0 %		Combine+: 1 volume Fixative A
glutaraldehyde		5.0 %	1 volume Fixative B
Na phosphate (monobasic)		0.2 M	
sucrose		3.0 %	
Millonig's osmium*	1.0 %		Combine+: 1 volume Fixative A
(Millonig: 1962)			1 volume Fixative B
formaldehyde		3.0 %	
Na phosphate (monobasic)	0.12 M	0.12 M	
glucose	0.5 %	0.5 %	
glutaraldehyde	0.5 %	0.5 %	
NaOH	0.1 M	0.1 M	

*Fixation time: $\frac{1}{2}$ hour
+Combine immediately before useage.

Table 3

Glutaraldehyde Fixation

Additives:	Fixative A*	Fixative B*	Fixative C*	Fixative D*	Post-Fixative*
glutaraldehyde Na cacodylate sucrose pH 7.4 (Connell: 1967)	3.0 % 0.1 M				1.0 % osmium 0.1 M 0.22 M
glutaraldehyde Na cacodylate sucrose pH 7.2 (Fahrenbach: 1969)	3.0 % 0.1 M 8.0 %				2.0 % osmium 0.1 M 8.0 %
glutaraldehyde Na phosphate (monobasic) s-collidine sucrose $CaCl_2$ pH 7.2 (Fahrenbach: 1969)	3.0 % 0.1 M 0.0 % 0.0015 M	3.0 % 0.1 M 3.0 % 0.0015 M	3.0 % 0.1 M 0.0 % 0.0015 M	3.0 % 0.1 M 3.0 % 0.0015 M	2.0 % osmium 0.1 M or 0.1 M 3.0 %
glutaraldehyde Sorensen buffer pH 7.3 (Maunsbach: 1966a)	1.0 % 0.135 M				Millonig's osmium (Millonig: 1962)

*Fixation time: $\frac{1}{2}$ hour

Table 4

Formaldehyde Fixation

Additives:	Fixative A*	Fixative B*	Fixative C*	Fixative D*	Fixative E*	Post-Fixative*
Brenner's formaldehyde (Brenner: 1969)						1.0 % osmium 1.0 % Na cacodylate 4.5 % sucrose (Anderson: 1970)
Karnovsky's formaldehyde (Karnovsky: 1965)						2.0 % osmium 0.1 M NaH_2PO_4 0.22 M sucrose
osmium						2.0 %
formaldehyde	4.0 %	4.0 %	3.0 %	3.0 %		
glutaraldehyde	1.0 %	1.0 %	1.0 %	1.0 %		
NaH_2PO_4	0.135 M	0.135 M	0.135 M	0.135 M		0.135 M
sucrose	0.0 %	3.0 %	0.0 %	3.0 %		3.0 %
pH 7.3						
osmium						2.0 %
formaldehyde	4.0 %	4.0 %	3.0 %	3.0 %		
glutaraldehyde	1.0 %	1.0 %	1.0 %	1.0 %		
Na cacodylate	0.1 M	0.1 M	0.1 M	0.1 M		0.1 M
sucrose	0.0 %	3.0 %	0.0 %	3.0 %		0.22 M
pH 7.2 (Fahrenbach: 1969)						(Connell: 1967)

*Fixation time: ½ hour

Table 4 (continued)

Formaldehyde Fixation

Additives:	Fixative A*	Fixative B*	Fixative C*	Fixative D*	Fixative E*	Post-Fixative*
osmium						2.0 %
formaldehyde	3.0 %	3.0 %	2.0 %	2.0 %		
glutaraldehyde	1.0 %	1.0 %	1.0 %	1.0 %		
s-collidine	0.2 M	0.2 M	0.2 M	0.2 M		0.2 M
sucrose	3.0 %	0.0 %	3.0 %	0.0 %		1.5 %
$CaCl_2$	0.01 M	0.01 M	0.01 M	0.01 M		0.01 M
$MgCl_2$	0.01 M	0.01 M	0.01 M	0.01 M		0.01 M
pH 7.3						
(Fahrenbach: 1969)						
formaldehyde	2.0 %	2.0 %	2.0 %	2.0 %	2.0 %	Millonig's osmium
glutaraldehyde	1.0 %	1.0 %	1.0 %	1.0 %	1.0 %	(Millonig: 1962)
NaH_2PO_4	0.135 M	0.135 M	0.135 M	0.135 M	0.135 M	
sucrose	2.5 %	2.0 %	1.5 %	1.0 %	0.5 %	
$CaCl_2$	0.01 M	0.01 M	0.01 M	0.01 M	0.01 M	
$MgCl_2$	0.01 M	0.01 M	0.01 M	0.01 M	0.01 M	
pH 7.3						
(Fahrenbach: 1969)						
osmium						1.0 %
formaldehyde	2.0 %	2.0 %	2.0 %	2.0 %		
glutaraldehyde	0.0 %	0.25 %	0.5 %	0.75 %		
s-collidine	0.2 M	0.2 M	0.2 M	0.2 M		0.1 %
sucrose						0.5 %
$CaCl_2$	0.01 M	0.01 M	0.01 M	0.01 M		
$MgCl_2$	0.01 M	0.01 M	0.01 M	0.01 M		
pH 7.3						

*Fixation time: ½ hour

Table 4 (continued)

Formaldehyde Fixation

Additives:	Fixative A	Fixative B	Fixative C	Fixative D	Fixative E	Post-Fixative*
formaldehyde	4.0 %	4.0 %	4.0 %	4.0 %		Millonig's osmium (Millonig: 1962)
glutaraldehyde	0.5 %	0.0 %	0.5 %	0.0 %		
NaH_2PO_4	0.12 M	0.12 M	0.12 M	0.12 M		
glucose	0.54 %	0.54 %	0.54 %	0.54 %		
NaOH	0.1 M	0.1 M	0.1 M	0.1 M		
fixation time	30 min.	30 min.	15 min.	15 min.		
pH 7.4 (Pease: 1964)						
osmium						1.0 %
formaldehyde	3.0 %	3.0 %	3.0 %			
glutaraldehyde	0.5 %	0.5 %	0.5 %			
NaH_2PO_4	0.12 M	0.12 M	0.12 M			0.12 M
glucose	0.5 %	0.5 %	0.5 %			0.5 %
NaOH	0.1 M	0.1 M	0.1 M			0.1 M
fixation time	30 min.	15 min.	10 min.			
pH 7.4 (Pease: 1964)						

*Fixation time: $\frac{1}{2}$ hour

Table 5

Physical Parameters of Experimental and Control Fetuses

	16-day Embryos* (Experimental)	16-day Embryos* (Control)	20-day Embryos* (Experimental)	20-day Embryos* (Control)
Total Number of Implants	107	116	98	107
Resorptions/ Implants	60/107 (56%)	6/116 (5%)	28/98 (29%)	7/107 (7%)
Normals/ Survivors	16/47 (34%)	109/110 (99%)	38/70 (54%)	100/100 (100%)
Malformed/ Survivors	31/47 (66%)	1/110 (1%)	32/70 (46%)	0/100 (0%)
Weight Ranges of Survivors	0.19-0.43 gm.	0.26-0.44 gm.	1.69-3.10 gm.	2.38-3.22 gm.
Average Weight of Survivors	0.31 gm.	0.35 gm.	2.40 gm.	2.80 gm.

*Eight maternal animals are included in each category.

Table 6

Malformations in 16- and 20-day Experimental Embryos

Malformations	16-Day Embryos*	20-Day Embryos*
Total malformations	57	50
Central nervous system (exencephaly, hydrocephalus, edema, meningocele)	16/57 (28%)	17/50 (34%)
Vertebral axis (spina bifida, deviation of axis)	11/57 (19%)	12/50 (24%)
Hindgut region (taillessness, atrophy of the tail, imperforate anus)	8/57 (14%)	9/50 (18%)
Generalized body hematomata or blisters	6/57 (11%)	2/50 (4%)
Eye (bilateral or unilateral anophthalmia)	5/57 (9%)	7/50 (14%)
Distension of pericardial sac	8/57 (14%)	--+
Generalized body edema	3/57 (5%)	2/50 (4%)
Other	0/57 (0%)	1/50 (2%)

*Multiple anomalies were observed in 26 embryos of 16-days gestation, and in 18 embryos of 20-days gestation.

+Any possible distensions of the pericardiac sac could not be ascertained in 20-day embryos.